BABAR Analysis Document #536, Version 6.0
January 15, 2004

A measurement of the lifetime difference $\Delta\Gamma/\Gamma$ and study of CPT and T violation using fully reconstructed CP and flavor eigenstates (Summer' 02 data sample)

Massimo Carpinelli, Francesco Forti, Marcello Giorgi, Fernando Martínez-Vidal[1,2], Nicola Neri, Francesco Sandrelli

INFN-Sezione di Pisa and Università di Pisa, Italy
for the Mixing AWG

Abstract

The time and flavor structure of the decay of $B^0_d\bar{B}^0_d$ mesons is exploited to perform the first measurement to date of the lifetime difference $\Delta\Gamma/\Gamma$ between the mass eigenstates. The analysis uses fully reconstructed B mesons into a flavor or CP (into charmonium) eigenstate and it is based on 81 fb^{-1} of data collected between 1999 and 2002 (Summer'02 data sample). The precision study of the time evolution of the $B^0_d\bar{B}^0_d$ mesons also provides a place for testing CPT and T invariance in a system where CP is violated outside the neutral kaon system, without restrictions imposed by the small expected value of the lifetime difference, opening the door to an alternative way for exploring new physics. Complications arise from the presence of theoretical and experimental competing effects, such as Doubly-CKM-Suppressed decays, direct CP violation and detector charge asymmetries. A global and simultaneous fit to the time distributions of tagged and untagged flavor and CP eigenstates allows the determination of the six independent parameters governing mixing (Δm, $\Delta\Gamma/\Gamma$), CPT/CP violation (Rez, Imz) and CP/T violation ($\frac{\mathrm{Im}\lambda_{CP}}{|\lambda_{CP}|}$, $|\,q/p\,|$), with maximal sensitivity and minimal correlation. The analysis results are:

$$\begin{aligned}
sign(\mathrm{Re}\lambda_{CP})\Delta\Gamma/\Gamma &= 0.008 \pm 0.037(\mathrm{stat}) \pm 0.018(\mathrm{syst}) \;\; [-0.068, 0.084] \\
|\,q/p\,| &= 1.029 \pm 0.013(\mathrm{stat}) \pm 0.011(\mathrm{syst}) \;\; [1.001, 1.057] \\
\frac{\mathrm{Re}\lambda_{CP}}{|\,\lambda_{CP}\,|}\mathrm{Re}z &= 0.014 \pm 0.035(\mathrm{stat}) \pm 0.034(\mathrm{syst}) \;\; [-0.072, 0.101] \\
\mathrm{Im}z &= 0.038 \pm 0.029(\mathrm{stat}) \pm 0.025(\mathrm{syst}) \;\; [-0.028, 0.104]
\end{aligned}$$

where the first error is statistical and the second systematics. The square brackets indicate the 90% confidence intervals. In the limit of CPT conservation ($z = 0$), the results are:

$$\begin{aligned}
sign(\frac{\mathrm{Re}\lambda_{CP}}{|\,\lambda_{CP}\,|})\Delta\Gamma/\Gamma &= 0.009^{+0.036}_{-0.037}(\mathrm{stat}) \pm 0.019(\mathrm{syst}) \;\; [-0.069, 0.087] \\
|\,q/p\,| &= 1.029 \pm 0.013(\mathrm{stat}) \pm 0.011(\mathrm{syst}) \;\; [1.001, 1.057]\,.
\end{aligned}$$

[1] Primary editor.
[2] Now at Instituto de Física Corpuscular (IFIC), CSIC-Universitat de València, València (Spain).

Contents

1 Introduction

The width difference $\Delta\Gamma$ between the mass eigenstates in the neutral B_d^0 system is a parameter usually neglected. In the Standard Model, the difference in the decay widths of the B_d^0 mesons is CKM-suppressed with respect to that in the B_s^0 system. A rough estimate leads to

$$\frac{\Delta\Gamma_d}{\Gamma_d} \sim \frac{\Delta\Gamma_s}{\Gamma_s} \times \lambda^2 \quad \approx \quad 0.5\% \tag{1}$$

where $\lambda = 0.225$ is the sine of the Cabibbo angle, and we have taken $\Delta\Gamma_s/\Gamma_s \approx 15\%$. Recently it has been discussed in the literature (see for example [1]) that a measurement of $\Delta\Gamma/\Gamma$ would be interesting since it could provide constraints (or signal, if the measured value turns out to be larger than the theoretical expectations) on new physics processes. No experimental measurement is currently available. Exploting the time and flavor structure of the decay of $B_d^0\bar{B}_d^0$ mesons, the analysis presented in this document will provide the first measurement of $\Delta\Gamma/\Gamma$ to date.

Nevertheless, the precision study of the time evolution of $B_d^0\bar{B}_d^0$ mesons opens the door for a broader class of studies, as an alternative way for exploring new physics. In a neutral-meson system, the violation of the CP symmetry includes the possibility of CPT violation. The CPT theorem [2, 3], based on very general principles of relativistic quantum field theories, states that any order of the triple product of the universal discrete symmetries C, P and T represent an exact symmetry. The CPT symmetry has been tested in a variety of experiments [4], remaining to date the only combination of C, P, T that is observed as an exact symmetry in nature. However, precisely because the CPT theorem represents an essential pillar of our present description of nature, it is appropiate to improve such studies in the B meson neutral system where the the $B^0\bar{B}^0$ interferometry provides an exceptionally sensitive framework [5]. On the other hand, superstring theories are not local and therefore do not necessarily fulfill the conditions of the CPT theorem. CPT invariance has also been questioned in the context of quantum gravity [6]. With CP violation in the B_d^0 system already well established [7], testing simultaneous and consistently the CP, T and CPT discrete symmetries of the effective Hamiltonian of evolution to disentangle whether the the CP violation is due to T or CPT violation (or both) is a natural step forward, and of great interest as outlined above. To date, all CPT violation tests in the B_d^0 system have been performed with inclusive methods in $B^0\bar{B}^0$ mixing [8], which provides information about CPT violation only if $\Delta\Gamma/\Gamma \neq 0$. This analysis will improve the situation significantly.

The outline of this document is as follows. In section 2 we summarize the formalism and derive the general time-dependent decay rates and likelihood function used in the analysis. Section 3 describes the decay modes, data and Monte Carlo samples. Section 4 provides some details about the resolution function treatment and justifies the motivation for the vertexing cuts applied. Section 5 describes the blinding strategy and in section 6 we describe the assumptions in the nominal fit. Sections 7 and 8 report the results and the consistency checks. Section 9 is devoted to the evaluation of the systematic errors. Finally, section 10 contains a summary of the analysis and the results.

Related (main) documentation

BAD#188 [10] Contains the details of the formalism used to calculate the time-dependent decay rates, as well as additional theoretical subtleties.

BAD#385 [12] Contains the feasibility and reach studies, together with the validation of most aspects of the fitting procedure, neglecting Doubly-CKM-Suppressed effects and exploiting untagged events in a different way. These two features are widely discussed in the present document (mainly in appendix A and B).

BAD#442 [9], BAD#452 [20] The Summer'02 $\sin 2\beta$ analysis documentation. Many of the inputs and systematics in this analysis are common with the standard $\sin 2\beta$ analysis, so the current document will focus on the aspects specific to this analysis. In some cases we will summary some particular aspects common with the $\sin 2\beta$ analysis.

BAD#125 [23] The hadronic mixing documentation.

BAD#436 [13] (not needed) Contains the blinded Winter'02 analysis. As the present analysis incorporates some new features (mainly the treatment of untagged events) and in order to simplify the reading, we kept BAD#536 completely independent of BAD#436.

2 Time-dependent decay rates and log-likelihood function

Starting from first principles we derive in this section the most general expression for the time-dependent decay rates in $\Upsilon(4S)$ decays as well as the final likelihood function including all the different experimental effects. In order to help our understanding of the main features of the PDF we also evaluate the time-dependence for different particular and simpler cases. For additional details about the formalism and the extraction of the decay rates, see reference [10].

2.1 Coherent B meson formalism

The neutral B meson system is a linear combination of the Schrödinger wave functions for the meson B^0 and its antimeson $\bar{B}^0$, $|\Psi\rangle = a|B^0\rangle + b|\bar{B}^0\rangle$. The time evolution of this combination is governed by the Schrödinger equation,

$$i\frac{\partial \Psi}{\partial t} = \tilde{H}\Psi \tag{2}$$

where $\tilde{H}$ is the 2×2 non-hermitian (probability is not conserved since the $B^0\bar{B}^0$ system decays) effective hamiltonian,

$$\tilde{H} = \tilde{M} - i\frac{\tilde{\Gamma}}{2} = \begin{pmatrix} M_{11} & M_{12} \\ M_{12}^* & M_{22} \end{pmatrix} - \frac{i}{2}\begin{pmatrix} \Gamma_{11} & \Gamma_{12} \\ \Gamma_{12}^* & \Gamma_{22} \end{pmatrix} . \tag{3}$$

$\tilde{M}$ and $\tilde{\Gamma}$ represent the mass (dispersive) and lifetime (absorptive) parts of the hamiltonian, both hermitian matrices[3].

The eigenvalues of (2) are

$$\lambda_{\pm} = \left(M - i\frac{\Gamma}{2}\right) \pm F' \tag{4}$$

[3]We use the notation H_{ij}, CP_{ij}, etc. to represent the matrix elements of the corresponding operators in the flavor basis, for instance $H_{12} \equiv \langle B^0|H|\bar{B}^0\rangle$.

where

$$F' = \sqrt{\left(M_{12}-i\frac{\Gamma_{12}}{2}\right)\left(M_{12}^{*}-i\frac{\Gamma_{12}^{*}}{2}\right)+\left(\delta M-i\frac{\delta\Gamma}{2}\right)^{2}} \tag{5}$$

$$M=\frac{M_{11}+M_{22}}{2} \quad , \quad \Gamma=\frac{\Gamma_{11}+\Gamma_{22}}{2} \tag{6}$$

$$\delta M=\frac{M_{11}-M_{22}}{2} \quad , \quad \delta\Gamma=\frac{\Gamma_{11}-\Gamma_{22}}{2} \ . \tag{7}$$

The corresponding eigenvectors are

$$\begin{aligned} \mid B_1\rangle &= \frac{1}{N_+}\left(p_+ \mid B^0\rangle - q_+ \mid \bar{B}^0\rangle\right) \\ \mid B_2\rangle &= \frac{1}{N_-}\left(p_- \mid B^0\rangle + q_- \mid \bar{B}^0\rangle\right) \end{aligned} \tag{8}$$

with $N_\pm^2 = \mid p_\pm \mid^2 + \mid q_\pm \mid^2$ and

$$q_\pm = -\left(M_{12}^{*}-i\frac{\Gamma_{12}^{*}}{2}\right) \tag{9}$$

$$p_\pm = \pm\left(\delta M-i\frac{\delta\Gamma}{2}\right)+F' \ . \tag{10}$$

Inverting (8) one can writte the $\mid B^0\rangle$ and $\mid \bar{B}^0\rangle$ states in terms of the evolution eigenstates,

$$\begin{aligned} \mid B^0\rangle &= \frac{1}{p_+q_- + p_-q_+}\left(N_+q_- \mid B_1\rangle + N_-q_+ \mid B_2\rangle\right) \\ \mid \bar{B}^0\rangle &= -\frac{1}{p_+q_- + p_-q_+}\left(N_+p_- \mid B_1\rangle - N_-p_+ \mid B_2\rangle\right) \ . \end{aligned} \tag{11}$$

Their time evolution is given by

$$\begin{aligned} \mid B^0(t)\rangle &= \frac{1}{p_+q_- + p_-q_+}\left(N_+q_-e^{-i\lambda_+t} \mid B_1\rangle + N_-q_+e^{-i\lambda_-t} \mid B_2\rangle\right) \\ \mid \bar{B}^0(t)\rangle &= -\frac{1}{p_+q_- + p_-q_+}\left(N_+p_-e^{-i\lambda_+t} \mid B_1\rangle - N_-p_+e^{-i\lambda_-t} \mid B_2\rangle\right) \ . \end{aligned} \tag{12}$$

When we pay attention to the restrictions imposed by discrete symmetries on the effective Hamiltonian (3) we see that ($CP_{12} = \langle B^0 \mid CP \mid \bar{B}^0\rangle$ is the relative unphysical phase between $\mid B^0\rangle$ and $\mid \bar{B}^0\rangle$):

- CP conservation imposes $\mathrm{Im}(M_{12}CP_{12}^{*}) = \mathrm{Im}(\Gamma_{12}CP_{12}^{*}) = 0$ and $H_{11} = H_{22}$;
- CPT invariance requires $H_{11} = H_{22}$;

- T invariance imposes $\mathrm{Im}(M_{12}CP^*_{12}) = \mathrm{Im}(\Gamma_{12}CP^*_{12}) = 0$.

As a consequence, the complex parameter

$$\Delta \;=\; 2\left(\delta M - i\frac{\delta\Gamma}{2}\right) \tag{13}$$

parameterizes any CPT violation. If either CPT or CP invariance leads to $\delta M = \delta\Gamma = 0$, we have

$$p \equiv p_+ = p_- \;=\; F \tag{14}$$

$$F \equiv F' \;=\; \sqrt{\left(M_{12} - i\frac{\Gamma_{12}}{2}\right)\left(M^*_{12} - i\frac{\Gamma^*_{12}}{2}\right)} \tag{15}$$

$$q \equiv q_+ = q_- \;= -\left(M^*_{12} - i\tfrac{\Gamma^*_{12}}{2}\right) \tag{16}$$

$$\frac{q}{p} = -\sqrt{\frac{M^*_{12} - i\frac{\Gamma^*_{12}}{2}}{M_{12} - i\frac{\Gamma_{12}}{2}}} \tag{17}$$

$$\lambda_\pm \;=\; \left(M - i\frac{\Gamma}{2}\right) \pm F \;\; . \tag{18}$$

As another consequence, if CP is conserved then $q = p$.

If there are no absortive parts in the effective hamiltonian ($\Gamma_{12} = 0$), then q/p is a pure phase, $\frac{q}{p} = e^{-i\chi}$ and $\mid q/p \mid = 1$. If there are absortive parts but $\mid \Gamma_{12}/M_{12} \mid$ is small,

$$\mid q/p \mid^2 \;\approx\; 1 - \mathrm{Im}\left[\frac{\Gamma_{12}}{M_{12}}\right] \;\; . \tag{19}$$

From (12) and (8), the time evolution of a state that is initially a pure B^0 or $\bar{B}^0$ is ($\vec{p} = (p_+, p_-)$, $\vec{q} = (q_+, q_-)$)

$$\begin{aligned} \mid B^0(t)\rangle \;&=\; f_+(\vec{p},\vec{q};t) \mid B^0\rangle + f_-(\vec{p},\vec{q};t) \mid \bar{B}^0\rangle \\ \mid \bar{B}^0(t)\rangle \;&=\; f_-(\vec{q},\vec{p};t) \mid B^0\rangle + f_+(\vec{q},\vec{p};t) \mid \bar{B}^0\rangle \end{aligned} \tag{20}$$

where

$$f_+(\vec{p},\vec{q};t) \;=\; \frac{1}{p_+q_- + p_-q_+}\left(p_+q_-e^{-i\lambda_+t} + p_-q_+e^{-i\lambda_-t}\right) \tag{21}$$

$$f_-(\vec{p},\vec{q};t) \;=\; -\frac{q_+q_-}{p_+q_- + p_-q_+}\left(e^{-i\lambda_+t} - e^{-i\lambda_-t}\right) \;\; . \tag{22}$$

With a little of algebra, equations (20) can be written in a more compact way as follows:

$$\begin{aligned} \mid B^0(t)\rangle &= [g_+(t)+zg_-(t)] \mid B^0\rangle - \frac{q}{p}\sqrt{1-z^2}g_-(t) \mid \bar{B}^0\rangle \\ \mid \bar{B}^0(t)\rangle &= -\frac{p}{q}\sqrt{1-z^2}g_-(t) \mid B^0\rangle + [g_+(t)-zg_-(t)] \mid \bar{B}^0\rangle \end{aligned} \tag{23}$$

where

$$z = \frac{\delta M - i\frac{\delta\Gamma}{2}}{F'} \tag{24}$$

$$g_\pm(t) = \frac{1}{2}\left(e^{-i\lambda_+ t} \pm e^{-i\lambda_- t}\right) \ . \tag{25}$$

The masses (m_1, m_2) and widths (Γ_1, Γ_2) of the eigenstates $\mid B_1\rangle$ and $\mid B_2\rangle$ are related to the eigenvalues (λ_+, λ_-) as:

$$m_1 = \mathrm{Re}(\lambda_+) \ , \quad m_2 = \mathrm{Re}(\lambda_-) \quad ; \qquad \Gamma_1 = -2\mathrm{Im}(\lambda_+) \ , \quad \Gamma_2 = -2\mathrm{Im}(\lambda_-) \ . \tag{26}$$

The oscillation parameters can then be defined as

$$\Delta\lambda = \frac{\lambda_+ - \lambda_-}{2} = \frac{1}{2}\left(\Delta m - i\frac{\Delta\Gamma}{2}\right) = F' \tag{27}$$

with

$$\Delta m = m_1 - m_2 = \mathrm{Re}(\lambda_+ - \lambda_-) \quad , \qquad \Delta\Gamma = \Gamma_1 - \Gamma_2 = 2\mathrm{Im}(\lambda_- - \lambda_+) \ . \tag{28}$$

Note that Δm is positive by definition. When $\Delta\Gamma = 0$ we have $\delta\Gamma = 0$ and $\mid q/p \mid = 1$.

For later use it is convenient also to define

$$\lambda = \frac{\lambda_+ + \lambda_-}{2} = M - i\frac{\Gamma}{2} \tag{29}$$

with

$$m = \frac{m_1 + m_2}{2} = \frac{\mathrm{Re}(\lambda_+ + \lambda_-)}{2} \equiv M \quad , \qquad \Gamma = \frac{1}{\tau} = \frac{\Gamma_1 + \Gamma_2}{2} = -\mathrm{Im}(\lambda_+ + \lambda_-) \ . \tag{30}$$

With these definitions, equations (5) and (24) can be rewritten, respectively, as

$$F' = \frac{1}{2}\left(\Delta m - i\frac{\Delta\Gamma}{2}\right) \tag{31}$$

and

$$z = 2\frac{\delta M - i\frac{\delta\Gamma}{2}}{\Delta m - i\frac{\Delta\Gamma}{2}} \ . \tag{32}$$

The complex-valued functions (25) in terms of the oscillation parameters are:

$$g_{\pm}(t) \;=\; \frac{1}{2}e^{-imt}e^{-t/2\tau}\left(e^{-i\Delta mt/2}e^{-\Delta\Gamma t/4} \pm e^{i\Delta mt/2}e^{\Delta\Gamma t/4}\right) \;. \tag{33}$$

In summary, we have four real parameters which carry information on the discrete symmetries of the effective Hamiltonian, according to the following list:

- $\mid q/p \mid \neq 1$ signals CP and T violation, with $\Delta\Gamma \neq 0$;
- $\arg q/p \neq 0$ indicates CP and T violation;
- $\delta M \neq 0$ (Rez $\neq 0$) means that CP and CPT violation exist;
- $\delta\Gamma \neq 0$ (Imz $\neq 0$) shows CP and CPT violation, with $\Delta\Gamma \neq 0$.

The fact that Rez is primarily connected to δM while Imz is to $\delta\Gamma$ makes Rez more interesting than Imz. Let us note that CPT or T violation requires CP violation, and CP violation implies T or CPT violation. As outlined in the introduction to this document, desintangle whether CP violation is due to T or CPT violation (or both) is one of the goals of this analysis.

So far we have considered the evolution of an isolated neutral B meson. Charge conjugation together with Bose statistics require that the $B^0\bar{B}^0$ state produced from the $\Upsilon(4S)$ decay is given in the eigenstate basis by

$$\mid \Upsilon\rangle \;=\; \frac{1}{\sqrt{2}}\left(\mid B_1\rangle \mid B_2\rangle - \mid B_2\rangle \mid B_1\rangle\right) \tag{34}$$

which evolves as

$$\mid \Upsilon(t_1,t_2)\rangle \;=\; \frac{1}{\sqrt{2}}\left(e^{-i\lambda_+ t_1}e^{-i\lambda_- t_2} \mid B_1\rangle \mid B_2\rangle - e^{-i\lambda_- t_1}e^{-i\lambda_+ t_2} \mid B_2\rangle \mid B_1\rangle\right) \;. \tag{35}$$

t_1 and t_2 are the proper times in the rest frames of the each B meson. If we make the change of variables

$$t = \frac{t_1+t_2}{2} \quad , \qquad \Delta t = t_2 - t_1 \;, \tag{36}$$

equation (35) can be rewritten as

$$\mid \Upsilon(t,\Delta t)\rangle \;=\; \frac{1}{\sqrt{2}}e^{-i2\lambda t}\left(e^{i\Delta\lambda\Delta t} \mid B_1\rangle \mid B_2\rangle - e^{-i\Delta\lambda\Delta t} \mid B_2\rangle \mid B_1\rangle\right) \;. \tag{37}$$

If one of the B mesons decays to a final state f_1 at time t_1, the partially projected state reads

$$\langle f_1 \mid \Upsilon(t,\Delta t)\rangle \;=\; \frac{1}{\sqrt{2}}e^{-i2\lambda t}\left(e^{i\Delta\lambda\Delta t}\langle f_1 \mid B_1\rangle \mid B_2\rangle - e^{-i\Delta\lambda\Delta t}\langle f_1 \mid B_2\rangle \mid B_1\rangle\right) \;. \tag{38}$$

Definining $A_1 = \langle f_1 \mid B^0 \rangle$ and $\overline{A}_1 = \langle f_1 \mid \overline{B}^0 \rangle$, from equation (8) we can expand,

$$\begin{aligned} \langle f_1 \mid B_1 \rangle &= \frac{1}{N_+}\left(p_+ A_1 - q_+ \overline{A}_1\right) \\ \langle f_1 \mid B_2 \rangle &= \frac{1}{N_-}\left(p_- A_1 + q_- \overline{A}_1\right) \quad . \end{aligned} \tag{39}$$

Using (39) and comparing with (12) for a single isolated B, the partially projected state (38) can be written as

$$\langle f_1 \mid \Upsilon(t_1, \Delta t) \rangle = -\frac{1}{\sqrt{2}} e^{-i2\lambda t_1} \frac{p_+ q_- + p_- q_+}{N_+ N_-} \left(\overline{A}_1 \mid B^0(\Delta t)\rangle - A_1 \mid \overline{B}^0(\Delta t)\rangle\right) \quad . \tag{40}$$

Let us note the change of variables from $(t, \Delta t)$ to $(t_1, \Delta t)$, since the overall exponential factor has a dependence with t_1.

If the other B meson decays to an state f_2 at time t_2 ($t_2 > t_1$, i.e. the collapse of the wave function occurs at t_1),

$$\langle f_1 f_2 \mid \Upsilon(t_1, \Delta t) \rangle = -\frac{1}{\sqrt{2}} e^{-i2\lambda t_1} \frac{p_+ q_- + p_- q_+}{N_+ N_-} \left(\overline{A}_1 \langle f_2 \mid B^0(\Delta t)\rangle - A_1 \langle f_2 \mid \overline{B}^0(\Delta t)\rangle\right) \quad . \tag{41}$$

The normalization factor $\frac{p_+ q_- + p_- q_+}{N_+ N_-}$ is phase-convention independent and depends only on z, $\mid q/p \mid$ and pq (see [10] for explicit dependence). When $\Delta t < 0$, the collapse of the wave function happens at t_2 but the above formalism and expressions are still valid.

2.2 Time-dependent decay rates for coherent B mesons

In order to calculate the decay rates, it is convenient to express the time-dependence of the decay amplitudes in terms of the $g_\pm$ functions. Using (23) and defining $A_2 = \langle f_2 \mid B^0 \rangle$ and $\overline{A}_2 = \langle f_2 \mid \overline{B}^0 \rangle$,

$$\overline{A}_1 \langle f_2 \mid B^0(\Delta t)\rangle - A_1 \langle f_2 \mid \overline{B}^0(\Delta t)\rangle = a_+ g_+(\Delta t) + a_- g_-(\Delta t) \tag{42}$$

where

$$\begin{aligned} a_+ &= \overline{A}_1 A_2 - A_1 \overline{A}_2 \\ a_- &= z\left(\overline{A}_1 A_2 + A_1 \overline{A}_2\right) - \sqrt{1-z^2}\left(\frac{q}{p}\overline{A}_1 \overline{A}_2 - \frac{p}{q} A_1 A_2\right) \quad . \end{aligned} \tag{43}$$

From (41), (42) and (43), we obtain the corresponding decay rate,

$$\begin{aligned} \mid \langle f_1 f_2 \mid \Upsilon(t_1, \Delta t)\rangle \mid^2 &= \frac{1}{2} e^{-2t_1/\tau} \frac{\mid p_+ q_- + p_- q_+ \mid^2}{\mid N_+ N_- \mid^2} \times \\ &\quad \left\{ \mid a_+ \mid^2 \mid g_+(\Delta t) \mid^2 + \mid a_- \mid^2 \mid g_-(\Delta t) \mid^2 + 2\mathrm{Re}\left[a_- a_+^* g_-(\Delta t) g_+^*(\Delta t)\right] \right\} \quad . \end{aligned} \tag{44}$$

We observe that the time dependence is described by two real-valued functions,

$$| g_{\pm}(\Delta t) |^2 = \frac{1}{2} e^{-\Delta t/\tau} [\cosh(\Delta\Gamma \Delta t/2) \pm \cos(\Delta m \Delta t)] \tag{45}$$

and the complex-valued function

$$g_+^*(\Delta t) g_-(\Delta t) = -\frac{1}{2} e^{-\Delta t/\tau} [\sinh(\Delta\Gamma \Delta t/2) + i \sin(\Delta m \Delta t)] \ . \tag{46}$$

If we replace (45) and (46) into (44),

$$\begin{aligned} | \langle f_1 f_2 | \Upsilon(t,\Delta t) \rangle |^2 &= \frac{1}{2} e^{-2t/\tau} \frac{| p_+ q_- + p_- q_+ |^2}{| N_+ N_- |^2} \times \\ &\left\{ \frac{1}{2} c_+ \cosh\left(\frac{\Delta\Gamma\Delta t}{2}\right) + \frac{1}{2} c_- \cos(\Delta m \Delta t) - \mathrm{Re}(s) \sinh\left(\frac{\Delta\Gamma\Delta t}{2}\right) + \mathrm{Im}(s) \sin(\Delta m \Delta t) \right\} \end{aligned} \tag{47}$$

where

$$c_{\pm} = | a_+ |^2 \pm | a_- |^2 \tag{48}$$

$$s = a_- a_+^* \ . \tag{49}$$

Note the change of variables from $(t_1, \Delta t)$ back to $(t, \Delta t)$.

The coefficients $c_{\pm}$ and s can be written in terms of the base of parameters

$$z \ , \quad u_{\pm} = \bar{A}_1 A_2 \pm A_1 \bar{A}_2 \ , \quad m = -\frac{q}{p} \bar{A}_1 \bar{A}_2 + \frac{p}{q} A_1 A_2 \tag{50}$$

as follows:

$$c_{\pm} = | u_- |^2 \pm \left[| z |^2 | u_+ |^2 + | 1 - z^2 | | m |^2 + 2\mathrm{Re}\left(z^* \sqrt{1-z^2} u_+^* m \right) \right] \tag{51}$$

$$s = z u_+ u_-^* + \sqrt{1-z^2} u_-^* m \ . \tag{52}$$

As experimentally the information available for the time sum t of the meson evolution is quite poor compared to Δt, it is appropiate to work with an integrated probability,

$$\begin{aligned} h_{12}(\Delta t) \equiv | \langle f_1 f_2 | \Upsilon(\Delta t) \rangle |^2 &= \int_{|\Delta t|/2}^{+\infty} dt \, | \langle f_1 f_2 | \Upsilon(t,\Delta t) \rangle |^2 = \frac{\tau}{4} e^{-|\Delta t|/\tau} \frac{| p_+ q_- + p_- q_+ |^2}{| N_+ N_- |^2} \times \\ &\left\{ \frac{1}{2} c_+ \cosh\left(\frac{\Delta\Gamma\Delta t}{2}\right) + \frac{1}{2} c_- \cos(\Delta m \Delta t) - \mathrm{Re}(s) \sinh\left(\frac{\Delta\Gamma\Delta t}{2}\right) + \mathrm{Im}(s) \sin(\Delta m \Delta t) \right\} \ . \end{aligned} \tag{53}$$

It is convenient to express the coefficients (51) and (52) in terms of the well-known convention independent parameter $\lambda = \frac{q}{p}\frac{\bar{A}}{A}$, where A and $\bar{A}$ are, respectively, the B^0 and $\bar{B}^0$ decay amplitudes into an arbitrary final state. Assuming that A_k and $A_{\bar{k}}$, with $k = 1,2$, are non-zero, we introduce the parameters

$$\lambda_k = \frac{q}{p}\frac{\bar{A}_k}{A_k} = \mid q/p \mid r_k e^{i\theta_k} \tag{54}$$

$$\bar{\lambda}_k = \frac{1}{\lambda_{\bar{k}}} = \frac{p}{q}\frac{A_{\bar{k}}}{A_{\bar{k}}} = \mid p/q \mid \bar{r}_k e^{i\bar{\theta}_k} \tag{55}$$

where

$$r_k = \mid \bar{A}_k \mid / \mid A_k \mid \tag{56}$$

$$\bar{r}_k = \frac{1}{r_{\bar{k}}} = \mid A_{\bar{k}} \mid / \mid \bar{A}_{\bar{k}} \mid \tag{57}$$

are the ratios of decay amplitudes of Doubly-CKM-Suppressed to favored processes, for $\mid f_k\rangle = \mid B^0\rangle$ and $\mid f_{\bar{k}}\rangle = \mid \bar{B}^0\rangle$ states, respectively. θ_k and $\bar{\theta}_k$ are the corresponding B^0 and $\bar{B}^0$ phases (overall phase of the ratio of decay amplitudes and the mixing phase). When there is one single process contributing to the favored and DCKM-supressed decays, $r_k = \bar{r}_k$. For $D^{(*)\pm}X^{\mp}$ final states, the amplitudes are expected to be dominated by the Standard Model $b \to c$ and $b \to u$ transitions for the favored and suppressed decays, respectively, as shown in figure 1. The expected relative amplitude of DCKM to favored decays can then be estimated to be $r_k = \bar{r}_k = \mid V_{ub}^* V_{cd} \mid\mid V_{cb}^* V_{ud} \mid \approx 0.02$, using the CKM matrix elements values from [26]. In this case we also have $\theta_k = -2\beta - \gamma - \delta_k$ and $\bar{\theta}_k = 2\beta + \gamma - \delta_k$, where 2β is the mixing (q/p) phase, γ the weak decay phase and δ_k the strong decay phase, which depends on the given final state. Semileptonic decays are free of DCKM-suppressed contributions.

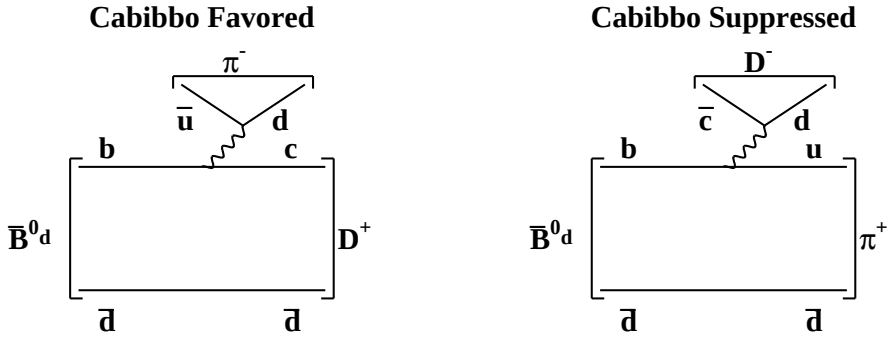

Figure 1: The CKM-allowed ($\sim \lambda^2$) and CKM-suppressed ($\sim \lambda^4$) diagrams for $B \to D^{(*\pm)}\pi^{\mp}/\rho^{\mp}/a_1^{\mp}$ decays. λ is the usual Wolfenstein paramater.

When $\mid f_k\rangle$ is a CP eigenstate ($k = CP$),

$$\lambda_{CP} = \frac{q}{p}\frac{\bar{A}_{CP}}{A_{CP}} = \mid q/p \mid r_{CP,CP} e^{i\theta_{CP}} \tag{58}$$

where

$$r_{CP,k} = \mid \bar{A}_{\bar{k}} \mid / \mid A_k \mid \tag{59}$$

parameterizes CP violation in decay ($k = 1,2,CP$). When there is one single process contributing, $r_{CP,k} = 1$. If the mechanisms contributing to the decay of CP eigenstates (f_{CP}) have the same weak phase for $\eta_{f_{CP}} = -1$ and $\eta_{f_{CP}} = +1$ modes,

$$\begin{aligned} \mathrm{Im}\lambda_{f_{CP}} &= -\eta_{f_{CP}}\mathrm{Im}\lambda_{CP} \\ \mathrm{Re}\lambda_{f_{CP}} &= \eta_{f_{CP}}\mathrm{Re}\lambda_{CP} \ . \end{aligned} \tag{60}$$

In order to evaluate (51) and (52) having λ_k and $\bar{\lambda}_k$ well defined, we must distinguish the 4 different final state configurations ($|\ f_1 f_2\rangle$, $|\ f_1^- f_2\rangle$, $|\ f_1 f_2^-\rangle$, $|\ f_1^- f_2^-\rangle$). For each case we then must evaluate $u_\pm$ and m, and finally

$$|\ u_\pm\ |^2 \ , \quad |\ m\ |^2 \ , \quad u_\pm^* m \ , \quad u_+ u_-^* \ . \tag{61}$$

These factors are renormalized so that $|\ A_1 A_2\ |^2 = 1$ (A_2 may be A_{CP}).

2.2.1 Case $|\ f_1 f_2\rangle$

$$\begin{aligned} u_\pm &= A_1 A_2 \frac{p}{q}(\lambda_1 \pm \lambda_2) \\ m &= -A_1 A_2 \frac{p}{q}(\lambda_1\lambda_2 - 1) \end{aligned} \tag{62}$$

$$\begin{aligned} |\ u_\pm\ |^2 &= |\ p/q\ |^2 \left\{ |\ \lambda_1\ |^2 + |\ \lambda_2\ |^2 \pm 2\,|\ \lambda_1\ ||\ \lambda_2\ |\,\mathrm{Re}\left(\lambda_1'\lambda_2'^*\right)\right\} \\ |\ m\ |^2 &= |\ p/q\ |^2 \left\{1 + |\ \lambda_1\ |^2 |\ \lambda_2\ |^2 - 2\,|\ \lambda_1\ ||\ \lambda_2\ |\,\mathrm{Re}\left(\lambda_1'\lambda_2'\right)\right\} \\ u_\pm^* m &= -|\ p/q\ |^2 \left\{ |\ \lambda_1\ |^2 |\ \lambda_2\ |\,\lambda_2' - |\ \lambda_1\ |\,\lambda_1'^* \pm |\ \lambda_2\ |^2 |\ \lambda_1\ |\,\lambda_1' \mp |\ \lambda_2\ |\,\lambda_2'^*\right\} \\ u_+ u_-^* &= |\ p/q\ |^2 \left\{ |\ \lambda_1\ |^2 - |\ \lambda_2\ |^2 + 2i\,|\ \lambda_1\ ||\ \lambda_2\ |\,\mathrm{Im}\left(\lambda_2'\lambda_1'^*\right)\right\} \end{aligned} \tag{63}$$

where

$$\lambda_k' = \frac{\lambda_k}{|\ \lambda_k\ |} \equiv e^{i\theta_k} \quad , \quad \bar{\lambda}_k' = \frac{\bar{\lambda}_k}{|\ \bar{\lambda}_k\ |} \equiv e^{i\bar{\theta}_k} \tag{64}$$

and

$$|\ \lambda_k\ | = |\ q/p\ |\, r_k \quad , \quad |\ \bar{\lambda}_k\ | = |\ p/q\ |\, \bar{r}_k \tag{65}$$

for flavor eigenstates ($k = 1,2$), and

$$|\ \lambda_{CP}\ | \ = \ |\ q/p\ |\, r_{CP,CP} \tag{66}$$

for CP eigenstates. Note that the sign convention in the definition of q/p can be changed just flipping the sign of λ_k and $\bar{\lambda}_k$.

2.2.2 Case $|\,\bar{f_1}f_2\rangle$

$$\begin{aligned} u_{\pm} &= \bar{A_1}A_2\left(1\pm\bar{\lambda}_1\lambda_2\right) \\ m &= -\bar{A_1}A_2\left(\lambda_2-\bar{\lambda}_1\right) \end{aligned} \tag{67}$$

$$\begin{aligned} |\,u_{\pm}\,|^2 &= r_{CP,1}^2\left\{1+|\,\bar{\lambda}_1\,|^2|\,\lambda_2\,|^2\pm 2\,|\,\bar{\lambda}_1\,||\,\lambda_2\,|\,\mathrm{Re}\left(\bar{\lambda}_1'\lambda_2'\right)\right\} \\ |\,m\,|^2 &= r_{CP,1}^2\left\{|\,\lambda_2\,|^2+|\,\bar{\lambda}_1\,|^2-2\,|\,\lambda_2\,||\,\bar{\lambda}_1\,|\,\mathrm{Re}\left(\lambda_2'\bar{\lambda}_1'^*\right)\right\} \\ u_{\pm}^*m &= -r_{CP,1}^2\left\{|\,\lambda_2\,|\,\lambda_2'-|\,\bar{\lambda}_1\,|\,\bar{\lambda}_1'\pm|\,\lambda_2\,|^2|\,\bar{\lambda}_1\,|\,\bar{\lambda}_1'^*\mp|\,\bar{\lambda}_1\,|^2|\,\lambda_2\,|\,\lambda_2'^*\right\} \\ u_+u_-^* &= r_{CP,1}^2\left\{1-|\,\bar{\lambda}_1\,|^2|\,\lambda_2\,|^2+2i\,|\,\bar{\lambda}_1\,||\,\lambda_2\,|\,\mathrm{Im}\left(\bar{\lambda}_1'\lambda_2'\right)\right\} \end{aligned} \tag{68}$$

2.2.3 Case $|\,f_1\bar{f_2}\rangle$

$$\begin{aligned} u_{\pm} &= A_1\bar{A_2}\left(\lambda_1\bar{\lambda}_2\pm 1\right) \\ m &= -A_1\bar{A_2}\left(\lambda_1-\bar{\lambda}_2\right) \end{aligned} \tag{69}$$

$$\begin{aligned} |\,u_{\pm}\,|^2 &= r_{CP,2}^2\left\{1+|\,\lambda_1\,|^2|\,\bar{\lambda}_2\,|^2\pm 2\,|\,\lambda_1\,||\,\bar{\lambda}_2\,|\,\mathrm{Re}\left(\lambda_1'\bar{\lambda}_2'\right)\right\} \\ |\,m\,|^2 &= r_{CP,2}^2\left\{|\,\lambda_1\,|^2+|\,\bar{\lambda}_2\,|^2-2\,|\,\lambda_1\,||\,\bar{\lambda}_2\,|\,\mathrm{Re}\left(\lambda_1'\bar{\lambda}_2'^*\right)\right\} \\ u_{\pm}^*m &= -r_{CP,2}^2\left\{|\,\lambda_1\,|^2|\,\bar{\lambda}_2\,|\,\bar{\lambda}_2'^*-|\,\bar{\lambda}_2\,||\,\lambda_1\,|\,\lambda_1'^*\pm|\,\lambda_1\,|\,\lambda_1'\mp|\,\bar{\lambda}_2\,|\,\bar{\lambda}_2'^*\right\} \\ u_+u_-^* &= r_{CP,2}^2\left\{|\,\lambda_1\,|^2|\,\bar{\lambda}_2\,|^2-1+2i\,|\,\lambda_1\,||\,\bar{\lambda}_2\,|\,\mathrm{Im}\left(\lambda_1'^*\bar{\lambda}_2'^*\right)\right\} \end{aligned} \tag{70}$$

2.2.4 Case $|\,\bar{f_1}\bar{f_2}\rangle$

$$\begin{aligned} u_{\pm} &= \bar{A_1}\bar{A_2}\frac{q}{p}\left(\bar{\lambda}_2\pm\bar{\lambda}_1\right) \\ m &= -\bar{A_1}\bar{A_2}\frac{q}{p}\left(1-\bar{\lambda}_1\bar{\lambda}_2\right) \end{aligned} \tag{71}$$

$$\begin{aligned} |\,u_{\pm}\,|^2 &= r_{CP,1}^2r_{CP,2}^2\,|\,q/p\,|^2\left\{|\,\bar{\lambda}_2\,|^2+|\,\bar{\lambda}_1\,|^2\pm 2\,|\,\bar{\lambda}_1\,||\,\bar{\lambda}_2\,|\,\mathrm{Re}\left(\bar{\lambda}_1'\bar{\lambda}_2'^*\right)\right\} \\ |\,m\,|^2 &= r_{CP,1}^2r_{CP,2}^2\,|\,q/p\,|^2\left\{1+|\,\bar{\lambda}_1\,|^2|\,\bar{\lambda}_2\,|^2-2\,|\,\bar{\lambda}_1\,||\,\bar{\lambda}_2\,|\,\mathrm{Re}\left(\bar{\lambda}_1'\bar{\lambda}_2'\right)\right\} \\ u_{\pm}^*m &= -r_{CP,1}^2r_{CP,2}^2\,|\,q/p\,|^2\left\{|\,\bar{\lambda}_2\,|^2\,\bar{\lambda}_2'^*-|\,\bar{\lambda}_2\,|^2|\,\bar{\lambda}_1\,|\,\lambda_1'\pm|\,\bar{\lambda}_1\,|\,\lambda_1'^*\mp|\,\bar{\lambda}_1\,|^2|\,\bar{\lambda}_2\,|\,\bar{\lambda}_2'^*\right\} \\ u_+u_-^* &= r_{CP,1}^2r_{CP,2}^2\,|\,q/p\,|^2\left\{|\,\bar{\lambda}_2\,|^2-|\,\bar{\lambda}_1\,|^2+2i\,|\,\bar{\lambda}_2\,||\,\bar{\lambda}_1\,|\,\mathrm{Im}\left(\bar{\lambda}_1'\bar{\lambda}_2'^*\right)\right\} \end{aligned} \tag{72}$$

2.2.5 Simplified expressions

In order to help our understanding of the main features of the time dependence, it is useful to evaluate the previous equations for several special cases. In some cases the coefficients $c_\pm$, Re(s) and Im(s) will be also given to first order in the CPT parameter z:

$$\begin{aligned} c_\pm &= |\,u_-\,|^2 \pm \left[|\,m\,|^2 + 2\mathrm{Re}(z^* u_+^* m)\right] \\ s &= z u_+ u_-^* + u_-^* m\,. \end{aligned} \tag{73}$$

Perfect tagging states

In the case when the flavor final states (reconstructed side in flavor events and tagging B) are perfect tagging states (λ_k and $\bar{\lambda}_k$, $k = 1,2$, are zero), the coefficients simplify to those given in tables 1 and 2, for flavor and CP eigenstates respectively. The same coefficients to first order in the CPT parameter z are given in tables 3 and 4.

In the following we identify $|\,f_1\rangle$ as the state used for B tagging ($k = 1 \equiv tag$), and $|\,f_2\rangle$ the reconstructed final state, flavor ($k = 2 \equiv flav$) or CP ($k = CP$).

Coefficient	$\|\,f_1 f_2\rangle$	$\|\,f_1 \bar{f}_2\rangle$	$\|\,\bar{f}_1 f_2\rangle$	$\|\,\bar{f}_1 \bar{f}_2\rangle$
$c_\pm$	$\pm\,\|\,q/p\,\|^{-2}\|\,1-z^2\,\|$	$r_{CP,1}^2\left(1\pm\|\,z\,\|^2\right)$	$r_{CP,2}^2\left(1\pm\|\,z\,\|^2\right)$	$\pm r_{CP,1}^2 r_{CP,2}^2\,\|\,q/p\,\|^2\|\,1-z^2\,\|$
s	0	$r_{CP,1}^2 z$	$-r_{CP,2}^2 z$	0

Table 1: Coefficients of the time-dependent decay rate for flavor eigenstates (perfect tagging states).

Coefficient	$\|\,f_1 f_{CP}\rangle$
$c_\pm$	$\|\,q/p\,\|^{-2}\left\{\|\,\lambda_{CP}\,\|^2 \pm \|\,z\,\|^2\|\,\lambda_{CP}\,\|^2 \pm \|\,1-z^2\,\| \pm 2\,\|\,\lambda_{CP}\,\|\,\mathrm{Re}\left(z^*\sqrt{1-z^2}\lambda_{CP}'^*\right)\right\}$
s	$-\,\|\,q/p\,\|^{-2}\left\{\|\,\lambda_{CP}\,\|^2 z + \|\,\lambda_{CP}\,\|\,\sqrt{1-z^2}\lambda_{CP}'^*\right\}$
	$\|\,\bar{f}_1 f_{CP}\rangle$
$c_\pm$	$r_{CP,1}^2\left\{1\pm\|\,z\,\|^2 \pm \|\,1-z^2\,\|\,\|\,\lambda_{CP}\,\|^2 \mp 2\,\|\,\lambda_{CP}\,\|\,\mathrm{Re}\left(z^*\sqrt{1-z^2}\lambda_{CP}'\right)\right\}$
s	$r_{CP,1}^2\left(z - \|\,\lambda_{CP}\,\|\,\sqrt{1-z^2}\lambda_{CP}'\right)$

Table 2: Coefficients of the time-dependent decay rate for CP eigenstates (perfect tagging states).

Coefficient	$\|\,f_1 f_2\rangle$	$\|\,f_1 \bar{f}_2\rangle$	$\|\,\bar{f}_1 f_2\rangle$	$\|\,\bar{f}_1 \bar{f}_2\rangle$
$c_\pm$	$\pm\,\|\,q/p\,\|^{-2}$	$r_{CP,1}^2$	$r_{CP,2}^2$	$\pm r_{CP,1}^2 r_{CP,2}^2\,\|\,q/p\,\|^2$
s	0	$r_{CP,1}^2 z$	$-r_{CP,2}^2 z$	0

Table 3: Coefficients of the time-dependent decay rate for flavor eigenstates (perfect tagging states), to first order in the CPT parameter z.

After a close inspection of tables 1, 2, 3 and 4, we observe that the coefficients $c_\pm$ and s remain unchanged under a simultaneous sign change of $\Delta\Gamma$, Rez and Reλ_{CP}'. This discrete ambiguity is resolved if we take Re$\lambda_{CP}' = +\sqrt{1-(\mathrm{Im}\lambda_{CP}')^2}$ and then consider as physical parameters $\Delta\Gamma \times sign(\mathrm{Re}\lambda_{CP}')$ and RezReλ_{CP}' instead of $\Delta\Gamma$ and Rez, respectively. We take the product RezReλ_{CP}' rather than Re$z \times sign(\mathrm{Re}\lambda_{CP}')$ because the CPT

Coefficient	$\mid f_1 f_{CP}\rangle$
$c_\pm$	$\mid q/p \mid^{-2} \left\{\mid \lambda_{CP} \mid^2 \pm 1 \pm 2 \mid \lambda_{CP} \mid [\mathrm{RezRe}\lambda'_{CP} - \mathrm{ImzIm}\lambda'_{CP}]\right\}$
s	$-\mid q/p \mid^{-2} \left\{\mid \lambda_{CP} \mid^2 z + \mid \lambda_{CP} \mid \lambda'^*_{CP}\right\}$
	$\mid f_1 f_{CP}\rangle$
$c_\pm$	$r^2_{CP,1}\left\{1 \pm \mid \lambda_{CP} \mid^2 \mp 2 \mid \lambda_{CP} \mid [\mathrm{RezRe}\lambda'_{CP} + \mathrm{ImzIm}\lambda'_{CP}]\right\}$
s	$r^2_{CP,1}(z - \mid \lambda_{CP} \mid \lambda'_{CP})$

Table 4: Coefficients of the time-dependent decay rate for CP eigenstates (perfect tagging states), to first order in the CPT parameter z.

asymmetries turn out to be proportional to $\mathrm{RezRe}\lambda'_{CP}$ [12, 15]. Therefore, the choice of independent physics parameters that model CPT/CP, CP/T and mixing is:

$$\boxed{\mathrm{Rez}\frac{\mathrm{Re}\lambda_{CP}}{|\lambda_{CP}|}\ ,\ \mathrm{Imz}\ ,\ \frac{\mathrm{Im}\lambda_{CP}}{|\lambda_{CP}|}\ ,\ |\,q/p\,|\ ,\ \Delta\Gamma/\Gamma \times sign(\mathrm{Re}\lambda_{CP})\ ,\ \Delta m\ ,\ \tau\,.}$$

The previous tables also provide very useful information about where the sensitivity to the different parameters comes from:

- the $\Delta\Gamma$ dependence for flavor eigenstates appears to be at second order in $\Delta\Gamma$ (from the cosh term) while it is to first order for CP eigenstates (sinh term). This implies that the precision on $\Delta\Gamma/\Gamma$ from CP events scales as $1/\sqrt{N}$ (N is here the number of events), constant as a function of $\Delta\Gamma/\Gamma$, while for flavor eigenstates the statistical error scales as $1/N^{1/4}$ for small values of $\Delta\Gamma/\Gamma$, while for large values it goes as $1/\sqrt{N}1/\Delta\Gamma$ [17]. Clearly, for small values of $\Delta\Gamma$ and in the presence of CP violation, even though the CP eigenstate sample is about 10 times smaller than the flavor eigenstate sample, it largely dominates the determination of $\Delta\Gamma$. Another consequence of the different $\Delta\Gamma$ dependence for flavor and CP states is the fact that the PDF for flavor events is symmetric with respect to $\Delta\Gamma$=0, so only CP events allow to extract information about the $\Delta\Gamma$ sign, up to the discrete ambiguity from $\mathrm{Re}\lambda_{CP}$;
- the dependence with Rez (even in Δt) is suppressed by terms linear in $\Delta\Gamma$ for flavor eigenstates. This implies, again, that for small values of $\Delta\Gamma$ and in the presence of CP violation, the CP eigenstate sample largely dominates the determination of Rez;
- the dependence with $\mathrm{Im}\lambda_{CP}$ (CP eigenstates) appears to be odd in Δt, and therefore can be resolved from the even dependence with Rez;
- the determination of $|\,q/p\,|$, Imz and Δm is dominated by the high statistics flavor sample due to the absence of suppression factors.

Overall, the combined use of flavor and CP samples provides maximal sensitivity to all the physics parameters, with small correlations, since they are determined either from different samples, either from different Δt dependencies. All these features were checked numerically using toy Monte Carlo [12].

Flavor eigenstates with $\lambda_2, \bar{\lambda}_2 \neq 0$, $\lambda_1 = \bar{\lambda}_1 = 0$, $z = 0$, $\Delta\Gamma = 0$ and $|\,q/p\,| = 1$

When $\lambda_1 = \bar{\lambda}_1 = 0$, $z = 0$, $\Delta\Gamma = 0$ and $|\,q/p\,| = 1$, we have, for flavor eigenstates

	$\mid f_1 f_2\rangle$	$\mid \bar{f}_1 f_2\rangle$	$\mid f_1 \bar{f}_2\rangle$	$\mid \bar{f}_1 \bar{f}_2\rangle$
$c_\pm$	$\mid \lambda_2 \mid^2 \pm 1$	$r^2_{CP,1}\left(1 \pm \mid \lambda_2 \mid^2\right)$	$r^2_{CP,2}\left(1 \pm \mid \lambda_2 \mid^2\right)$	$r^2_{CP,1} r^2_{CP,2}\left(\mid \lambda_2 \mid^2 \pm 1\right)$
$\mathrm{Im}(s)$	$\mid \lambda_2 \mid \mathrm{Im}\lambda'_2$	$-r^2_{CP,1} \mid \lambda_2 \mid \mathrm{Im}\lambda'_2$	$-r^2_{CP,2} \mid \bar{\lambda}_2 \mid \mathrm{Im}\lambda'_2$	$r^2_{CP,1} r^2_{CP,2} \mid \bar{\lambda}_2 \mid \mathrm{Im}\lambda'_2$

and for CP eigenstates

	$\mid f_1 f_{CP}\rangle$	$\mid f_1^- f_{CP}\rangle$
$c_\pm$	$\mid \lambda_{CP} \mid^2 \pm 1$	$r_{CP,1}^2 \left(1 \pm \mid \lambda_{CP} \mid^2\right)$
$\mathrm{Im}(s)$	$\mid \lambda_{CP} \mid \mathrm{Im}\lambda'_{CP}$	$-r_{CP,1}^2 \mid \lambda_{CP} \mid \mathrm{Im}\lambda'_{CP}$

where $\mathrm{Im}\lambda'_2 = -\sin(2\beta+\gamma+\delta)$, $\mathrm{Im}\bar{\lambda}'_2 = \sin(2\beta+\gamma-\delta)$ and $\mathrm{Im}\lambda'_{CP} = -\sin(2\beta+\delta)$, δ being the strong phase. For $B^0 \to J/\psi K^0$ decays, $\mathrm{Im}\lambda'_{CP} = -\eta_{CP}\sin(2\beta)$. We recover here the usual expressions used in the $\sin(2\beta)$, $\sin(2\alpha)$ and $\sin(2\beta+\gamma)$ analyses.

Flavor eigenstates with $\lambda_1, \bar{\lambda}_1 \neq 0$ and $\lambda_2 = \bar{\lambda}_2 = 0$

This corresponds to the case when the fully reconstructed B mesons are perfect tagging states (i.e. from semileptonic decays) but the tagging B's are not:

- Case $\mid f_1 f_2\rangle$

$$\begin{aligned} \mid u_\pm \mid^2 &= \mid p/q \mid^2 \mid \lambda_1 \mid^2 \\ \mid m \mid^2 &= \mid p/q \mid^2 \\ u_\pm^* m &= \mid p/q \mid^2 \mid \lambda_1 \mid \lambda_1'^* \\ u_+ u_-^* &= \mid p/q \mid^2 \mid \lambda_1 \mid^2 \end{aligned}$$

To first order in z,

$$\begin{aligned} c_\pm &= \mid p/q \mid^2 \left\{ \mid \lambda_1 \mid^2 \pm 1 \pm 2\mathrm{Re}z \mid \lambda_1 \mid \mathrm{Re}\lambda'_1 \mp 2\mathrm{Im}z \mid \lambda_1 \mid \mathrm{Im}\lambda'_1 \right\} \\ \mathrm{Re}(s) &= \mid p/q \mid^2 \left\{ \mid \lambda_1 \mid^2 \mathrm{Re}z + \mid \lambda_1 \mid \mathrm{Re}\lambda'_1 \right\} \\ \mathrm{Im}(s) &= \mid p/q \mid^2 \left\{ \mid \lambda_1 \mid^2 \mathrm{Im}z - \mid \lambda_1 \mid \mathrm{Im}\lambda'_1 \right\} \end{aligned}$$

- Case $\mid f_1^- f_2\rangle$

$$\begin{aligned} \mid u_\pm \mid^2 &= r_{CP,1}^2 \\ \mid m \mid^2 &= r_{CP,1}^2 \mid \bar{\lambda}_1 \mid^2 \\ u_\pm^* m &= r_{CP,1}^2 \mid \bar{\lambda}_1 \mid \bar{\lambda}'_1 \\ u_+ u_-^* &= r_{CP,1}^2 \end{aligned}$$

To first order in z,

$$\begin{aligned} c_\pm &= r_{CP,1}^2 \left\{ 1 \pm \mid \bar{\lambda}_1 \mid^2 \pm 2\mathrm{Re}z \mid \bar{\lambda}_1 \mid \mathrm{Re}\bar{\lambda}'_1 \pm 2\mathrm{Im}z \mid \bar{\lambda}_1 \mid \mathrm{Im}\bar{\lambda}'_1 \right\} \\ \mathrm{Re}(s) &= r_{CP,1}^2 \left\{ \mathrm{Re}z + \mid \bar{\lambda}_1 \mid \mathrm{Re}\bar{\lambda}'_1 \right\} \\ \mathrm{Im}(s) &= r_{CP,1}^2 \left\{ \mathrm{Im}z + \mid \bar{\lambda}_1 \mid \mathrm{Im}\bar{\lambda}'_1 \right\} \end{aligned}$$

- Case $|\, f_1 \bar{f}_2\rangle$

$$\begin{aligned} |\, u_\pm \,|^2 &= r^2_{CP,2} \\ |\, m \,|^2 &= r^2_{CP,2}\,|\,\lambda_1\,|^2 \\ u^*_\pm m &= \mp r^2_{CP,2}\,|\,\lambda_1\,|\,\lambda'_1 \\ u_+ u^*_- &= -r^2_{CP,2} \end{aligned}$$

To first order in z,

$$\begin{aligned} c_\pm &= r^2_{CP,2}\left\{1\pm |\,\lambda_1\,|^2 \mp 2\mathrm{Re}z\,|\,\lambda_1\,|\,\mathrm{Re}\lambda'_1 \mp 2\mathrm{Im}z\,|\,\lambda_1\,|\,\mathrm{Re}\lambda'_1\right\} \\ \mathrm{Re}(s) &= r^2_{CP,2}\left\{-\mathrm{Re}z+\,|\,\lambda_1\,|\,\mathrm{Re}\lambda'_1\right\} \\ \mathrm{Im}(s) &= r^2_{CP,2}\left\{-\mathrm{Im}z+\,|\,\lambda_1\,|\,\mathrm{Im}\lambda'_1\right\} \end{aligned}$$

- Case $|\, f_1 f_2\rangle$

$$\begin{aligned} |\, u_\pm \,|^2 &= r^2_{CP,1} r^2_{CP,2}\,|\,q/p\,|^2 |\,\bar{\lambda}_1\,|^2 \\ |\, m \,|^2 &= r^2_{CP,1} r^2_{CP,2}\,|\,q/p\,|^2 \\ u^*_\pm m &= \mp r^2_{CP,1} r^2_{CP,2}\,|\,q/p\,|^2 |\,\bar{\lambda}_1\,|\,\bar{\lambda}'^*_1 \\ u_+ u^*_- &= -r^2_{CP,1} r^2_{CP,2}\,|\,q/p\,|^2 |\,\bar{\lambda}_1\,|^2 \end{aligned}$$

To first order in z,

$$\begin{aligned} c_\pm &= r^2_{CP,1} r^2_{CP,2}\,|\,q/p\,|^2 \left\{|\,\bar{\lambda}_1\,|^2 \pm 1 \mp 2\mathrm{Re}z\,|\,\bar{\lambda}_1\,|\,\mathrm{Re}\bar{\lambda}'_1 \pm 2\mathrm{Im}z\,|\,\bar{\lambda}_1\,|\,\mathrm{Im}\bar{\lambda}'_1\right\} \\ \mathrm{Re}(s) &= -r^2_{CP,1} r^2_{CP,2}\,|\,q/p\,|^2 \left\{|\,\bar{\lambda}_1\,|^2\,\mathrm{Re}z-\,|\,\bar{\lambda}_1\,|\,\mathrm{Re}(\bar{\lambda}'_1)\right\} \\ \mathrm{Im}(s) &= -r^2_{CP,1} r^2_{CP,2}\,|\,q/p\,|^2 \left\{|\,\bar{\lambda}_1\,|^2\,\mathrm{Im}z+\,|\,\bar{\lambda}_1\,|\,\mathrm{Im}\lambda'_1\right\} \end{aligned}$$

From these expressions we observe that DCKM decays in the tagging side induce a sign ambiguity similar to that described previously, but now involving $\mathrm{Re}\lambda'_1$ ($\mathrm{Re}\bar{\lambda}'_1$) instead of $\mathrm{Re}\lambda'_{CP}$, for $B^0(\bar{B}^0)$ tags. It can also be seen that the parameter Rez always appears either multiplied by or added to a term proportional to $\mathrm{Re}\lambda'_1$ ($\mathrm{Re}\bar{\lambda}'_1$). Similarly, Imz is always accompanied by a term proportional to $\mathrm{Im}\lambda'_1$ ($\mathrm{Im}\bar{\lambda}'_1$). This implies that Rez(Imz) will be mainly affected by (correlated with) the DCKM real(imaginary) parts. The dominant dependence with λ'_1 and $\bar{\lambda}'_1$ is in all cases linear in $|\,\lambda_1\,|$ and $|\,\bar{\lambda}_1\,|$. A similar analysis for $\lambda_1, \bar{\lambda}_1 \neq 0$, $\lambda_2 = \bar{\lambda}_2 = 0$ reveals the same features for the reconstructed B (flavor sample). In this case, however, given that the flavor eigenstate sample is analyzed in combination with the CP sample, it is expected the DCKM effects to be smaller, as will be discussed later.

CP eigenstates ($\lambda_2 = \lambda_{CP}$) with $\lambda_1, \bar{\lambda}_1 \neq 0$

This corresponds to the most general case for fully reconstructed CP eigenstates:

- Case $|\, f_1 f_{CP}\rangle$

$$\begin{aligned}
|\,u_\pm\,|^2 &= |\,p/q\,|^2\left\{|\,\lambda_1\,|^2+|\,\lambda_{CP}\,|^2\pm 2\,|\,\lambda_1\,||\,\lambda_{CP}\,|\,\mathrm{Re}\left(\lambda'_1\lambda'^*_{CP}\right)\right\}\\
|\,m\,|^2 &= |\,p/q\,|^2\left\{1+|\,\lambda_1\,|^2|\,\lambda_{CP}\,|^2-2\,|\,\lambda_1\,||\,\lambda_{CP}\,|\,\mathrm{Re}\left(\lambda'_1\lambda'_{CP}\right)\right\}\\
u^*_\pm m &= -|\,p/q\,|^2\left\{|\,\lambda_1\,|^2|\,\lambda_{CP}\,|\,\lambda'_{CP}-|\,\lambda_1\,|\,\lambda'^*_1\pm|\,\lambda_{CP}\,|^2|\,\lambda_1\,|\,\lambda'_1\mp|\,\lambda_{CP}\,|\,\lambda'^*_{CP}\right\}\\
u_+u^*_- &= |\,p/q\,|^2\left\{|\,\lambda_1\,|^2-|\,\lambda_{CP}\,|^2+2i\,|\,\lambda_1\,||\,\lambda_{CP}\,|\,\mathrm{Im}\left(\lambda'_{CP}\lambda'^*_1\right)\right\}
\end{aligned}\tag{74}$$

- Case $|\, f_1^- f_{CP}\rangle$

$$\begin{aligned}
|\,u_\pm\,|^2 &= r^2_{CP,1}\left\{1+|\,\bar\lambda_1\,|^2|\,\lambda_{CP}\,|^2\pm 2\,|\,\bar\lambda_1\,||\,\lambda_{CP}\,|\,\mathrm{Re}\left(\bar\lambda'_1\lambda'_{CP}\right)\right\}\\
|\,m\,|^2 &= r^2_{CP,1}\left\{|\,\lambda_{CP}\,|^2+|\,\bar\lambda_1\,|^2-2\,|\,\lambda_{CP}\,||\,\bar\lambda_1\,|\,\mathrm{Re}\left(\lambda'_{CP}\bar\lambda'^*_1\right)\right\}\\
u^*_\pm m &= -r^2_{CP,1}\left\{|\,\lambda_{CP}\,|\,\lambda'_{CP}-|\,\bar\lambda_1\,|\,\bar\lambda'_1\pm|\,\lambda_{CP}\,|^2|\,\bar\lambda_1\,|\,\bar\lambda'^*_1\mp|\,\bar\lambda_1\,|^2|\,\lambda_{CP}\,|\,\lambda'^*_{CP}\right\}\\
u_+u^*_- &= r^2_{CP,1}\left\{1-|\,\bar\lambda_1\,|^2|\,\lambda_{CP}\,|^2+2i\,|\,\bar\lambda_1\,||\,\lambda_{CP}\,|\,\mathrm{Im}\left(\bar\lambda'_1\lambda'_{CP}\right)\right\}
\end{aligned}\tag{75}$$

Substituting equations (74) and (75) into (73), it can easily be seen that the coefficients $c_\pm$ and s remain unchanged under the simultaneous sign change of $\Delta\Gamma$, Rez, $\mathrm{Re}\lambda'_{CP}$, $\mathrm{Re}\lambda'_1$ and $\mathrm{Re}\bar\lambda'_1$. The ambiguity can be resolved if we take $\mathrm{Re}\lambda'_{CP}=+\sqrt{1-(\mathrm{Im}\lambda'_{CP})^2}$ and the consider as physical parameters $\Delta\Gamma sign(\mathrm{Re}\lambda'_{CP})$ and $\mathrm{Rez}\mathrm{Re}\lambda'_{CP}$ instead of $\Delta\Gamma$ and Rez, respectively. This solves mathametically the complete ambiguity. In practice, due to the poor resolution on $\mathrm{Re}\lambda'_1$ and $\mathrm{Re}\bar\lambda'_1$ we may need to fix these parameters. The dependence with λ'_1 and $\bar\lambda'_1$ is, for all terms, linear in $|\,\lambda_1\,|$ and $|\,\bar\lambda_1\,|$. Finally, let us note that the dependence of $\mathrm{Im}\lambda'_{CP}$ with $\mathrm{Im}\lambda'_1$ is to first order in Δm, while with $\mathrm{Re}\lambda'_1$ is to second order in Δm as well as in $\Delta\Gamma$.

Flavor eigenstates with $\lambda_2,\bar\lambda_2\neq 0$ and $\lambda_1,\bar\lambda_1\neq 0$

This corresponds to the most general case for fully reconstructed flavor eigenstates. For our purposes here, it is enough to analyze the case $|\, f_1 f_2\rangle$, given by equation (63):

$$\begin{aligned}
|\,u_\pm\,|^2 &= |\,p/q\,|^2\left\{|\,\lambda_1\,|^2+|\,\lambda_2\,|^2\pm 2\,|\,\lambda_1\,||\,\lambda_2\,|\,\mathrm{Re}\left(\lambda'_1\lambda'^*_2\right)\right\}\\
|\,m\,|^2 &= |\,p/q\,|^2\left\{1+|\,\lambda_1\,|^2|\,\lambda_2\,|^2-2\,|\,\lambda_1\,||\,\lambda_2\,|\,\mathrm{Re}\left(\lambda'_1\lambda'_2\right)\right\}\\
u^*_\pm m &= -|\,p/q\,|^2\left\{|\,\lambda_1\,|^2|\,\lambda_2\,|\,\lambda'_2-|\,\lambda_1\,|\,\lambda'^*_1\pm|\,\lambda_2\,|^2|\,\lambda_1\,|\,\lambda'_1\mp|\,\lambda_2\,|\,\lambda'^*_2\right\}\\
u_+u^*_- &= |\,p/q\,|^2\left\{|\,\lambda_1\,|^2-|\,\lambda_2\,|^2+2i\,|\,\lambda_1\,||\,\lambda_2\,|\,\mathrm{Im}\left(\lambda'_2\lambda'^*_1\right)\right\}
\end{aligned}$$

We observe again the sign ambiguity, now involving $\mathrm{Re}\lambda'_2$ ($\mathrm{Re}\bar\lambda'_2$) instead of $\mathrm{Re}\lambda'_{CP}$, for $B^0(\bar B^0)$. Mathematically the ambiguity is already resolved once we have solved it for CP eigenstates (assuming a combined analysis of the flavor and CP eigenstates). In practice, as before, due to the poor resolution on $\mathrm{Re}\lambda'_{1/2}$ and $\mathrm{Re}\bar\lambda'_{1/2}$ we may need to fix these parameters. Let us note that in this case the dependence with $\lambda'_{1/2}$ and $\bar\lambda'_{1/2}$ is linear in $|\,\lambda_{1/2}\,|$ and $|\,\bar\lambda_{1/2}\,|$ only for the $u^*_\pm m$ term, while it is quadratic for the rest.

2.3 Note about sign conventions

As described in sections 2.2 and 2.1, the sign convention adopted in this document to define q/p makes use of the lighter eigenstate. This convention is the same as in the BaBar Physics Book [11] and in the PDG2002

[26], but opposite to that used in the current version of reference [10]. The $\Delta\Gamma$ sign convention, equation (28), is the same as in the BaBar Physics Book [11] and reference [10], but opposite to that of PDG2002 [26]. All the analysis results presented in this document are consistent with the q/p convention in the text, but for $\Delta\Gamma$ is the opposite. The consistency of sign conventions between the text and the analysis results can be obtained just flipping the sign of the $\Delta\Gamma/\Gamma$ results.

2.4 $\{\mid q/p \mid, \lambda, z\}$ vs $\{\varepsilon, \delta\}$ formalisms

Alternative formalisms can be used to describe flavor and CP mixing [14, 10]. One of these alternative choices is a phase-convention independent formalism similar to that used in kaon system phenomenology [15] ($\{\varepsilon, \delta\}$). To first order in the CPT parameter Δ -the same as defined in equation 13-, the parameters ε and δ parameterize CP/T and CP/CPT violation, and are defined as [15, 12]:

$$\varepsilon = \frac{\mathrm{Im}(\Gamma_{12}CP^*_{12}) + 2i\mathrm{Im}(M_{12}CP^*_{12})}{2\mathrm{Re}(M_{12}CP^*_{12}) - i\mathrm{Re}(\Gamma_{12}CP^*_{12}) + 2F'} \tag{76}$$

$$\delta = \frac{2\Delta}{2\mathrm{Re}(M_{12}CP^*_{12}) - i\mathrm{Re}(\Gamma_{12}CP^*_{12}) + 2F'} \tag{77}$$

where $CP_{12} = \langle B^0 \mid CP \mid \bar{B}^0 \rangle = e^{-i\alpha}$ is the unphysical relative phase between $\mid B^0 \rangle$ and $\mid \bar{B}^0 \rangle$. The main difference with respect to the standard $\{\mid q/p \mid, \lambda, z\}$ formalism is that it relies on the base of CP eigenstates, rather than flavor eigenstates. This is then used to make the formalism phase-convention independent without the need of introducing a specific decay process to unambiguosly define the unphysical relative phase between B^0 and $\bar{B}^0$. This requires, however, of a CP-conserving decay into a definite CP final state. If the decay does not fall into a CP-conserving direction (i.e there is CP violation in the decay and/or not perfect tagging states), corrections are needed in order to define the CP tag appropiately [15]. These corrections are in practice not easy to introduce, limiting the application of the formalism.

After some algebra one can obtain, to first order in CPT and assuming CP conserving decays and perfect tagging states, the relations connecting the two formalisms [12]:

$$\frac{\delta}{1-\varepsilon^2} = z \tag{78}$$

and

$$\frac{q}{p}e^{i\alpha} = \frac{1-\varepsilon}{1+\varepsilon}\,. \tag{79}$$

From (78) and (79) and taking first order in $\mathrm{Re}\varepsilon$ we found the following relations:

$$\frac{2\mathrm{Re}\varepsilon}{1+\mid \varepsilon \mid^2} \equiv \frac{1-\mid q/p \mid^2}{1+\mid q/p \mid^2} \tag{80}$$

$$\frac{\mathrm{Im}\varepsilon}{1+\mid \varepsilon \mid^2} \equiv -\frac{1}{2}\frac{\mathrm{Im}\lambda_{CP}}{\mid \lambda_{CP} \mid} \tag{81}$$

$$\frac{1-|\,\varepsilon\,|^2}{1+|\,\varepsilon\,|^2} \equiv \frac{\mathrm{Re}\lambda_{CP}}{|\,\lambda_{CP}\,|} \tag{82}$$

$$\frac{\mathrm{Re}\delta}{1+|\,\varepsilon\,|^2}\frac{1-|\,\varepsilon\,|^2}{1+|\,\varepsilon\,|^2} \equiv \mathrm{Re}z\frac{\mathrm{Re}\lambda_{CP}}{|\,\lambda_{CP}\,|} \tag{83}$$

$$\frac{\mathrm{Im}\delta}{1+|\,\varepsilon\,|^2} \equiv \mathrm{Im}z\,. \tag{84}$$

2.5 Mistag fractions, $B^0\bar{B}^0$ differences in tagging and reconstruction efficiencies and direct CP violation in tagging and flavor eigenstates

The time-dependent decay rates given in equation (53) have to be corrected by the fraction w^α of events with wrongly assigned flavor in tagging category α, the *mistag fraction*. On the other hand, differences in reconstruction and tagging efficiencies for B^0 and $\bar{B}^0$ can induce biases in the decay time distributions due to the presence of even terms in Δt (odd terms do not contribute). Let us define first the quantities used to parameterize all these effects (we use the same definitions as in [9]).

$w^\alpha_{B^0}$ is defined as the fraction of true B^0 but are incorrectly tagged as $\bar{B}^0$ for tagging category α, and similarly for $w^\alpha_{\bar{B}^0}$. As the mistag fraction can be different for B^0 and $\bar{B}^0$ due to differences in the material interactions (especially for kaons), it is convenient to define

$$w^\alpha = \frac{w^\alpha_{B^0} + w^\alpha_{\bar{B}^0}}{2} \tag{85}$$

and

$$\Delta w^\alpha = w^\alpha_{B^0} - w^\alpha_{\bar{B}^0} \tag{86}$$

which give, respectively, the mean value and the difference of the mistag fractions for B^0 and $\bar{B}^0$. With these definitions,

$$w^\alpha_{B^0} = w^\alpha + \Delta w^\alpha/2 \tag{87}$$

and

$$w^\alpha_{\bar{B}^0} = w^\alpha - \Delta w^\alpha/2\ . \tag{88}$$

Let us define now

$$\mu^\alpha = \frac{t_1^\alpha - t_1^{\bar{\alpha}}}{t_1^\alpha + t_1^{\bar{\alpha}}} \tag{89}$$

and

$$\nu \;=\; \frac{t_2 - t_{\bar{2}}}{t_2 + t_{\bar{2}}} \tag{90}$$

where $t^{\alpha}_{1/\bar{1}}$ is the tagging efficiency for $B^0/\bar{B}^0$ and tagging category α. Similarly $t_{2/\bar{2}}$ is the reconstruction efficiency for $B^0/\bar{B}^0$. If we call T^{α} and R the average tagging and reconstruction efficiencies ($T^{\alpha} = \frac{t^{\alpha}_1 + t^{\alpha}_{\bar{1}}}{2}$ and $R = \frac{t_2 + t_{\bar{2}}}{2}$), we have

$$t^{\alpha}_1 = T^{\alpha}(1+\mu^{\alpha}) \quad , \quad t^{\alpha}_{\bar{1}} = T^{\alpha}(1-\mu^{\alpha}) \tag{91}$$

and

$$t_2 = R(1+\nu) \quad , \quad t_{\bar{2}} = R(1-\nu) \;\; . \tag{92}$$

The corrected expressions read, for flavor eigenstates (B_{flav}):

$$h^{\alpha}_{k_1 k_2}(\Delta t) \;=\; t_{k_2}\left\{ t^{\alpha}_{k_1}(1-w^{\alpha}_{k_1}) h_{k_1 k_2}(\Delta t) + t^{\alpha}_{\bar{k}_1} w^{\alpha}_{k_1} h_{\bar{k}_1 k_2}(\Delta t) \right\} \tag{93}$$

and for CP eigenstates (B_{CP}):

$$h^{\alpha}_{k_1 k_2}(\Delta t) \;=\; t^{\alpha}_{k_1}(1-w^{\alpha}_{k_1}) h_{k_1 k_2}(\Delta t) + t^{\alpha}_{\bar{k}_1} w^{\alpha}_{k_1} h_{\bar{k}_1 k_2}(\Delta t) \tag{94}$$

where $k_1 = 1, \bar{1}$ and $k_2 = 2, \bar{2}, CP$. The difference among equations (93) and (94) is because $\eta_{f_{CP}} = -1$ (B_{CP-}) and $\eta_{f_{CP}} = +1$ (B_{CP+}) states are normalized separately, while B^0_{flav} and $\overline{B}^0_{flav}$ are normalized together.

For untagged events ($\alpha = UnTagged$), expressions (93) and (94) still hold, with the following relations being satisfied:

$$w_1^{UnTagged} = w_{\bar{1}}^{UnTagged} \;=\; \frac{1}{2} \tag{95}$$

$$t_1^{UnTagged} \;=\; 1 - \sum_{\alpha_{Tagged}} t_1^{\alpha_{Tagged}} \tag{96}$$

$$t_{\bar{1}}^{UnTagged} \;=\; 1 - \sum_{\alpha_{Tagged}} t_{\bar{1}}^{\alpha_{Tagged}} \;\; . \tag{97}$$

where α_{Tagged} is the tagging category index for tagged events only. From (91), (96) and (97) it can easily be verified that

$$T^{UnTagged} \;=\; 1 - \sum_{\alpha_{Tagged}} T^{\alpha_{Tagged}} \tag{98}$$

and

$$\mu^{UnTagged} \;=\; -\frac{\sum_{\alpha_{Tagged}} T^{\alpha_{Tagged}} \mu^{\alpha_{Tagged}}}{T^{UnTagged}} \;\; . \tag{99}$$

CP violation in the decay of B tagging states and flavor eigenstates was explicitely included in equation (53) and terms (63), (68), (70) and (72). Alternatively, it can be included in equations (93) and (94) with the replacement $t_1^{\alpha} \to t_1^{\alpha} r_{CP,1}^2$ and $t_2^- \to t_2^- r_{CP,2}^2$ (t_1^{α} and t_2 remain unchanged). Equations (89) and (90) should then be rewritten as

$$\mu^{\alpha} = \frac{t_1^{\alpha} - t_1^{\alpha} r_{CP,1}^2}{t_1^{\alpha} + t_1^{\alpha} r_{CP,1}^2} \tag{100}$$

and

$$\nu = \frac{t_2 - t_2^- r_{CP,2}^2}{t_2 + t_2^- r_{CP,2}^2} \, . \tag{101}$$

From these expressions we see that the net effect of any possible CP violation in the decay of B tagging states and/or flavor eigenstates cannot be distinguished from a charge asymmetry of the detector response.

2.6 Δt resolution function

The introduction of the resolution effects requires the convolution of equations (93) and (94) with the resolution function $\mathcal{R}(\Delta t - \Delta t', \sigma_{\Delta t}; \vec{q}_{\alpha})$:

$$h_{k_1 k_2}^{\alpha,resol}(\Delta t, \sigma_{\Delta t}) = \int_{-\infty}^{+\infty} \mathcal{R}(\Delta t - \Delta t', \sigma_{\Delta t}; \vec{q}_{\alpha}) h_{k_1 k_2}^{\alpha}(\Delta t') d\Delta t' \, . \tag{102}$$

The problem can be reduced to the convolution of a set of basis functions,

$$\frac{1}{2\tau} \exp\left(\mp \tau_{eff} \Delta t'\right) \exp\left(i \Delta m \Delta t'\right) \tag{103}$$

with (123), where

$$\tau_{eff} = \frac{2\tau}{2 \mp \tau \Delta\Gamma} = \frac{\tau}{1 \mp \Delta\Gamma/2\Gamma} \tag{104}$$

and $\tau = 1/\Gamma$. The $-(+)$ sign applies for $\Delta t' > 0$ ($\Delta t' < 0$). The normalization of (102) over a given (finite or infinite) domain $(\Delta t_1, \Delta t_2)$ can then be calculated from the integral

$$H_{k_1 k_2}^{\alpha,resol}(\sigma_{\Delta t}) = \int_{\Delta t_1}^{\Delta t_2} h_{k_1 k_2}^{\alpha,resol}(\Delta t, \sigma_{\Delta t}) d\Delta t \, . \tag{105}$$

All the integrals (102) and their normalizations (105) can be calculated analytically, and expressed in terms of complex exponentials and the complementary complex error function [18]. The integration limits Δt_1 and Δt_2 can be the acceptance cuts on Δt (finite normalization) or infinity (asymptotic normalization). Asymptotic normalization is used by default in this analysis. The specific resolution models used in this analysis are discussed in section 4.

2.7 Background treatment

In the presence of backgrounds, the PDF has to be extended to include a term for each significant background source. The backgrounds for B_{flav} and $B_{CPK^0_S} \equiv B_{CP-}$ states are small and mostly combinatoric. They are estimated from the beam-energy substituted mass (m_{ES}) sideband, assuming a single Gaussian distribution for the signal and an Argus parameterization for the background. From unbinned maximum likelihood fits to the m_{ES} spectrum, an event-by-event signal probability, $p^{\alpha}_{sig}(m_{ES})$, for each tagging category α, is calculated. The corrected general PDF can then be written as

$$\begin{aligned} h^{\alpha,obs}_{k_1k_2}(\Delta t,\sigma_{\Delta t}) &= (1-f^{\alpha}_{peak})\,p^{\alpha}_{sig}(m_{ES})\,h^{\alpha,resol,sig}_{k_1k_2}(\Delta t,\sigma_{\Delta t}) + \\ & f^{\alpha}_{peak}\,p^{\alpha}_{sig}(m_{ES})\,h^{\alpha,resol,peak}_{k_1k_2}(\Delta t,\sigma_{\Delta t}) + \\ & \left\{1-p^{\alpha}_{sig}(m_{ES})\right\}\sum_{\beta} f^{\alpha}_{\beta}\,h^{\alpha,resol,\beta}_{k_1k_2}(\Delta t,\sigma_{\Delta t}) \end{aligned} \tag{106}$$

where f^{α}_{β} and f^{α}_{peak} are the combinatorial and peaking background component fractions for the given sample. It is verified that

$$\sum_{\beta} f^{\alpha}_{\beta} = 1 \ . \tag{107}$$

The signal probability is calculated separately for each tagging category.

For each individual signal and background component, $j = sig, peak, \beta$, and tagging category α, the distributions (106) are normalized so that:

$$\sum_{k_1=1,\bar{1}} H^{\alpha,resol,j}_{k_1k_2}(\sigma_{\Delta t})\,d\Delta t = 1 \ , \quad \forall\ j,\alpha \tag{108}$$

for B_{CP} events, and

$$\sum_{k_2=2,\bar{2}}\ \sum_{k_1=1,\bar{1}} H^{\alpha,resol,j}_{k_1k_2}(\sigma_{\Delta t})\,d\Delta t = 1 \ , \quad \forall\ j,\alpha \tag{109}$$

for B_{flav} events.

For the $B^0 \to J/\psi K^0_L$ channel ($B_{CPK^0_L} \equiv B_{CP+}$ sample) the background level is significantly higher with significant non-combinatorial component, therefore requiring an special treatment [20]. The data are used to determine the relative amount of signal, background from $B \to J/\psi X$ events and events from a misreconstructed $J/\psi \to \ell\ell$ candidate. The Monte Carlo simulation is then used to evaluate the channels that contribute to the $B \to J/\psi X$ background. All this information is used to determine the composition of the $B^0 \to J/\psi K^0_L$ sample from a fit to the ΔE spectrum after flavor tagging. Moreover, some of the decay modes in the inclusive J/ψ background have an expected CP structure. The PDF can then be formulated as

$$
\begin{aligned}
h^{\alpha,obs}_{k_1k_2}(\Delta t,\sigma_{\Delta t}) &= f^{\alpha}_{sig}(\Delta E)h^{\alpha,resol,sig}_{k_1k_2}(\Delta t,\sigma_{\Delta t}) + \\
&\sum_{j=J/\psi\ X} f^{\alpha}_{j}(\Delta E)h^{\alpha,resol,j}_{k_1k_2}(\Delta t,\sigma_{\Delta t}) + \\
&f^{\alpha}_{non-J/\psi}(\Delta E)\left[f^{\alpha}_{prompt}h^{\alpha.resol,prompt}_{k_1k_2}(\Delta t,\sigma_{\Delta t}) + f^{\alpha}_{non-prompt}h^{\alpha,resol,non-prompt}_{k_1k_2}(\Delta t,\sigma_{\Delta t})\right]
\end{aligned}
\tag{110}
$$

where

$$
f^{\alpha}_{prompt} + f^{\alpha}_{non-prompt} = 1 \tag{111}
$$

and

$$
f^{\alpha}_{sig}(\Delta E) + \sum_{j=J/\psi\ X} f^{\alpha}_{j}(\Delta E) + f^{\alpha}_{non-J/\psi}(\Delta E) = 1\ . \tag{112}
$$

2.8 The log-likelihood function

The log-likelihood function for tagging category α ($\equiv \alpha_{Tagged}, UnTagged$) is finally defined as

$$
\begin{aligned}
\ln\mathcal{L}_{\alpha} = &\sum_{i}^{N^{\alpha}_{B^0_{tag}B_{CP-}}} \ln h^{\alpha,obs}_{B^0_{tag}B_{CP-}}(\Delta t_i,\sigma_{\Delta t,i}) + \sum_{i}^{N^{\alpha}_{\overline{B}^0_{tag}B_{CP-}}} \ln h^{\alpha,obs}_{\overline{B}^0_{tag}B_{CP-}}(\Delta t_i,\sigma_{\Delta t,i}) + \\
&\sum_{i}^{N^{\alpha}_{B^0_{tag}B_{CP+}}} \ln h^{\alpha,obs}_{B^0_{tag}B_{CP+}}(\Delta t_i,\sigma_{\Delta t,i}) + \sum_{i}^{N^{\alpha}_{\overline{B}^0_{tag}B_{CP+}}} \ln h^{\alpha,obs}_{\overline{B}^0_{tag}B_{CP+}}(\Delta t_i,\sigma_{\Delta t,i}) + \\
&\sum_{i}^{N^{\alpha}_{B^0_{tag}B^0_{flav}}} \ln h^{\alpha,obs}_{B^0_{tag}B^0_{flav}}(\Delta t_i,\sigma_{\Delta t,i}) + \sum_{i}^{N^{\alpha}_{\overline{B}^0_{tag}\overline{B}^0_{flav}}} \ln h^{\alpha,obs}_{\overline{B}^0_{tag}\overline{B}^0_{flav}}(\Delta t_i,\sigma_{\Delta t,i}) + \\
&\sum_{i}^{N^{\alpha}_{B^0_{tag}\overline{B}^0_{flav}}} \ln h^{\alpha,obs}_{B^0_{tag}\overline{B}^0_{flav}}(\Delta t_i,\sigma_{\Delta t,i}) + \sum_{i}^{N^{\alpha}_{\overline{B}^0_{tag}B^0_{flav}}} \ln h^{\alpha,obs}_{\overline{B}^0_{tag}B^0_{flav}}(\Delta t_i,\sigma_{\Delta t,i})
\end{aligned}
\tag{113}
$$

where $N^{\alpha}_{k_1k_2}$ is the total number of k_2 events tagged as k_1 in tagging category α. The global likelihood function for all tagging categories is then calculated as

$$
\ln\mathcal{L} = \sum_{\alpha}\ln\mathcal{L}_{\alpha}\ . \tag{114}
$$

The use of untagged events provides fundamental advantages, discussed in detail in appendix A: i) allows the extraction of the detector charge asymmetries simultaneously with the physics asymmetries, ii) provides additional sensitivity to the determination of $\Delta\Gamma/\Gamma$, and iii) improves the resolution function determination.

An standalone fitting program, called `cptNagFit`, has been developped to find the solution of (148) and the errors on the fitted parameters. The program has been interfaced to the NAG library [31] and the

MINUIT package [32]. All the numerical and minimization routines are based on the NAG library, and the error estimation relies on the HESSE and MINOS methods of MINUIT. This simultaneous interfacing allows direct comparison and cross-checking of the fitting results using two completely different libraries. As described in section 8, the `cptNagFit` fitting program has been cross-checked performing standard $\sin 2\beta$ fits with the widely used `RootFitTools` package [18].

2.9 Parameter counting

From the expressions we derived in this section, especially in subsection 2.2 and 2.5, we can determine the parameters that contribute to the most general time dependence ($c_\pm$, $\mathrm{Re}(s)$ and $\mathrm{Im}(s)$ coefficients and Δt dependence itself), assming a single final state contributes to $|\, f_1\rangle$, $|\, \bar{f_1}\rangle$, $|\, f_2\rangle$ and $|\, \bar{f_2}\rangle$:

- $|\, A_1 A_2\,|^2$ is a global normalization factor, therefore irrelevant for any time-dependent analysis;
- $r_{CP,k}$ can be used to parameterize CP violation in decay (3 parameters):
  - $r_{CP,1}$, for tagging side,
  - $r_{CP,2}$, for reconstructed side, flavor sample,
  - $r_{CP,CP}$, for reconstructed side, CP sample;
- $\Delta\Gamma/\Gamma$, the width difference among B^0 mass eigenstates, and Δm, the oscillation frequency (2 parameters);
- Rez and Imz, the CPT/CP violation parameters (2 parameters);
- $|\, q/p\,|$, the T/CP violation parameter (1 parameter);
- r_k and $\bar{r_k}$ are the ratios of the magnitudes of decay amplitudes of DCKM to favored processes, for B^0 and $\bar{B}^0$ (4 parameters):
  - r_1,$\bar{r_1}$, for tagging side,
  - r_2,$\bar{r_2}$, for reconstructed side, flavor sample;
- θ_k and $\bar{\theta}_k$ are the overall B^0 and $\bar{B}^0$ phases of the ratio of decay amplitudes and the mixing phase (5 parameters):
  - θ_1,$\bar{\theta}_1$, for tagging side,
  - θ_2,$\bar{\theta}_2$, for reconstructed side, flavor sample,
  - θ_{CP}, for reconstructed side, CP sample.
- w and Δw, average mistag fractions and its $B^0\bar{B}^0$ asymmetry (2 parameters)
- ν and μ, the reconstruction and tagging efficiency asymmetry (2 parameters)

When we consider a combined analysis of the flavor and CP eigenstates, we have a total of 8 different final state configurations: 6 for flavor eigenstates, including untagged events ($B^0_{flav}B^0_{tag}$, $\bar{B}^0_{flav}B^0_{tag}$, $B^0_{flav}\bar{B}^0_{tag}$, $\bar{B}^0_{flav}\bar{B}^0_{tag}$, untagged B^0_{flav} and untagged $\bar{B}^0_{flav}$) and 2 for CP eigenstates (B^0_{tag}, $\bar{B}^0_{tag}$). Here we considered all tagged events as belonging to a single class, and the untagged events only for flavor eigenstates as a source of time-integrated information as needed for the simultaneous determination of ν, μ and $|\, q/p\,|$ (see appendix A). For each specific final state configuration the number of independent coefficients in the decay rate is, up to a

sign ambiguity, 2. This can be seen as follows (see [10] for details). From (48) and (49) it can be shown that the coefficients $c_\pm$ and s satisfy the constraint

$$c_+^2 - c_-^2 \;=\; 4\left(\mathrm{Re}(s)^2 + \mathrm{Im}(s)^2\right) \;. \tag{115}$$

Since c_+ is always positive we can re-parameterize the decay rate (53) in terms of the coefficients of the sinh, cos and sin terms relative to the cosh term:

$$\begin{aligned} |\,\langle f_1 f_2 \,|\, \Upsilon(\Delta t)\rangle\,|^2 \;\propto\; & \frac{\tau}{4} e^{-|\Delta t|/\tau}\left\{\cosh\left(\frac{\Delta\Gamma\Delta t}{2}\right) + C_{12}\cos(\Delta m\Delta t) + \right. \\ & \left. \sigma_{12}\sqrt{1-C_{12}^2-S_{12}^2}\sinh\left(\frac{\Delta\Gamma\Delta t}{2}\right) + S_{12}\sin(\Delta m\Delta t)\right\} \end{aligned} \tag{116}$$

where

$$C_{12} \;=\; \frac{|\,a_+\,|^2 - |\,a_-\,|^2}{|\,a_+\,|^2 + |\,a_-\,|^2} \tag{117}$$

$$S_{12} \;=\; 2\frac{\mathrm{Im}(a_+^* a_-)}{|\,a_+\,|^2 + |\,a_-\,|^2} \;. \tag{118}$$

The parameter σ_{12} can only take the values ± 1 since equation (115) fixes only the magnitude of the sinh coefficient, but not its sign. This gives the 2 independent coefficients per configurations, resulting in a total of 16 independent observations. The basic problem now is that the total number of parameters above is 21, so we require additional assumptions:

- $r_{CP,1}$, $r_{CP,2}$ and $r_{CP,CP}$ can be assumed to be 1 ($r_{CP,1}$ and $r_{CP,2}$ are in fact reabsorbed in the μ and ν parameters, respectively);
- r_1 and r_2 can be assumed to be equal to $\bar{r_1}$ and $\bar{r_2}$, respectively, and assume to be known (≈ 0.02 according to the CKM matrix elements [26]).

With these (reasonable) assumptions we reduce to 14 parameters, which gives, in principle, enough observations to extract all the other parameters. In practice, as discussed in section 2.10 and appendix B, sign ambiguities and small sensitivity to some of these parameters require additional assumptions.

2.10 Discussion about Doubly-CKM-Suppressed effects

The numerical sensitivity of the CPT/T/CPT/oscillation parameters to DCKM effects in the tagging and reconstructed (flavor sample) sides was investigated using toy Monte Carlo[4], as described in detail in appendix B.1. The studies confirmed the main features described in section 2.2.5. First, Rez is mainly correlated with the DCKM real parts, while Imz is correlated with DCKM imaginary parts. Second, the sensitivity to the DCKM real parts is poor ($\frac{\mathrm{Re}\lambda_{tag}}{|\lambda_{tag}|}$ and $\frac{\mathrm{Re}\bar{\lambda}_{tag}}{|\lambda_{tag}|}$) or none ($\frac{\mathrm{Re}\lambda_{flav}}{|\lambda_{flav}|}$ and $\frac{\mathrm{Re}\bar{\lambda}_{flav}}{|\lambda_{flav}|}$). The poor sensitivities together with the discrete ambiguities involved will require to fix (e.g. to zero) these parameters. Third, DCKM effects on Δm and $\Delta\Gamma$

[4] All the feasibility, reach and validation studies when DCKM effects are neglected were described in detail in [12].

are small since most of the impact is absorbed by the coefficients of the time dependence. Four, the tagging side gives the largest contribution (assuming a single channel contributing to the sample, see discussion below). This is expected in a combined analysis of flavor and CP eigenstates since the tagging side effects are common to all samples, while the CP sample would contribute to reduce dependencies from the reconstructed side of the flavor sample. In the extreme case of parameters dominated by the CP sample (e.g. Rez, Imλ'_{CP}) we expect the effects from the reconstructed side of the flavor sample to be very small or negligible, as seen in the toy Monte Carlo studies. From these studies we concluded that the optimal trade-off between statistical precision and systematic uncertainties induced by DCKM decays requires the introduction of new fit parameters (to be added to the 6 CPT/T/CP/oscillation parameters), the sines of the DCKM phases, 2 for the tagging side (common to all samples) and 2 for the reconstructed side (flavor sample). Using toy Monte Carlo, it was verified (for different DCKM phase configurations) that this fitting configuration provides unbiassed estimates for all the parameters, and the Gaussian errors reported by the fit give a good estimation of the statistical reach, within 10%.

Supposse now that we identify f_2 accurately, but we have a probability w_1 of misidentifying f_1 as $f_{\bar{1}}$, and a probability $\bar{w_1}$ of misidentifying $f_{\bar{1}}$ as f_1. From equation (41), the time-dependent decay rate can be written as

$$\begin{aligned} |\langle f_1 f_2 \mid \Upsilon(t_1,\Delta t)\rangle|^2 &= \frac{1}{2}e^{-2t_1/\tau}\frac{|\, p_+q_- + p_-q_+\,|^2}{|\, N_+N_-\,|^2}\Big\{|\langle f_2 \mid B^0(\Delta t)\rangle|^2\left[(1-w_1)\,|\,\bar{A_1}\,|^2 + \bar{w_1}\,|\,\bar{A_{\bar{1}}}\,|^2\right] + \\ &\quad |\langle f_2 \mid \bar{B}^0(\Delta t)\rangle|^2\left[(1-w_1)\,|\,A_1\,|^2 + \bar{w_1}\,|\,A_{\bar{1}}\,|^2\right] - \\ &\quad 2\mathrm{Re}\left[\langle f_2 \mid B^0(\Delta t)\rangle\langle f_2 \mid \bar{B}^0(\Delta t)\rangle^*\left((1-w_1)\bar{A_1}A_1^* + \bar{w_1}\bar{A_{\bar{1}}}A_{\bar{1}}^*\right)\right]\Big\} \quad . \end{aligned} \tag{119}$$

with the following relations being satisfied:

$$\begin{aligned} |\,\bar{A_1}\,|^2 &= r_1^2\,|\,A_1\,|^2 \\ |\,\bar{A_{\bar{1}}}\,|^2 &= r_{CP,1}^2\,|\,A_1\,|^2 \\ |\,A_{\bar{1}}\,|^2 &= \bar{r}_1^2 r_{CP,1}^2\,|\,A_1\,|^2 \\ \bar{A_1}A_1^* &= r_1 e^{i\phi_1}\,|\,A_1\,|^2 \\ \bar{A_{\bar{1}}}A_{\bar{1}}^* &= \bar{r}_1 r_{CP,1}^2 e^{-i\bar{\phi}_1}\,|\,A_1\,|^2 \quad . \end{aligned} \tag{120}$$

$\phi_1(\bar{\phi}_1)$ is the relative phase of $\bar{A_1}(A_{\bar{1}})$ with respect to $A_1(\bar{A_{\bar{1}}})$. From equations (119) and (120) it can easily be seen that a change in r_1 and $\bar{r}_1$ can be completely absorbed in a redefinition of w_1, $\bar{w_1}$, Re$(e^{i\phi_1})$, Im$(e^{i\phi_1})$, Re$(e^{-i\bar{\phi}_1})$ and Im$(e^{-i\bar{\phi}_1})$. The dependence with r_1 and $\bar{r}_1$ is quadratic for the former and linear for the latter. Of course, if the real and imaginary parts are either fixed or constrained to be within the physical region this is anymore true since the complete absortion of the effect requires the simultaneous change of all the above quantities. If for example (our case) Re$(e^{i\phi_1})$ and Re$(e^{-i\bar{\phi}_1})$ are fixed to zero, the systematics from their variation from -1 to $+1$ will scale linearly with the largest possible value assumed for r_1 and $\bar{r}_1$, while the uncertainty from r_1 and $\bar{r}_1$ in the sine terms will be absorbed in a redefinition of the fitted value of Im$(e^{i\phi_1})$ and Im$(e^{-i\bar{\phi}_1})$. This feature was verified using toy Monte Carlo, as described in appendix B.2.

So far we assumed that the final states f_1 and f_2 receive contributions from a single channel. In practice, the B sample used for B tagging and the flavor eigenstate sample are an admixture of different channels. When we consider semi-inclusive measurements that do not distinguish between different final states, the decay rate distribution has to be expressed as

$$|\langle f_1 f_2 \mid \Upsilon(\Delta t)\rangle|^2 \propto \sum_j \omega_j\,|\langle f_{1,j} f_{2,j} \mid \Upsilon(\Delta t)\rangle|^2 \tag{121}$$

where the set of final states has been denoted by $\{f_1 f_2\}_j$. ω_j are the weights for each final state, and include relative normalization factors and experimental efficiencies. The decay rate distribution can be written in the form of equation (53) with the following substitutions:

$$
\begin{aligned}
\mid u_{\pm} \mid^2 &\rightarrow \sum_j \omega_j \mid u_{\pm,} \mid^2 \\
\mid m \mid^2 &\rightarrow \sum_j \omega_j \mid m_j \mid^2 \\
u_{\pm}^* m &\rightarrow \sum_j \omega_j u_{\pm,j}^* m_j \\
u_+ u_-^* &\rightarrow \sum_j \omega_j u_{+,j} u_{-,j}^*
\end{aligned}
$$

It is therefore expected that multiple channels would result in an effective single channel which overall effect would be a weigthed average of each individual channel. As a consequence, the effects from more than one channel should always be smaller than the worse possible single channel. This was confirmed by a toy Monte Carlo study, described in appendix B.3. This proves that the DCKM systematics extracted under the single channel assumptio will be conservative.

3 Decay modes, data and Monte Carlo samples

The decay modes considered for the analysis are:

$B_{CPK_S^0}$ **sample:** $B^0 \rightarrow J/\psi K_S^0(\pi^+\pi^-$ and $\pi^0\pi^0)$, $B^0 \rightarrow \psi(2S) K_S^0(\pi^+\pi^-)$, $\chi_{c1}\, K_S^0(\pi^+\pi^-)$; $J/\psi \rightarrow e^+e^-, \mu^+\mu^-$; $\psi(2S) \rightarrow e^+e^-, \mu^+\mu^-, J/\psi\pi^+\pi^-$; $\chi_{c1} \rightarrow J/\psi\gamma$;

$B_{CPK_L^0}$ **sample:** $B^0 \rightarrow J/\psi K_L^0$;

B_{flav} **sample:** $B^0 \rightarrow \mathrm{D}^{(*)}\pi(\rho, \mathrm{a}_1)$ and $B^0 \rightarrow J/\psi K^{*0}$. Charmed mesons are reconstructed in the following modes: $\mathrm{D}^{*-} \rightarrow \overline{\mathrm{D}}^0\pi^-$ with $\overline{\mathrm{D}}^0 \rightarrow \mathrm{K}^+\pi^-, \mathrm{K}^+\pi^-\pi^0, \mathrm{K}^+\pi^+\pi^-\pi^-, \mathrm{K}_S^0\pi^+\pi^-$; $\mathrm{D}^- \rightarrow \mathrm{K}^+\pi^-\pi^-, \mathrm{K}_S^0\pi^-$; $\rho^- \rightarrow \pi^-\pi^0$, $a_1 \rightarrow \pi^+\pi^-\pi^+$, $K^{*0} \rightarrow K^+\pi^-$.

Control sample: $B^+ \rightarrow \overline{\mathrm{D}}^{(*)0}\pi^+$, $B^+ \rightarrow J/\psi K^+$, $B^+ \rightarrow \psi(2S)K^+$, $B^+ \rightarrow \chi_{c1}\, K^+$ and $B^+ \rightarrow J/\psi K^{*+}(K_S^0\pi^+)$. Charmonium and $\overline{\mathrm{D}}^0$ mesons are reconstructed in the same channels as the neutral modes. $\overline{\mathrm{D}}^{*0}$ mesons are reconstructed in the $\overline{\mathrm{D}}^{*0} \rightarrow \overline{\mathrm{D}}^0\pi^0$ mode.

Each of these samples is separated by tagging category, with a total of 4 tagging categories: the default tagger used here is the Moriond Tagger [22] (`Lepton, Kaon+KPi, Kaon+SlowPi, Other`), while the Elba Tagger [21] (`Lepton, Kaon, NT1, NT2`) will be used as cross-check. `UnTagged` events are also used in this analysis as an additional tagging category.

The selection cuts for all the modes are the same as those used in [9, 20, 23]. The data sample corresponds to an integrated luminosity of approximately 81 fb^{-1}, accumulated during 5 running periods:

- run1: 9933-17106 (L: 20.78 fb^{-1})

- run2a: 18245-20851 (L: 9.07 fb^{-1})
- run2b: 20852-25007 (L: 26.58 fb^{-1})
- run2c: 25281-28831 (L: 22.45 fb^{-1})
- run2d: 28838-29326 (L: 2.27 fb^{-1})

Table 5 summarizes the event yields on the full data sample for all the open charm and charmonium modes. In each case, the $\sigma(m_{ES})$, yield and purity (estimated as the signal fraction for events with $m_{ES} > 5.27$ GeV for modes other than $J/\psi K_L^0$ and $\mid \Delta E \mid < 10$ MeV for $J/\psi K_L^0$) are given separately for each mode, and in the case of charmonium modes it is given for *ee* and $\mu\mu$. Figures 2 to 15 show the unbinned maximum likelihood fit used to extract the yields and purities given in table 5. The fits are performed to the beam-energy substituted mass, $m_{ES} = \sqrt{E^{*2} - p^{*2}}$, using a Gaussian plus Argus background shape. The $J/\psi K_L^0$ channel is handled differently, using the variable $\Delta E = E^*_{J/\psi} + E^*_{K_L^0} - E_{beam}$. See [20] for details. The fit results to the ΔE distributions are shown in figures 9 and 10. Table 6 summarizes the signal event yields per sample and tagging category, after vertexing cuts. These yields have been obtained from the m_{ES} fits in the case of the B_{flav} and $B_{CPK_S^0}$ sample, and multiplying by the signal fraction in the $\mid \Delta E \mid < 10$ MeV interval for the $B_{CPK_L^0}$ sample.

Two different Monte Carlo samples are used: an standard sample, the same as used in [9, 20], and a dedicated one. The values of the physics parameters used in the generation of the two samples are shown in table 7. Each sample contains B_{flav}, $B_{CPK_S^0}$ and $B_{CPK_L^0}$ decay modes. The standard sample itself has two subsamples, one with exclusive charmonium decays and the other with inclusive decays. The dedicated sample has only exclusive charmonium decays. The statistics of reconstructed *B* mesons (before vertexing cuts and tagging) is given in table 8, for each mode and sample separately. It must be noted that the relative statistics among the samples as we have in the data was not kept here.

`ASCII` files input to the fits are taken from:

`/nfs/farm/babar/AWG36/CPTAnalysis/input/summer02/anal-13/`

4 Resolution function and vertexing cuts

The decay time difference Δt between the two decaying *B* mesons is calculated from the *z* positions of the reconstructed vertices, using the *average* τ_B *approximation* [27], which uses the measured $\Upsilon(4S)$ boost (determined on a run-by-run basis) as well as the polar angle of the reconstructed *B*, therefore accounting for the boost of the *B* mesons with respect to the $\Upsilon(4S)$. The standard *BABAR* algorithm, `BtaSelFit`, with default configuration (beam constraints) is used for the Δz reconstruction [27]. Only events satisfying that $\mid \Delta t \mid < 20$ ps and $\sigma_{\Delta t} < 1.4$ ps are accepted, the same as using in the hadronic mixing analysis [23]. The nominal fit (section 6) does not include in the normalization of the PDF the Δt cut. The fit including the limited Δt range will be done as well and used to estimate a systematic uncertainty due to this assumption. Fits in different Δt and $\sigma_{\Delta t}$ ranges will be performed as well as cross-check.

The Δt resolution is modelled using two different parameterizations [29].

The first approach, called thereafter *GG model*, assumes three Gaussians [23]. The *core* component tries to describe well measured vertices, meanwhile the *tail* part accounts for poorly measured decay times. Finally, there is a small fraction of *outliers* (a few per mille) where Δt is badly reconstructed, partly due to mistakes in the track reconstruction, partly to tracks from secondary decays (long living particles and hard scatters). As the reconstructed Δt error provides a good (approximate) representation of the resolution for the core (tail)

Fig.	Mode		$\sigma\, m_{ES}$ (MeV)	m_{ES} Yield (ΔE for $J/\psi K_L^0$)	Purity (%)
2	$D^*\pi$		2.56 ± 0.04	7529 ± 110	92.0 ± 0.5
	$D^*\rho$		2.97 ± 0.06	4769 ± 91	84.1 ± 1.0
	$D^* a_1$		2.57 ± 0.07	3533 ± 92	77.8 ± 1.9
3	$D\pi$		2.50 ± 0.04	8408 ± 136	80.9 ± 1.3
	$D\rho$		2.87 ± 0.07	4786 ± 113	75.9 ± 1.0
	Da_1		2.46 ± 0.08	2689 ± 89	65.6 ± 1.0
4	$J/\psi K^{*0}$	e^+e^-	2.76 ± 0.09	1477 ± 45	95.1 ± 0.9
	$(K^\pm\pi^\mp)$	$\mu^+\mu^-$	2.53 ± 0.09	1217 ± 40	95.9 ± 0.9
	all B_{flav}		2.64 ± 0.02	34390 ± 275	81.9 ± 0.2
5	$J/\psi K_S^0$	e^+e^-	2.68 ± 0.16	683 ± 33	93.2 ± 1.4
	$(\pi^+\pi^-)$	$\mu^+\mu^-$	2.62 ± 0.11	746 ± 30	98.1 ± 0.7
6	$J/\psi K_S^0$	e^+e^-	2.8 ± 0.4	112 ± 16	83 ± 3
	$(\pi^0\pi^0)$	$\mu^+\mu^-$	3.3 ± 0.4	143 ± 16	91 ± 4
7	$\psi(2S)K_S^0$	e^+e^-	3.0 ± 0.5	110 ± 17	85 ± 5
		$\mu^+\mu^-$	2.6 ± 0.3	106 ± 12	94 ± 4
8	$\chi_{c1}K_S^0$	e^+e^-	3.2 ± 0.5	56 ± 9	96 ± 4
		$\mu^+\mu^-$	2.6 ± 0.5	55 ± 9	94 ± 5
	all $B_{CPK_S^0}$		2.74 ± 0.08	2015 ± 55	94.1 ± 0.8
9	$J/\psi K_L^0$(EMC)	e^+e^-	—	200 ± 17	49 ± 3
		$\mu^+\mu^-$	—	233 ± 20	45 ± 3
10	$J/\psi K_L^0$(IFR)	e^+e^-	—	224 ± 20	69 ± 4
		$\mu^+\mu^-$	—	231 ± 20	68 ± 4
11	$D^0\pi$		2.55 ± 0.03	15546 ± 183	82.3 ± 0.4
	$D^{*0}\pi$		2.98 ± 0.05	6177 ± 109	88.6 ± 0.4
	all $B^+ \to$charm		2.66 ± 0.03	21770 ± 214	84.0 ± 0.5
12	$J/\psi K$	e^+e^-	2.75 ± 0.07	2820 ± 68	92.7 ± 0.7
		$\mu^+\mu^-$	2.52 ± 0.06	2844 ± 61	96.7 ± 0.5
13	$\psi(2S)K$	e^+e^-	2.79 ± 0.16	457 ± 26	93.3 ± 1.9
		$\mu^+\mu^-$	2.51 ± 0.15	409 ± 23	96.1 ± 1.6
14	$\chi_{c1}K$	e^+e^-	3.23 ± 0.23	295 ± 20	96.2 ± 1.9
		$\mu^+\mu^-$	2.38 ± 0.18	260 ± 19	93 ± 3
15	$J/\psi K^*$	e^+e^-	2.99 ± 0.18	448 ± 26	93.6 ± 1.8
	$(K_S^0\pi)$	$\mu^+\mu^-$	2.62 ± 0.21	353 ± 24	91 ± 3
	all $B^+ \to$charmonium		2.67 ± 0.04	7882 ± 108	94.4 ± 0.4

Table 5: Event yields, signal resolutions, and signal purities for all the open charm and charmonium decay modes, from 81 fb^{-1} of data (Summer'02 data sample). Results are shown separately for $J/\psi \to e^+e^-$ and $J/\psi \to \mu^+\mu^-$ channels. The errors on these quantities are the statistical errors from the distribution. The m_{ES} results, yields and purities were determined from a fit to a Gaussian plus Argus background in a 3σ ΔE window (the purity was estimated for the region $m_{ES} > 5.27$ GeV/c^2), as shown in figures 2 to 15.

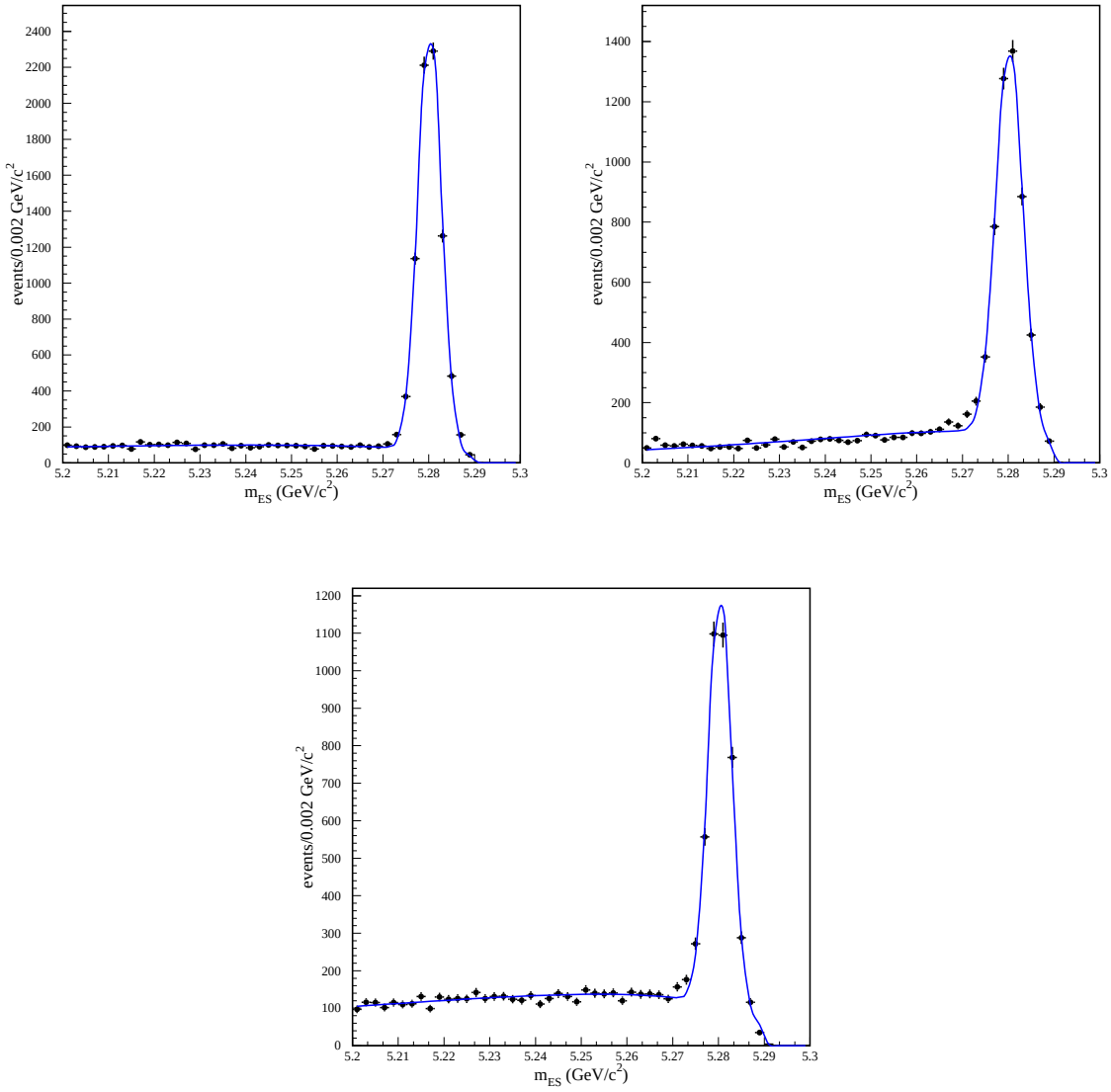

Figure 2: Fits to the m_{ES} distributions in the $B^0 \to \mathrm{D}^*\pi$ (top/left), $B^0 \to \mathrm{D}^*\rho$ (top/right) and $B^0 \to \mathrm{D}^* a_1$ (bottom) channels. Vertexing cuts have not been applied.

Gaussian, it is used to weight the events on a event-by-event basis, rather than to use a global resolution, therefore increasing the sensitivity of the analysis to well measured events. As the error is still not a perfect representation of the resolution (especially for the tail component) we allow for two global scale factors. On the contrary, the event-by-event Δt error is not a good representation of the resolution for the outliers component, and in this case a global and fixed (8 ps) resolution is used instead. In addition to the increase of the sensitivity, the weighting of the events according to the reconstructed Δt error largely eliminates small differences in resolution between the different classes of events entering in the analysis. Very small residual effects due to differences in the scale factors can then be considered as part of the systematic uncertainties. Figure 16 shows the distributions of the per-event error on Δt for the B_{flav} and $B_{CPK^0_S}$ data samples, for signal ($m_{ES} > 5.27$ GeV) and sideband ($5.2 < m_{ES} < 5.27$ GeV) region events. The curves correspond to the unbinned maximum likelihood fit to a Crystall Ball shape.

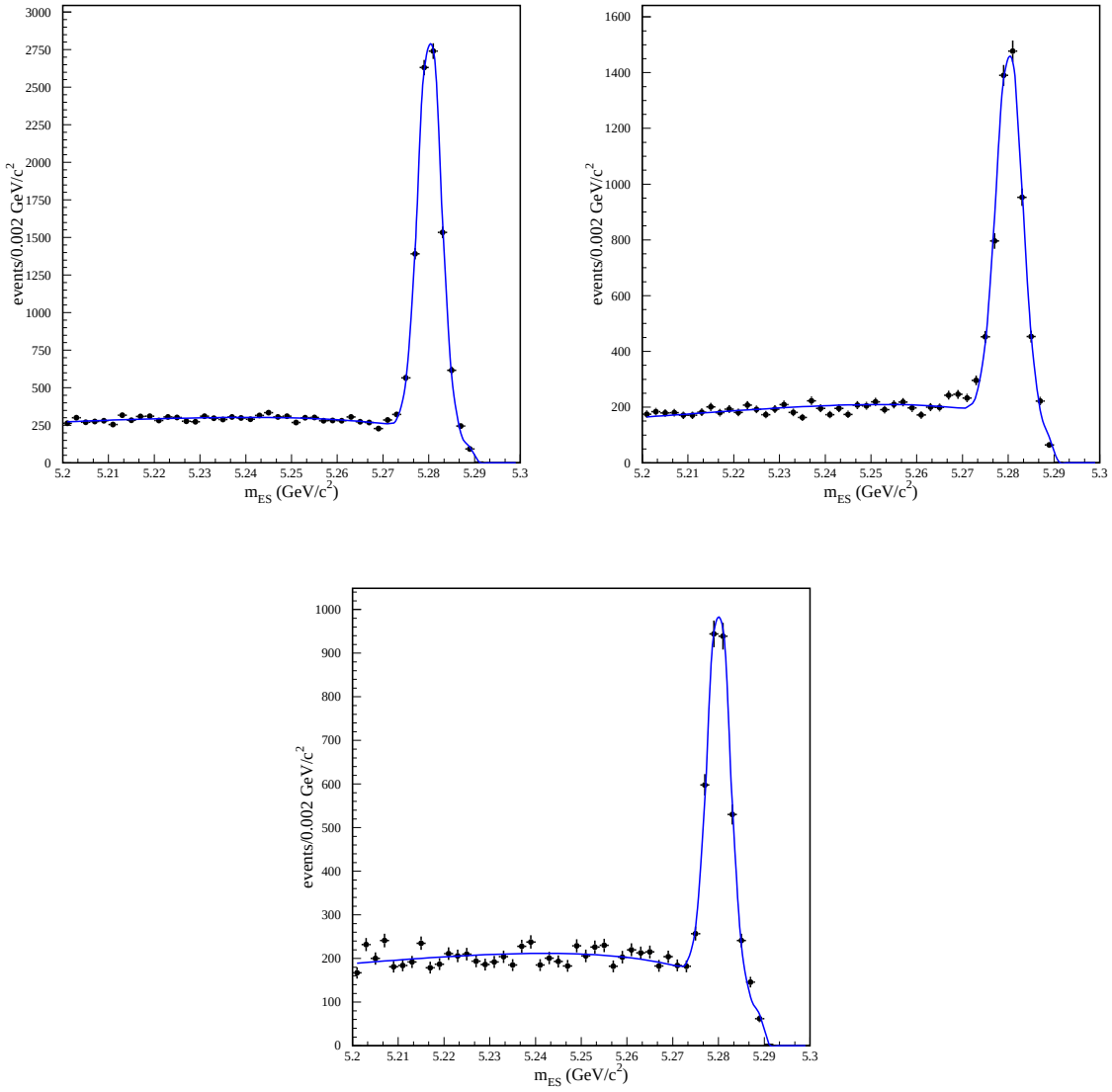

Figure 3: Fits to the m_{ES} distributions in the $B^0 \to D\pi$ (top/left), $B^0 \to D\rho$ (top/right) and $B^0 \to Da_1$ (bottom) channels. Vertexing cuts have not been applied.

Although the vertex reconstruction algorithm minimizes biases due to the secondary charm decays and V^0's in the tagging side, the z_{TAG} position is on average biased towards positive z values, resulting in a negative shift in Δt. This effect is accounted in the resolution function by introducing a shift in the central value of the core and tail Gaussians. Due to the different B decay channels populating the different tagging categories, the average bias is category dependent. It was found that introducing a different bias in each tagging category for the core component but having a common tail bias provides the optimal trade-off between systematic effects and number of different parameters in the resolution [23].

The second parameterization, called *GExp*, uses one Gaussian with variable width and zero bias plus the same Gaussian convoluted with an exponential which effective lifetime is intended to describe the charm bias [29]. Similarly to the *GG* model, the reconstructed Δt error is used to weight the events, and different effective lifetimes and fractions of the exponential part are assumed for each tagging category, in order to take into

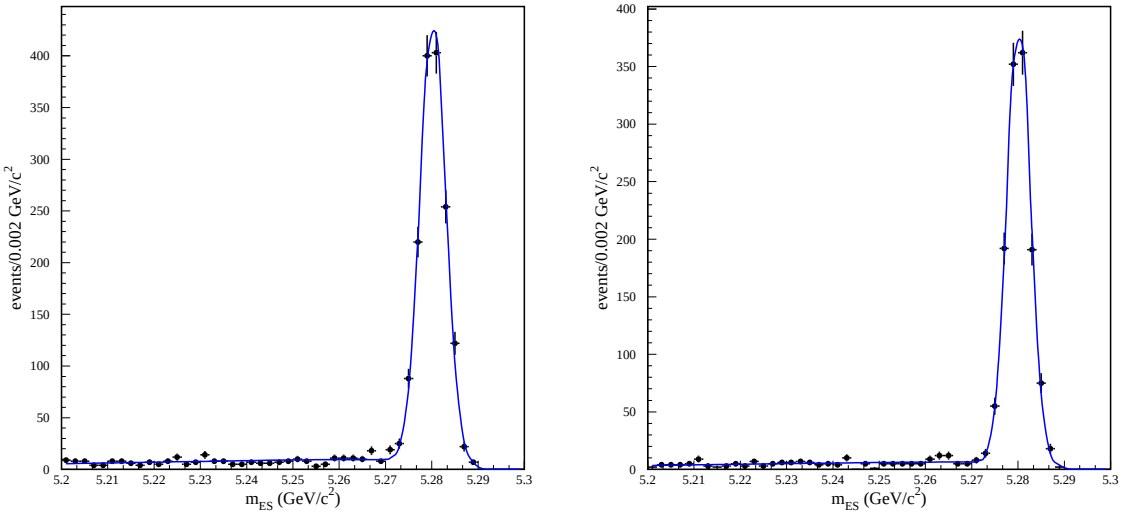

Figure 4: Fits to the m_{ES} distributions in the $B^0 \to J/\psi K^*$ ($K^{\pm}\pi^{\mp}$) channel for the e^+e^- (left) and $\mu^+\mu^-$ (right) modes. Vertexing cuts have not been applied.

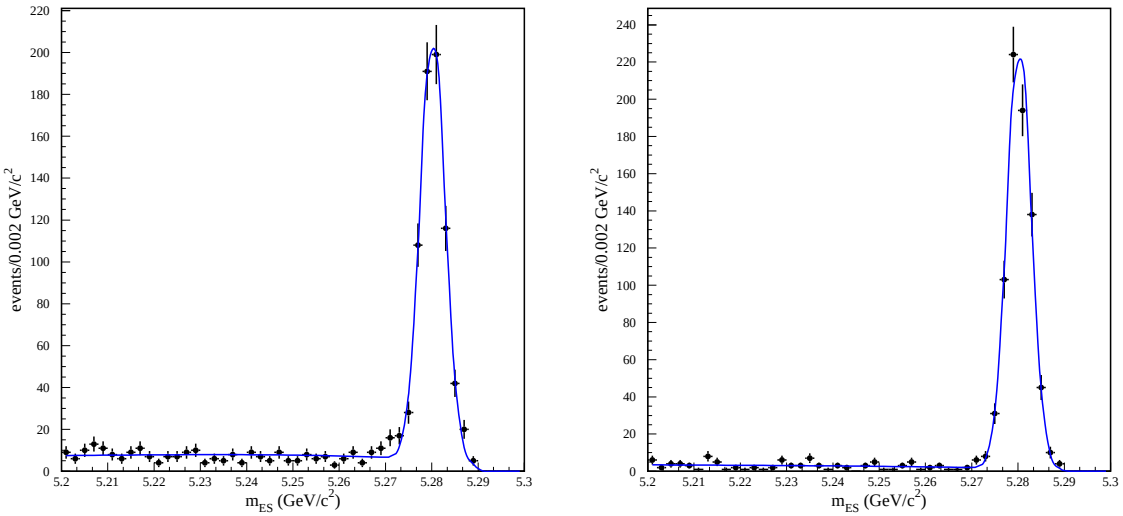

Figure 5: Fits to the m_{ES} distributions in the $B^0 \to J/\psi K^0_S$ ($\pi^+\pi^-$) channel for the e^+e^- (left) and $\mu^+\mu^-$ (right) modes. Vertexing cuts have not been applied.

account the different B decay channels populating each tagging category. The outlier component in this model is assumed the same as in the *GG* parameterization.

In summary, for an event with reconstructed $(\Delta t, \sigma_{\Delta t})$, the *GG* resolution function for tagging category α reads

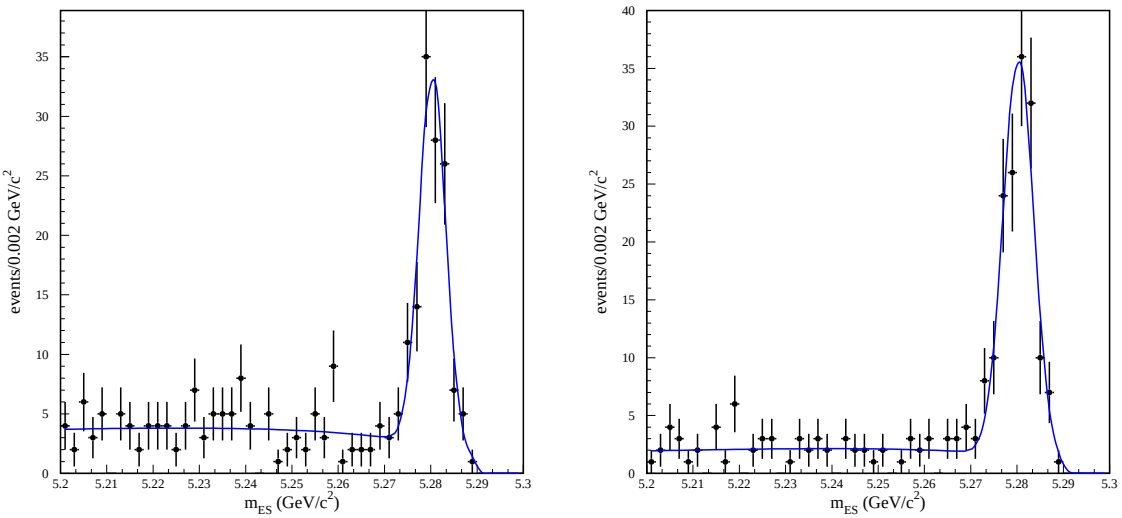

Figure 6: Fits to the m_{ES} distributions in the $B^0 \to J/\psi K^0_S$ ($\pi^0\pi^0$) channel for the e^+e^- (left) and $\mu^+\mu^-$ (right) modes. Vertexing cuts have not been applied.

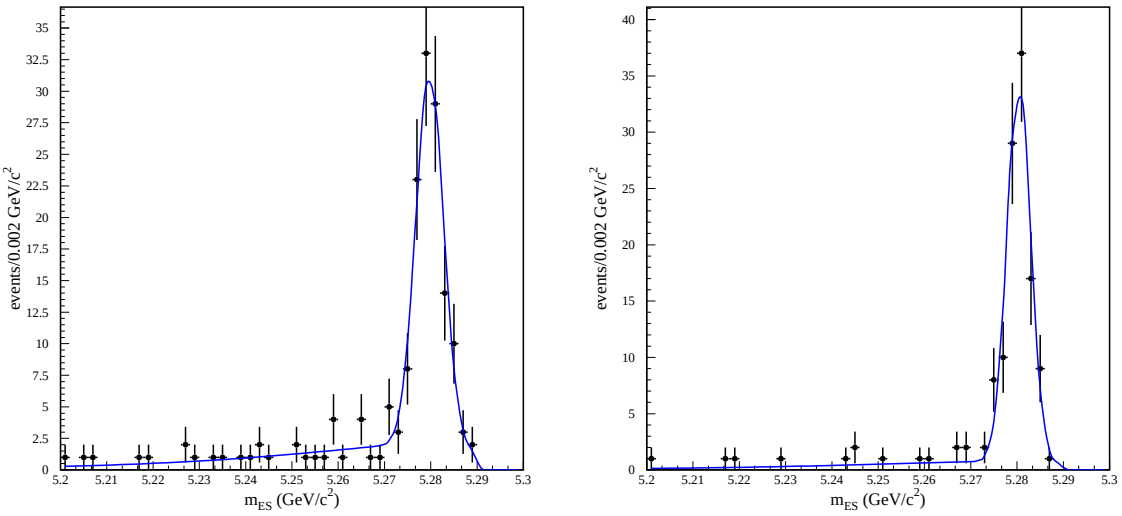

Figure 7: Fits to the m_{ES} distributions in the $B^0 \to \psi(2S)K^0_S$ channel for the e^+e^- (left) and $\mu^+\mu^-$ (right) modes. Vertexing cuts have not been applied.

$$\begin{aligned}\mathcal{R}(\Delta t - \Delta t', \sigma_{\Delta t}; \vec{q}_\alpha) &= (1 - f_{tail} - f_{outlier}) h_G(\Delta t - \Delta t'; \delta^\alpha_{core}, S_{core}\sigma_{\Delta t}) + \\ &\quad f_{tail} h_G(\Delta t - \Delta t'; \delta_{tail}, S_{tail}\sigma_{\Delta t}) + \\ &\quad f_{outlier} h_G(\Delta t - \Delta t', ; \delta_{outlier}, \sigma_{outlier}) \end{aligned} \tag{122}$$

where

$$h_G(t; \delta, \sigma) = \frac{1}{\sqrt{2\pi}\sigma} \exp(-(t-\delta)^2/(2\sigma^2)) \ . \tag{123}$$

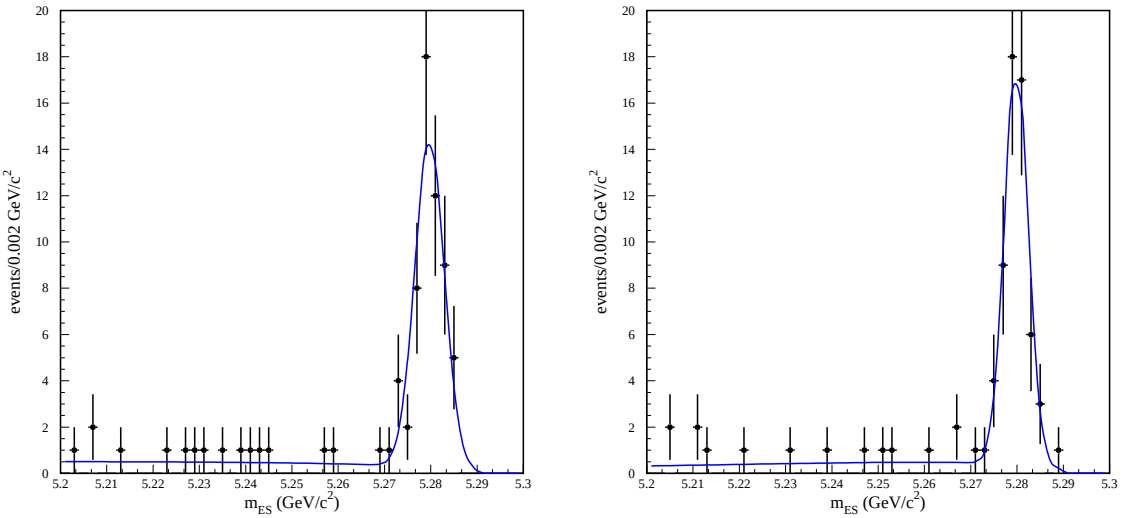

Figure 8: Fits to the m_{ES} distributions in the $B^0 \to \chi_{c1} K_S^0$ channel for the e^+e^- (left) and $\mu^+\mu^-$ (right) modes. Vertexing cuts have not been applied.

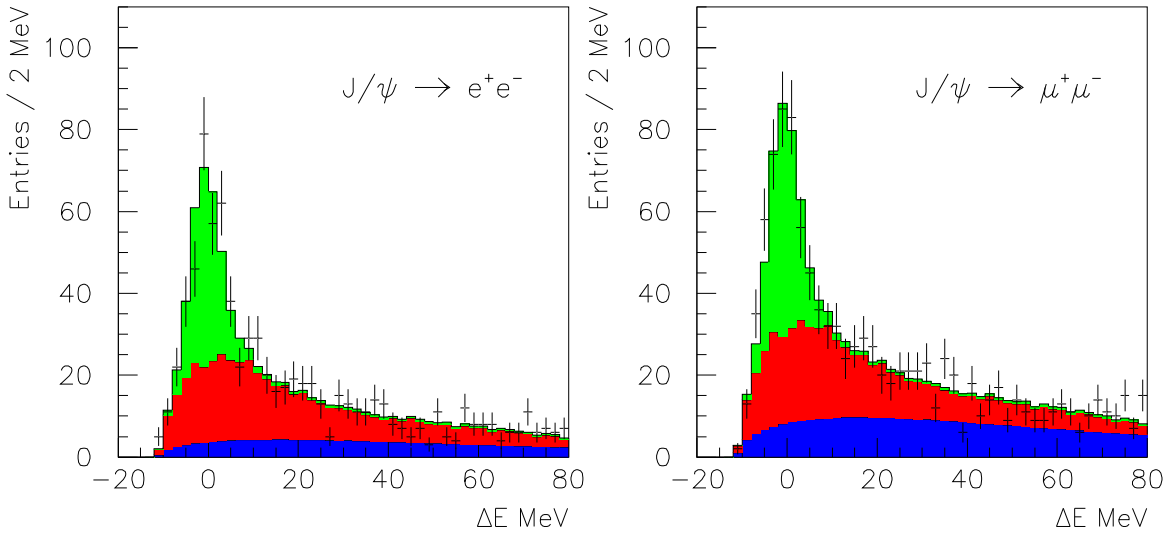

Figure 9: Fits to the ΔE distribution in the $B^0 \to J/\psi K_L^0$ channel for K_L^0 detected in the Emc. Vertexing cuts have not been applied. The red (blue) histogram is the fitted inclusive J/ψ (fake J/ψ) background contribution.

The equivalent *GExp* resolution function for tagging category α reads

$$\begin{aligned}\mathcal{R}(\Delta t - \Delta t', \sigma_{\Delta t}; \vec{q}_\alpha) &= (1 - f_{Exp}^\alpha - f_{outlier}) h_G(\Delta t - \Delta t'; \delta = 0, S\sigma_{\Delta t}) + \\ & f_{Exp}^\alpha \frac{1}{2\sigma_{\Delta t}\tau_r^\alpha}\left[\exp\left(\frac{S^2}{2(\tau_r^\alpha)^2} + \frac{\Delta t - \Delta t'}{\sigma_{\Delta t}\tau_r^\alpha}\right) erfc\left(\frac{S}{\sqrt{2}\tau_r^\alpha} + \frac{\Delta t - \Delta t'}{\sqrt{2}S\sigma_{\Delta t}}\right)\right] + \\ & f_{outlier} h_G(\Delta t - \Delta t', ; \delta_{outlier}, \sigma_{outlier}) \end{aligned} \quad (124)$$

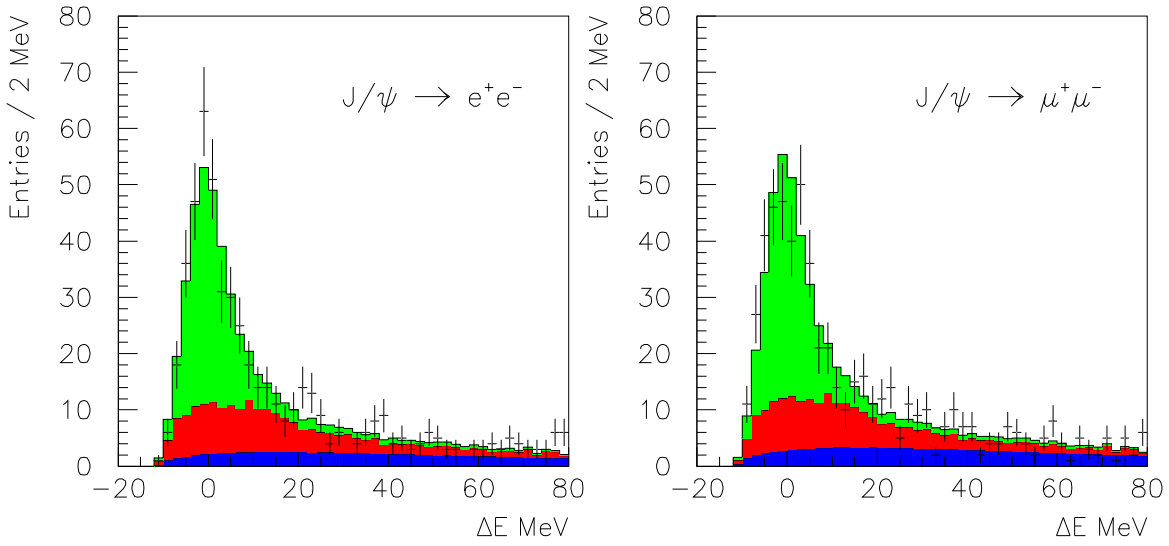

Figure 10: Fits to the ΔE distribution in the $B^0 \to J/\psi K_L^0$ channel for K_L^0 detected in the IFR. Vertexing cuts have not been applied. The red (blue) histogram is the fitted inclusive J/ψ (fake J/ψ) background contribution.

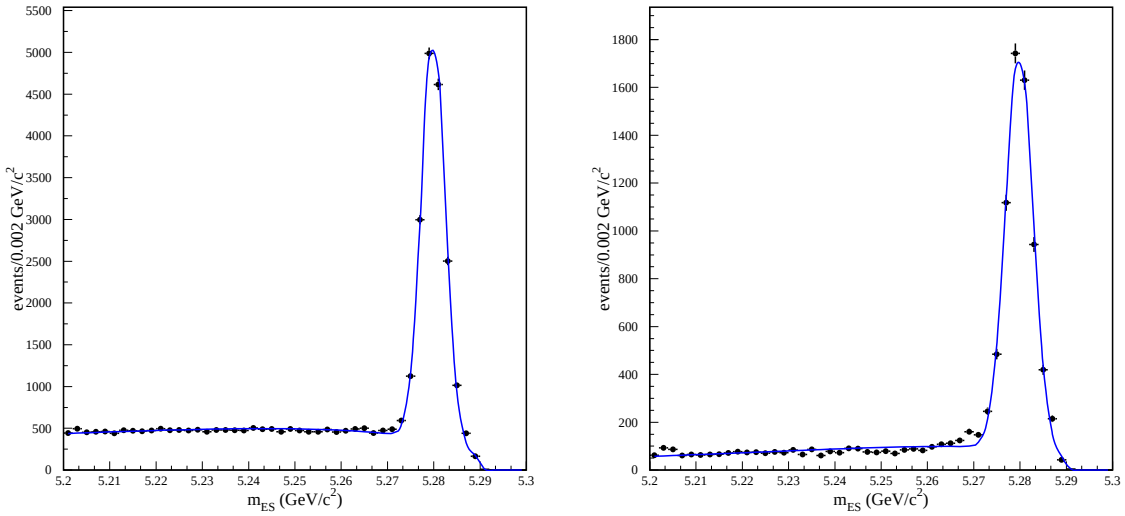

Figure 11: Fits to the m_{ES} distributions in the $B^+ \to \overline{D}^0 \pi^+$ (left) and $B^+ \to \overline{D}^{*0} \pi^+$ (right) channels. Vertexing cuts have not been applied.

The complete signal resolution function for all tagging categories is therefore represented by 11 parameters in the *GG* model,

$$\vec{q} = \left\{ S_{core}, \delta_{core}^{leptons}, \delta_{core}^{kaons}, \delta_{core}^{NT1}, \delta_{core}^{NT2}, f_{tail}, \delta_{tail}, S_{tail}, f_{outlier}, \delta_{outlier}, \sigma_{outlier} \right\} \tag{125}$$

and 12 in the *GExp* parameterization,

$$\vec{q} = \left\{ S, \tau_r^{leptons}, \tau_r^{kaons}, \tau_r^{NT1}, \tau_r^{NT2}, f_{Exp}^{leptons}, f_{Exp}^{kaons}, f_{Exp}^{NT1}, f_{Exp}^{NT2}, f_{outlier}, \delta_{outlier}, \sigma_{outlier} \right\} \quad . \tag{126}$$

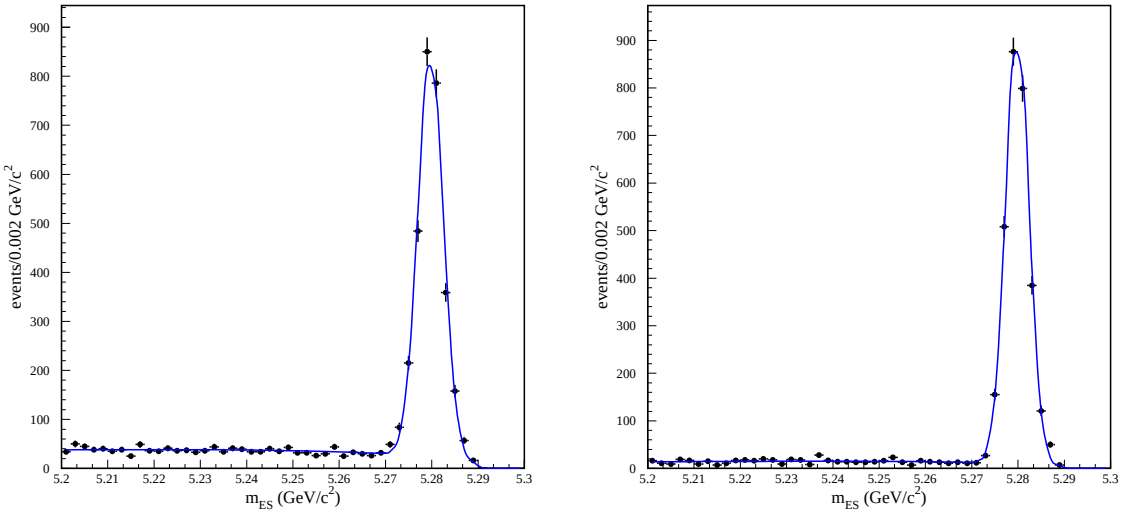

Figure 12: Fits to the m_{ES} distributions in the $B^+ \to J/\psi K^+$ channel for the e^+e^- (left) and $\mu^+\mu^-$ (right) modes. Vertexing cuts have not been applied.

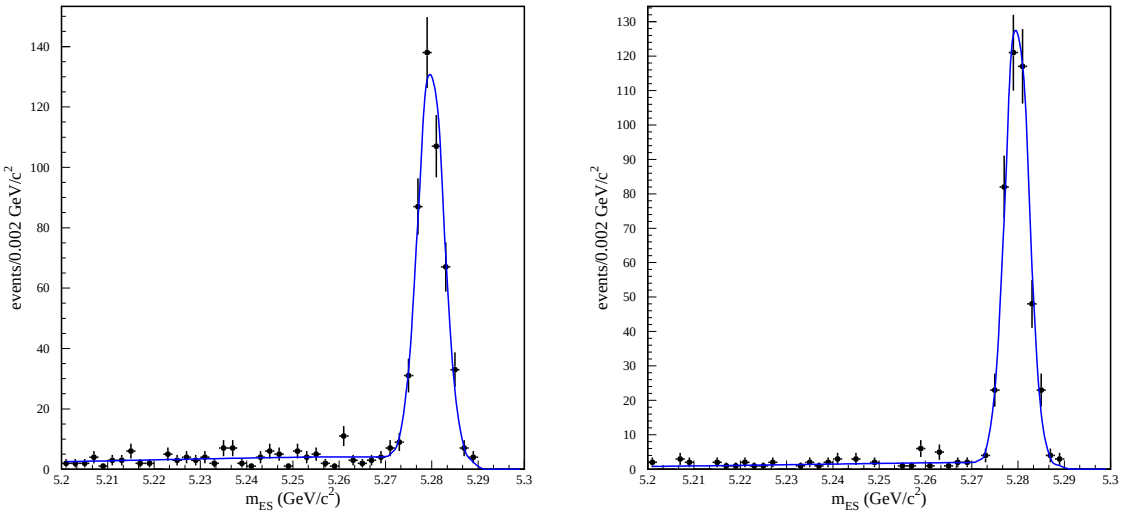

Figure 13: Fits to the m_{ES} distributions in the $B^+ \to \psi(2S)K^+$ channel for the e^+e^- (left) and $\mu^+\mu^-$ (right) modes. Vertexing cuts have not been applied.

$\sigma_{outlier}$ and $\delta_{outlier}$ are fixed, respectively, to 8 and 0 ps.

In the *GG* model all offsets δ^{α}_{core} and δ_{tail} are modeled to be proportional to the reconstructed error $\sigma_{\Delta t}$, since it was found that events with high $\sigma_{\Delta t}$ tend to have high Δt residual [34]. Figure 17, extracted from [23], shows the dependence of the mean (and RMS) of the Monte Carlo Δt residual in bins of the reconstructed $\sigma_{\Delta t}$. It can be seen that the linear scaling is a good approximation for $\sigma_{\Delta t} < 1.4$ ps. Above this value the observed dependence diverges from the linear model, although the statistics there is small. The *GExp* model accounts implicitely for this observed correlation [34].

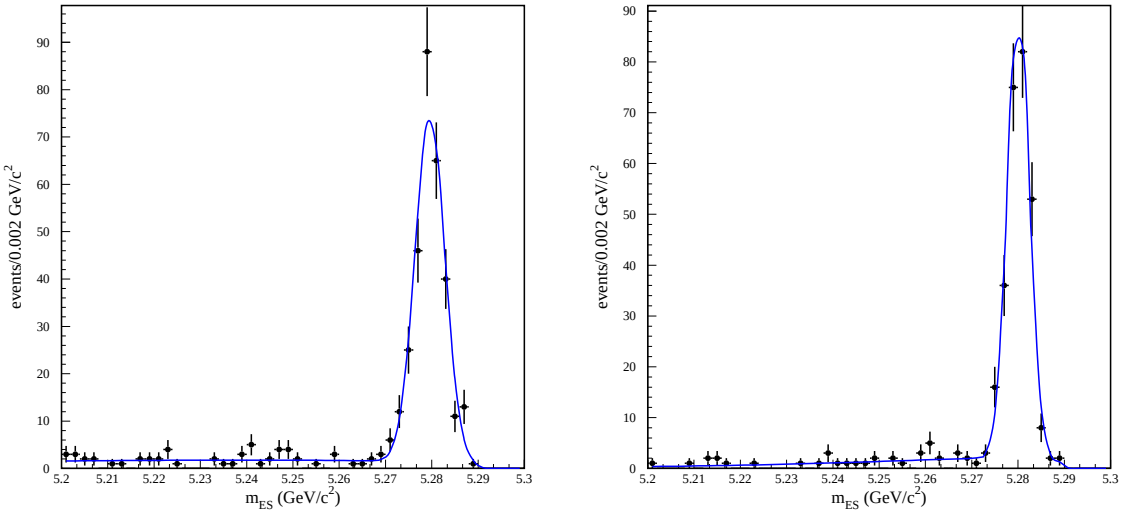

Figure 14: Fits to the m_{ES} distributions in the $B^+ \to \chi_{c1} K^+$ channel for the e^+e^- (left) and $\mu^+\mu^-$ (right) modes. Vertexing cuts have not been applied.

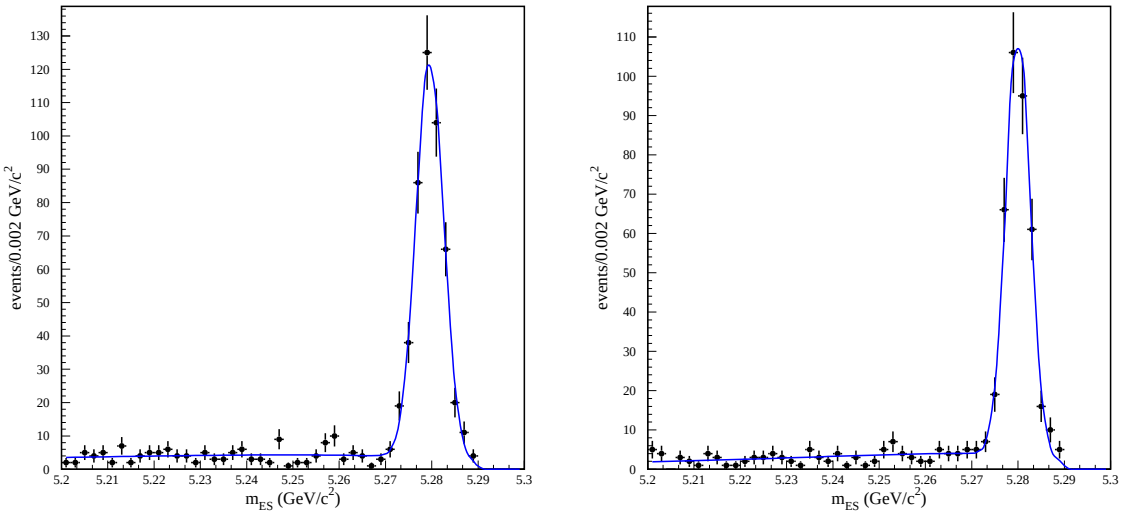

Figure 15: Fits to the m_{ES} distributions in the $B^+ \to J/\psi K^{*+}$ ($K^0_S\pi^+$) channel for the e^+e^- (left) and $\mu^+\mu^-$ (right) modes. Vertexing cuts have not been applied.

The reconstructed event-by-event Δt error ($\sigma_{\Delta t}$) is used to weight the events in the fitting procedure [12]. It is therefore important to make sure that there are no significant correlations among this variable and the variables parameterizing the tagging performance, w^α (average mistag) and Δw^α ($B^0\bar{B}^0$ mistag difference), and if there are, then model them properly. As shown in figure 18(top), obtained from the Monte Carlo sample, there is an almost perfect linear correlation between the mean wrong tag fraction, w^α, and the Δt error, especially for tagging categories involving kaons, being much weaker or negligible for the `Lepton` category. We then model the wrong tag fraction according to the following model:

	B_{flav}			$B_{CPK^0_S}$			$B_{CPK^0_L}$		
Tag	B^0	$\bar{B}^0$	Tot	B^0	$\bar{B}^0$	Tot	B^0	$\bar{B}^0$	Tot
Lepton	1478	1419	2897	96	98	194	35	35	70
Kaon+KPi	2665	2672	5337	154	175	329	74	65	139
Kaon+SlowPi	3183	2976	6159	181	188	369	85	66	151
Other	3197	3014	6211	184	172	356	78	72	150
UnTagged		10423			585			260	

Table 6: Signal event yields, obtained from the m_{ES} fits for the B_{flav} and $B_{CPK^0_S}$ samples and multiplying by the signal fraction in the $|\,\Delta E\,| < 10$ MeV interval for the $B_{CPK^0_L}$ sample, after vertexing requirements.

Parameter	Standard Monte Carlo (exclusive and inclusive)	Dedicated Monte Carlo (exclusive)
$\Delta\Gamma/\Gamma$	0.00	0.20
$\mid q/p \mid$	1.00	1.04
$\frac{\mathrm{Im}\lambda_{CP}}{\lvert\lambda_{CP}\rvert}$	0.70	0.70
Δm	0.472	0.472
$\frac{\mathrm{Re}\lambda_{CP}}{\lvert\lambda_{CP}\rvert}$Rez	0.00	0.00
Imz	0.00	0.00

Table 7: Physics parameter values of the standard and dedicated Monte Carlo samples.

Sample	Standard Monte Carlo	Dedicated Monte Carlo
B^0 cocktail	125250	85048
exclusive $B^0 \to J/\psi K^0_S(\pi^+\pi^-)$	228945	9194
exclusive $B^0 \to J/\psi K^0_S(\pi^0\pi^0)$	54729	3664
exclusive $B^0 \to \psi(2S) K^0_S$	43999	5248
exclusive $B^0 \to \chi_{c1}\, K^0_S$	24414	5050
exclusive $B^0 \to J/\psi K^0_L$	146276	5431
inclusive $B^0 \to J/\psi K^0_S(\pi^+\pi^-)$	10088	
inclusive $B^0 \to J/\psi K^0_S(\pi^0\pi^0)$	2116	
inclusive $B^0 \to \psi(2S) K^0_S$	235	
inclusive $B^0 \to \chi_{c1}\, K^0_S$	561	
inclusive $B^0 \to J/\psi K^0_L$	16203	

Table 8: Standard and dedicated Monte Carlo statistics (after reconstruction and before vertexing cuts and tagging). The values of the physics parameters for each generation were shown in table 7. For the $J/\psi K^0_L$ mode the statistics is given for the ΔE interval $[-20, 80]$ MeV.

$$w^\alpha = w^\alpha_0 + w^\alpha_{slope}\sigma_{\Delta t}\ . \tag{127}$$

As it can be seen in figure 18(top), for kaons this linear model applies better for $\sigma_{\Delta t} < 1.4$ ps. Detailed studies to explain the mechanism of this observed correlation can be found in [33]. The difference of the mistag fractions for B^0 and $\bar{B}^0$, Δw^α, is well constant over the full $\sigma_{\Delta t}$ range, for all tagging categories, as shown in figure 18(bottom). Similarly, the $B^0\bar{B}^0$ differences in reconstruction and tagging efficiency (ν and μ^α parameters) are checked to be constant over the $\sigma_{\Delta t}$ range, as shown in figure 19, which shows the difference in the number

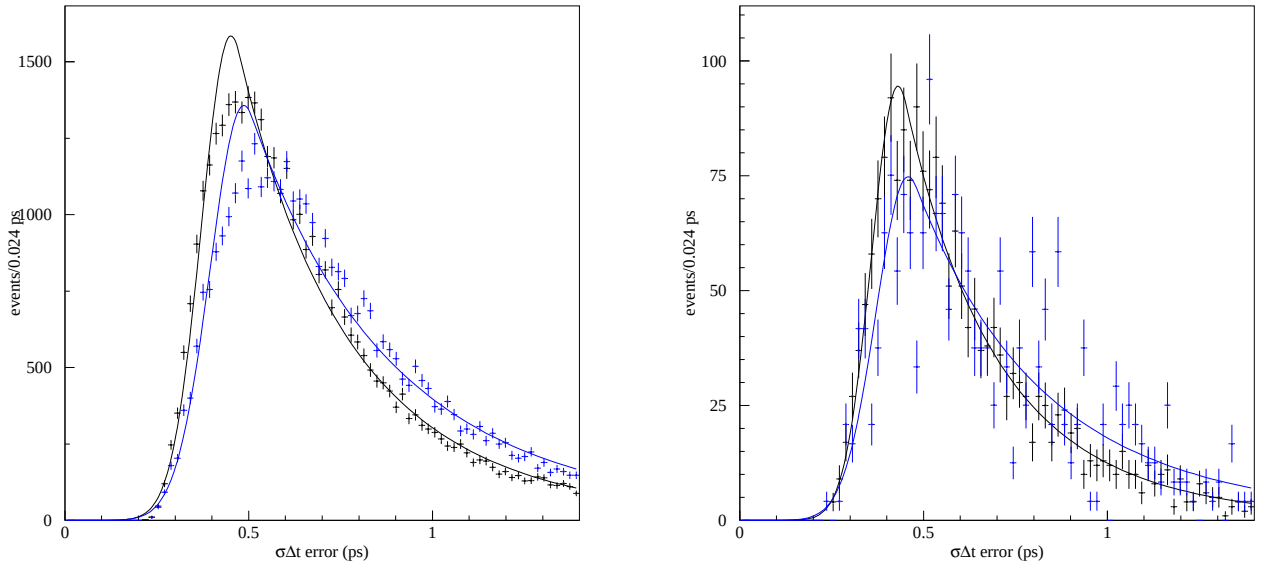

(a) (b)

Figure 16: Event-by-event error on Δt for the (a) B_{flav} and (b) $B_{CPK^0_S}$ data samples, for for signal ($m_{ES} > 5.27$ GeV, black) and sideband ($5.2 < m_{ES} < 5.27$ GeV, blue) region events. The sideband statistics has been normalized to the same number of signal events. The curves currespond to the fit to a Crystall Ball shape.

of B^0 and $\overline{B}^0$ tagged (bottom) and reconstructed (bottom) events in the B_{flav} sample. Similar distributions are observed in the Monte Carlo.

Finally, figures 20 and 21 show the stability of w^α, Δw^α and μ^α, ν with the reconstructed Δt, from Monte Carlo (figure 20) and B_{flav} data sample (figure 21), for each tagged category.

5 Blinding

The blinding strategy used the hidden offset method [25]. A fixed hidden offset is added to the measured parameter in one of two ways: i) $x_{blind} = x_{unblind} + x_{offset}$ or ii) $x_{blind} = 2\mu - x_{unblind} + x_{offset}$, where μ is the central value and x_{offset} is the random offset taken from a Gaussian distribution with mean zero and RMS σ. Either i) or ii) is used, the choice is made randomly and kept hidden. The use of ii) hides whether the result moves up or down when changes in the analysis are made. The standard tools (`BlindTools` package) have been used. Table 9 summarizes the blinding strings, as well as the central values (μ) and RMS (σ) of the blinding for each parameter and fit configuration. Δm and τ_B (when τ_B is free) are unblinded. Common blinding strings for Analysis 1 and Analysis 2 (see section 6), as well as for B_{CP}, $B_{CPK^0_S}$ only and $B_{CPK^0_L}$ only fits, are used. The time distributions and asymmetries are hidden.

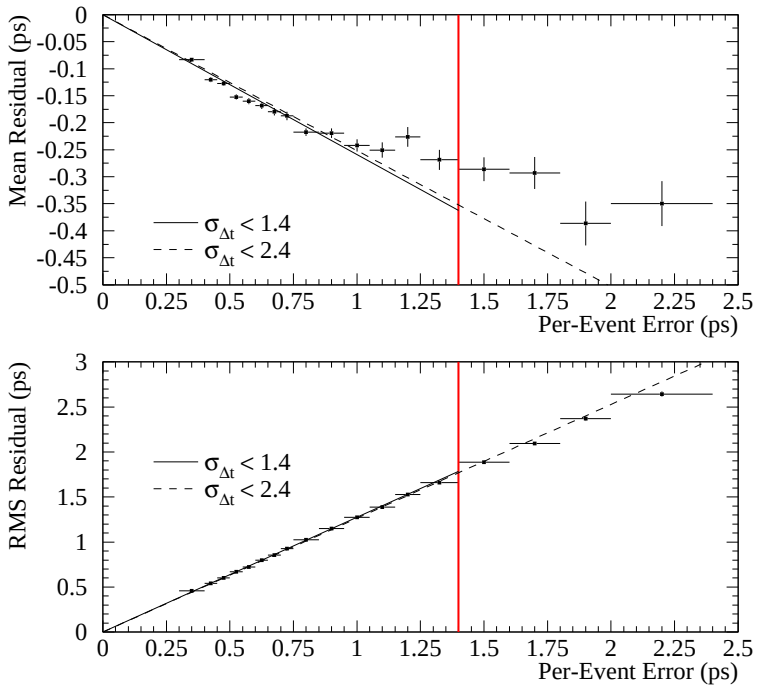

Figure 17: Mean and width of the MC Δt residual in bins of the per-event error $\sigma_{\Delta t}$. Fits are shown to a line constrained to pass through the origin for $\sigma_{\Delta t} < 1.4$ and $\sigma_{\Delta t} < 2.4$ ps.

6 Description of the nominal fit

The complete log-likelihood function used in this analysis was described in detail in section 2. The assumptions made in the nominal fit are the following:

- Two configurations (Analyses):

  Analysis 1: fit for $\Delta\Gamma/\Gamma \times sign(\frac{\mathrm{Re}\lambda_{CP}}{|\lambda_{CP}|})$, Δm, $|\,q/p\,|$ and $\frac{\mathrm{Im}\lambda_{CP}}{|\lambda_{CP}|}$ (4 parameters). Thus this analysis assumes CPT conservation.

  Analysis 2: fit for $\Delta\Gamma/\Gamma \times sign(\frac{\mathrm{Re}\lambda_{CP}}{|\lambda_{CP}|})$, Δm, $|\,q/p\,|$, $\frac{\mathrm{Im}\lambda_{CP}}{|\lambda_{CP}|}$, $\mathrm{Rez}\frac{\mathrm{Re}\lambda_{CP}}{|\lambda_{CP}|}$ and Imz (6 parameters).

Parameter	Central value	RMS	Blinding String
$\Delta\Gamma/\Gamma$	0.00	0.50	Here we blind the width difference (summer02 sample)
$\|\,q/p\,\|$	1.00	0.04	Here we blind absqoverp (summer02 sample)
$\frac{\mathrm{Im}\lambda_{CP}}{\|\lambda_{CP}\|}$	0.60	0.20	Here we blind imagLambda (summer02 sample)
$\frac{\mathrm{Re}\lambda_{CP}}{\|\lambda_{CP}\|}\mathrm{Rez}$	0.00	0.50	Here we blind realZ (summer02 sample)
Imz	0.00	0.50	Here we blind imagZ (summer02 sample)

Table 9: Central values, RMS and strings of the blinding strategy.

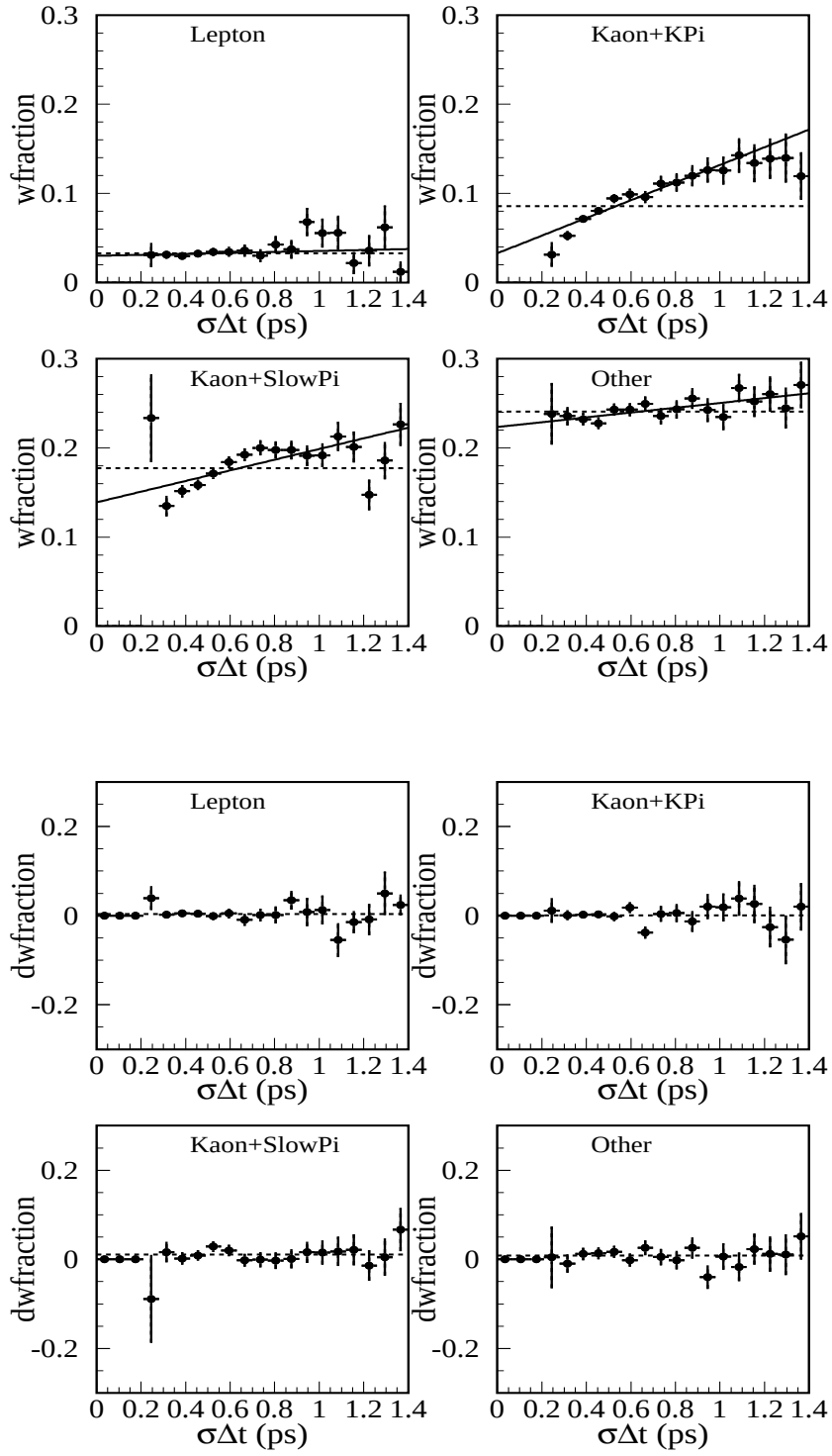

Figure 18: (Top) Mistag fraction from Monte Carlo in bins of per-event error $\sigma_{\Delta t}$, for each tagging category. (Bottom) $B^0\overline{B}^0$ mistag fraction differences from Monte Carlo in bins of per-event error $\sigma_{\Delta t}$, for each tagging category. The straight lines are the result of a simple binned fit to the points (with slope and origin free).

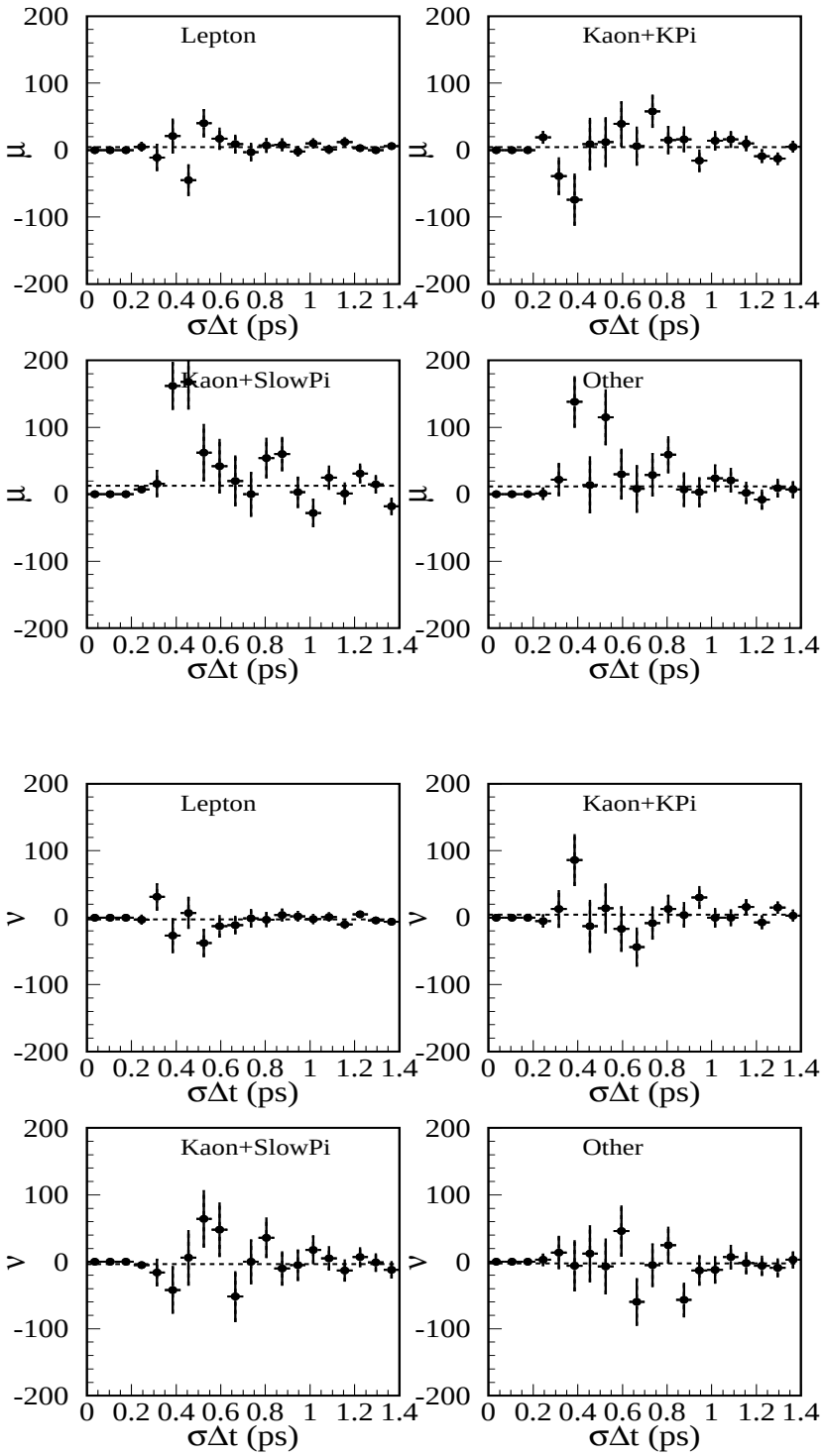

Figure 19: (Top) Difference in the number of B^0 and $\bar{B}^0$ tagged events ($\propto \mu^{\alpha}$) from the B_{flav} data sample in bins of per-event error $\sigma_{\Delta t}$, for each tagging category. (Bottom) Difference in the number of B^0 and $\bar{B}^0$ reconstructed events ($\propto \nu$) from the B_{flav} data sample in bins of per-event error $\sigma_{\Delta t}$, for each tagging category. The straight lines are the result of a simple binned fit to the points.

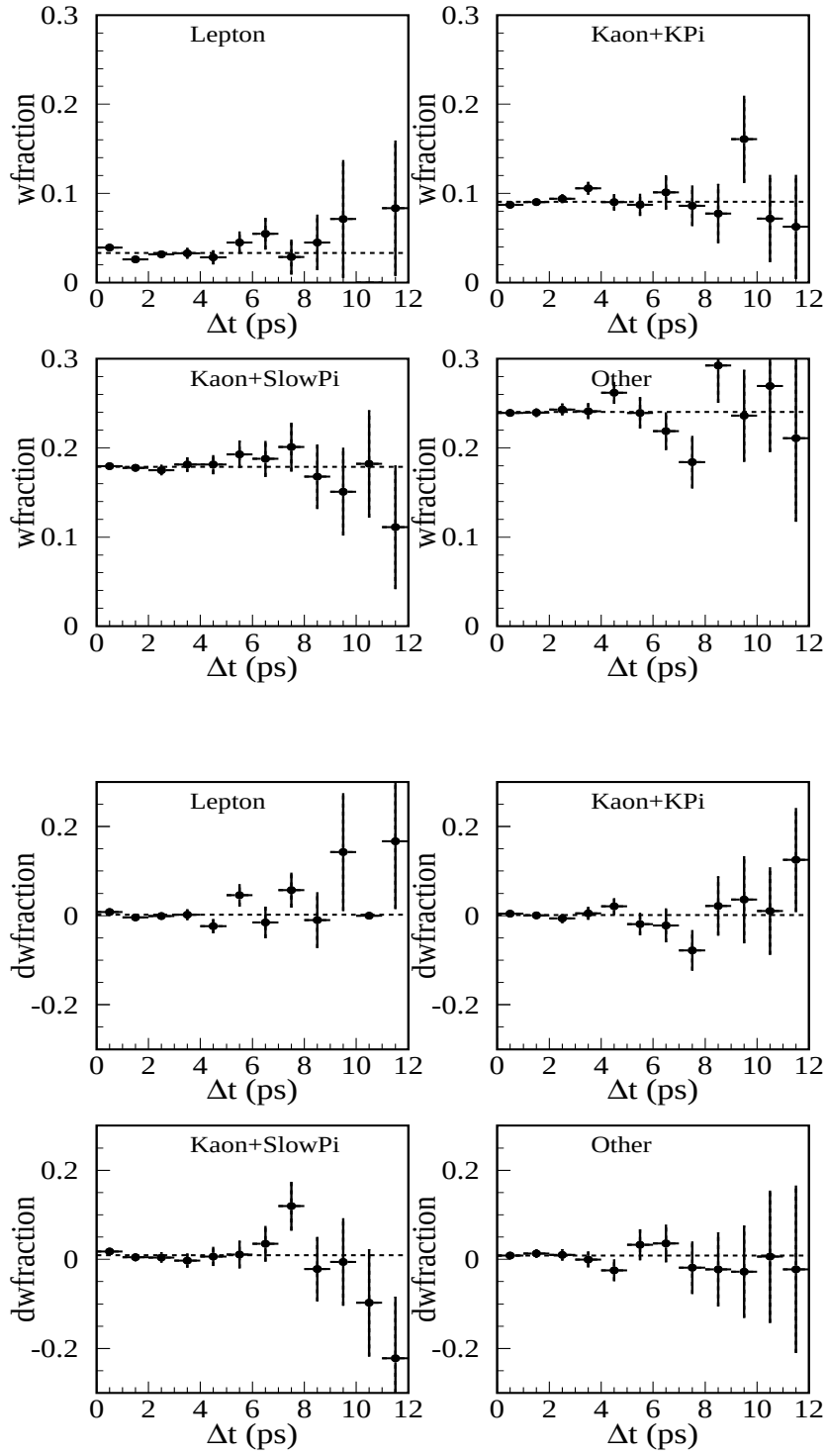

Figure 20: (Top) Mistag fraction from Monte Carlo in bins of Δt, for each tagging category. (Bottom) $B^0\bar{B}^0$ mistag fraction differences from Monte Carlo in bins of Δt, for each tagging category. The straight lines are the result of a simple binned fit to the points.

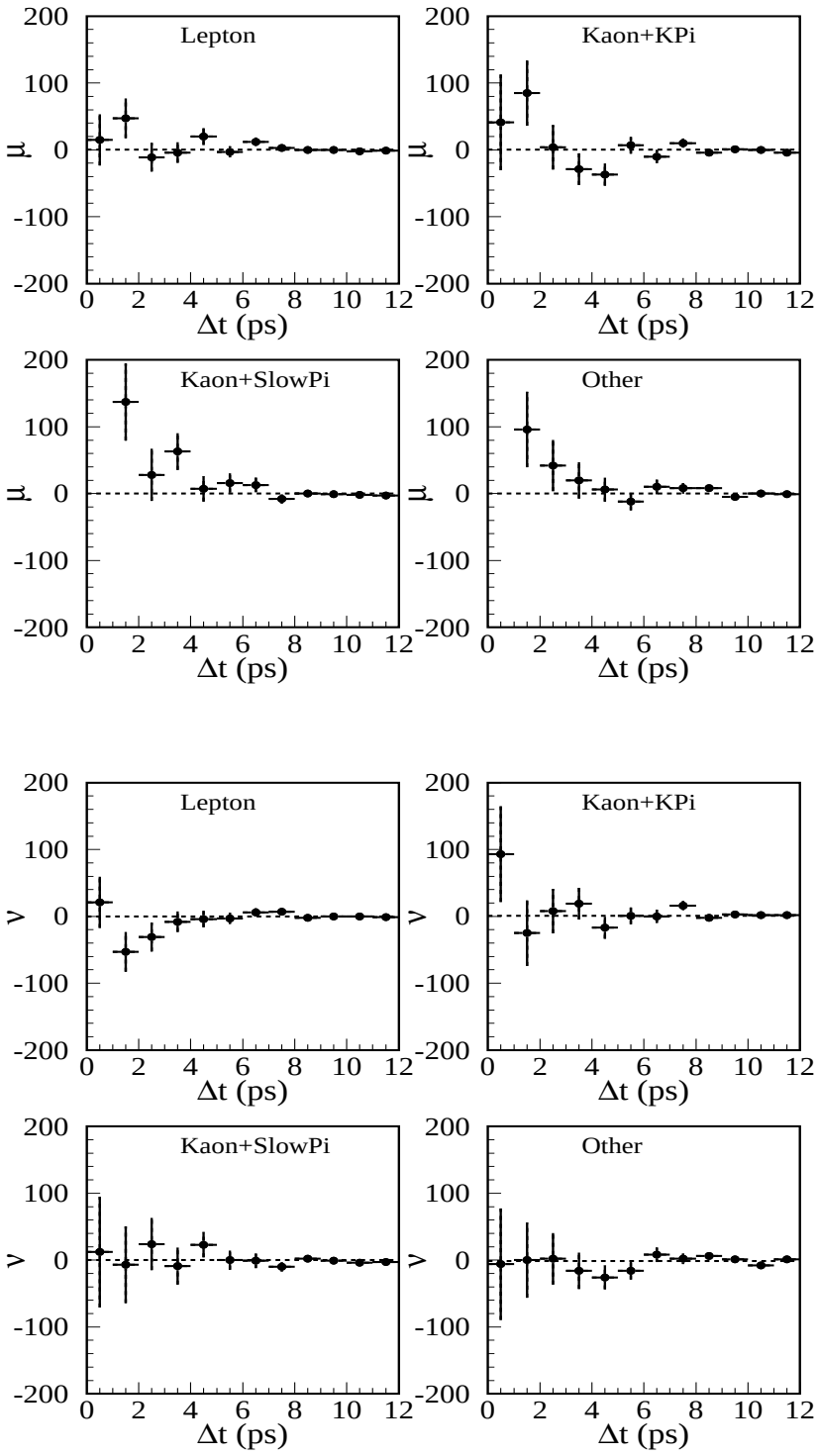

Figure 21: (Top) Difference in the number of B^0 and $\overline{B}^0$ tagged events ($\propto \mu^{\alpha}$) from the B_{flav} data sample in bins of Δt, for each tagging category. (Bottom) Difference in the number of B^0 and $\overline{B}^0$ reconstructed events ($\propto \nu$) from the B_{flav} data sample in bins of Δt, for each tagging category. The straight lines are the result of a simple binned fit to the points.

τ will be kept as fixed parameter. Although all the parameters (except τ) are left free in the nominal fit (as required in order to have a theoretically consistent scenario), only measurements of $\Delta\Gamma/\Gamma \times sign(\frac{\mathrm{Re}\lambda_{CP}}{|\lambda_{CP}|})$, $\mathrm{Re}z\frac{\mathrm{Re}\lambda_{CP}}{|\lambda_{CP}|}$, Im$z$ and $\mid q/p \mid$ will be provided. Δm and $\frac{\mathrm{Im}\lambda_{CP}}{|\lambda_{CP}|}$ will be used as cross-checks. Fits with τ free will also be performed as cross-check. $\frac{\mathrm{Re}\lambda_{CP}}{|\lambda_{CP}|}$ is extracted as $\frac{\mathrm{Re}\lambda_{CP}}{|\lambda_{CP}|} = +\sqrt{1-\left(\frac{\mathrm{Im}\lambda_{CP}}{|\lambda_{CP}|}\right)^2}$, so it is constrained to be within the physical region, i.e. $1-\left(\frac{\mathrm{Im}\lambda_{CP}}{|\lambda_{CP}|}\right)^2 \geq 0$;

- assume that the mechanisms contributing to the decay of CP eigenstates have the same weak phase for $\eta_{f_{CP}} = -1$ and $\eta_{f_{CP}} = +1$ modes;
- assume a single effective channel in the tagging and flavor eigenstate B sides and fit for the imaginary parts of the corresponding doubly-CKM-suppressed phases: $\frac{\mathrm{Im}\lambda_{tag}}{|\lambda_{tag}|}$, $\frac{\mathrm{Im}\bar{\lambda}_{tag}}{|\bar{\lambda}_{tag}|}$, $\frac{\mathrm{Im}\lambda_{flav}}{|\lambda_{flav}|}$, $\frac{\mathrm{Im}\bar{\lambda}_{flav}}{|\bar{\lambda}_{flav}|}$ (4 parameters). The real parts are all fixed to zero. The ratios of the decay amplitudes of DCKM to favored processes, r_{tag} and r_{flav} are also fixed to the value discussed in section 7.1.4. The corresponding ratios for $\bar{B}^0$, $\bar{r}_{tag}$ and $\bar{r}_{flav}$, are assumed to be the same as for B^0;
- a total of 10(12) parameters are used to describe the signal resolution function with the GG($GExp$) model:

  GG: scale factors of the core and tails components, S_{core} and S_{tail}; tagging category dependent core bias, δ^{α}_{core}; common tail bias, δ_{tail}; fraction of tail and outlier Gaussians, f_{tail} and $f_{outlier}$; the width and bias of the outlier Gaussian were fixed to 8 ps and 0 respectively. This is the model used for the central value;

  GExp: scale factor of the Gaussian, S, tagging category dependent effective lifetime (τ^{α}_{r}) and exponential component fraction (f^{α}_{Exp}); the width and bias of the outlier Gaussian were fixed to 8 ps and 0 respectively. This model is used as cross-check and to estimate a systematic uncertainty due to the resolution model parameterization;

- a total of 11 parameters are used to describe the signal mistags: for each tagging category (Tagged events only), the average mistag fraction (origin, w^{α}_{0}, and slope w^{α}_{slope}) and the $B^0\bar{B}^0$ differences, Δw^{α}. w^{Lepton}_{slope} was fixed to zero;
- 3 background components are assumed for the B_{flav} sample (17 parameters):
  - a prompt (zero lifetime) and non-prompt (non-vanishing and free lifetime -1 parameter-) components, with their own effective wrong tag fraction (w^{α}_{slope} and Δw^{α} fixed to zero) (8 parameters) and a common resolution function, described as a common single Gaussian distribution with a scale factor S_{backg} and a bias δ_{backg} (GG model) or a common single unbiassed Gaussian with a scale factor S_{backg} plus the same Gaussian convoluted with an exponential function with effective lifetime $\tau_{r,backg}$ ($GExp$ model), and an outlier fraction $f_{backg,outlier}$ (3 parameters); the width of the outlier component is taken to be fixed at 8 ps with zero bias; the relative $f^{\alpha}_{prompt,B_{flav}}$ fraction of prompt background for each tagging category (UnTagged events included) are also considered as free parameters (5 parameters);
  - a peaking contribution due to B^+ decays, which resolution function is the same as that of the signal, with B^+ lifetime fixed to the PDG2002 value (1.674 ± 0.018) [26]; the peaking background fraction is fixed;
  - no oscillatory/CPT/CP/T structure is assumed for the non-prompt combinatorial background component;
- 3 background components are assumed for the $B_{CPK^0_S}$ sample (5 parameters):

– prompt, non-prompt and peaking background, where the peaking background fraction is also fixed, and a common (averaged over tagging categories) prompt fraction is assumed, independently for each $B_{CPK^0_S}$ sample (4 parameters). The wrong tag fraction parameters, lifetime and resolution function of the peaking background component is assumed to be the same as those of the signal. The lifetime of the non-prompt background is left free (1 parameter) and assumed the same for all tagging categories. No CPT/T/CP/oscillation structure in the background is assumed. Finally, the resolution function parameters of the prompt and non-prompt components are assumed the same as those of the prompt and non-prompt background components of the B_{flav} sample;

- the background treatment in the $B_{CPK^0_L}$ sample is performed as outlined in section 7.1.5 and described in detail in [20], with only one difference. While in [20] the resolution function parameters of the non-J/ψ background are extracted from an external fit to the J/ψ dilepton mass sideband, here we assume them to be same as for the prompt and non-prompt background components of the B_{flav} sample, similarly as it is done for the $B_{CPK^0_S}$ sample. Only the fraction of prompt component and the lifetime of the non-prompt one are fixed to the values extracted from the external fit. As in [20], due to different background composition, the $B_{CPK^0_L}$ sample is splitted according to the K^0_L type (IFR and EMC), J/ψ channel (e^-e^- and $\mu^+\mu^-$) and Lepton and non-Lepton tag;

- the signal $B^0\bar{B}^0$ differences in reconstruction and tagging efficiencies, ν and μ^α, are extracted simultaneously together with the other parameters (5 parameters). For combinatorial background components they are assumed zero;

- assume direct CP conservation for B_{CP} samples;

- the parameters of the signal probablity obtained from the m_{ES} fits are taken as fixed (B_{flav} and $B_{CPK^0_S}$ samples).

- the overall tagging efficiencies T^α ($\alpha = \alpha_{Tagged}$) are fixed to the values extracted from simple counting of events in the B_{flav} sample.

- the *GG* resolution model is adopted for the nominal fit configuration (central value) while the *GExp* model will be used to assign the systematics from the resolution function parameterization. An exhaustive comparison of the two models was made in reference [12], section 4.1. From these studies there was no evidence of advantages of any of the two models, from the point of view of the biases and statistical reach. For compatibility with the *BABAR* hadronic mixing and $\sin 2\beta$ analyses we adopted the *GG* model for the nominal fit configuration. Fits with the *GExp* model are, however, significantly slower than those using the *GG* parameterization.

The total number of parameters is therefore:

Analysis 1: 56 with *GG* model, 58 with *GExp*;

Analysis 2: 58 with *GG* model, 60 with *GExp*.

Results in the $\{\varepsilon, \delta\}$ formalism will be also provided to first order in $\mathrm{Re}\varepsilon$ and δ, using the relations given in section 2.4.

7 Results

7.1 Fit inputs

7.1.1 Mistag fractions for charged B's and B^+B^- differences in reconstruction and tagging efficiencies

The mistags and detector charge asymmtries of charged B mesons are extracted from a maximum likelihood fit to the B^+ sample (open charm) alone. The lifetime of B^+ mesons is left free. All the other oscillation/CPT/T/CP and DCKM parameters were assumed to be zero (except obviously $\mid q/p \mid$=1). The fitting strategy is the same as for the B_{flav} sample (excluding the $B_{CPK^0_S}$ and $B_{CPK^0_L}$ samples). The peaking background component due to B^0 decays was assumed to be $(2.0 \pm 1.5)\%$ [29]. The mistags for the peaking background are assumed the same as for the signal (no corrections are assumed here due to the known differences of mistags for neutral and charged B mesons since would propagate to our measurements at second or third order, as will be shown in section 9.8). The results of the fit with the *GG* and *GExp* resolution models are shown in tables 10 and 11, respectively. The lifetime is unblinded. Note that the obtained lifetime is about two sigma (statistical) below the PDG2002 value for the `GG` model, while it is consistent (about one sigma below) for the `GExp`. This feature is known from earlier lifetime studies [29]: the `GG` model provides slightly biased estimates of the lifetime while the `GExp` approach gives the optimal trade-off between statistical reach and systematics (included biases). However, what matters here is the fact that the mistag fractions and the B^+B^- differences in reconstruction efficiencies obtained with the two resolution models are completely consistent. Figure 22 shows the normalized residuals (defined as the difference between the data and the fit projection onto the Δt axis divided by the data error), separately for each tagging category and for B^- and B^+ events (signal region, $m_{ES} > 5.27$ GeV/c^2).

7.1.2 m_{ES} fit results

An event-by-event signal probability, $p^{\alpha}_{sig}(m_{ES})$, for the B_{flav} and $B_{CPK^0_S}$ samples is estimated from unbinned maximum likelihood fits to the m_{ES} spectra, assuming a Gaussian plus an Argus background shape, in a 3σ ΔE window. The m_{ES} fits are performed separately for each sample –B_{flav}, $B^0 \to J/\psi K^0_S(\pi^+\pi^-)$, $B^0 \to J/\psi K^0_S(\pi^0\pi^0)$, $B^0 \to \psi(2S)K^0_S$, χ_{c1} K^0_S– and tagging category. Due to the lack of statistics, the fits were performed for all tagging categories together in the case of the $B^0 \to \psi(2S)K^0_S$ and $B^0 \to \chi_{c1}$ K^0_S decay modes. e^+e^- and $\mu^+\mu^-$ channels were treated together. The results of these fits for each tagging category are shown in figures 23 and 24, for the B_{flav} and $B_{CPK^0_S}$ (all combined) samples, respectively. The parameters describing the signal probability obtained from these fits are fixed in the final likelihood fit.

7.1.3 Peaking background for B_{flav} and $B_{CPK^0_S}$ samples

The amount of charged B background that peaks in the m_{ES} B_{flav} distribution was estimated by using generic Monte Carlo. In addition, a cocktail Monte Carlo sample of charged B's containing the main sources of the background in the generic Monte Carlo was also generated and used [23]. The signal events from all reconstructed modes are removed from the Monte Carlo and a fit is performed to the remaining distribution including a Gaussian term plus an Argus background. The f^{α}_{peak} fraction was finally estimated to be $(1.5 \pm 0.6)\%$ [23]. In the case of the $B_{CPK^0_S}$ sample, the inclusive J/ψ Monte Carlo was used [9], and the amount of peaking background was estimated similarly, but now for each channel separately. Table 12 summarizes the averaged over tagging categories value of f^{α}_{peak}, for each $B_{CPK^0_S}$ sample.

Parameter	B^+ fit results (*GG* model)
τ	1.625 ± 0.024
S_{core}	1.105 ± 0.088
$\delta_{core}^{\text{Lepton}}$	-0.218 ± 0.100
$\delta_{core}^{\text{Kaon1}}$	-0.293 ± 0.079
$\delta_{core}^{\text{Kaon+SlowPi}}$	-0.288 ± 0.072
$\delta_{core}^{\text{Other}}$	-0.219 ± 0.073
$\delta_{core}^{\text{Untag}}$	-0.286 ± 0.056
f_{tail}	0.101 ± 0.045
δ_{tail}	-0.02 ± 0.45
$f_{outlier}$	$(3.8 \pm 1.8) \cdot 10^{-3}$
w_0^{Lepton}	$(9.8 \pm 2.9) \cdot 10^{-3}$
$w_0^{\text{Kaon+KPi}}$	$(1.3 \pm 1.5) \cdot 10^{-2}$
$w_0^{\text{Kaon+SlowPi}}$	0.111 ± 0.019
w_0^{Other}	0.204 ± 0.022
$w_{slope}^{\text{Kaon+KPi}}$	0.116 ± 0.028
$w_{slope}^{\text{Kaon+SlowPi}}$	$(9.6 \pm 3.0) \cdot 10^{-2}$
w_{slope}^{Other}	0.118 ± 0.035
Δw^{Lepton}	$(7.7 \pm 5.6) \cdot 10^{-3}$
$\Delta w^{\text{Kaon+KPi}}$	$(-2.1 \pm 9.3) \cdot 10^{-3}$
$\Delta w^{\text{Kaon+SlowPi}}$	$(-2.9 \pm 1.3) \cdot 10^{-2}$
Δw^{Other}	$(-2.7 \pm 1.6) \cdot 10^{-2}$

Parameter	B^+ fit results (*GG* model)
ν	$(9.9 \pm 7.6) \cdot 10^{-3}$
μ^{Lepton}	$(-0.7 \pm 2.3) \cdot 10^{-2}$
$\mu^{\text{Kaon+KPi}}$	$(1.4 \pm 1.6) \cdot 10^{-2}$
$\mu^{\text{Kaon+SlowPi}}$	$(2.1 \pm 1.5) \cdot 10^{-2}$
μ^{Other}	$(-2.1 \pm 1.6) \cdot 10^{-2}$
$f_{prompt,B_{flav}}^{\text{Lepton}}$	0.123 ± 0.088
$f_{prompt,B_{flav}}^{\text{Kaon+KPi}}$	0.622 ± 0.027
$f_{prompt,B_{flav}}^{\text{Kaon+SlowPi}}$	0.652 ± 0.024
$f_{prompt,B_{flav}}^{\text{Other}}$	0.710 ± 0.022
$f_{prompt,B_{flav}}^{\text{Untag}}$	0.783 ± 0.016
S_{back}	1.321 ± 0.016
δ_{back}	$(-0.6 \pm 1.3) \cdot 10^{-2}$
$f_{back,outlier}$	$(1.40 \pm 0.18) \cdot 10^{-2}$
$w_{0,prompt}^{\text{Lepton}}$	0.08 ± 0.20
$w_{0,prompt}^{\text{Kaon+KPi}}$	0.113 ± 0.014
$w_{0,prompt}^{\text{Kaon+SlowPi}}$	0.220 ± 0.014
$w_{0,prompt}^{\text{Other}}$	0.352 ± 0.015
$w_{0,non-prompt}^{\text{Lepton}}$	0.157 ± 0.041
$w_{0,non-prompt}^{\text{Kaon+KPi}}$	0.185 ± 0.022
$w_{0,non-prompt}^{\text{Kaon+SlowPi}}$	0.260 ± 0.024
$w_{0,non-prompt}^{\text{Other}}$	0.381 ± 0.031
$\tau_{non-prompt}$	1.329 ± 0.053

Table 10: Fit results for B^+ data (*GG* resolution model). The lifetime is unblinded.

Parameter	B^+ fit results (*GExp* model)
τ	1.650 ± 0.021
S	1.130 ± 0.070
τ_r^{Lepton}	0.195 ± 0.085
$\tau_r^{\text{Kaon+KPi}}$	0.35 ± 0.42
$\tau_r^{\text{Kaon+SlowPi}}$	0.77 ± 0.38
τ_r^{Other}	1.10 ± 0.59
τ_r^{Untag}	0.95 ± 0.39
f_{Exp}^{Lepton}	1.0000 ± 0.0037
$f_{Exp}^{\text{Kaon+KPi}}$	0.78 ± 0.94
$f_{Exp}^{\text{Kaon+SlowPi}}$	0.37 ± 0.19
f_{Exp}^{Other}	0.20 ± 0.12
f_{Exp}^{Untag}	0.30 ± 0.13
$f_{outlier}$	$(3.7 \pm 1.8) \cdot 10^{-3}$
w_0^{Lepton}	$(9.8 \pm 2.9) \cdot 10^{-3}$
$w_0^{\text{Kaon+KPi}}$	$(1.3 \pm 1.5) \cdot 10^{-2}$
$w_0^{\text{Kaon+SlowPi}}$	0.111 ± 0.019
w_0^{Other}	0.204 ± 0.022
$w_{slope}^{\text{Kaon+KPi}}$	0.115 ± 0.028
$w_{slope}^{\text{Kaon+SlowPi}}$	$(9.6 \pm 3.0) \cdot 10^{-2}$
w_{slope}^{Other}	0.118 ± 0.035
Δw^{Lepton}	$(7.7 \pm 5.6) \cdot 10^{-3}$
$\Delta w^{\text{Kaon+KPi}}$	$(-2.1 \pm 9.3) \cdot 10^{-3}$
$\Delta w^{\text{Kaon+SlowPi}}$	$(-2.9 \pm 1.3) \cdot 10^{-2}$
Δw^{Other}	$(-2.7 \pm 1.6) \cdot 10^{-2}$

Parameter	B^+ fit results (*GExp* model)
ν	$(9.9 \pm 7.6) \cdot 10^{-3}$
μ^{Lepton}	$(-0.6 \pm 2.3) \cdot 10^{-2}$
$\mu^{\text{Kaon+KPi}}$	$(1.4 \pm 1.6) \cdot 10^{-2}$
$\mu^{\text{Kaon+SlowPi}}$	$(2.1 \pm 1.5) \cdot 10^{-2}$
μ^{Other}	$(-2.1 \pm 1.6) \cdot 10^{-2}$
$f_{prompt,B_{flav}}^{\text{Lepton}}$	0.120 ± 0.088
$f_{prompt,B_{flav}}^{\text{Kaon+KPi}}$	0.622 ± 0.027
$f_{prompt,B_{flav}}^{\text{Kaon+SlowPi}}$	0.654 ± 0.025
$f_{prompt,B_{flav}}^{\text{Other}}$	0.711 ± 0.022
$f_{prompt,B_{flav}}^{\text{Untag}}$	0.785 ± 0.017
S_{back}	1.319 ± 0.016
$\tau_{r,back}$	-2.2 ± 1.9
$f_{back,outlier}$	$(1.38 \pm 0.19) \cdot 10^{-2}$
$w_{0,prompt}^{\text{Lepton}}$	0.08 ± 0.21
$w_{0,prompt}^{\text{Kaon+KPi}}$	0.113 ± 0.014
$w_{0,prompt}^{\text{Kaon+SlowPi}}$	0.220 ± 0.014
$w_{0,prompt}^{\text{Other}}$	0.352 ± 0.015
$w_{0,non-prompt}^{\text{Lepton}}$	0.156 ± 0.040
$w_{0,non-prompt}^{\text{Kaon+KPi}}$	0.185 ± 0.022
$w_{0,non-prompt}^{\text{Kaon+SlowPi}}$	0.260 ± 0.025
$w_{0,non-prompt}^{\text{Other}}$	0.381 ± 0.031
$\tau_{non-prompt}$	1.324 ± 0.053

Table 11: Fit results for B^+ data (*GExp* resolution model).

$B_{CPK_S^0}$ Mode	Fraction of peaking background (%)
$J/\psi K_S^0(\pi^+\pi^-)$	0.28 ± 0.11 %
$J/\psi K_S^0(\pi^0\pi^0)$	1.76 ± 0.57%
$\psi(2S)K_S^0$	1.17 ± 3.10%
$\chi_{c1}K_S^0$	3.54 ± 1.44%

Table 12: Peaking background contributions for the $B_{CPK_S^0}$ channels. The errors are the statistical errors from the m_{ES} fits.

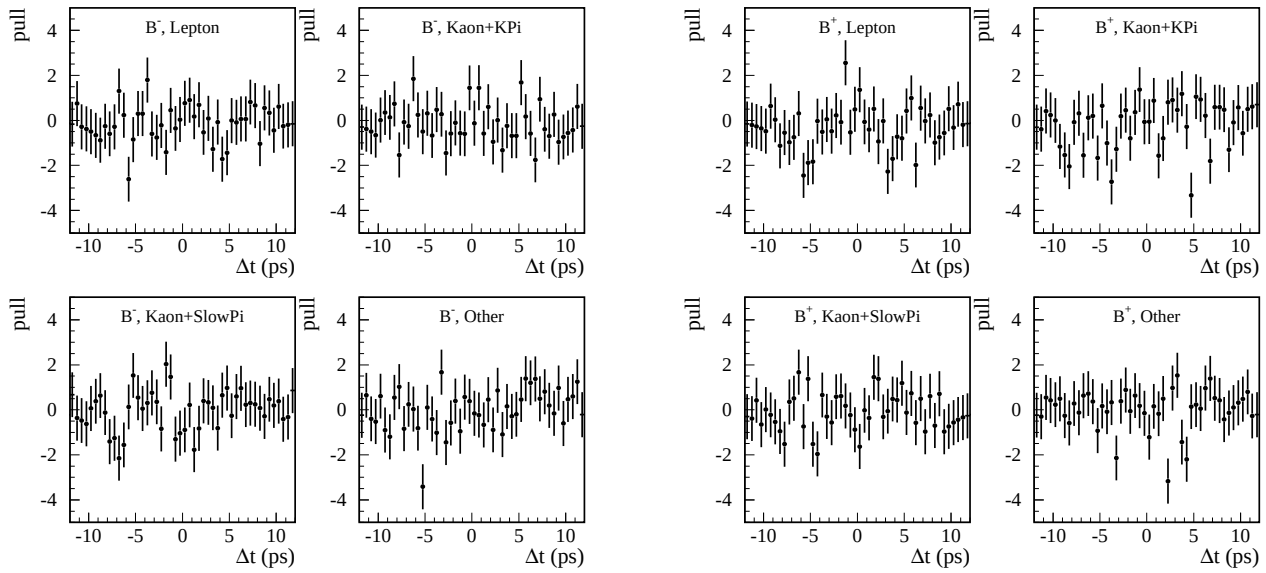

(a) (b)

Figure 22: Normalized residuals of the Δt projections of the nominal fit to the charged B data for (a) B^- and (b) B^+ events (signal region, $m_{ES} > 5.27$ GeV/c^2), for the different tagging categories (GG model).

7.1.4 Doubly-CKM-Suppressed decays

The expected relative amplitude of DCKM to favored decays, r_k and $\bar{r_k}$ ($k = tag, flav$), was fixed to 0.02, as our best estimate assuming that the amplitudes are dominated by the Standard Model $b \to c$ and $b \to u$ transitions, $|V_{ub}^* V_{cd}|\,/\,|V_{cb}^* V_{ud}|$, for the favored and suppressed decays, respectively (figure 1), using the CKM matrix elements values from [26] and neglecting corrections due to the ratio of the suppressed to allowed decay constants. We assumed the same value for tagging and reconstructed B sides. In the case of the `Lepton` tagging category, largely dominated by semileptonic decays (more than 95%) the values of of r_{tag} and $\bar{r}_{tag}$ were assumed to be 0.

7.1.5 $B^0 \to J/\psi K_L^0$ background parameters

Fit inputs to the $B_{CPK_L^0}$ sample are basically the same as those in [20]. More than 90% of the events that pass the K_L^0 selection cuts contain a real J/ψ[20]. Table 13 lists the signal and total inclusive J/ψ fractions, broken down by the top seven decay modes of the J/ψ, and the K_L^0 reconstruction type, for events that pass the selection cuts, in a window $|\Delta E| < 10$ MeV. The effective η_{CP} is also shown.

Events from the J/ψ dilepton invariant mass sideband are used to determine the properties of the non-J/ψ background. From a comparison of the flavor tagging efficiency in the data sideband with those of the B_{flav} data it is found that the lepton category tagging efficiency in the data sideband does not agree very well with those of the B_{flav} data (and inclusive J/ψ Monte Carlo). This is consequence of the loose PID requirement on the muons in the $J/\psi \to \mu\mu$ selection [20]. A a result of this difference, the sample composition has been splitted

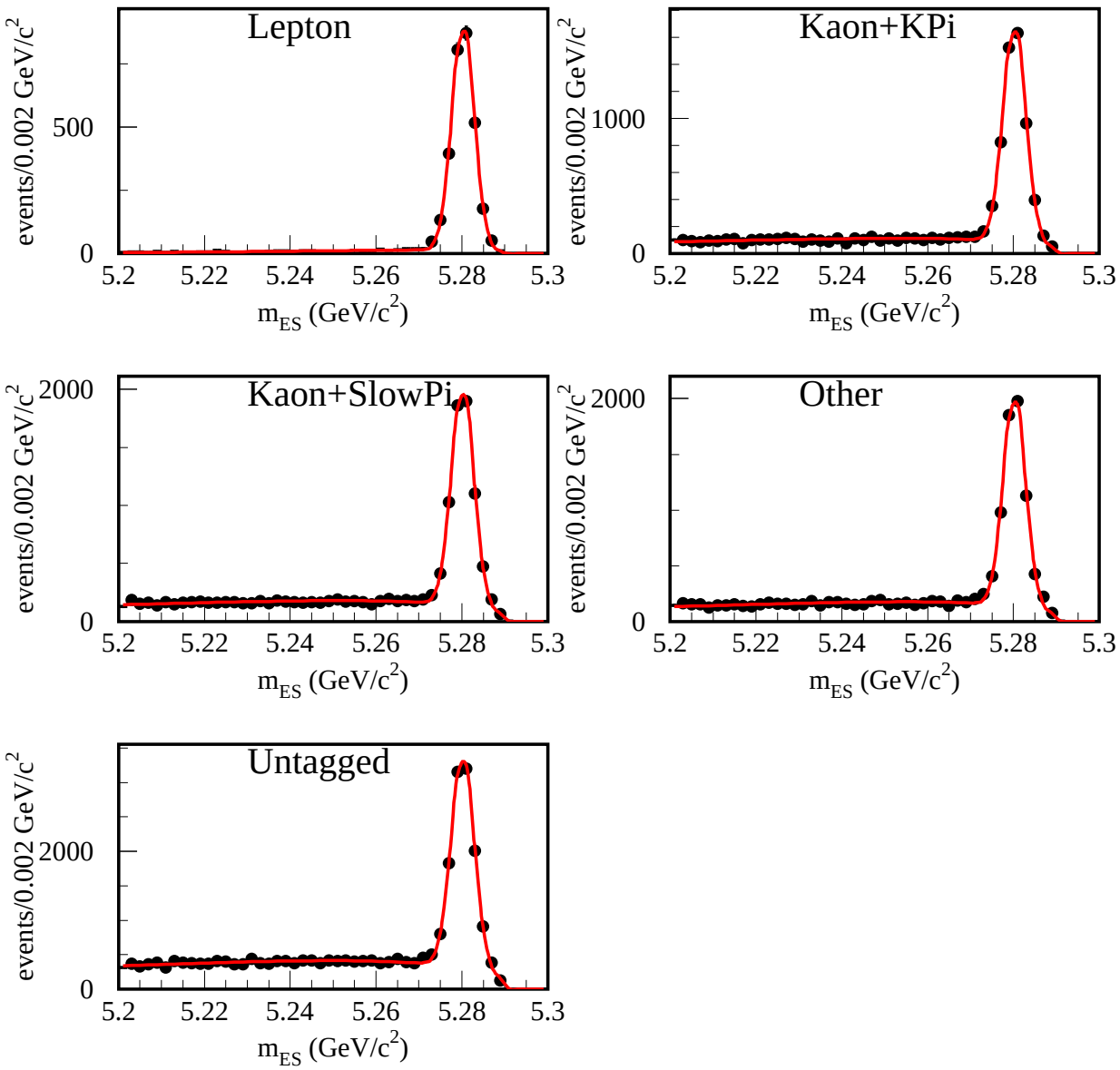

Figure 23: m_{ES} fits to each tagging category for the B_{flav} sample, after vertex cuts.

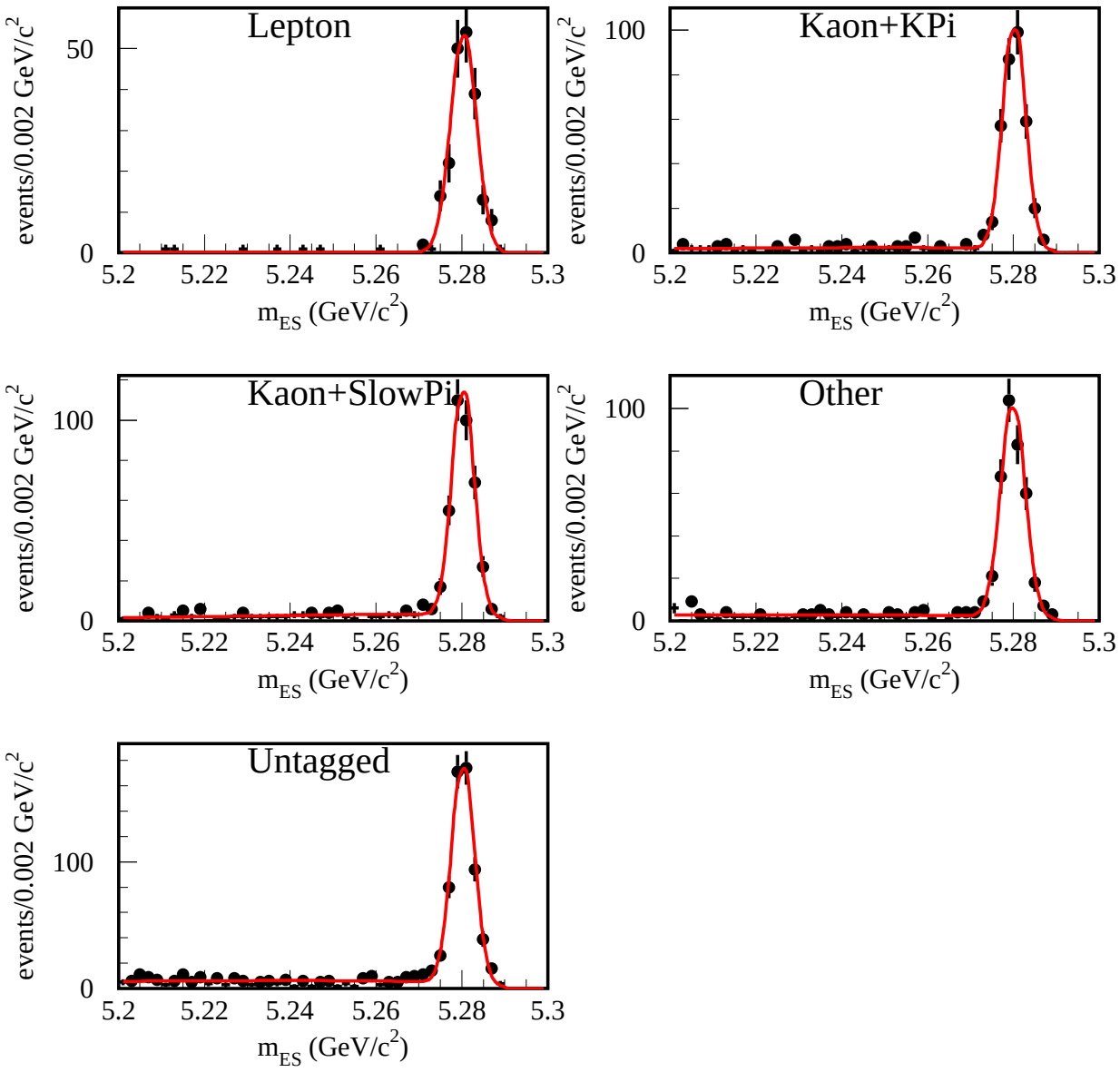

Figure 24: m_{ES} fits to each tagging category for the $B_{CPK^0_S}$ sample, after vertex cuts.

K_L type	EMC	IFR	η_{CP}
$J/\psi K_L$	0.622	0.732	+1
$J/\psi K^{*0}$	0.077	0.064	-0.68
$J/\psi K^{*+}$	0.109	0.114	0
$J/\psi K_s$	0.031	0.009	-1
$J/\psi K_L\pi^0$	0.004	0.002	0
$J/\psi K_L\pi^+$	0.004	0.007	0
$\chi_c K_L$	0.011	0.015	+1
$J/\psi X$ other	0.142	0.056	0
$non-J/\psi$	0	0	0.21(EMC)/0.24(IFR)

Table 13: Sample composition fractions for $J/\psi K_L$ inclusive charmonium Monte Carlo.

K_L type	EMC				IFR			
Tag type	Lepton		non-Lepton		Lepton		non-Lepton	
J/ψ mode	ee	$\mu\mu$	ee	$\mu\mu$	ee	$\mu\mu$	ee	$\mu\mu$
$J/\psi K_L$	0.4788	0.4696	0.5007	0.4746	0.6315	0.6270	0.6548	0.6440
$J/\psi K^{*0}$	0.0863	0.0840	0.0722	0.0679	0.0830	0.0826	0.0688	0.0678
$J/\psi K^{*+}$	0.1256	0.1223	0.1051	0.0988	0.1579	0.1570	0.1309	0.1290
$J/\psi K_s$	0.0610	0.0594	0.0510	0.0480	0.0104	0.0104	0.0086	0.0085
$J/\psi K_L\pi^0$	0.0052	0.0051	0.0044	0.0041	0.0026	0.0026	0.0022	0.0021
$J/\psi K_L\pi^+$	0.0062	0.0060	0.0051	0.0048	0.0055	0.0055	0.0046	0.0045
$\chi_c K_L$	0.0170	0.0166	0.0142	0.0134	0.0212	0.0210	0.0175	0.0173
$J/\psi X$ other	0.1821	0.1772	0.1523	0.1433	0.0641	0.0638	0.0532	0.0524
non-J/ψ	0.0379	0.0598	0.0949	0.1451	0.0238	0.0301	0.0593	0.0743

Table 14: Sample composition fractions for $J/\psi K_L$ data.

by flavor tag, allowing for the Lepton-tagged events to be treated separately from other events. The fractions for the non-Lepton tag categories are the same.

A binned likelihood fit to the ΔE spectrum in the data is used to determine the relative amounts of signal, inclusive J/ψ background and non-J/ψ background. In these fits, the signal and inclusive-J/ψ distributions are obtained from inclusive J/ψ Monte Carlo, while the non-J/ψ distribution is obtained from the J/ψ dilepton mass sideband. The fit is performed separately for each K_L^0 reconstruction type (EMC and IFR), due to differences in purity and background composition. The sample is further splitted into lepton type ($J/\psi \to e^+e^-$ and $J/\psi \to \mu^+\mu^-$). The $J/\psi \to ee$ and $J/\psi \to \mu\mu$ fits are performed simultaneously by constraining the ratio of $J/\psi K_L^0$ events to inclusive J/ψ events in $J/\psi \to ee$ and $J/\psi \to \mu\mu$ to be within the precision of the Monte Carlo [20]. The different inclusive J/ψ backgrounds from Monte Carlo are then renormalized to the J/ψ background fraction extracted from the data. The fractions are adjusted for Lepton-tagged and non-Lepton tagged events in order to adecuate for the observed differences in flavor tagging efficiencies in the J/ψ sideband events relative to the B_{flav} and inclusive J/ψ Monte Carlo (see [20] for details). The sample omposition fractions finally obtained with the procedure in the data are given in table 14.

The variable ΔE is used on an event-by-event basis to discriminate between signal and background. As the J/ψ Lepton type is not expected to influence the ΔE shape, the PDFs were used without regard to lepton type. The ΔE PDFs where used separately for EMC and IFR K_L^0 type, and they were grouped for $J/\psi K_L^0$ (signal), $J/\psi K_S^0$ background, J/ψ X background (excluding $J/\psi K_S^0$) and non-J/ψ. The ΔE PDF's are taken from the fits

contained in the hbook file:

```
/nfs/farm/babar/AWG/sin2b/data_run2/klong-input/de-pdfs-summer-2002-v1.hbook.
```

According to the studies reported in [20], the different decay modes contributing to the $J/\psi K_L^0$ mode are statistically consistent with having the same mistag fractions as in the B_{flav} sample. In this analysis, the resolution function of the signal and inclusive-J/ψ background was assumed to be same as for the B_{flav} sample. The resolution function for the non-J/ψ component (combinatoric in nature) was assumed the same as the prompt and non-prompt background components of the B_{flav} and $B_{CPK_S^0}$ samples. As the relative fraction of prompt to non-prompt component and the effective lifetime of the non-prompt in the non-J/ψ background are not necessarily the same as in the B_{flav} and $B_{CPK_S^0}$ samples, an external fit to the J/ψ dileptopn mass sideband was performed, and then were fixed in the nominal fit. The external fit was performed to all events using a *GG* resolution model with the scale of the tail Guassian, S_{tail}, fixed to 3.0. The results obtained are those reported in table 15. Therefore the prompt fraction and effective lifetime, input to the nominal fit, were, respectively, 0.68 ± 0.08 and 1.8 ± 0.3.

Parameter	Fit result
S_{core}	1.35 ± 0.10
δ_{core}	-0.00 ± 0.10
f_{tail}	0.04 ± 0.07
S_{tail}	3.0
δ_{tail}	-2 ± 3
$f_{outlier}$	0.011 ± 0.012
$f_{prompt,B_{CPK_L^0}}$	0.68 ± 0.08
$\tau_{non-prompt,B_{CPK_L^0}}$	1.8 ± 0.3

Table 15: Results from the external unbinned likelihood fit of the J/ψ dilepton mass sideband data, used to extract the fraction of prompt to non-prompt background and the effective lifetime for the non-J/ψ $J/\psi K_L^0$ background component.

7.1.6 Direct CP violation

The nominal fit includes in the PDF (via the parameters ν and μ^α) any possible violation of CP in the decay of tagging and flavor states (see section 2.5). In the case of CP eigenstates we assume CP conservation in the decay ($r_{CP,CP}$=1). A systematic error will be assigned due to this source by varying $r_{CP,CP}$ by $\pm$10%.

7.2 Analysis 1 results

Tables 16 and 17 report the fitted parameters for Analysis 1, for the *GG* and *GExp* resolution models, respectively (combined fit, B_{flav}+$B_{CPK_S^0}$+$B_{CPK_L^0}$). The unblind result for Δm is consistent with the *BABAR* hadronic mixing measurement [23] and the 2003 world average [24]. The difference between the *GG* and *GExp* resolution models, about 0.7σ (statistical), is due to the correlation of Δm with τ_B (-30%) and the slightly biased estimation of τ_B (towards low values) with the *GG* model, as discussed in section 8.1. The differences in the values of $\frac{\mathrm{Im}\lambda_{flav}}{|\lambda_{flav}|}$, $\frac{\mathrm{Im}\lambda_{flav}}{|\lambda_{flav}|}$, $\frac{\mathrm{Im}\lambda_{tag}}{|\lambda_{tag}|}$, $\frac{\mathrm{Im}\bar{\lambda}_{tag}}{|\lambda_{tag}|}$ between the two resolution models are due to the non-negligible correlation with the charm bias resolution function parameters, δ^α_{core} and τ^α_r (about 30% the larger). Tables 18 and 19 give the correlations among the 4 physics parameters, again for *GG* and *GExp*.

7.3 Analysis 2 results

Similarly, tables 20 and 21 report the fitted parameters from Analysis 2, for the *GG* and *GExp* resolution models, respectively (combined fit, B_{flav}+$B_{CPK^0_S}$+$B_{CPK^0_L}$). The unblind result for Δm is consistent with the *BABAR* hadronic mixing measurement [23] and the 2003 world average [24]. The difference between the *GG* and *GExp* resolution models, about 0.7σ (statistical), is due to the correlation of Δm with τ_B (-30%) and the slightly biased estimation of τ_B (towards low values) with the *GG* model, as discussed in section 8.1. The differences in the values of $\frac{\mathrm{Im}\lambda_{flav}}{|\lambda_{flav}|}$, $\frac{\mathrm{Im}\lambda_{flav}}{|\lambda_{flav}|}$, $\frac{\mathrm{Im}\lambda_{tag}}{|\lambda_{tag}|}$, $\frac{\mathrm{Im}\lambda_{tag}}{|\lambda_{tag}|}$ between the two resolution models are due to the non-negligible correlation with the charm bias resolution function parameters, δ^{α}_{core} and τ^{α}_{r} (about 30% the larger). Note the negligible change of Δm between Analysis 2 and Analysis 1. The differences in these same parameters between Analysis 1 and Analysis 2 are due to the correlation with Imz. Tables 22 and 23 give the correlations among the 6 physics parameters, again for *GG* and *GExp*.

The normalized residuals, defined as the difference between the data and the fit projection (nominal fit to all samples together) onto the Δt axis divided by the data error, for the B_{flav}, $B_{CPK^0_S}$ and $B_{CPK^0_L}$ samples and the different tagging categories (signal region, $m_{ES} > 5.27$ GeV/c^2 for B_{flav} and $B_{CPK^0_S}$, $\mid \Delta E \mid < 10$ MeV for $B_{CPK^0_L}$) are shown in figures 25, 26 and 27. The time distributions themselves are hidden.

7.4 Asymmetric (MINOS) errors

The statistical errors shown in all the previous tables are those obtained assuming that all the parameters are Gaussian. Deviations from an ideal Gaussian behaviour can be expected from toy Monte Carlo studies. It is therefore important to provide the asymmetric error estimates (MINOS). They can be found in tables 25, for the two analyses. None of the parameters is showing a significant asymmetric error behaviour.

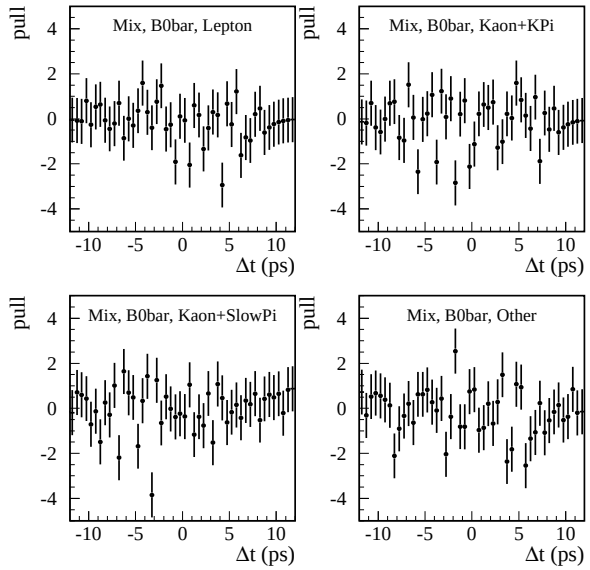

(a)

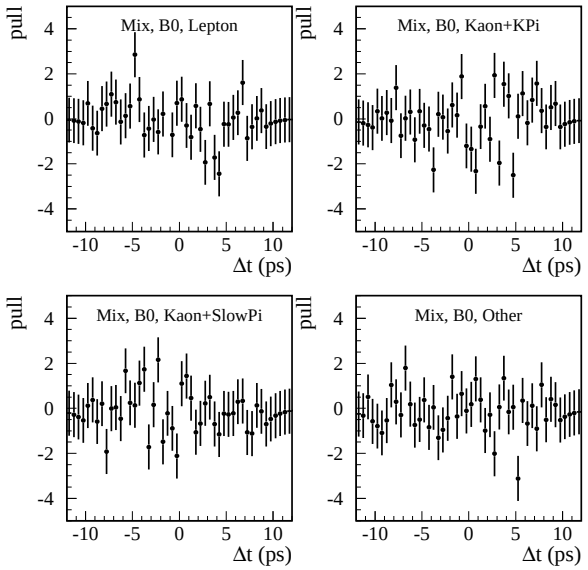

(b)

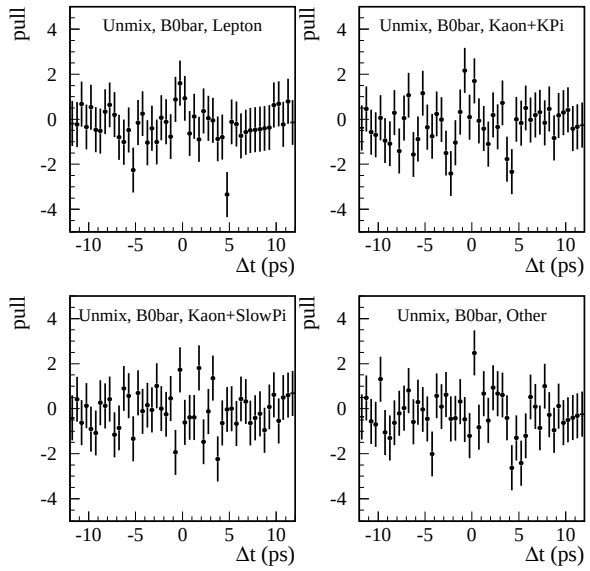

(c)

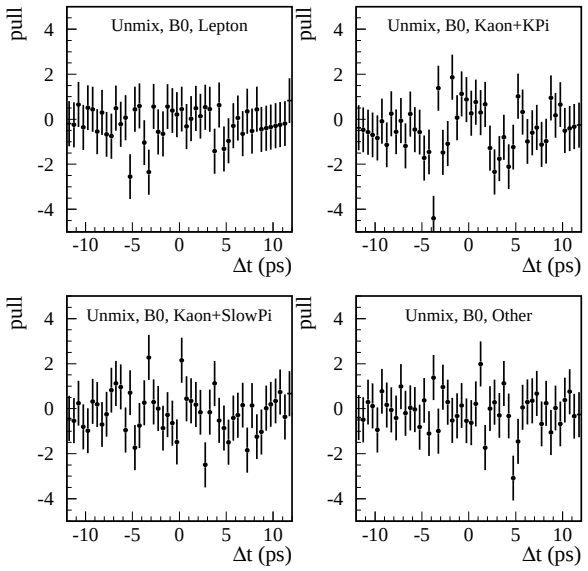

(d)

Figure 25: Normalized residuals of the Δt projections of the nominal fit (Analysis 2) for the B_{flav} sample: (a) mixed $\overline{B}^0$ tagged, (b) mixed B^0 tagged, (c) unmixed $\overline{B}^0$ tagged and (d) unmixed B^0 tagged (GG model), for each tagging category (signal region, $m_{ES} > 5.27$ GeV/c^2).

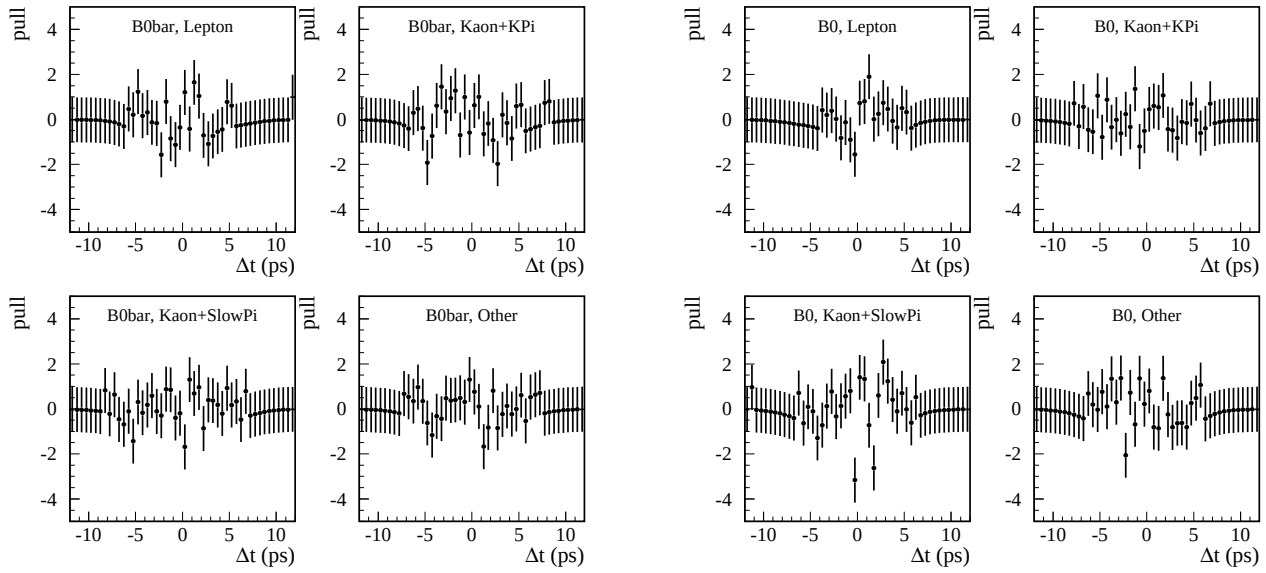

(a) (b)

Figure 26: Normalized residuals of the Δt projections of the nominal fit (Analysis 2) for the $B_{CPK^0_S}$ sample: (a) $\overline{B}^0$ tagged, (b) B^0 tagged (*GG* model), for each tagging category (signal region, $m_{ES} > 5.27$ GeV/c^2).

Parameter	B^0 fit results (GG model)
Δm	0.5253 ± 0.0076
$\Delta\Gamma/\Gamma$	-0.188 ± 0.037
$\mid q/p \mid$	0.925 ± 0.013
$\frac{\mathrm{Im}\lambda_{CP}}{\lvert\lambda_{CP}\rvert}$	0.339 ± 0.067
S_{core}	1.245 ± 0.039
$\delta_{core}^{\mathsf{Lepton}}$	$(2.3 \pm 6.5) \cdot 10^{-2}$
$\delta_{core}^{\mathsf{Kaon+KPi}}$	-0.273 ± 0.048
$\delta_{core}^{\mathsf{Kaon+SlowPi}}$	-0.322 ± 0.042
$\delta_{core}^{\mathsf{Other}}$	-0.295 ± 0.043
$\delta_{core}^{\mathsf{Untag}}$	-0.277 ± 0.033
f_{tail}	$(3.39 \pm 0.98) \cdot 10^{-2}$
S_{tail}	5.65 ± 0.81
δ_{tail}	-1.45 ± 0.49
$f_{outlier}$	$(0.8 \pm 1.2) \cdot 10^{-3}$
w_0^{Lepton}	$(2.59 \pm 0.65) \cdot 10^{-2}$
$w_0^{\mathsf{Kaon+KPi}}$	$(1.9 \pm 2.0) \cdot 10^{-2}$
$w_0^{\mathsf{Kaon+SlowPi}}$	0.158 ± 0.024
w_0^{Other}	0.264 ± 0.025
$w_{slope}^{\mathsf{Kaon+KPi}}$	0.133 ± 0.036
$w_{slope}^{\mathsf{Kaon+SlowPi}}$	$(7.1 \pm 3.6) \cdot 10^{-2}$
$w_{slope}^{\mathsf{Other}}$	$(7.4 \pm 3.8) \cdot 10^{-2}$
$\Delta w^{\mathsf{Lepton}}$	$(-1.2 \pm 1.2) \cdot 10^{-2}$
$\Delta w^{\mathsf{Kaon+KPi}}$	$(-2.6 \pm 1.2) \cdot 10^{-2}$
$\Delta w^{\mathsf{Kaon+SlowPi}}$	$(-4.1 \pm 1.3) \cdot 10^{-2}$
$\Delta w^{\mathsf{Other}}$	$(-2.8 \pm 1.3) \cdot 10^{-2}$
ν	$(9.9 \pm 8.3) \cdot 10^{-3}$
μ^{Lepton}	$(2.3 \pm 2.2) \cdot 10^{-2}$
$\mu^{\mathsf{Kaon+KPi}}$	$(-2.2 \pm 1.7) \cdot 10^{-2}$
$\mu^{\mathsf{Kaon+SlowPi}}$	$(1.4 \pm 1.6) \cdot 10^{-2}$
μ^{Other}	$(1.4 \pm 1.6) \cdot 10^{-2}$

Parameter	B^0 fit results (GG model)
$\frac{\mathrm{Im}\lambda_{flav}}{\lvert\lambda_{flav}\rvert}$	1.42 ± 0.94
$\frac{\mathrm{Im}\lambda_{flav}}{\lvert\lambda_{flav}\rvert}$	0.15 ± 0.94
$\frac{\mathrm{Im}\lambda_{tag}}{\lvert\lambda_{tag}\rvert}$	0.46 ± 0.98
$\frac{\mathrm{Im}\lambda_{tag}}{\lvert\lambda_{tag}\rvert}$	0.8 ± 1.0
$f_{prompt,B_{flav}}^{\mathsf{Lepton}}$	0.251 ± 0.065
$f_{prompt,B_{flav}}^{\mathsf{Kaon+KPi}}$	0.601 ± 0.022
$f_{prompt,B_{flav}}^{\mathsf{Kaon+SlowPi}}$	0.622 ± 0.020
$f_{prompt,B_{flav}}^{\mathsf{Other}}$	0.651 ± 0.019
$f_{prompt,B_{flav}}^{\mathsf{Untag}}$	0.704 ± 0.015
S_{back}	1.334 ± 0.014
δ_{back}	$(-3.41 \pm 0.97) \cdot 10^{-2}$
$f_{back,outlier}$	$(1.40 \pm 0.14) \cdot 10^{-2}$
$w_{0,prompt}^{\mathsf{Lepton}}$	-0.21 ± 0.14
$w_{0,prompt}^{\mathsf{Kaon+KPi}}$	0.173 ± 0.015
$w_{0,prompt}^{\mathsf{Kaon+SlowPi}}$	0.304 ± 0.012
$w_{0,prompt}^{\mathsf{Other}}$	0.419 ± 0.012
$w_{0,non-prompt}^{\mathsf{Lepton}}$	0.397 ± 0.046
$w_{0,non-prompt}^{\mathsf{Kaon+KPi}}$	0.352 ± 0.022
$w_{0,non-prompt}^{\mathsf{Kaon+SlowPi}}$	0.342 ± 0.019
$w_{0,non-prompt}^{\mathsf{Other}}$	0.465 ± 0.021
$\tau_{non-prompt}$	1.313 ± 0.037
$\tau_{non-prompt,B_{CPK_S^0}}$	1.63 ± 0.27
$f_{prompt,J/\psi K_S(\pi^+\pi^-)}$	0.587 ± 0.077
$f_{prompt,J/\psi K_S(\pi^0\pi^0)}$	0.622 ± 0.087
$f_{prompt,\psi(2S)K_S}$	0.69 ± 0.17
$f_{prompt,\chi_{c1}K_S}$	0.22 ± 0.25

Table 16: Analysis 1 results, GG resolution model.

Parameter	B^0 fit results (*GExp* model)
Δm	0.5198 ± 0.0076
$\Delta\Gamma/\Gamma$	-0.180 ± 0.041
$\mid q/p \mid$	0.923 ± 0.013
$\frac{\mathrm{Im}\lambda_{CP}}{\mid\lambda_{CP}\mid}$	0.339 ± 0.066
S	1.125 ± 0.035
τ_r^{Lepton}	2.5 ± 1.4
$\tau_r^{\mathrm{Kaon+KPi}}$	1.09 ± 0.29
$\tau_r^{\mathrm{Kaon+SlowPi}}$	1.28 ± 0.21
τ_r^{Other}	2.17 ± 0.34
τ_r^{Untag}	1.88 ± 0.27
$f_{Exp}^{\mathrm{Lepton}}$	$(3.6 \pm 3.2) \cdot 10^{-2}$
$f_{Exp}^{\mathrm{Kaon+KPi}}$	0.284 ± 0.088
$f_{Exp}^{\mathrm{Kaon+SlowPi}}$	0.289 ± 0.058
f_{Exp}^{Other}	0.163 ± 0.035
f_{Exp}^{Untag}	0.174 ± 0.031
$f_{outlier}$	$(3.6 \pm 1.1) \cdot 10^{-3}$
w_0^{Lepton}	$(2.93 \pm 0.65) \cdot 10^{-2}$
$w_0^{\mathrm{Kaon+KPi}}$	$(2.1 \pm 2.0) \cdot 10^{-2}$
$w_0^{\mathrm{Kaon+SlowPi}}$	0.161 ± 0.024
w_0^{Other}	0.265 ± 0.025
$w_{slope}^{\mathrm{Kaon+KPi}}$	0.134 ± 0.036
$w_{slope}^{\mathrm{Kaon+SlowPi}}$	$(6.9 \pm 3.6) \cdot 10^{-2}$
$w_{slope}^{\mathrm{Other}}$	$(7.1 \pm 3.8) \cdot 10^{-2}$
$\Delta w^{\mathrm{Lepton}}$	$(-1.2 \pm 1.2) \cdot 10^{-2}$
$\Delta w^{\mathrm{Kaon+KPi}}$	$(-2.4 \pm 1.2) \cdot 10^{-2}$
$\Delta w^{\mathrm{Kaon+SlowPi}}$	$(-4.1 \pm 1.3) \cdot 10^{-2}$
$\Delta w^{\mathrm{Other}}$	$(-2.8 \pm 1.3) \cdot 10^{-2}$
ν	$(1.05 \pm 0.83) \cdot 10^{-2}$
μ^{Lepton}	$(2.4 \pm 2.2) \cdot 10^{-2}$
$\mu^{\mathrm{Kaon+KPi}}$	$(-2.1 \pm 1.7) \cdot 10^{-2}$
$\mu^{\mathrm{Kaon+SlowPi}}$	$(1.4 \pm 1.6) \cdot 10^{-2}$
μ^{Other}	$(1.5 \pm 1.6) \cdot 10^{-2}$

Parameter	B^0 fit results (*GExp* model)
$\frac{\mathrm{Im}\lambda_{flav}}{\mid\lambda_{flav}\mid}$	0.98 ± 0.90
$\frac{\mathrm{Im}\lambda_{flav}}{\mid\lambda_{flav}\mid}$	-0.36 ± 0.91
$\frac{\mathrm{Im}\lambda_{tag}}{\mid\lambda_{tag}\mid}$	0.13 ± 0.95
$\frac{\mathrm{Im}\lambda_{tag}}{\mid\lambda_{tag}\mid}$	0.41 ± 0.98
$f_{prompt,B_{flav}}^{\mathrm{Lepton}}$	0.236 ± 0.068
$f_{prompt,B_{flav}}^{\mathrm{Kaon+KPi}}$	0.614 ± 0.024
$f_{prompt,B_{flav}}^{\mathrm{Kaon+SlowPi}}$	0.639 ± 0.021
$f_{prompt,B_{flav}}^{\mathrm{Other}}$	0.668 ± 0.020
$f_{prompt,B_{flav}}^{\mathrm{Untag}}$	0.725 ± 0.016
S_{back}	1.323 ± 0.014
$\tau_{r,back}$	2.39 ± 0.25
$f_{back,outlier}$	$(1.19 \pm 0.14) \cdot 10^{-2}$
$w_{0,prompt}^{\mathrm{Lepton}}$	-0.25 ± 0.17
$w_{0,prompt}^{\mathrm{Kaon+KPi}}$	0.170 ± 0.015
$w_{0,prompt}^{\mathrm{Kaon+SlowPi}}$	0.303 ± 0.013
$w_{0,prompt}^{\mathrm{Other}}$	0.420 ± 0.013
$w_{0,non-prompt}^{\mathrm{Lepton}}$	0.397 ± 0.047
$w_{0,non-prompt}^{\mathrm{Kaon+KPi}}$	0.362 ± 0.024
$w_{0,non-prompt}^{\mathrm{Kaon+SlowPi}}$	0.345 ± 0.021
$w_{0,non-prompt}^{\mathrm{Other}}$	0.466 ± 0.023
$\tau_{non-prompt}$	1.257 ± 0.039
$\tau_{non-prompt}$	1.257 ± 0.039
$\tau_{non-prompt,B_{CPK_S^0}}$	1.60 ± 0.29
$f_{prompt,J/\psi K_S(\pi^+\pi^-)}$	0.599 ± 0.080
$f_{prompt,J/\psi K_S(\pi^0\pi^0)}$	0.654 ± 0.091
$f_{prompt,\psi(2S)K_S}$	0.71 ± 0.18
$f_{prompt,\chi_{c1}K_S}$	0.23 ± 0.26

Table 17: Analysis 1 results, *GExp* resolution model.

	$\Delta\Gamma/\Gamma$	$\mid q/p \mid$	$\frac{\mathrm{Im}\lambda_{CP}}{\mid\lambda_{CP}\mid}$
Δm	-0.9%	-2.8%	-5.3%
$\Delta\Gamma/\Gamma$		10.7%	0.2%
$\mid q/p \mid$			-1.5%

Table 18: Correlations among the 4 physics parameters, Analysis 1, *GG* resolution model.

	$\Delta\Gamma/\Gamma$	$\mid q/p \mid$	$\frac{\mathrm{Im}\lambda_{CP}}{\mid\lambda_{CP}\mid}$
Δm	-1.5%	-3.4%	-5.0%
$\Delta\Gamma/\Gamma$		11.8%	2.2%
$\mid q/p \mid$			-1.5%

Table 19: Correlations among the 4 physics parameters, Analysis 1, *GExp* resolution model.

Parameter	B^0 fit results (*GG* model)
Δm	0.5254 ± 0.0076
$\Delta\Gamma/\Gamma$	-0.189 ± 0.037
$\mid q/p \mid$	0.925 ± 0.013
$\frac{\mathrm{Im}\lambda_{CP}}{\lvert\lambda_{CP}\rvert}$	0.327 ± 0.066
$\frac{\mathrm{Re}\lambda_{CP}}{\lvert\lambda_{CP}\rvert}\mathrm{Rez}$	-0.120 ± 0.035
Imz	0.258 ± 0.029
S_{core}	1.245 ± 0.039
$\delta_{core}^{\mathsf{Lepton}}$	$(2.3 \pm 6.5) \cdot 10^{-2}$
$\delta_{core}^{\mathsf{Kaon+KPi}}$	-0.273 ± 0.048
$\delta_{core}^{\mathsf{Kaon+SlowPi}}$	-0.322 ± 0.042
$\delta_{core}^{\mathsf{Other}}$	-0.295 ± 0.043
$\delta_{core}^{\mathsf{Untag}}$	-0.277 ± 0.033
f_{tail}	$(3.40 \pm 0.98) \cdot 10^{-2}$
S_{tail}	5.65 ± 0.80
δ_{tail}	-1.45 ± 0.49
$f_{outlier}$	$(0.8 \pm 1.2) \cdot 10^{-3}$
w_0^{Lepton}	$(2.59 \pm 0.65) \cdot 10^{-2}$
$w_0^{\mathsf{Kaon+KPi}}$	$(2.0 \pm 2.0) \cdot 10^{-2}$
$w_0^{\mathsf{Kaon+SlowPi}}$	0.159 ± 0.024
w_0^{Other}	0.265 ± 0.025
$w_{slope}^{\mathsf{Kaon+KPi}}$	0.133 ± 0.036
$w_{slope}^{\mathsf{Kaon+SlowPi}}$	$(7.1 \pm 3.6) \cdot 10^{-2}$
$w_{slope}^{\mathsf{Other}}$	$(7.4 \pm 3.8) \cdot 10^{-2}$
$\Delta w^{\mathsf{Lepton}}$	$(-1.2 \pm 1.2) \cdot 10^{-2}$
$\Delta w^{\mathsf{Kaon+KPi}}$	$(-2.7 \pm 1.3) \cdot 10^{-2}$
$\Delta w^{\mathsf{Kaon+SlowPi}}$	$(-4.2 \pm 1.3) \cdot 10^{-2}$
$\Delta w^{\mathsf{Other}}$	$(-2.9 \pm 1.3) \cdot 10^{-2}$
ν	$(1.11 \pm 0.84) \cdot 10^{-2}$
μ^{Lepton}	$(2.4 \pm 2.2) \cdot 10^{-2}$
$\mu^{\mathsf{Kaon+KPi}}$	$(-2.2 \pm 1.7) \cdot 10^{-2}$
$\mu^{\mathsf{Kaon+SlowPi}}$	$(1.4 \pm 1.6) \cdot 10^{-2}$
μ^{Other}	$(1.4 \pm 1.6) \cdot 10^{-2}$

Parameter	B^0 fit results (*GG* model)
$\frac{\mathrm{Im}\lambda_{flav}}{\lvert\lambda_{flav}\rvert}$	2.3 ± 1.1
$\frac{\mathrm{Im}\lambda_{flav}}{\lvert\lambda_{flav}\rvert}$	-0.6 ± 1.1
$\frac{\mathrm{Im}\lambda_{tag}}{\lvert\lambda_{tag}\rvert}$	1.5 ± 1.2
$\frac{\mathrm{Im}\lambda_{tag}}{\lvert\lambda_{tag}\rvert}$	-0.1 ± 1.2
$f_{prompt,B_{flav}}^{\mathsf{Lepton}}$	0.252 ± 0.065
$f_{prompt,B_{flav}}^{\mathsf{Kaon+KPi}}$	0.601 ± 0.022
$f_{prompt,B_{flav}}^{\mathsf{Kaon+SlowPi}}$	0.622 ± 0.020
$f_{prompt,B_{flav}}^{\mathsf{Other}}$	0.651 ± 0.019
$f_{prompt,B_{flav}}^{\mathsf{Untag}}$	0.704 ± 0.015
S_{back}	1.334 ± 0.014
δ_{back}	$(-3.41 \pm 0.97) \cdot 10^{-2}$
$f_{back,outlier}$	$(1.40 \pm 0.14) \cdot 10^{-2}$
$w_{0,prompt}^{\mathsf{Lepton}}$	-0.21 ± 0.14
$w_{0,prompt}^{\mathsf{Kaon+KPi}}$	0.173 ± 0.015
$w_{0,prompt}^{\mathsf{Kaon+SlowPi}}$	0.304 ± 0.012
$w_{0,prompt}^{\mathsf{Other}}$	0.419 ± 0.012
$w_{0,non-prompt}^{\mathsf{Lepton}}$	0.397 ± 0.047
$w_{0,non-prompt}^{\mathsf{Kaon+KPi}}$	0.352 ± 0.022
$w_{0,non-prompt}^{\mathsf{Kaon+SlowPi}}$	0.342 ± 0.019
$w_{0,non-prompt}^{\mathsf{Other}}$	0.465 ± 0.021
$\tau_{non-prompt}$	1.313 ± 0.037
$\tau_{non-prompt,B_{CPK_S^0}}$	1.63 ± 0.27
$f_{prompt,J/\psi K_S(\pi^+\pi^-)}$	0.587 ± 0.077
$f_{prompt,J/\psi K_S(\pi^0\pi^0)}$	0.622 ± 0.087
$f_{prompt,\psi(2S)K_S}$	0.69 ± 0.17
$f_{prompt,\chi_{c1}K_S}$	0.22 ± 0.25

Table 20: Analysis 2 results, *GG* resolution model.

Parameter	B^0 fit results (*GExp* model)
Δm	0.5201 ± 0.0076
$\Delta\Gamma/\Gamma$	-0.182 ± 0.042
$\mid q/p \mid$	0.924 ± 0.013
$\frac{\mathrm{Im}\lambda_{CP}}{\mid\lambda_{CP}\mid}$	0.328 ± 0.065
$\frac{\mathrm{Re}\lambda_{CP}}{\mid\lambda_{CP}\mid}\mathrm{Re}z$	-0.112 ± 0.041
$\mathrm{Im}z$	0.262 ± 0.029
S	1.125 ± 0.035
τ_r^{Lepton}	2.5 ± 1.4
$\tau_r^{\mathrm{Kaon+KPi}}$	1.09 ± 0.29
$\tau_r^{\mathrm{Kaon+SlowPi}}$	1.28 ± 0.21
τ_r^{Other}	2.17 ± 0.34
τ_r^{Untag}	1.88 ± 0.27
$f_{Exp}^{\mathrm{Lepton}}$	$(3.6 \pm 3.2) \cdot 10^{-2}$
$f_{Exp}^{\mathrm{Kaon+KPi}}$	0.283 ± 0.088
$f_{Exp}^{\mathrm{Kaon+SlowPi}}$	0.290 ± 0.057
f_{Exp}^{Other}	0.164 ± 0.035
f_{Exp}^{Untag}	0.174 ± 0.031
$f_{outlier}$	$(3.6 \pm 1.1) \cdot 10^{-3}$
w_0^{Lepton}	$(2.93 \pm 0.65) \cdot 10^{-2}$
$w_0^{\mathrm{Kaon+KPi}}$	$(2.1 \pm 2.0) \cdot 10^{-2}$
$w_0^{\mathrm{Kaon+SlowPi}}$	0.162 ± 0.024
w_0^{Other}	0.266 ± 0.025
$w_{slope}^{\mathrm{Kaon+KPi}}$	0.134 ± 0.036
$w_{slope}^{\mathrm{Kaon+SlowPi}}$	$(6.9 \pm 3.6) \cdot 10^{-2}$
$w_{slope}^{\mathrm{Other}}$	$(7.1 \pm 3.8) \cdot 10^{-2}$
$\Delta w^{\mathrm{Lepton}}$	$(-1.2 \pm 1.2) \cdot 10^{-2}$
$\Delta w^{\mathrm{Kaon+KPi}}$	$(-2.5 \pm 1.3) \cdot 10^{-2}$
$\Delta w^{\mathrm{Kaon+SlowPi}}$	$(-4.1 \pm 1.3) \cdot 10^{-2}$
$\Delta w^{\mathrm{Other}}$	$(-2.8 \pm 1.3) \cdot 10^{-2}$
ν	$(1.09 \pm 0.83) \cdot 10^{-2}$
μ^{Lepton}	$(2.5 \pm 2.2) \cdot 10^{-2}$
$\mu^{\mathrm{Kaon+KPi}}$	$(-2.1 \pm 1.7) \cdot 10^{-2}$
$\mu^{\mathrm{Kaon+SlowPi}}$	$(1.4 \pm 1.6) \cdot 10^{-2}$
μ^{Other}	$(1.5 \pm 1.6) \cdot 10^{-2}$

Parameter	B^0 fit results (*GExp* model)
$\frac{\mathrm{Im}\lambda_{flav}}{\mid\lambda_{flav}\mid}$	1.8 ± 1.1
$\frac{\mathrm{Im}\lambda_{flav}}{\mid\lambda_{flav}\mid}$	-1.1 ± 1.1
$\frac{\mathrm{Im}\lambda_{tag}}{\mid\lambda_{tag}\mid}$	1.1 ± 1.2
$\frac{\mathrm{Im}\lambda_{tag}}{\mid\lambda_{tag}\mid}$	-0.4 ± 1.2
$f_{prompt,B_{flav}}^{\mathrm{Lepton}}$	0.236 ± 0.068
$f_{prompt,B_{flav}}^{\mathrm{Kaon+KPi}}$	0.614 ± 0.024
$f_{prompt,B_{flav}}^{\mathrm{Kaon+SlowPi}}$	0.639 ± 0.021
$f_{prompt,B_{flav}}^{\mathrm{Other}}$	0.668 ± 0.020
$f_{prompt,B_{flav}}^{\mathrm{Untag}}$	0.725 ± 0.016
S_{back}	1.323 ± 0.014
$\tau_{r,back}$	2.39 ± 0.25
$f_{back,outlier}$	$(1.19 \pm 0.14) \cdot 10^{-2}$
$w_{0,prompt}^{\mathrm{Lepton}}$	-0.25 ± 0.17
$w_{0,prompt}^{\mathrm{Kaon+KPi}}$	0.170 ± 0.015
$w_{0,prompt}^{\mathrm{Kaon+SlowPi}}$	0.303 ± 0.013
$w_{0,prompt}^{\mathrm{Other}}$	0.420 ± 0.013
$w_{0,non-prompt}^{\mathrm{Lepton}}$	0.397 ± 0.047
$w_{0,non-prompt}^{\mathrm{Kaon+KPi}}$	0.362 ± 0.024
$w_{0,non-prompt}^{\mathrm{Kaon+SlowPi}}$	0.345 ± 0.021
$w_{0,non-prompt}^{\mathrm{Other}}$	0.466 ± 0.023
$\tau_{non-prompt}$	1.257 ± 0.039
$\tau_{non-prompt}$	1.257 ± 0.039
$\tau_{non-prompt,B_{CPK_S^0}}$	1.60 ± 0.29
$f_{prompt,J/\psi K_S(\pi^+\pi^-)}$	0.599 ± 0.080
$f_{prompt,J/\psi K_S(\pi^0\pi^0)}$	0.654 ± 0.091
$f_{prompt,\psi(2S)K_S}$	0.71 ± 0.18
$f_{prompt,\chi_{c1}K_S}$	0.23 ± 0.26

Table 21: Analysis 2 results, *GExp* resolution model.

	$\Delta\Gamma/\Gamma$	$\mid q/p \mid$	$\frac{\mathrm{Im}\lambda_{CP}}{\mid\lambda_{CP}\mid}$	$\frac{\mathrm{Re}\lambda_{CP}}{\mid\lambda_{CP}\mid}$Rez	Imz
Δm	-1.3%	-2.8%	-5.6%	7.0%	-0.2%
$\Delta\Gamma/\Gamma$		11.0%	0.4%	-7.9%	-1.8%
$\mid q/p \mid$			-1.0%	-2.4%	-1.1%
$\frac{\mathrm{Im}\lambda_{CP}}{\mid\lambda_{CP}\mid}$				-10.9%	17.4%
$\frac{\mathrm{Re}\lambda_{CP}}{\mid\lambda_{CP}\mid}$Rez					-3.4%

Table 22: Correlations among the 6 physics parameters, Analysis 2, *GG* resolution model.

	$\Delta\Gamma/\Gamma$	$\mid q/p \mid$	$\frac{\mathrm{Im}\lambda_{CP}}{\mid\lambda_{CP}\mid}$	$\frac{\mathrm{Re}\lambda_{CP}}{\mid\lambda_{CP}\mid}$Rez	Imz
Δm	-2.7%	-3.7%	-5.4%	13.6%	-1.0%
$\Delta\Gamma/\Gamma$		12.9%	2.1%	-9.0%	-3.6%
$\mid q/p \mid$			-1.1%	-2.3%	-2.6%
$\frac{\mathrm{Im}\lambda_{CP}}{\mid\lambda_{CP}\mid}$				-10.6%	17.1%
$\frac{\mathrm{Re}\lambda_{CP}}{\mid\lambda_{CP}\mid}$Rez					-5.6%

Table 23: Correlations among the 6 physics parameters, Analysis 2, *GExp* resolution model.

	$\Delta\Gamma/\Gamma$	$\mid q/p \mid$	$\frac{\mathrm{Im}\lambda_{CP}}{\mid\lambda_{CP}\mid}$	$\frac{\mathrm{Re}\lambda_{CP}}{\mid\lambda_{CP}\mid}$Rez	Imz	$\frac{\mathrm{Im}\lambda_{flav}}{\mid\lambda_{flav}\mid}$	$\frac{\mathrm{Im}\overline{\lambda}_{flav}}{\mid\overline{\lambda}_{flav}\mid}$	$\frac{\mathrm{Im}\lambda_{tag}}{\mid\lambda_{tag}\mid}$	$\frac{\mathrm{Im}\overline{\lambda}_{tag}}{\mid\overline{\lambda}_{tag}\mid}$
Δm	-1.3%	-2.8%	-5.6%	7.0%	-0.2%	1.0%	1.5%	1.0%	2.2%
$\Delta\Gamma/\Gamma$		11.0%	0.4%	-7.9%	-1.8%	-0.6%	-1.4%	-0.0%	-0.4%
$\mid q/p \mid$			-1.0%	-2.4%	-1.1%	1.6%	1.3%	0.7%	2.3%
$\frac{\mathrm{Im}\lambda_{CP}}{\mid\lambda_{CP}\mid}$				-10.9%	17.4%	13.6%	-6.1%	14.4%	-5.5%
$\frac{\mathrm{Re}\lambda_{CP}}{\mid\lambda_{CP}\mid}$Rez					-3.4%	-1.4%	0.7%	-2.0%	0.6%
Imz						57.7%	-53.9%	61.6%	-56.6%
$\frac{\mathrm{Im}\lambda_{flav}}{\mid\lambda_{flav}\mid}$							3.9%	77.9%	9.8%
$\frac{\mathrm{Im}\overline{\lambda}_{flav}}{\mid\overline{\lambda}_{flav}\mid}$								9.2%	79.2%
$\frac{\mathrm{Im}\lambda_{tag}}{\mid\lambda_{tag}\mid}$									18.7%

Table 24: Correlations among the physics parameters and DCKM phases, Analysis 2, *GG* resolution model.

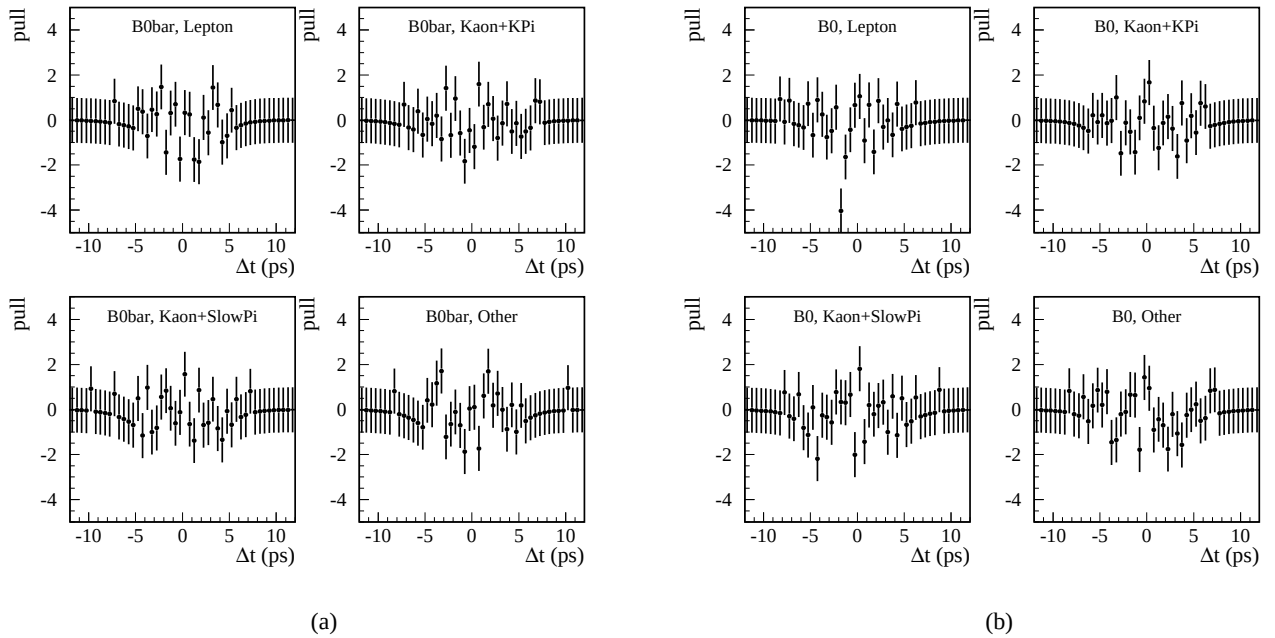

(a) (b)

Figure 27: Normalized residuals of the Δt projections of the nominal fit (Analysis 2) for the $B_{CPK^0_L}$ sample: (a) $\bar{B}^0$ tagged, (b) B^0 tagged (*GG* model), for each tagging category (signal region, $|\,\Delta E\,| < 10$ MeV).

Parameter	Analysis 1 *GG*	Analysis 2 *GG*
Δm	$0.5253^{+0.0076}_{-0.0076}$	$0.5254^{+0.0076}_{-0.0076}$
$\Delta\Gamma/\Gamma$	$-0.188^{+0.036}_{-0.037}$	$-0.189^{+0.037}_{-0.037}$
$\mid q/p \mid$	$0.925^{+0.013}_{-0.013}$	$0.925^{+0.013}_{-0.013}$
$\frac{\mathrm{Im}\lambda_{CP}}{\mid\lambda_{CP}\mid}$	$0.339^{+0.066}_{-0.067}$	$0.327^{+0.065}_{-0.067}$
$\frac{\mathrm{Re}\lambda_{CP}}{\mid\lambda_{CP}\mid}\mathrm{Re}z$	—	$-0.120^{+0.035}_{-0.035}$
$\mathrm{Im}z$	—	$0.258^{+0.029}_{-0.029}$

Table 25: Results with asymmetric errors from Analysis 1 and 2 data fits, *GG* model.

7.5 Goodness-of-fit and expected errors

The estimation of the goodness-of-fit and expected statistical errors has been done using a sofisticated toy Monte Carlo. The toy MC samples were made with exactly the same number of events per sample -B_{flav}, $B^0 \to J/\psi K_S^0(\pi^+\pi^-)$, $B^0 \to J/\psi K_S^0(\pi^0\pi^0)$, $B^0 \to \psi(2S) K_S^0$, χ_{c1} K_S^0, $B^0 \to J/\psi K_L^0$(IFR e^+e^-, IFR $\mu^+\mu^-$, EMC e^+e^-, EMC $\mu^+\mu^-$)- and tagging category -`Lepton, Kaon+KPi, Kaon+SlowPi, Other, UnTagged`- as the data sample. Each toy sample used the set of m_{ES} (ΔE) and $\sigma_{\Delta t}$ values taken from the non-K_L^0 (K_L^0) sample. The values of the physics parameters generated were those obtained from the data fit, after internal unblinding by the generation code. From the set of $m_{ES}(\Delta E)$ and $\sigma_{\Delta t}$ values the event is generated to be signal or background and B^0 or $\overline{B}^0$, using the time-integrated PDF within the Δt cut limits ($\pm$ 20 ps) with limited Δt resolution, equation (105), normalized according to (108) and (109). In this way the mistag rates for B^0 and $\overline{B}^0$, tagging-vertexing correlations, $B^0\overline{B}^0$ differences in reconstruction and tagging efficiencies, $B^0\overline{B}^0$ physics asymmetries (mainly $|\, q/p \,|$) and signal/background components are generated according to the values measured in the data [5]. The Δt distribution (truth+smearing) is finally generated for each event class and set of $m_{ES}(\Delta E)$ and $\sigma_{\Delta t}$ values.

Comparing the likelihood distribution coming from about 300 toy Monte Carlo experiments with the value obtained in the nominal data fit (see figure 28), the goodness-of-fit of the data is evaluated to be 73% for Analysis 1 and 76% for Analysis 2. Figures 29, 30, 31, 32 and 33 compare the likelihood distribition from the experiments and the data for each subsample separately, for Analysis 1 and 2.

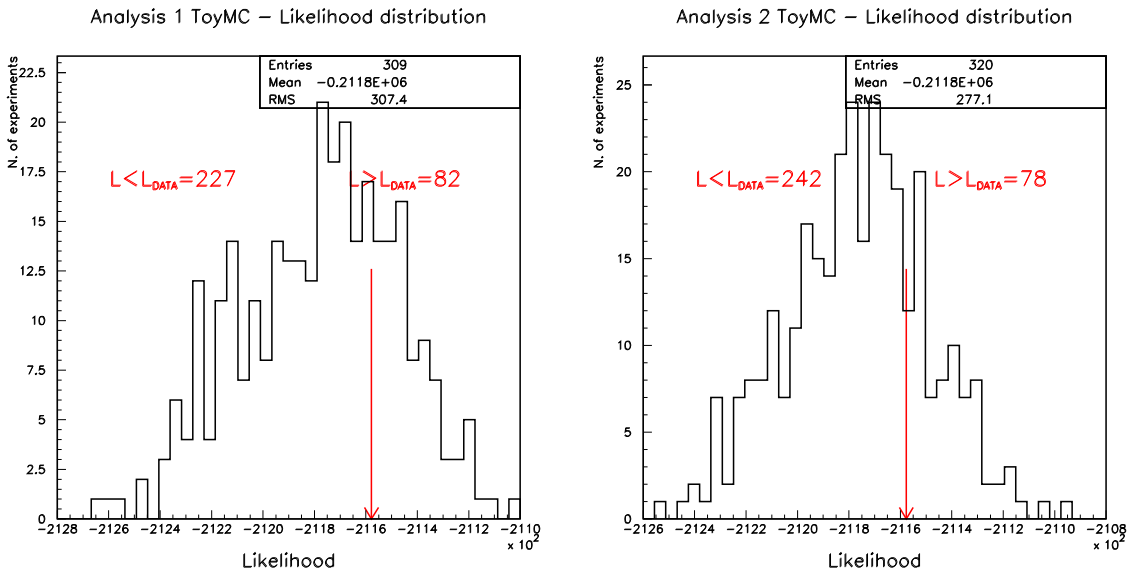

Figure 28: Likelihood distribution from toy Monte Carlo experiments (Analysis 1 and 2). The arrow shows the value obtained from the nominal data fit. The number of experiments with likelihood value smaller and greater than the data is quoted. The probability that the toy Monte Carlo experiments are less likely (larger negative log-likelihood) than the data is evaluated to be 73% for Analysis 1 and 76% for Analysis 2.

The (Gaussian) errors on the physical parameters coming from the toy Monte Carlo fits are compared with the RMS of the residual distribution and the errors extracted from the nominal data fit, as shown in figure 34,

[5] Let us note that all the signal and background components are fluctuated, while some of them are fixed in the nominal fit (peaking background fractions and $J/\psi K_L^0$ fractions). This implies that the toy Monte Carlo samples include fluctuations in quantities that are fixed in the fit. As a consequence, the RMS and fit errors are expected to be slightly larger than in the data, and the goodness-of-fit slightly overestimated. The gross effects are however already well reproduced by the toy samples.

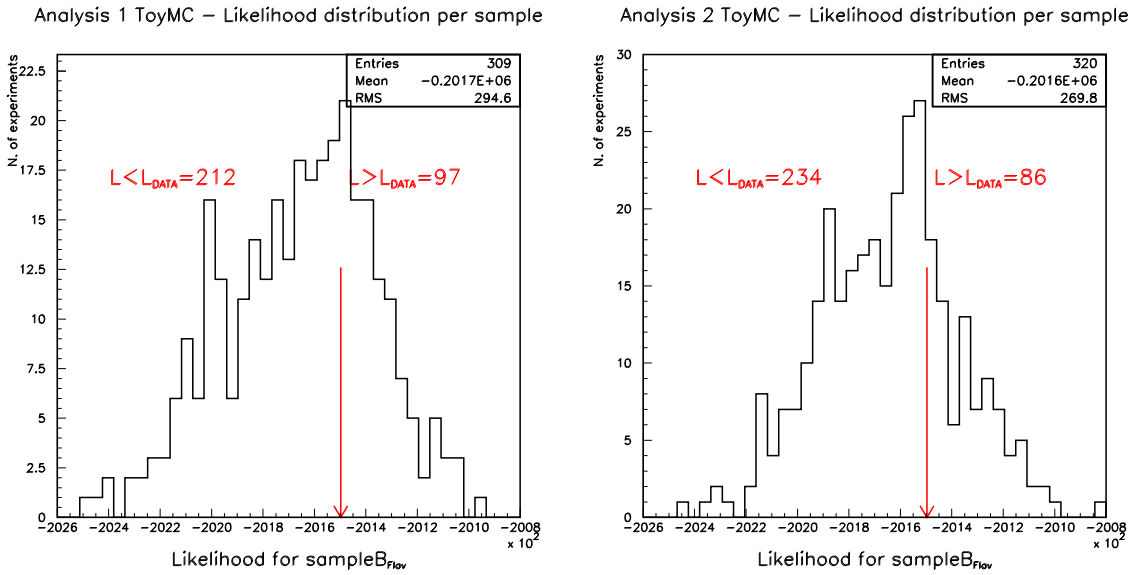

Figure 29: Likelihood distribution from toy Monte Carlo experiments (Analysis 1 and 2) for the B_{flav} sample only. The arrow shows the value obtained from the nominal data fit.

for Analysis 2 (similar distributions are obtained for Analysis 1). These figures deserve several remarks. First, Gaussian errors give a good estimate of the resolution as extracted from the RMS of the residual distributions, within 10%. The small deviations are due in part to statistical fluctuations and in part to small non-Gaussian effects. Second, there is a good agreement between the error extracted from the data sample fit and the Gaussian error distribution obtained from the toy samples. Third, the biases (if any) from the residual distributions are in all cases very small compared with the current statistical precision. The larger between the bias and its error will be assigned as systematic error due to the fitting procedure (see section 9.14).

The correlation coefficients and the scatter distributions among all the CPT/T/CP/oscillation parameters (here we also include the fitted Doubly-CKM-Suppressed parameters) from the toy Monte Carlo fits are also compared with the values extracted from the nominal data fit in figures 36 and 40, for Analysis 2. In all cases the data values fall into the expected range.

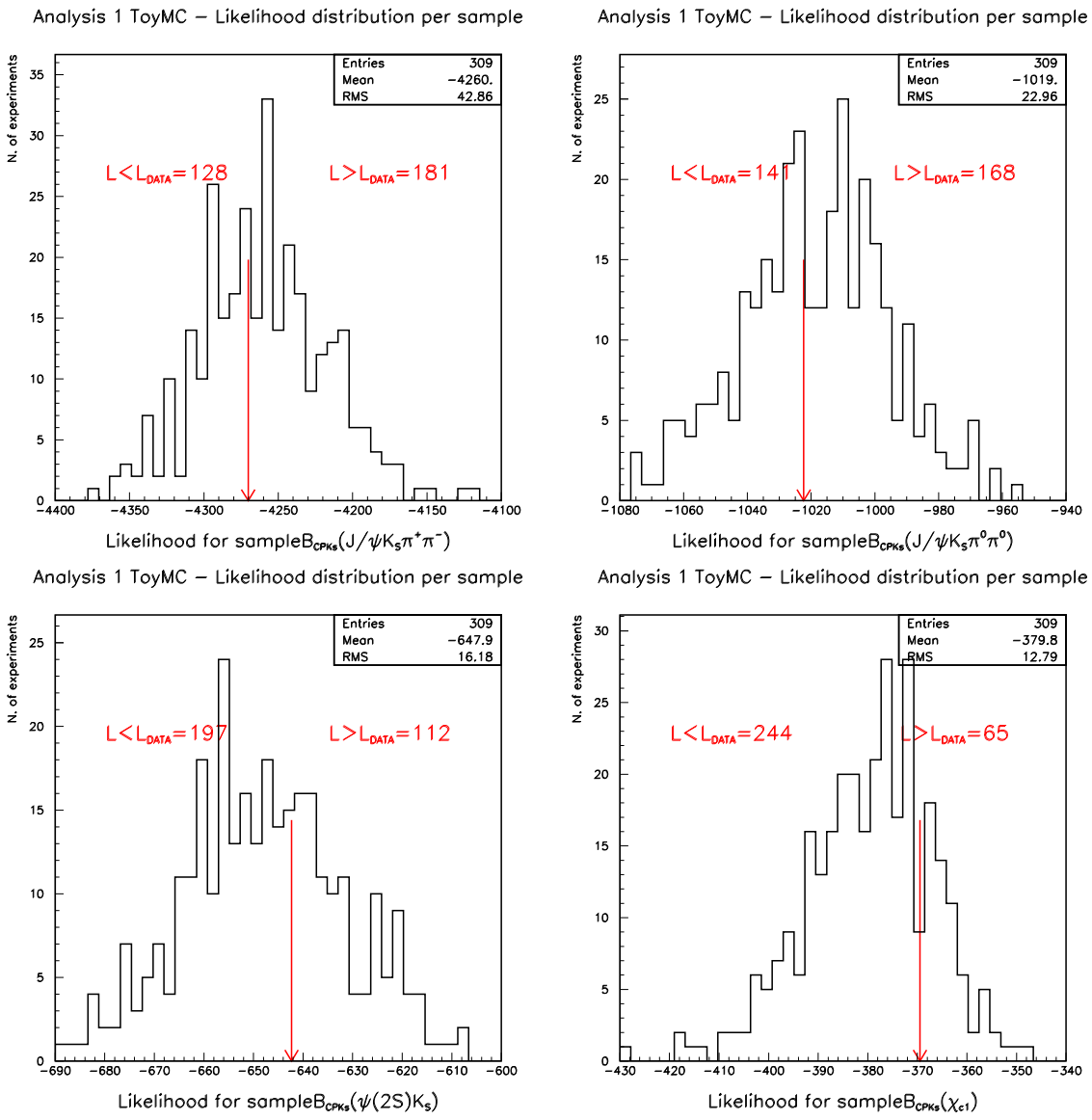

Figure 30: Likelihood distribution from toy Monte Carlo experiments (Analysis 1) for the $B_{CPK^0_S}$ subsamples. Channels are (from left to right and from top to bottom): $B^0 \to J/\psi K^0_S(\pi^+\pi^-)$, $B^0 \to J/\psi K^0_S(\pi^0\pi^0)$, $B^0 \to \psi(2S)K^0_S$, $B^0 \to \chi_{c1}\, K^0_S(\pi^+\pi^-)$. The arrow shows the value obtained from the nominal data fit.

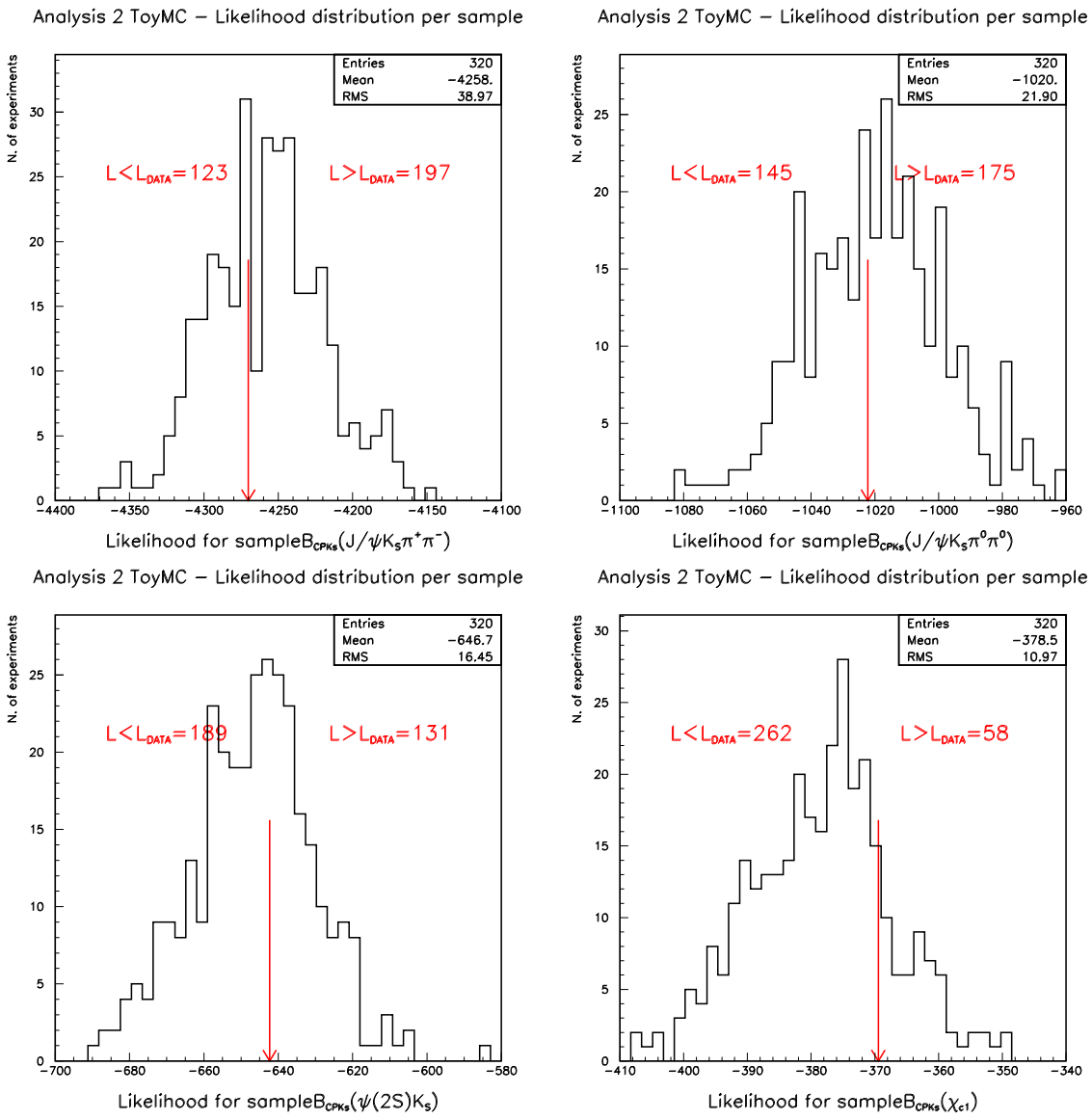

Figure 31: Likelihood distribution from toy Monte Carlo experiments (Analysis 2) for the $B_{CPK_S^0}$ subsamples. Channels are (from left to right and from top to bottom): $B^0 \to J/\psi K_S^0(\pi^+\pi^-)$, $B^0 \to J/\psi K_S^0(\pi^0\pi^0)$, $B^0 \to \psi(2S)K_S^0$, $B^0 \to \chi_{c1}\, K_S^0(\pi^+\pi^-)$. The arrow shows the value obtained from the nominal data fit.

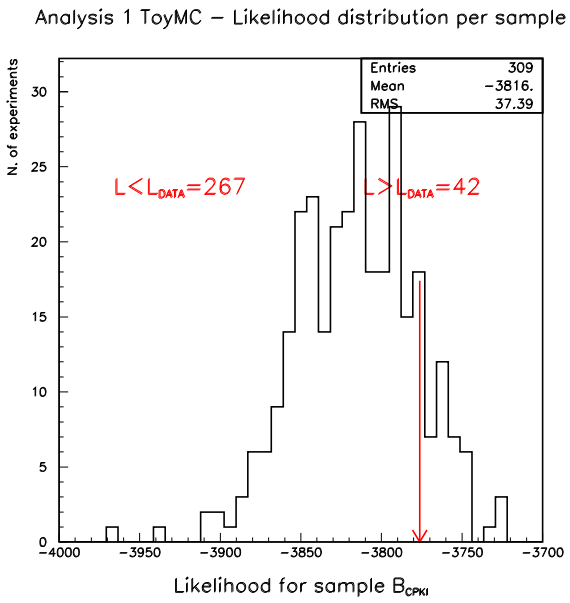

Figure 32: Likelihood distribution from toy Monte Carlo experiments (Analysis 1) for the $B_{CPK_L^0}$ subsample. The arrow shows the value obtained from the nominal data fit.

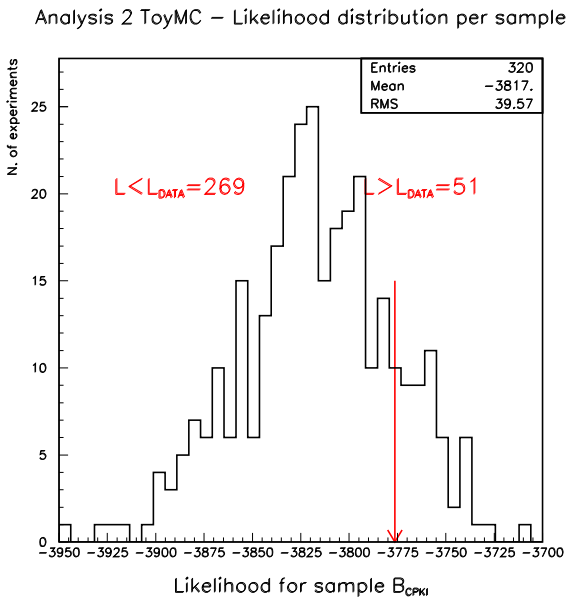

Figure 33: Likelihood distribution from toy Monte Carlo experiments (Analysis 2) for the $B_{CPK_L^0}$ subsamples. The arrow shows the value obtained from the nominal data fit.

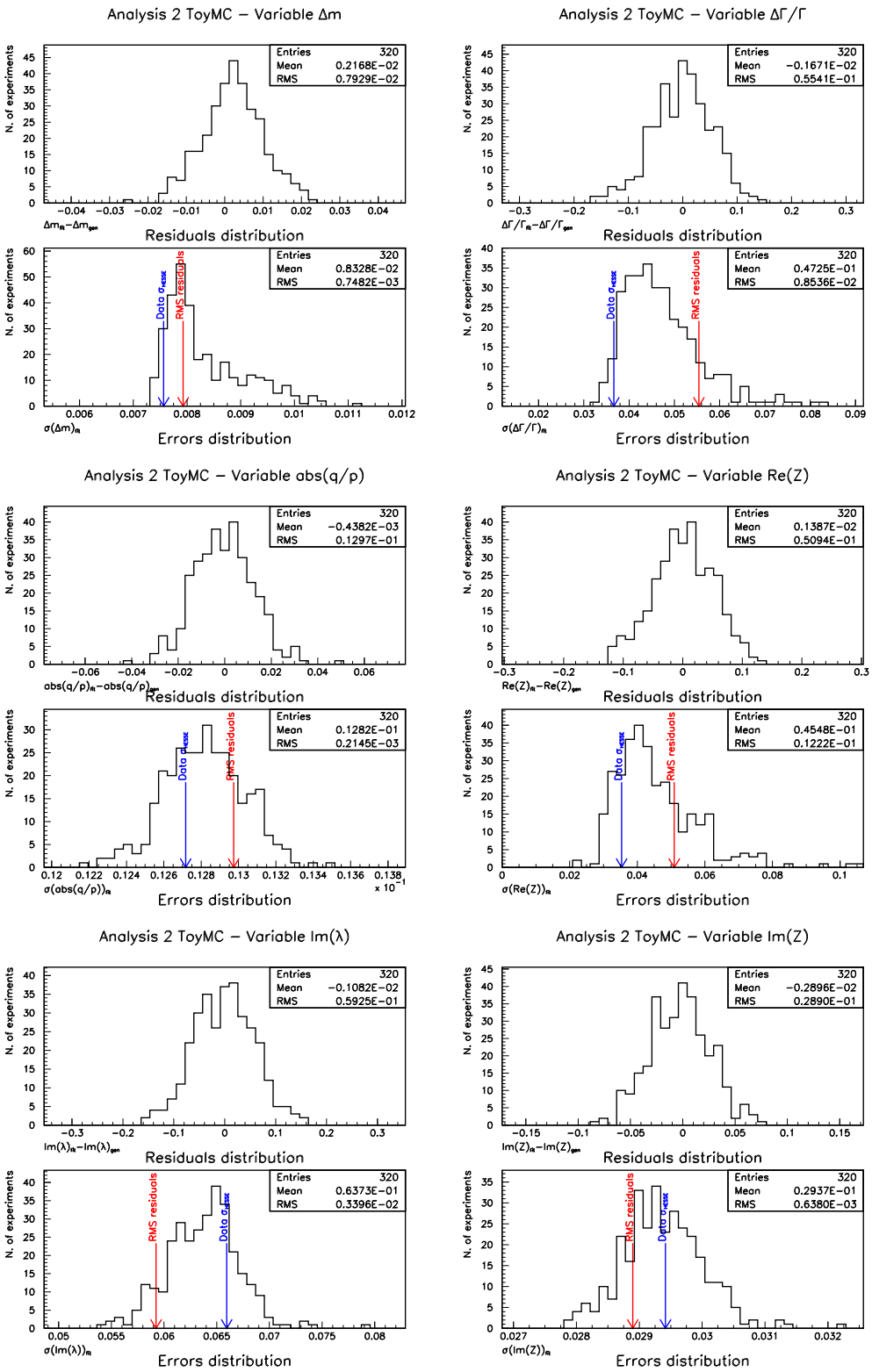

Figure 34: The residual and Gaussian error distributions for the oscillation/CPT/T/CP parameters from Analysis 2 of toy Monte Carlo experiments. In the error distribution indicated are the RMS of the residual distribution (red arrow) and the values of the Gaussian error (blue arrow) extracted from the data fit.

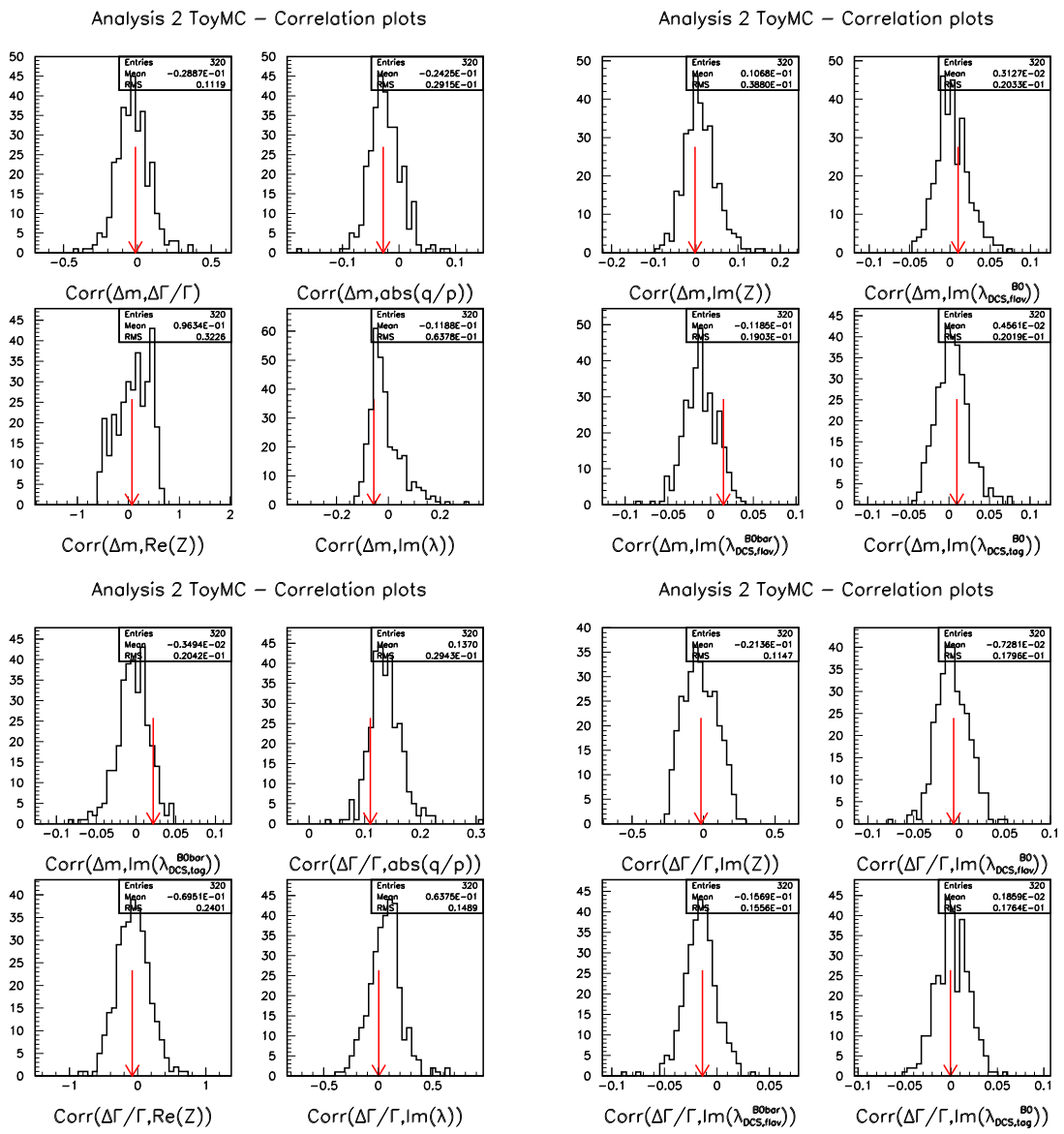

Figure 35: Distribution of the correlation coefficients among the physical and DCKM parameters from Analysis 2 of toy Monte Carlo experiments. The values corresponding to the nominal data fit (red arrow) are indicated.

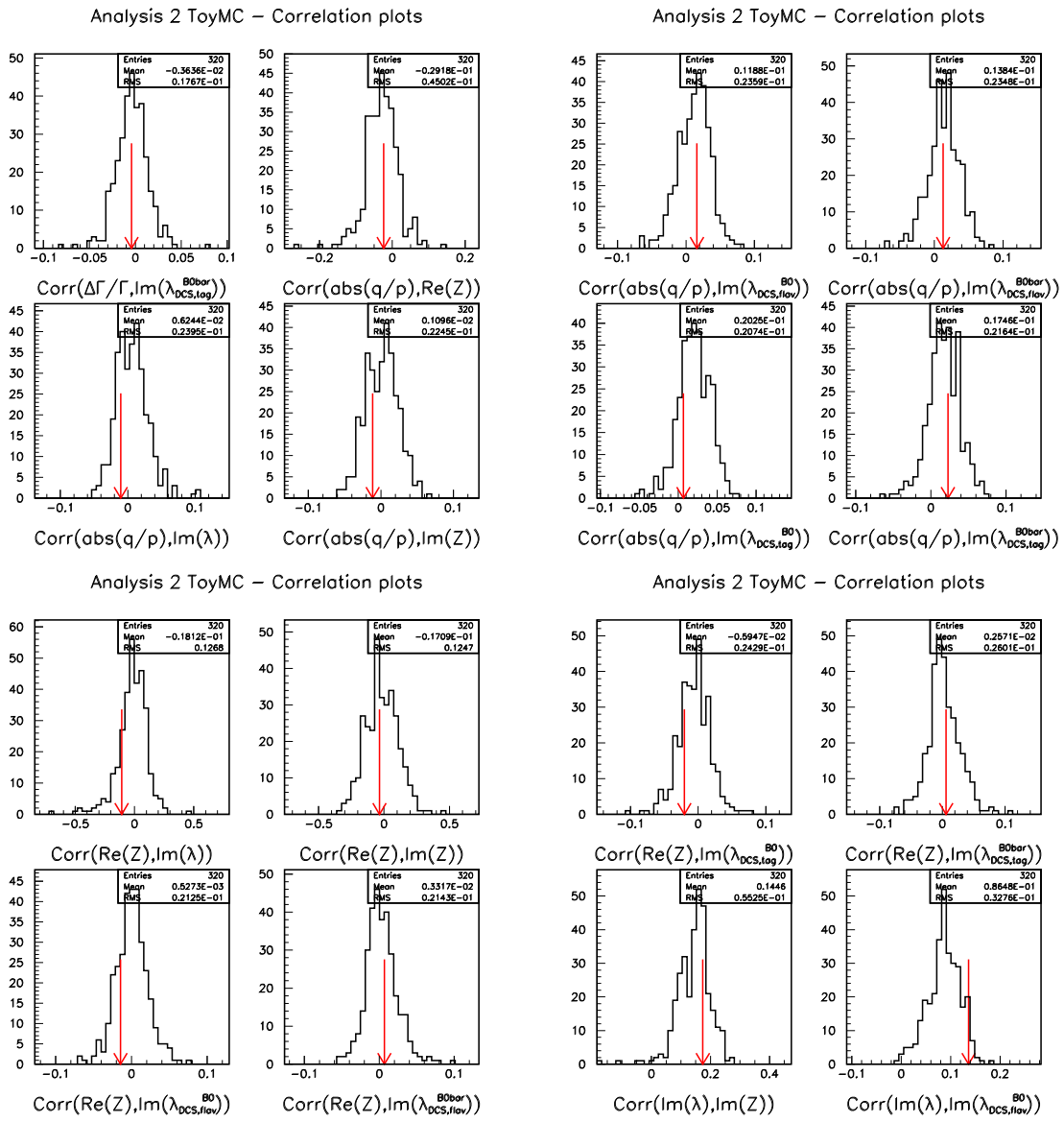

Figure 36: Distribution of the correlation coefficients among the physical and DCKM parameters from Analysis 2 of toy Monte Carlo experiments. The values corresponding to the nominal data fit (red arrow) are indicated (con't).

An additional goodness-of-fit check was performed from a χ^2 comparison of the results of the unbinned maximum likelihood fit and the Δt projections (sum of normalized residuals shown in figures 25, 26 and 27 for non-empty bins). The results are reported in table 26, for each sample and B^0 and $\bar{B}^0$ flavors separately.

Sample/B^0-$\bar{B}^0$ tag	Analysis 1	Analysis 2
B_{flav} Mixed B^0 tag	30.5/44	30.6/44
B_{flav} Mixed $\bar{B}^0$ tag	26.6/54	26.4/54
B_{flav} Unmixed B^0 tag	48.5/54	48.1/54
B_{flav} Unmixed $\bar{B}^0$ tag	46.3/49	46.5/49
$B_{CPK^0_S}$ B^0 tag	23.6/31	23.7/31
$B_{CPK^0_S}$ $\bar{B}^0$ tag	25.5/38	25.9/38
$B_{CPK^0_L}$ B^0 tag	28.8/33	28.6/33
$B_{CPK^0_L}$ $\bar{B}^0$ tag	23.2/29	23.5/29

Table 26: χ^2/dof per sample and B^0-$\bar{B}^0$ flavor for the nominal fit, for tagged only and signal region events ($m_{ES} > 5.27$ GeV/c^2 for B_{flav} and $B_{CPK^0_S}$, and $\mid \Delta E \mid < 10$ MeV for $B_{CPK^0_L}$).

Finally, data-sized full exclusive Monte Carlo fits (see section 9.14 for details) were also performed and compared to the data results. Table 27 summarizes the average Gaussian error obtained from the data-size exclusive MC fits, obtained from all combinations of 6 different B_{flav} and 84 CP samples. There is a good agreement with the error obtained from the fit to the data sample.

Parameter	Analysis 1	Analysis 2
Δm	0.0074	0.0076
$\Delta\Gamma/\Gamma$	0.0404	0.0404
$\mid q/p \mid$	0.0129	0.0129
$\frac{\mathrm{Im}\lambda_{CP}}{\mid\lambda_{CP}\mid}$	0.0637	0.0639
$\frac{\mathrm{Re}\lambda_{CP}}{\mid\lambda_{CP}\mid}$Rez	—	0.0430
Imz	—	0.0288

Table 27: Average error from the data-sized full Monte Carlo fits.

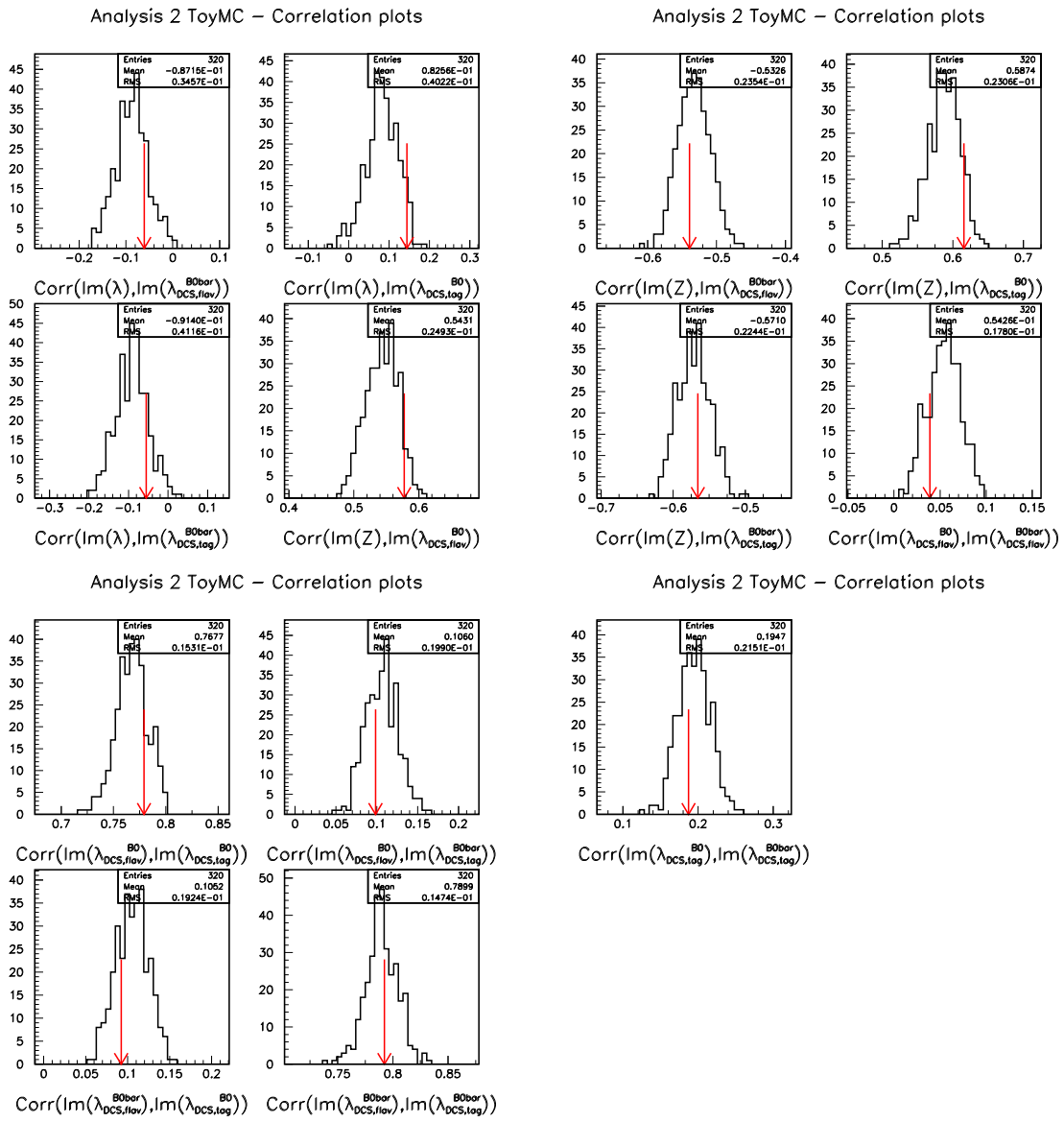

Figure 37: Distribution of the correlation coefficients among the physical and DCKM parameters from Analysis 2 of toy Monte Carlo experiments. The values corresponding to the nominal data fit (red arrow) are indicated (con't).

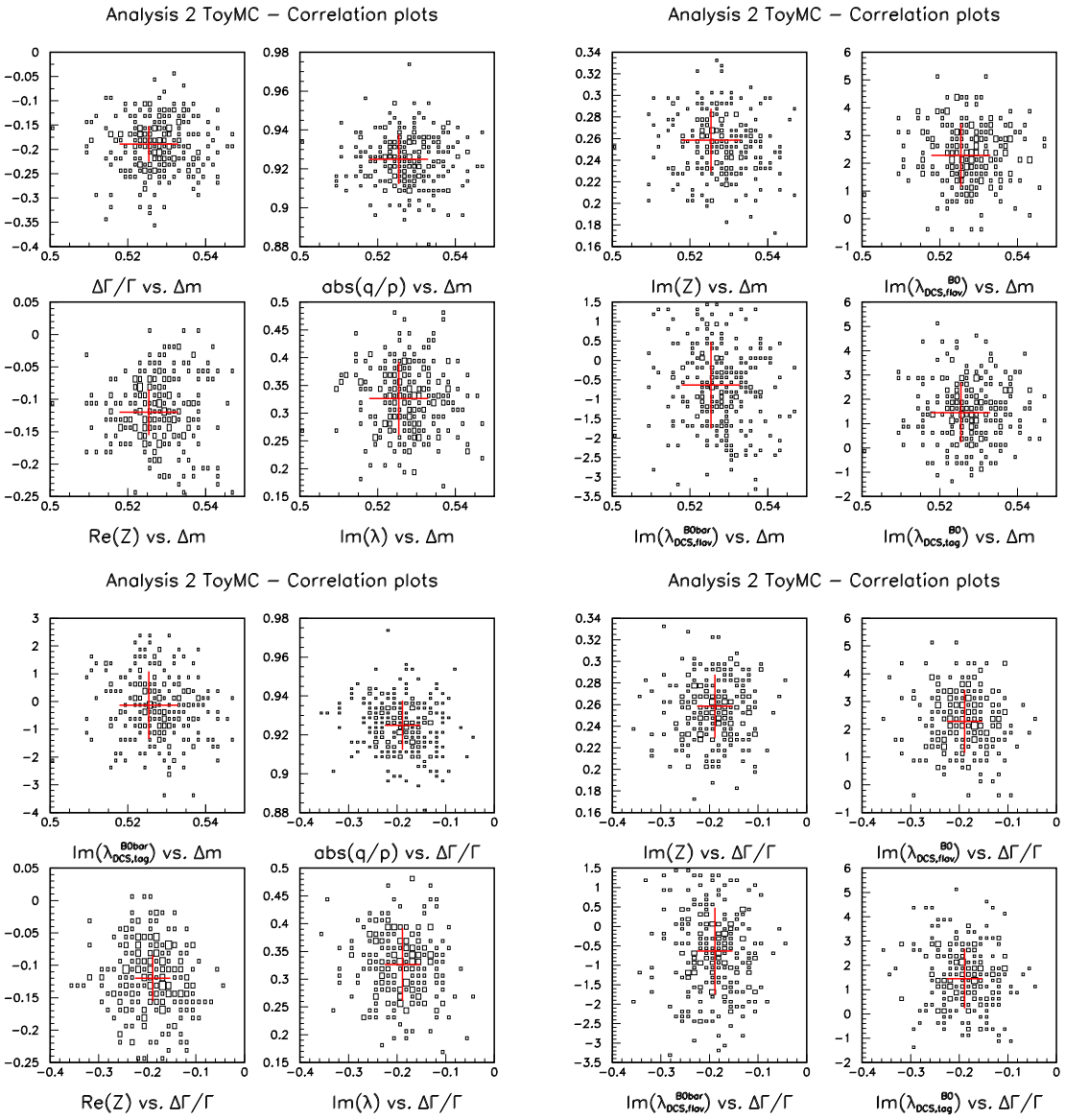

Figure 38: Scatter distributions among the physical and DCKM parameters from Analysis 2 of toy Monte Carlo experiments. The values corresponding to the nominal data fit (red arrow) are indicated.

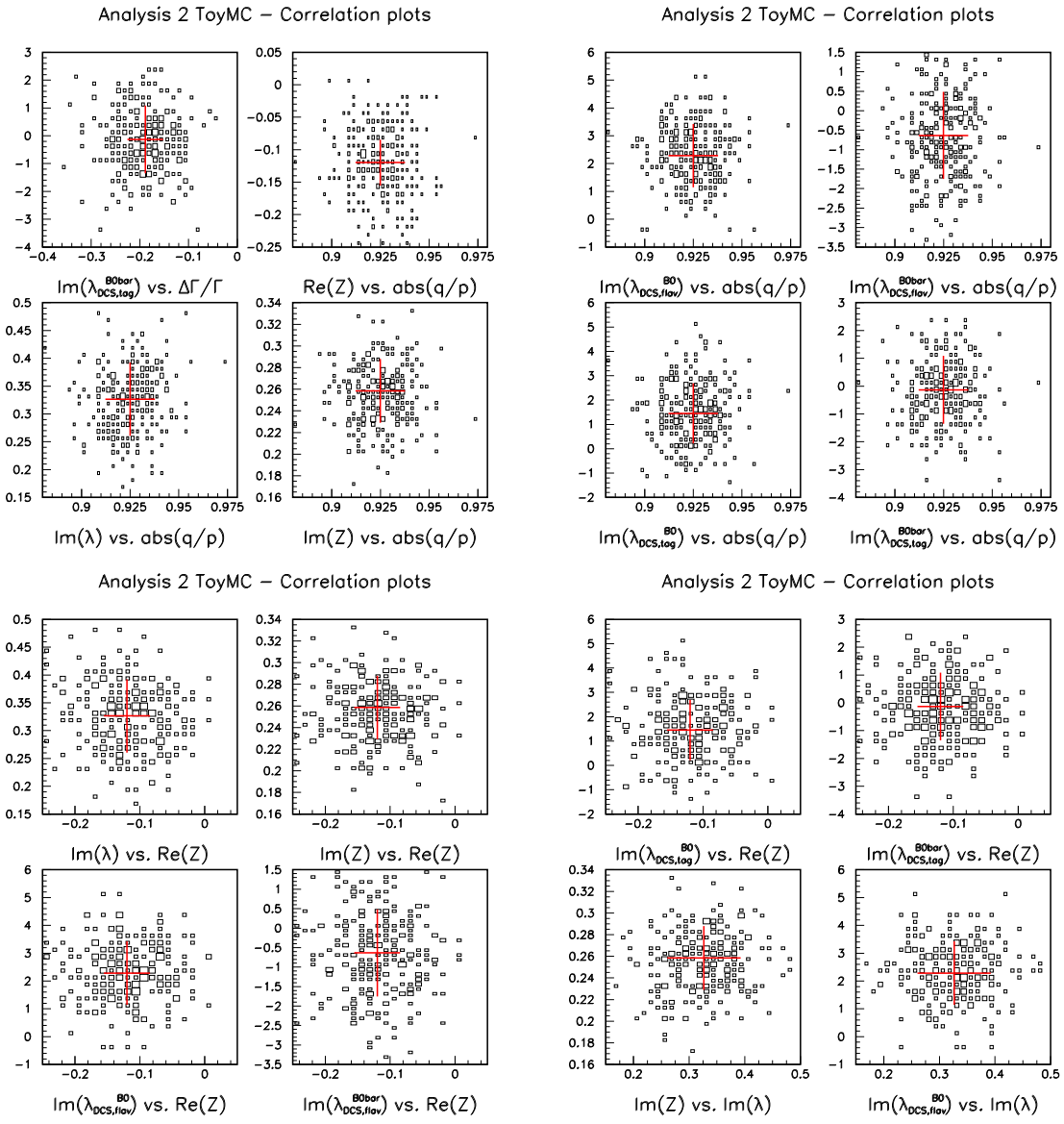

Figure 39: Scatter distributions among the physical and DCKM parameters from Analysis 2 of toy Monte Carlo experiments. The values corresponding to the nominal data fit (red arrow) are indicated (con't).

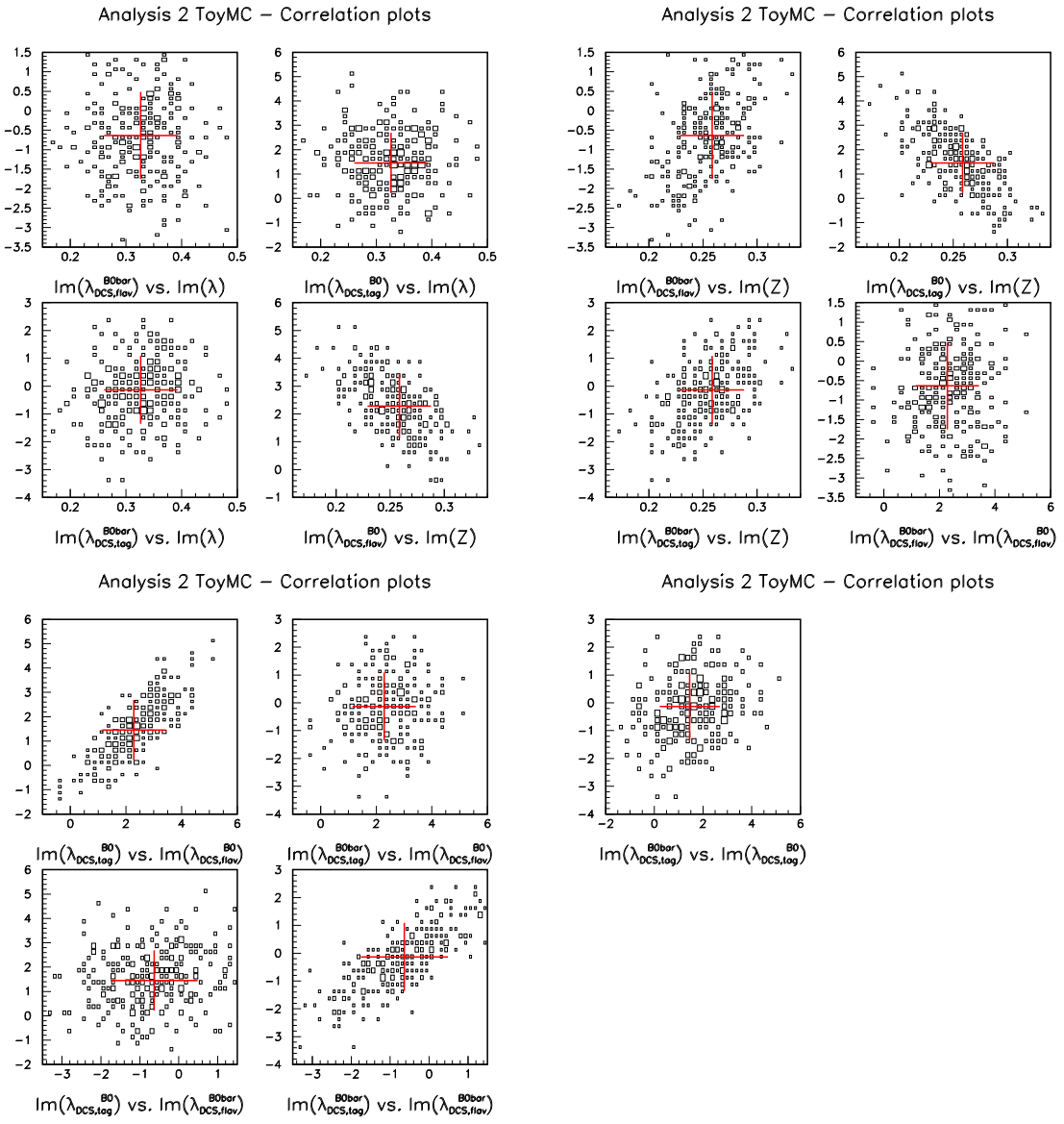

Figure 40: Scatter distributions among the physical and DCKM parameters from Analysis 2 of toy Monte Carlo experiments. The values corresponding to the nominal data fit (red arrow) are indicated (con't).

7.6 Unblind results

On February 12, 2003, the analysis was unblinded. The values for the physics parameters were

$$\begin{aligned} sign(\mathrm{Re}\lambda_{CP})\Delta\Gamma/\Gamma &= 0.008 \pm 0.037 \\ |\, q/p \,| &= 1.029 \pm 0.013 \\ \frac{\mathrm{Re}\lambda_{CP}}{|\,\lambda_{CP}\,|}\mathrm{Re}z &= 0.014 \pm 0.035 \\ \mathrm{Im}z &= 0.038 \pm 0.029 \end{aligned}$$

for Analysis 2, and

$$\begin{aligned} sign(\frac{\mathrm{Re}\lambda_{CP}}{|\,\lambda_{CP}\,|})\Delta\Gamma/\Gamma &= 0.009^{+0.036}_{-0.037} \\ |\, q/p \,| &= 1.029 \pm 0.013 \end{aligned}$$

for Analysis 1. The fit projections (global fit with all samples) onto the Δt axis for each sample and tagging category separately are shown in figures 41 (B_{flav}) and 42 ($B_{CPK^0_S}$ and $B_{CPK^0_L}$).

7.7 Asymmetries

By comparing the fit projections onto the Δt axis of the time-dependent decay rates for the different processes one can build a total of 14 (not all independent) asymmetries (see reference [12] -which follows the discussion in [15]- for details) which are sensitive to the different parameters of interest in this analysis:

- the mixing asymmetry, figure 43(a):

$$A_{Mixing}(\Delta t) \equiv \frac{N_{\overline{B}^0_{tag}B^0_{flav}}(\Delta t) + N_{B^0_{tag}\overline{B}^0_{flav}}(\Delta t) - N_{B^0_{tag}B^0_{flav}}(\Delta t) - N_{\overline{B}^0_{tag}\overline{B}^0_{flav}}(\Delta t)}{N_{\overline{B}^0_{tag}B^0_{flav}}(\Delta t) + N_{B^0_{tag}\overline{B}^0_{flav}}(\Delta t) + N_{B^0_{tag}B^0_{flav}}(\Delta t) + N_{\overline{B}^0_{tag}\overline{B}^0_{flav}}(\Delta t)} \tag{128}$$

  proportional to $\frac{\cos(\Delta m\Delta t)}{\cosh(\Delta\Gamma\Delta t/2)}$;

- the T flavor asymmetry (Kabir asymmetry), figure 43(b):

$$A_{T,flav}(\Delta t) \equiv \frac{N_{B^0_{tag}B^0_{flav}}(\Delta t) - N_{\overline{B}^0_{tag}\overline{B}^0_{flav}}(\Delta t)}{N_{B^0_{tag}B^0_{flav}}(\Delta t) + N_{\overline{B}^0_{tag}\overline{B}^0_{flav}}(\Delta t)} \tag{129}$$

  primarily proportional to $2\frac{1-|q/p|^2}{1+|q/p|^2}$ and independent of Δt. In the limit $\Delta\Gamma = 0$ this asymmetry vanishes;

- the CPT flavor asymmetry, figure 43(c):

$$A_{CPT,flav}(\Delta t) \equiv \frac{N_{\overline{B}^0_{tag}B^0_{flav}}(\Delta t) - N_{B^0_{tag}\overline{B}^0_{flav}}(\Delta t)}{N_{\overline{B}^0_{tag}B^0_{flav}}(\Delta t) + N_{B^0_{tag}\overline{B}^0_{flav}}(\Delta t)} \tag{130}$$

  primarily proportional to $2\frac{\mathrm{Re}z\sinh(\Delta\Gamma\Delta t/2)+\mathrm{Im}z\sin(\Delta m\Delta t)}{\cosh(\Delta\Gamma\Delta t/2)+\cos(\Delta m\Delta t)}$, so it vanishes for $\Delta\Gamma$=0 since it is linear in both $\Delta\Gamma$ and z;

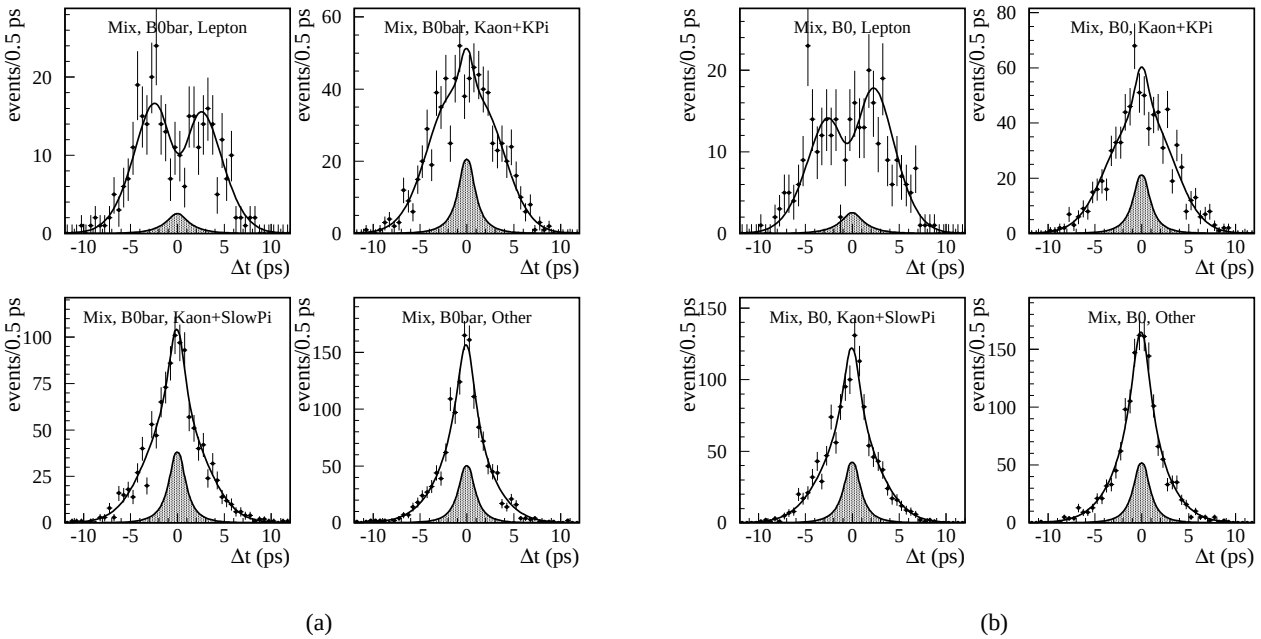

(a) (b)

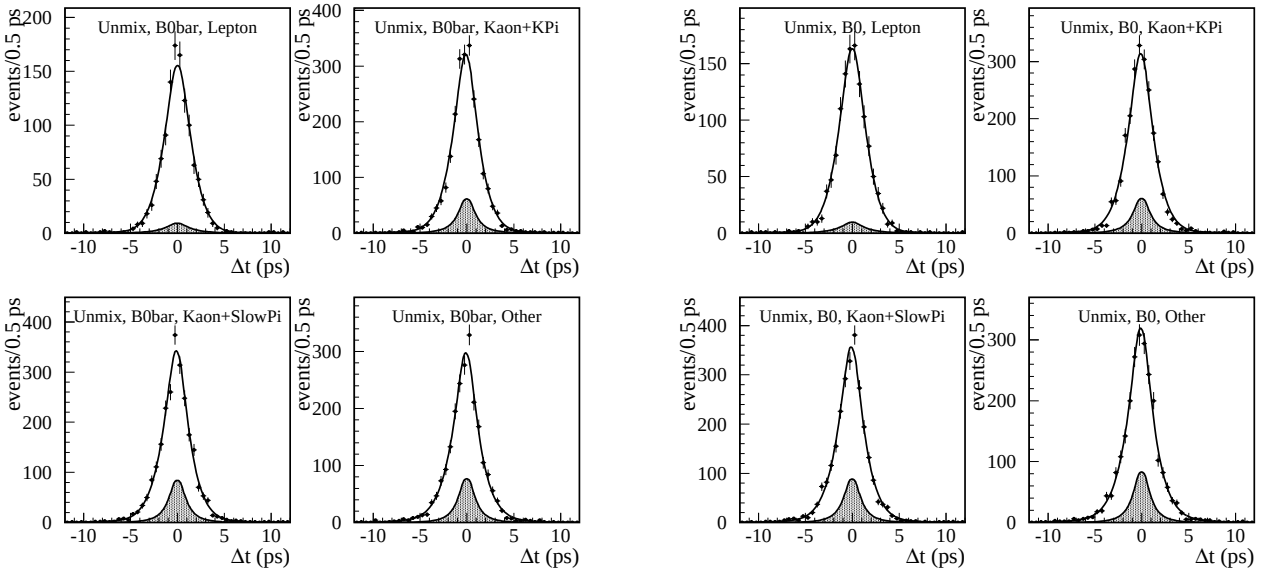

(c) (d)

Figure 41: Δt projections of the nominal fit (Analysis 2) for the B_{flav} data sample: (a) mixed $\bar{B}^0$ tagged, (b) mixed B^0 tagged, (c) unmixed $\bar{B}^0$ tagged and (d) unmixed B^0 tagged (*GG* model), for each tagging category.

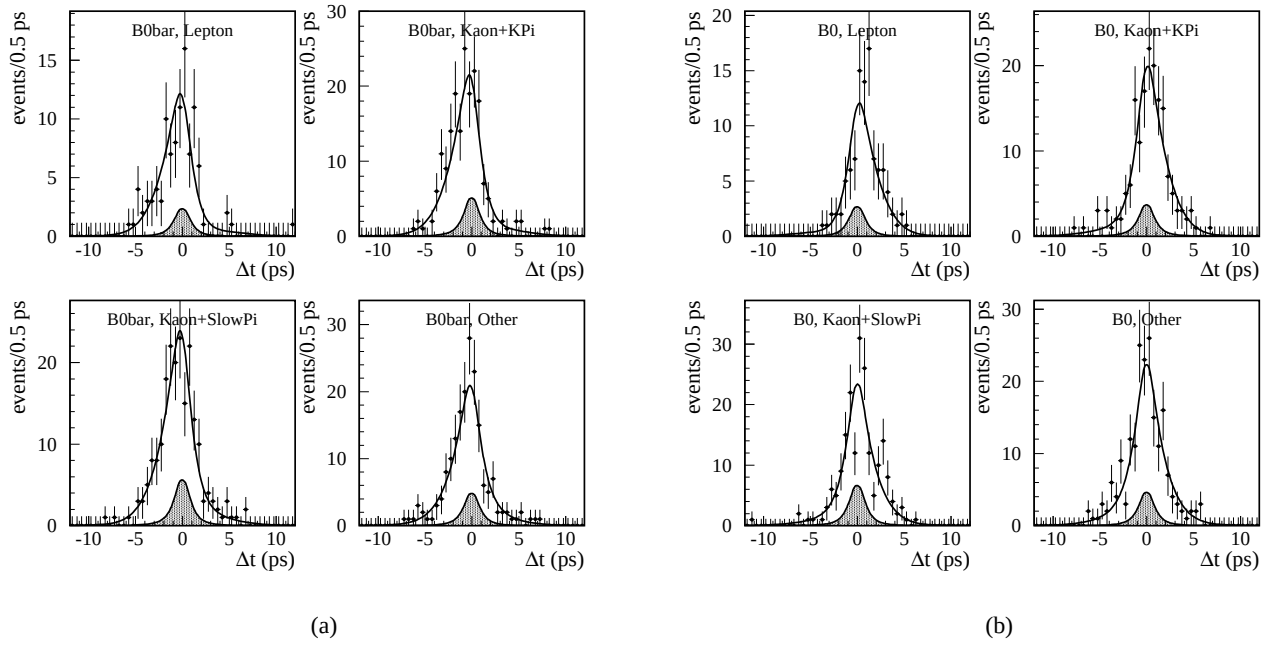

(a) (b)

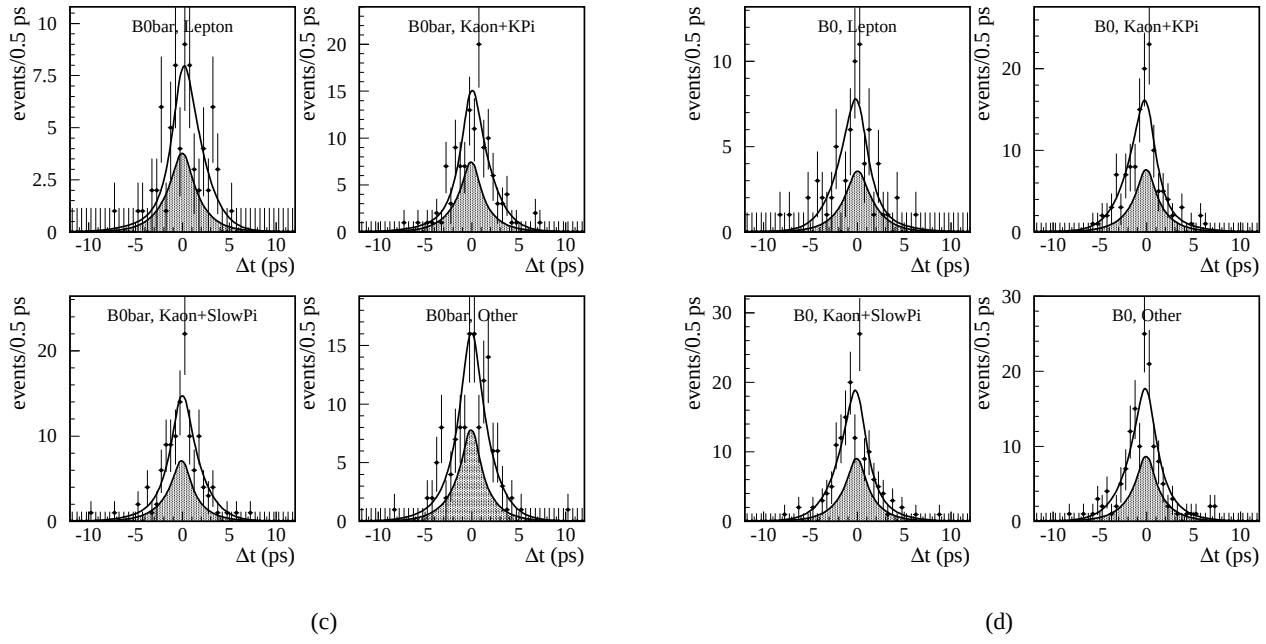

(c) (d)

Figure 42: Δt projections of the nominal fit in data (Analysis 2) for $B_{CPK^0_S}$ (a) $\bar{B}^0$ and (b) B^0 tagged and for bcpkl (c) $\bar{B}^0$ and (d) B^0 tagged (*GG* model), for each tagging category.

- the CP asymmetries, figure 43(d)(e):

$$
\begin{aligned}
A_{CP,B_{CPK_S^0}}(\Delta t) &\equiv \frac{N_{B^0_{tag}B_{CPK_S^0}}(\Delta t) - N_{\overline{B}^0_{tag}B_{CPK_S^0}}(\Delta t)}{N_{B^0_{tag}B_{CPK_S^0}}(\Delta t) + N_{\overline{B}^0_{tag}B_{CPK_S^0}}(\Delta t)} \\
A_{CP,B_{CPK_L^0}}(\Delta t) &\equiv \frac{N_{B^0_{tag}B_{CPK_L^0}}(\Delta t) - N_{\overline{B}^0_{tag}B_{CPK_L^0}}(\Delta t)}{N_{B^0_{tag}B_{CPK_L^0}}(\Delta t) + N_{\overline{B}^0_{tag}B_{CPK_L^0}}(\Delta t)}
\end{aligned}
\tag{131}
$$

  which have contributions from CP/T-violating (odd Δt dependence) and CP/CPT-violating (even Δt dependence) terms, independent of $\Delta\Gamma$. The asymmetry also containts correction terms which are proportional to $\Delta\Gamma$, but cannot introduce fake effects since those terms are at the same time proportional to CP/T and CP/CPT-violating terms;

- the non-genuine[6] T asymmetries (Δt asymmetries), figure 43(f)(g)(h)(i):

$$
\begin{aligned}
A_{\Delta t,B_{CPK_S^0},\bar{B}^0}(\Delta t) &\equiv \frac{N_{\overline{B}^0_{tag}B_{CPK_S^0}}(\Delta t) - N_{\overline{B}^0_{tag}B_{CPK_S^0}}(-\Delta t)}{N_{\overline{B}^0_{tag}B_{CPK_S^0}}(\Delta t) + N_{\overline{B}^0_{tag}B_{CPK_S^0}}(-\Delta t)} \\
A_{\Delta t,B_{CPK_S^0},B^0}(\Delta t) &\equiv \frac{N_{B^0_{tag}B_{CPK_S^0}}(\Delta t) - N_{B^0_{tag}B_{CPK_S^0}}(-\Delta t)}{N_{B^0_{tag}B_{CPK_S^0}}(\Delta t) + N_{B^0_{tag}B_{CPK_S^0}}(-\Delta t)} \\
A_{\Delta t,B_{CPK_L^0},\bar{B}^0}(\Delta t) &\equiv \frac{N_{\overline{B}^0_{tag}B_{CPK_L^0}}(\Delta t) - N_{\overline{B}^0_{tag}B_{CPK_L^0}}(-\Delta t)}{N_{\overline{B}^0_{tag}B_{CPK_L^0}}(\Delta t) + N_{\overline{B}^0_{tag}B_{CPK_L^0}}(-\Delta t)} \\
A_{\Delta t,B_{CPK_L^0},B^0}(\Delta t) &\equiv \frac{N_{B^0_{tag}B_{CPK_L^0}}(\Delta t) - N_{B^0_{tag}B_{CPK_L^0}}(\Delta t)}{N_{B^0_{tag}B_{CPK_L^0}}(\Delta t) + N_{B^0_{tag}B_{CPK_L^0}}(-\Delta t)}
\end{aligned}
\tag{132}
$$

  which have contributions from CP/T and CP/CPT violating terms as well as $\Delta\Gamma$ terms which do not depend on CP/T and CP/CPT violating parameters and therefore are a potencial source of fake effects. In the limit $\Delta\Gamma$=0 this asymmetry equals to the genuine T asymmetry;

- the genuine T asymmetry, figure 43(j):

$$
A_T(\Delta t) \equiv \frac{N_{B^0_{tag}B_{CPK_S^0}}(\Delta t) - N_{\overline{B}^0_{tag}B_{CPK_L^0}}(-\Delta t)}{N_{B^0_{tag}B_{CPK_S^0}}(\Delta t) + N_{\overline{B}^0_{tag}B_{CPK_L^0}}(-\Delta t)}
\tag{133}
$$

  which includes CP/T and CP/CPT violating terms. $\Delta\Gamma$ correction terms are also proportional to CP/T and CP/CPT violating parameters so $\Delta\Gamma \neq 0$ cannot introduce fake effects. In the limit $\Delta\Gamma = 0$ the asymmetry is primarily proportional to CP/T violation (odd in Δt);

[6] By non-genuine asymmetries we mean asymmetries which do not involve processes conected by any fundamental discrete symmetry but that in the limit $\Delta\Gamma$=0 they turn out to be equivalent to the genuine case, i.e. the asymmetries defined with the processes related by that fundamental symmetry [15].

- the non-genuine CPT asymmetries (CPΔt asymmetries), figure 43(k)(l):

$$\begin{aligned} A_{CP\Delta t,B_{CPK^0_S}}(\Delta t) &\equiv \frac{N_{B^0_{tag}B_{CPK^0_S}}(\Delta t) - N_{\overline{B}^0_{tag}B_{CPK^0_S}}(-\Delta t)}{N_{B^0_{tag}B_{CPK^0_S}}(\Delta t) + N_{\overline{B}^0_{tag}B_{CPK^0_S}}(-\Delta t)} \\ A_{CP\Delta t,B_{CPK^0_L}}(\Delta t) &\equiv \frac{N_{B^0_{tag}B_{CPK^0_L}}(\Delta t) - N_{\overline{B}^0_{tag}B_{CPK^0_L}}(-\Delta t)}{N_{B^0_{tag}B_{CPK^0_L}}(\Delta t) + N_{\overline{B}^0_{tag}B_{CPK^0_L}}(-\Delta t)} \end{aligned} \tag{134}$$

  which have, similarly to the non-genuine T asymmetries, contributions from CP/T and CP/CPT violating terms as well as $\Delta\Gamma$ terms which do not depend on CP/T and CP/CPT parameters, and therefore are a potencial source of fake effects. In the limit $\Delta\Gamma$=0 this asymmetry equals to the genuine CPT asymmetry;

- the genuine CPT asymmetries, figure 43(m)(n):

$$\begin{aligned} A_{CPT,B^0}(\Delta t) &\equiv \frac{N_{B^0_{tag}B_{CPK^0_S}}(\Delta t) - N_{B^0_{tag}B_{CPK^0_L}}(-\Delta t)}{N_{B^0_{tag}B_{CPK^0_S}}(\Delta t) + N_{B^0_{tag}B_{CPK^0_L}}(-\Delta t)} \\ A_{CPT,\bar{B}^0}(\Delta t) &\equiv \frac{N_{\overline{B}^0_{tag}B_{CPK^0_S}}(\Delta t) - N_{\overline{B}^0_{tag}B_{CPK^0_L}}(-\Delta t)}{N_{\overline{B}^0_{tag}B_{CPK^0_S}}(\Delta t) + N_{\overline{B}^0_{tag}B_{CPK^0_L}}(-\Delta t)} \end{aligned} \tag{135}$$

  which also contain CP/T and CP/CPT violation terms but is primarily even in Δt and mainly proportional to Rez. To leading order, this asymmetry has no $\Delta\Gamma$ terms. A non-vanishing value of Rez will genuinely manifest in this asymmetry.

Figure 44 shows the corresponding residual distributions, where the residual is defined as the difference between the data and the fit projection onto the Δt axis divided by the data error. Summing over all the asymmetry bins we can perform a χ^2 check of the 14 asymmetries (as said, not all all independent). To make this check bins with no events were excluded. A good χ^2 probability was found in all cases. This test should be seen as an additional check of the goodness-of-fit.

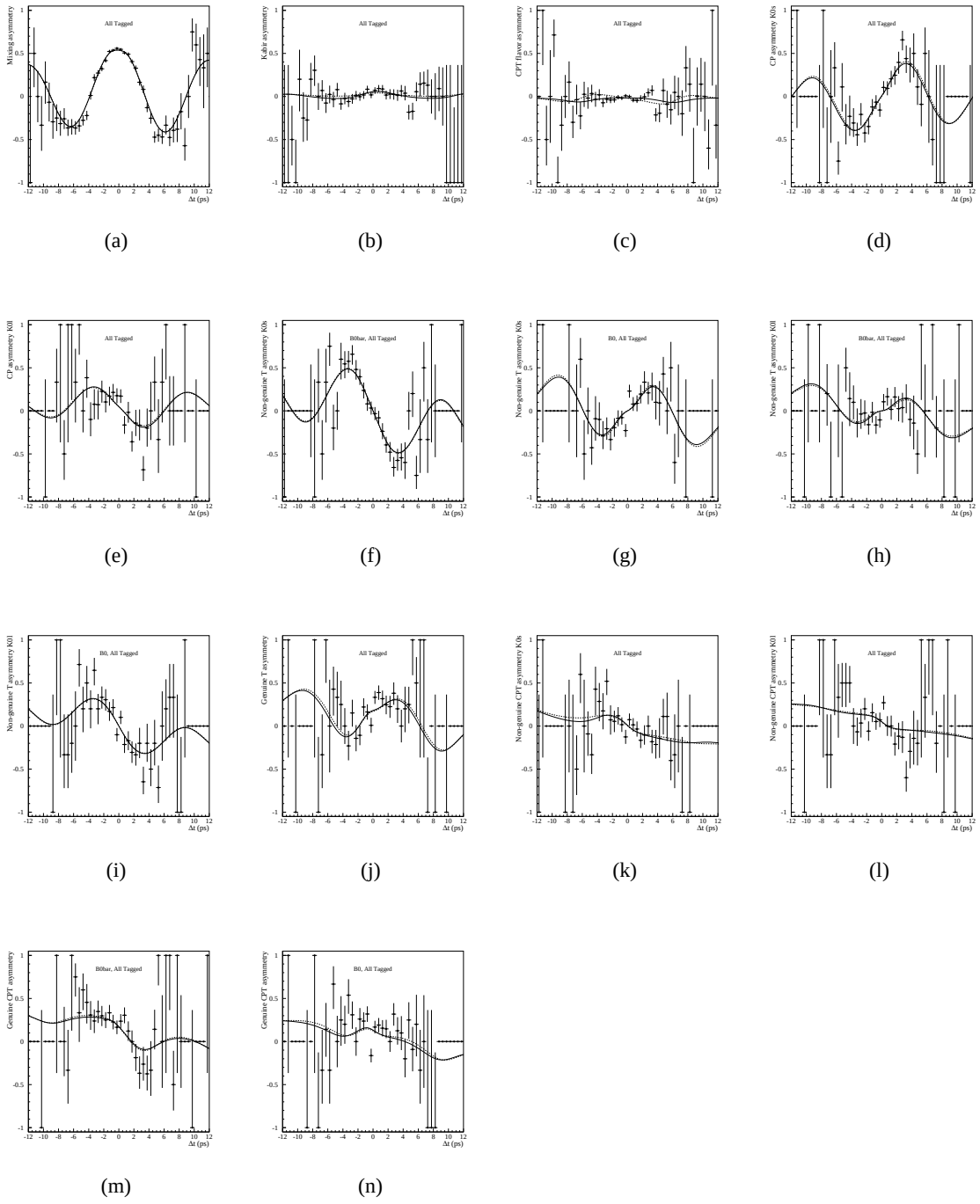

(a) (b) (c) (d)

(e) (f) (g) (h)

(i) (j) (k) (l)

(m) (n)

Figure 43: All possible asymmetries resulting from the comparison of the time-dependent decay rates fit projections onto the Δt axis for the different processes and all tagged events (Analysis 2): (a) $A_{Mixing}(\Delta t)$, Eq. (128); (b) $A_{T,flav}(\Delta t)$, Eq. (129); (c) $A_{CPT,flav}(\Delta t)$, Eq. (130); (d) $A_{CP,B_{CPK^0_S}}(\Delta t)$, Eq. (131); (e) $A_{CP,B_{CPK^0_L}}(\Delta t)$, Eq. (131); (f) $A_{\Delta t,B_{CPK^0_S},\bar{B}^0}(\Delta t)$, Eq. (132); (g) $A_{\Delta t,B_{CPK^0_S},B^0}(\Delta t)$, Eq. (132); (h) $A_{\Delta t,B_{CPK^0_L},\bar{B}^0}(\Delta t)$, Eq. (132); (i) $A_{\Delta t,B_{CPK^0_L},B^0}(\Delta t)$, Eq. (132); (j) $A_T(\Delta t)$, Eq. (133); (k) $A_{CP\Delta t,B_{CPK^0_S}}(\Delta t)$, Eq. (134); (l) $A_{CP\Delta t,B_{CPK^0_L}}(\Delta t)$, Eq. (134); (m) $A_{CPT,\bar{B}^0}(\Delta t)$, Eq. (135); (n) $A_{CPT,B^0}(\Delta t)$, Eq. (135). The dotted curves are obtained assumming $\Delta\Gamma/\Gamma$=0, $\mid q/p \mid$=1, $z = 0$. Hidden while Analysis 2 is blinded.

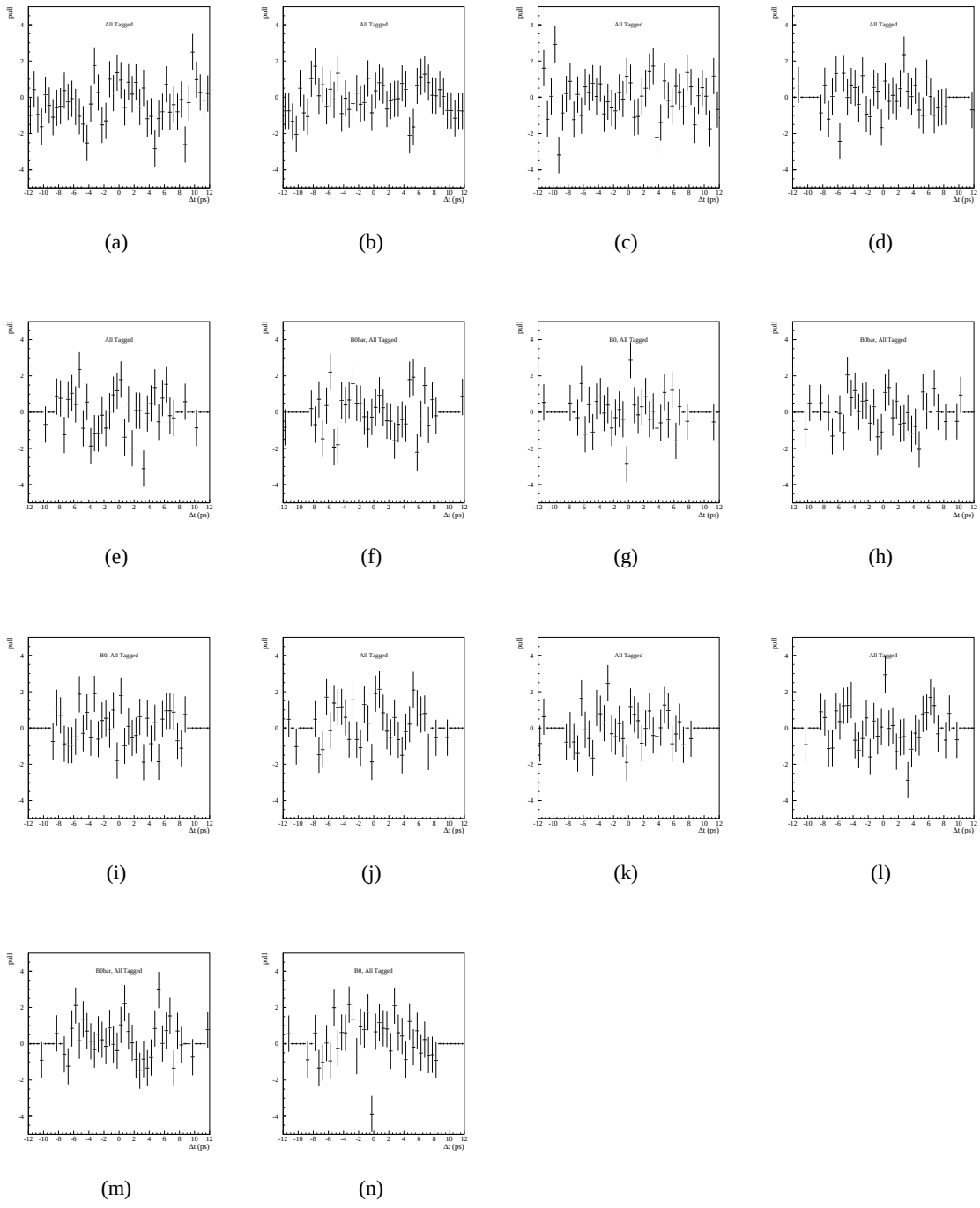

Figure 44: Residuals of all possible asymmetries resulting from the comparison of the time-dependent decay rates fit projections onto the Δt axis for the different processes and all tagged events (Analysis 2): (a) $A_{Mixing}(\Delta t)$, Eq. (128); (b) $A_{T,flav}(\Delta t)$, Eq. (129); (c) $A_{CPT,flav}(\Delta t)$, Eq. (130); (d) $A_{CP,B_{CPK^0_S}}(\Delta t)$, Eq. (131); (e) $A_{CP,B_{CPK^0_L}}(\Delta t)$, Eq. (131); (f) $A_{\Delta t,B_{CPK^0_S},\bar{B}^0}(\Delta t)$, Eq. (132); (g) $A_{\Delta t,B_{CPK^0_S},B^0}(\Delta t)$, Eq. (132); (h) $A_{\Delta t,B_{CPK^0_L},\bar{B}^0}(\Delta t)$, Eq. (132); (i) $A_{\Delta t,B_{CPK^0_L},B^0}(\Delta t)$, Eq. (132); (j) $A_T(\Delta t)$, Eq. (133); (k) $A_{CP\Delta t,B_{CPK^0_S}}(\Delta t)$, Eq. (134); (l) $A_{CP\Delta t,B_{CPK^0_L}}(\Delta t)$, Eq. (134); (m) $A_{CPT,\bar{B}^0}(\Delta t)$, Eq. (135); (n) $A_{CPT,B^0}(\Delta t)$, Eq. (135).

8 Cross-checks

We have performed several checks, both on data and Monte Carlo, to test the consistency of the measurements and the robustness of the results. They following subsections resume the results of our tests.

8.1 Average B^0 lifetime results

The average B^0 lifetime was fixed in the nominal fit configuration to the PDG2002 value [26], $\tau_B = 1.542 \pm 0.016$. This value, however, was obtained by averaging measurements based on flavor eigenstate samples obtained neglecting effects from non-zero values of $\Delta\Gamma$, $\mid q/p \mid -1$ and CPT violation ($z = 0$). Summing up the $\mid 1\rangle$, $\mid \bar{1}\rangle$, $\mid 2\rangle$ and $\mid \bar{2}\rangle$ contributions of table 3 (valid to first order in z), we observe that the dependence on CPT violation cancels out (the coefficient s is zero). The coefficients of the $\Delta m\Delta t$ and $\Delta\Gamma\Delta t$ dependence, c_- and c_+, become 0 and 4, respectively, up to order $(\mid q/p \mid -1)^2$. From this simple analysis we conclude that only a second order dependence on $\Delta\Gamma$ survives, and all the other cancel out up to second order in CPT violation and T violation in mixing. A fully consistent approach would therefore require to fit also for τ_B. Nevertheless the effect turns out to be only at second order. By this reason and in order to improve the robustness and speed of the fit we fixed the average B^0 lifetime, and then we assigned as systematics twice the world average error (see section 9.6). In addition, as a consistency check, the fit was redone in data for several configurations (`GG`/`GExp` models and Analysis 1 and 2), with τ_B free. The comparison of the fitted B^0 lifetime with the nominal fixed value, together with the variation of the oscillation/CPT/CP/T parameters, provides a powerful consistency check. The results for Analysis 1 and Analysis 2, compared to the nominal fits, are shown in tables 28 and 29, for the `GG` resolution model. The corresponding results for the `GExp` model are reported in tables 30 and 31. The τ_B results obtained using the `GG` resolution model are about two sigma (statistical) below the PDG2002 value, while the values from the `GExp` model are consistent. This feature is known from earlier lifetime studies [29]: the `GG` model provides slightly biased estimates of the lifetime while the `GExp` approach gives the optimal trade-off between statistical reach and systematics (included biases). The change on Δm (about 0.6 sigma) is due to its correlation with the lifetime. All the other parameters are consistent within statistical differences. The difference between the PDG2002 τ_B and the value obtained from the fit with the nominal `GG` resolution model is also about twice the PDG2002 error, justifying the prescription used to estimate the systematics from fixing τ_B (section 9.6).

Parameter	Nominal fit	τ_B free
τ	—	1.518 ± 0.016
Δm	0.5253 ± 0.0076	0.5303 ± 0.0084
$\Delta\Gamma/\Gamma$	-0.188 ± 0.037	-0.185 ± 0.040
$\mid q/p \mid$	0.925 ± 0.013	0.924 ± 0.013
$\frac{\mathrm{Im}\lambda_{CP}}{\mid\lambda_{CP}\mid}$	0.339 ± 0.067	0.334 ± 0.067

Table 28: Analysis 1 results including B^0 lifetime among free parameters. For comparison, nominal fit results are reported as well. *GG* resolution model.

8.2 $B_{CPK_S^0}$ and $B_{CPK_L^0}$ separately

We performed the nominal fit separately for the $B_{CPK_S^0}$ and $B_{CPK_L^0}$ samples only. Results are summarized in tables 32 and 33, and they are compared to the nominal fits, for Analysis 1 and 2 respectively. Let us remark

Parameter	Nominal fit	τ_B free
τ	—	1.518 ± 0.016
Δm	0.5254 ± 0.0076	0.5302 ± 0.0084
$\Delta\Gamma/\Gamma$	-0.189 ± 0.037	-0.186 ± 0.040
$\mid q/p \mid$	0.925 ± 0.013	0.924 ± 0.013
$\frac{\mathrm{Im}\lambda_{CP}}{\lvert\lambda_{CP}\rvert}$	0.327 ± 0.066	0.323 ± 0.066
$\frac{\mathrm{Re}\lambda_{CP}}{\lvert\lambda_{CP}\rvert}\mathrm{Re}z$	-0.120 ± 0.035	-0.122 ± 0.033
$\mathrm{Im}z$	0.258 ± 0.029	0.259 ± 0.030

Table 29: Analysis 2 results including B^0 lifetime among free parameters . For comparison, nominal fit results are reported as well. *GG* model resolution model.

Parameter	Nominal fit	τ_B free
τ	—	1.531 ± 0.014
Δm	0.5198 ± 0.0076	0.5216 ± 0.0080
$\Delta\Gamma/\Gamma$	-0.180 ± 0.041	-0.177 ± 0.045
$\mid q/p \mid$	0.923 ± 0.013	0.923 ± 0.013
$\frac{\mathrm{Im}\lambda_{CP}}{\lvert\lambda_{CP}\rvert}$	0.339 ± 0.066	0.337 ± 0.066

Table 30: Analysis 1 results including B^0 lifetime among free parameters. For comparison, the fits with the lifetime fixed are reported as well. *GExp* resolution model.

Parameter	Nominal fit	τ_B free
τ	—	1.531 ± 0.015
Δm	0.5201 ± 0.0076	0.5218 ± 0.0080
$\Delta\Gamma/\Gamma$	-0.182 ± 0.042	-0.179 ± 0.044
$\mid q/p \mid$	0.924 ± 0.013	0.923 ± 0.013
$\frac{\mathrm{Im}\lambda_{CP}}{\lvert\lambda_{CP}\rvert}$	0.328 ± 0.065	0.327 ± 0.065
$\frac{\mathrm{Re}\lambda_{CP}}{\lvert\lambda_{CP}\rvert}\mathrm{Re}z$	-0.112 ± 0.041	-0.114 ± 0.040
$\mathrm{Im}z$	0.262 ± 0.029	0.262 ± 0.029

Table 31: Analysis 2 results including B^0 lifetime among free parameters. For comparison, the fits with the lifetime fixed are reported as well. *GExp* resolution model.

that the fact that the blinding is in this case the same as for the Analysis 1 and 2 fits but this does not unblind the actual fitted values of the other parameters since the correlation among these parameters is small.

8.3 $\sin 2\beta$ only fits

Analysis 1 fits with $\Delta\Gamma/\Gamma$ and $\mid q/p \mid$ fixed to 0 and 1 ($\sin 2\beta$ only fits), respectively, were also performed, for all B_{CP} modes together as well as for $B_{CPK_S^0}$ and $B_{CPK_L^0}$ separately. The results, with $\frac{\mathrm{Im}\lambda_{CP}}{\lvert\lambda_{CP}\rvert}$ unblinded, can be found in table 34.

In order to have a better comparison with the standard $\sin 2\beta$ analysis [9] we repeated the fits but now

Parameter	all CP (nominal)	$B_{CPK^0_S}$ sample	$B_{CPK^0_L}$ sample
Δm	0.5253 ± 0.0076	0.5246 ± 0.0076	0.5276 ± 0.0077
$\Delta\Gamma/\Gamma$	-0.188 ± 0.037	-0.193 ± 0.040	-0.189 ± 0.047
$\mid q/p \mid$	0.925 ± 0.013	0.924 ± 0.013	0.923 ± 0.013
$\frac{\mathrm{Im}\lambda_{CP}}{\mid\lambda_{CP}\mid}$	0.339 ± 0.067	0.327 ± 0.074	0.40 ± 0.15

Table 32: Comparison of Analysis 1 nominal fit, with the full CP, $B_{CPK^0_S}$ and $B_{CPK^0_L}$ samples. The blinding string of the results is the same for all the columns.

Parameter	all CP (nominal)	$B_{CPK^0_S}$ sample	$B_{CPK^0_L}$ sample
Δm	0.5254 ± 0.0076	0.5247 ± 0.0076	0.5277 ± 0.0077
$\Delta\Gamma/\Gamma$	-0.189 ± 0.037	-0.194 ± 0.040	-0.188 ± 0.047
$\mid q/p \mid$	0.925 ± 0.013	0.924 ± 0.013	0.923 ± 0.013
$\frac{\mathrm{Im}\lambda_{CP}}{\mid\lambda_{CP}\mid}$	0.327 ± 0.066	0.302 ± 0.071	0.44 ± 0.16
$\frac{\mathrm{Re}\lambda_{CP}}{\mid\lambda_{CP}\mid}\mathrm{Re}z$	-0.120 ± 0.035	-0.128 ± 0.035	-0.120 ± 0.049
$\mathrm{Im}z$	0.258 ± 0.029	0.251 ± 0.030	0.258 ± 0.031

Table 33: Comparison of Analysis 2 nominal fit, with the full CP, $B_{CPK^0_S}$ and $B_{CPK^0_L}$ samples. The blinding string of the results is the same for all the columns.

Parameter	$\sin 2\beta$ full CP sample	$\sin 2\beta$ $B_{CPK^0_S}$ sample	$\sin 2\beta$ $B_{CPK^0_L}$ sample
Δm	0.5255 ± 0.0076	0.5249 ± 0.0076	0.5277 ± 0.0077
$\frac{\mathrm{Im}\lambda_{CP}}{\mid\lambda_{CP}\mid}$	0.751 ± 0.067	0.762 ± 0.073	0.70 ± 0.15

Table 34: Comparison of $\sin 2\beta$ only fits (Analysis 1 with $\Delta\Gamma/\Gamma$ and $\mid q/p \mid$ fixed to 0 and 1), using the full CP, $B_{CPK^0_S}$ and $B_{CPK^0_L}$ samples. $\frac{\mathrm{Im}\lambda_{CP}}{\mid\lambda_{CP}\mid}$ is unblinded.

adding the η_c decay modes [9] to the $B_{CPK^0_S}$ sample. The results are given in table 35. To have an even better comparison, the fits (including η_c decay modes) were repeated with the following simplifications: i) i) Δm, σ_{tail} and r_k ($k = tag, \underline{flav}$) were fixed respectively to 0.489 ps^{-1}, 3.0 and 0 (therefore we did not fit for $\frac{\mathrm{Im}\lambda_{tag}}{\mid\lambda_{tag}\mid}$, $\frac{\mathrm{Im}\bar{\lambda}_{tag}}{\mid\lambda_{tag}\mid}$, $\frac{\mathrm{Im}\lambda_{flav}}{\mid\lambda_{flav}\mid}$ and $\frac{\mathrm{Im}\bar{\lambda}_{flav}}{\mid\lambda_{flav}\mid}$); ii) the tagging/vertexing correlations were neglected; iii) common prompt combinatorial background fraction for all $B_{CPK^0_S}$ subsamples; iv) the lifetime of the non-prompt combinatorial background fixed to the B^0 lifetime (1.542); iv) the cut on $\sigma_{\Delta t}$ was relaxed to 2.5 ps; v) do not use untagged events. The results from these fits are shown in table 36. The $\frac{\mathrm{Im}\lambda_{CP}}{\mid\lambda_{CP}\mid}(\sin 2\beta)$ values are before the MC bias correction (-0.0138 ± 0.005) applied in [9].

Parameter	$\sin 2\beta$ η_c full CP	$\sin 2\beta$ η_c $B_{CPK^0_S}$	$\sin 2\beta$ η_c $B_{CPK^0_L}$
Δm	0.5258 ± 0.0076	0.5252 ± 0.0076	0.5277 ± 0.0077
$\frac{\mathrm{Im}\lambda_{CP}}{\mid\lambda_{CP}\mid}$	0.746 ± 0.065	0.754 ± 0.072	0.70 ± 0.15

Table 35: Comparison of $\sin 2\beta$ only fits (Analysis 1 with $\Delta\Gamma/\Gamma$ and $\mid q/p \mid$ fixed to 0 and 1), using the full CP, $B_{CPK^0_S}$ and $B_{CPK^0_L}$ samples, but including also the η_c sample. $\frac{\mathrm{Im}\lambda_{CP}}{\mid\lambda_{CP}\mid}$ is unblinded.

Parameter	$\sin 2\beta$ Standard full CP	$\sin 2\beta$ Standard $B_{CPK_S^0}$	$\sin 2\beta$ Standard $B_{CPK_L^0}$
$\frac{\mathrm{Im}\lambda_{CP}}{\lvert\lambda_{CP}\rvert}$	0.769 ± 0.067	0.777 ± 0.074	0.74 ± 0.16

Table 36: Comparison of $\sin 2\beta$ only fits (Analysis 1 with $\Delta\Gamma/\Gamma$ and $\mid q/p \mid$ fixed to 0 and 1), using the full CP, $B_{CPK_S^0}$ and $B_{CPK_L^0}$ samples, including the η_c sample, with the simplifications described in the text and used in the standard $\sin 2\beta$ fit (see [9]).

Parameter	Analysis 1	Analysis 2
Δm	0.5251 ± 0.0075	0.5253 ± 0.0076
$\Delta\Gamma/\Gamma$	-0.188 ± 0.037	-0.187 ± 0.037
$\mid q/p \mid$	0.936 ± 0.043	0.933 ± 0.043
$\frac{\mathrm{Im}\lambda_{CP}}{\lvert\lambda_{CP}\rvert}$	0.340 ± 0.067	0.326 ± 0.066
$\frac{\mathrm{Re}\lambda_{CP}}{\lvert\lambda_{CP}\rvert}$Rez	—	-0.148 ± 0.038
Imz	—	0.259 ± 0.029

Table 37: Shape only fit for analysis 1 and 2. See text for explanation. These results must be compared to those of tables 16 and 20.

8.4 $B^0\bar{B}^0$ shape only fit

The normalization of the PDF (section 2) is performed for all mixed/unmixed/$B^0/\bar{B}^0$ events together, but separately for the B_{flav}, $B_{CPK_S^0}$ and $B_{CPK_L^0}$ samples. As a cross-check, the fit was also performed normalizing separately also for B^0 and $\bar{B}^0$ events. Taking out this constraint implies to perform a fit to the $B^0\bar{B}^0$ Δt shape only fit, being therefore insensitive to the total number of B^0, $\bar{B}^0$ events. The results are reported in table 37, for Analysis 1 and Analysis 2 respectively (to be compared with tables 16 and 20). Let us note the much larger statistical error on $\mid q/p \mid$, as expected since the sensitivity to $\mid q/p \mid$ comes mainly from the relative B^0-$\bar{B}^0$ rates and not the Δt shape itself. The results are compatible within the statistical differences.

8.5 Results per tagging category

The fit has also been performed for each tagging category separately. In these fits the resolution function and mistags are extracted as in the nominal fit but now the physics parameters are allowed to be different for each tagging category. However, allowing 6 independent physics parameters for each category increase very significantly the total number of parameters, reducing the robustness and stability of the fit. To overcome this problem, Δm and $\frac{\mathrm{Im}\lambda_{CP}}{\lvert\lambda_{CP}\rvert}$ were fitted for all tagging categories together (as in the nominal fit), and only $\Delta\Gamma/\Gamma$, $\mid q/p \mid$, Rez and Imz were allowed to float for each category. The parameters of the `UnTagged` category were merged with those of the `Lepton` category, which only matters for $\Delta\Gamma/\Gamma$. The results from this check are shown in table 38, for Analysis 1 and Analysis 2 respectively. In the case of Analysis 2 they are also shown separately for $B_{CPK_S^0}$ and $B_{CPK_L^0}$. The results are in all cases compatible within statistics.

8.6 Tagging efficiency per sample

In the nominal fit, overall tagging efficiencies are extracted from the B_{flav} sample and then fixed and assummed common for all samples. We also tried to extract and fix them for each sample separately. No changes

Parameter	Analysis 1	Analysis 2 all CP	Analysis 2 $B_{CPK^0_S}$ sample	Analysis 2 $B_{CPK^0_L}$ sample
Δm	0.5254 ± 0.0076	0.5263 ± 0.0077	0.5252 ± 0.0077	0.5288 ± 0.0079
$\Delta\Gamma/\Gamma$(Lepton)	-0.170 ± 0.059	-0.170 ± 0.059	-0.168 ± 0.064	-0.199 ± 0.075
$\Delta\Gamma/\Gamma$(Kaon + KPi)	-0.219 ± 0.082	-0.220 ± 0.083	-0.223 ± 0.092	-0.20 ± 0.12
$\Delta\Gamma/\Gamma$(Kaon + SlowPi)	-0.140 ± 0.073	-0.148 ± 0.071	-0.146 ± 0.082	-0.173 ± 0.086
$\Delta\Gamma/\Gamma$(Other)	-0.243 ± 0.078	-0.244 ± 0.081	-0.260 ± 0.084	-0.17 ± 0.11
$\mid q/p \mid$ (Lepton)	0.925 ± 0.017	0.925 ± 0.017	0.925 ± 0.017	0.922 ± 0.018
$\mid q/p \mid$ (Kaon + KPi)	0.928 ± 0.022	0.928 ± 0.022	0.929 ± 0.023	0.927 ± 0.023
$\mid q/p \mid$ (Kaon + SlowPi)	0.944 ± 0.022	0.945 ± 0.023	0.944 ± 0.023	0.940 ± 0.023
$\mid q/p \mid$ (Other)	0.896 ± 0.025	0.897 ± 0.024	0.895 ± 0.025	0.900 ± 0.025
$\frac{\mathrm{Im}\lambda_{CP}}{\lvert\lambda_{CP}\rvert}$	0.341 ± 0.066	0.327 ± 0.065	0.300 ± 0.069	0.46 ± 0.16
$\frac{\mathrm{Re}\lambda_{CP}}{\lvert\lambda_{CP}\rvert}$ Rez(Lepton)	—	-0.119 ± 0.060	-0.121 ± 0.057	-0.132 ± 0.085
$\frac{\mathrm{Re}\lambda_{CP}}{\lvert\lambda_{CP}\rvert}$ Rez(Kaon + KPi)	—	-0.132 ± 0.050	-0.135 ± 0.049	-0.128 ± 0.069
$\frac{\mathrm{Re}\lambda_{CP}}{\lvert\lambda_{CP}\rvert}$ Rez(Kaon + SlowPi)	—	$(-5.6 \pm 7.1) \cdot 10^{-2}$	$(-8.2 \pm 8.8) \cdot 10^{-2}$	$(-4.2 \pm 9.9) \cdot 10^{-2}$
$\frac{\mathrm{Re}\lambda_{CP}}{\lvert\lambda_{CP}\rvert}$ Rez(Other)	—	-0.14 ± 0.15	-0.14 ± 0.15	-0.14 ± 0.23
Imz(Lepton)	—	0.265 ± 0.030	0.257 ± 0.031	0.263 ± 0.031
Imz(Kaon + KPi)	—	0.238 ± 0.038	0.228 ± 0.039	0.237 ± 0.040
Imz(Kaon + SlowPi)	—	0.255 ± 0.040	0.242 ± 0.041	0.253 ± 0.041
Imz(Other)	—	0.233 ± 0.041	0.227 ± 0.043	0.233 ± 0.042

Table 38: Results per tagging category. GG resolution model was used.

Parameter	Analysis 1	Analysis 2
Δm	0.5253 ± 0.0076	0.5254 ± 0.0076
$\Delta\Gamma/\Gamma$	-0.188 ± 0.037	-0.189 ± 0.037
$\mid q/p \mid$	0.925 ± 0.013	0.925 ± 0.013
$\frac{\mathrm{Im}\lambda_{CP}}{\lvert\lambda_{CP}\rvert}$	0.339 ± 0.067	0.327 ± 0.066
$\frac{\mathrm{Re}\lambda_{CP}}{\lvert\lambda_{CP}\rvert}$ Rez	—	-0.120 ± 0.035
Imz	—	0.258 ± 0.029

Table 39: Results extracting tagging efficiencies separately for each sample. These results must be compared to those of tables 16 and 20.

were observed with respect to the nominal configuration, as seen in table 39.

8.7 Δt and $\sigma_{\Delta t}$ cuts variation

Likelihood fits were performed for different values of the Δt and $\sigma_{\Delta t}$ cuts. The chosen Δt cut values were $5, 10, 15, 20, 25, 30$ ps (20 is the nominal one). The set of cuts taken for $\sigma_{\Delta t}$ were $0.6, 1.0, 1.4, 1.8, 2.2$ ps (1.4 is the nominal). In the first case, finite normalization, according to equation (105), was used instead of the asymptotic one used in the nominal fit. The stability of the results compared to the nominal cuts is shown in figures 45 and 46.

8.8 Results from standard full Monte Carlo

The nominal fits were performed on the high statistics standard Monte Carlo (exclusive and inclusive charmonium), described in section 3. The fit results corresponding to Analysis 2 are given in tables 40 and 41, for the *GG* and *GExp* resolution models. Table 42 summarizes the Analysis 2 results (restricted to physical parameters) obtained from the exclusive and inclusive charmonium samples, all B_{CP} or $B_{CPK^0_S}$ and $B_{CPK^0_L}$ only

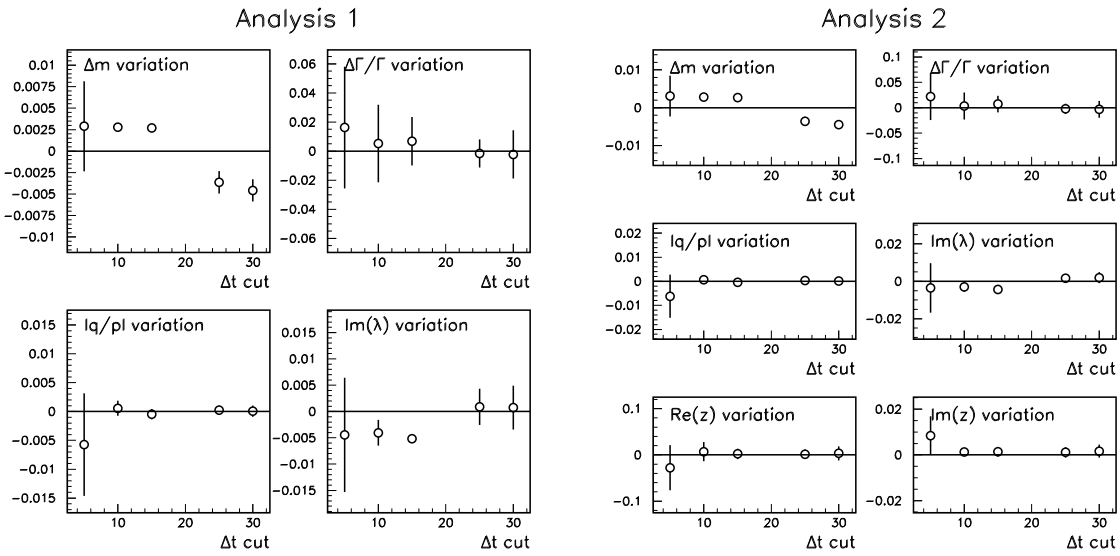

Figure 45: Stability of the fitted physical parameters from Analysis 1 and 2 against the Δt cut. The variation with respect to the nominal configuration is shown.

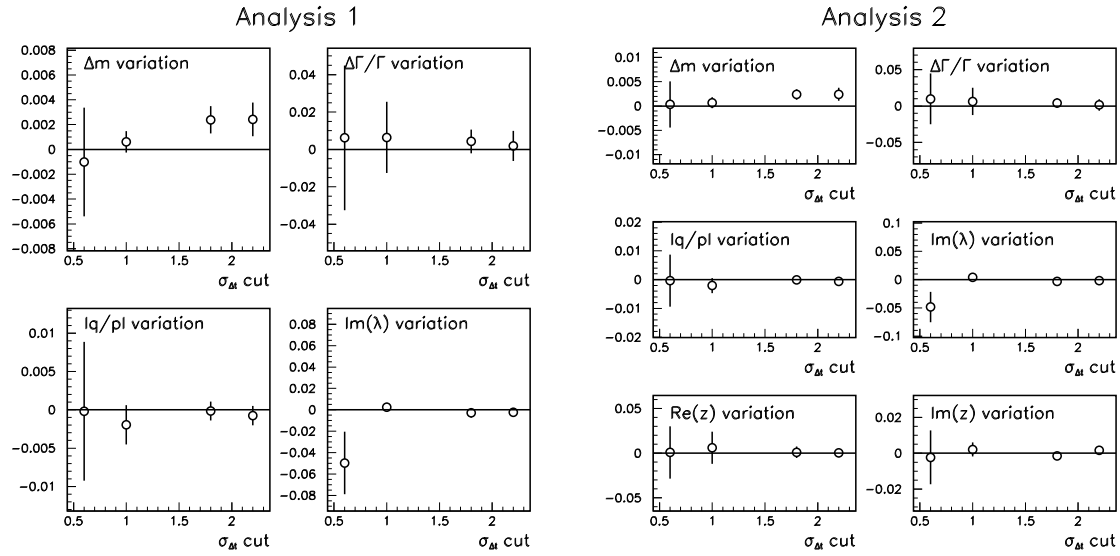

Figure 46: Stability of the fitted physical parameters from Analysis 1 and 2 against the $\sigma_{\Delta t}$ cut. The variation with respect to the nominal configuration is shown.

separately. The B_{flav} peaking background in these fits was assumed to be 0. The $B_{CPK_S^0}$ peaking background in the exclusive sample was taken also 0, and 1.5% in the inclusive one. The non-J/ψ background components in the $J/\psi K_L^0$ sample were taken 0. The fit projections (global fit with all samples) onto the Δt axis and the corresponding normalized residuals (defined as the difference between the data and the fit projection), for each standard Monte Carlo (inclusive charmonium) sample abd tagging category separately are shown in figures 47, 48 (B_{flav}), 49 ($B_{CPK_S^0}$) and 50 ($B_{CPK_L^0}$). Let us note that for this check we did not keep the relative fractions of B_{flav}, $B_{CPK_S^0}$ and $B_{CPK_L^0}$ events as observed in the data but we just put together the maximum available standard Monte Carlo statistics.

8.9 Results from dedicated full Monte Carlo

The nominal fits were also performed on the high statistics dedicated Monte Carlo described in section 3. As in the case of the standard Monte Carlo sample, we did not keep the relative fractions of B_{flav}, $B_{CPK_S^0}$ and $B_{CPK_L^0}$ events as observed in the data but we just used all the available statistics. Fits to Monte Carlo truth (perfect resolution, perfect tag) were first applied in order to check the correctness of the truth values in this dedicated Monte Carlo production. The results of these MC truth fits are given in table 43.

The fit results corresponding to Analysis 1 and Analysis 2, for the *GG* and *GExp* resolution models, are given in tables 44–47. All peaking backgrounds in these fits were assumed zero.

8.10 Results from reweighted dedicated full Monte Carlo

The dedicated full Monte Carlo was also used to "generate" samples with CPT violation ($z \neq 0$) and DCKM effects ($\lambda_{tag}, \bar{\lambda}_{tag}, \lambda_{flav}, \lambda_{flav} \neq 0$). This was done using reweighting techniques.

8.10.1 Strategy

The reweighting of the dedicated Monte Carlo events is performed using the truth values of Δt and the flavors of the two B mesons in the event. The flavor of the B mesons allows us to classify the B_{flav} and B_{CP} events according to 4 categories each: (B^0_{tag} B^0_{flav}, $\overline{B}^0_{tag}$ B^0_{flav}, B^0_{tag} $\overline{B}^0_{flav}$ and $\overline{B}^0_{tag}$ $\overline{B}^0_{flav}$) and (B^0_{tag} $\eta_{CP} = -1, \overline{B}^0_{tag}$ $\eta_{CP} = -1, B^0_{tag}$ $\eta_{CP} = +1, \overline{B}^0_{tag}$ $\eta_{CP} = +1$), respectively. For each event class, we then calculate the ratio of the new and original (standard events) PDF's. While doing this, special attention must be put to the fact that the new physics parameters change the time-integrated rates. As with this technique we only want to change the physics but not the detector effects, the two PDF's entering into the ratio must use a common normalization, i.e. the new PDF must not be renormalized with the new physics parameter values. In this way, the change in the number of events in each event category is purely due to physics. Figure 51 shows the PDF ratios (new/original), corresponding to the physics paramaters of the CPT reweighted configuration given in table 48.

8.10.2 Results from Monte Carlo truth fits

Fits to Monte Carlo truth (perfect resolution, perfect tag) were first applied in order to check that the generated values are correct. r_{tag}, $\bar{r}_{tag}$, $\frac{\mathrm{Im}\lambda_{tag}}{|\lambda_{tag}|}$, $\frac{\mathrm{Im}\bar{\lambda}_{tag}}{|\lambda_{tag}|}$, r_{flav}, $\bar{r}_{flav}$, $\frac{\mathrm{Im}\lambda_{flav}}{|\lambda_{flav}|}$ and $\frac{\mathrm{Im}\lambda_{flav}}{|\lambda_{flav}|}$ were fixed in all cases to the truth values. The results of these fits are given in table 49.

Parameter	B^0 fit results (*GG* model)
Δm	0.4815 ± 0.0038
$\Delta\Gamma/\Gamma$	$(-1.4 \pm 1.7) \cdot 10^{-2}$
$\lvert q/p \rvert$	1.0058 ± 0.0065
$\frac{\mathrm{Im}\lambda_{CP}}{\lvert\lambda_{CP}\rvert}$	0.674 ± 0.026
$\frac{\mathrm{Re}\lambda_{CP}}{\lvert\lambda_{CP}\rvert}\mathrm{Rez}$	$(-0.7 \pm 1.9) \cdot 10^{-2}$
Imz	$(0.5 \pm 1.4) \cdot 10^{-2}$
S_{core}	1.267 ± 0.023
$\delta_{core}^{\mathrm{Lepton}}$	-0.125 ± 0.032
$\delta_{core}^{\mathrm{Kaon+KPi}}$	-0.323 ± 0.025
$\delta_{core}^{\mathrm{Kaon+SlowPi}}$	-0.316 ± 0.022
$\delta_{core}^{\mathrm{Other}}$	-0.265 ± 0.022
$\delta_{core}^{\mathrm{Untag}}$	-0.305 ± 0.018
f_{tail}	$(3.83 \pm 0.90) \cdot 10^{-2}$
S_{tail}	4.41 ± 0.40
δ_{tail}	-1.50 ± 0.32
$f_{outlier}$	$(2.47 \pm 0.58) \cdot 10^{-3}$
w_0^{Lepton}	$(2.97 \pm 0.33) \cdot 10^{-2}$
$w_0^{\mathrm{Kaon+KPi}}$	$(3.15 \pm 0.93) \cdot 10^{-2}$
$w_0^{\mathrm{Kaon+SlowPi}}$	0.141 ± 0.012
w_0^{Other}	0.255 ± 0.012
$w_{slope}^{\mathrm{Kaon+KPi}}$	$(9.5 \pm 1.7) \cdot 10^{-2}$
$w_{slope}^{\mathrm{Kaon+SlowPi}}$	$(9.6 \pm 1.8) \cdot 10^{-2}$
$w_{slope}^{\mathrm{Other}}$	$(8.0 \pm 1.8) \cdot 10^{-2}$
$\Delta w^{\mathrm{Lepton}}$	$(-5.6 \pm 6.1) \cdot 10^{-3}$
$\Delta w^{\mathrm{Kaon+KPi}}$	$(-0.7 \pm 5.8) \cdot 10^{-3}$
$\Delta w^{\mathrm{Kaon+SlowPi}}$	$(-2.62 \pm 0.63) \cdot 10^{-2}$
$\Delta w^{\mathrm{Other}}$	$(-3.52 \pm 0.65) \cdot 10^{-2}$
ν	$(6.5 \pm 3.9) \cdot 10^{-3}$
μ^{Lepton}	$(2.9 \pm 1.0) \cdot 10^{-2}$
$\mu^{\mathrm{Kaon+KPi}}$	$(7.2 \pm 7.9) \cdot 10^{-3}$
$\mu^{\mathrm{Kaon+SlowPi}}$	$(2.5 \pm 7.8) \cdot 10^{-3}$
μ^{Other}	$(-9.3 \pm 8.0) \cdot 10^{-3}$

Parameter	B^0 fit results (*GG* model)
$\frac{\mathrm{Im}\lambda_{flav}}{\lvert\lambda_{flav}\rvert}$	-0.25 ± 0.54
$\frac{\mathrm{Im}\lambda_{flav}}{\lvert\lambda_{flav}\rvert}$	-0.10 ± 0.54
$\frac{\mathrm{Im}\lambda_{tag}}{\lvert\lambda_{tag}\rvert}$	0.62 ± 0.59
$\frac{\mathrm{Im}\lambda_{tag}}{\lvert\lambda_{tag}\rvert}$	0.21 ± 0.58
$f_{prompt,B_{flav}}^{\mathrm{Lepton}}$	$(0.00 \pm 0.24) \cdot 10^{-3}$
$f_{prompt,B_{flav}}^{\mathrm{Kaon+KPi}}$	$(0.00 \pm 0.14) \cdot 10^{-3}$
$f_{prompt,B_{flav}}^{\mathrm{Kaon+SlowPi}}$	$(0.00 \pm 0.32) \cdot 10^{-3}$
$f_{prompt,B_{flav}}^{\mathrm{Other}}$	$(5.3 \pm 4.0) \cdot 10^{-2}$
$f_{prompt,B_{flav}}^{\mathrm{Untag}}$	0.117 ± 0.038
S_{back}	1.374 ± 0.069
δ_{back}	-0.199 ± 0.033
$f_{back,outlier}$	$(1.60 \pm 0.37) \cdot 10^{-2}$
$w_{0,non-prompt}^{\mathrm{Lepton}}$	0.178 ± 0.022
$w_{0,non-prompt}^{\mathrm{Kaon+KPi}}$	0.219 ± 0.013
$w_{0,non-prompt}^{\mathrm{Kaon+SlowPi}}$	0.333 ± 0.012
$w_{0,non-prompt}^{\mathrm{Other}}$	0.369 ± 0.015
$\tau_{non-prompt}$	1.340 ± 0.034
$\tau_{non-prompt,B_{CPK_S^0}}$	1.89 ± 0.16
$f_{prompt,J/\psi K_S(\pi^+\pi^-)}$	0.124 ± 0.076
$f_{prompt,J/\psi K_S(\pi^0\pi^0)}$	0.302 ± 0.093
$f_{prompt,\psi(2S)K_S}$	0.17 ± 0.20
$f_{prompt,\chi_{c1}K_S}$	0.30 ± 0.14

Table 40: Analysis 2 results, *GG* resolution model for the standard full Monte Carlo sample (inclusive charmonium).

Parameter	B^0 fit results (*GExp* model)
Δm	0.4766 ± 0.0038
$\Delta\Gamma/\Gamma$	$(-1.4 \pm 1.8) \cdot 10^{-2}$
$\mid q/p \mid$	1.0053 ± 0.0066
$\frac{\mathrm{Im}\lambda_{CP}}{\mid\lambda_{CP}\mid}$	0.672 ± 0.026
$\frac{\mathrm{Re}\lambda_{CP}}{\mid\lambda_{CP}\mid}\mathrm{Re}z$	$(-0.9 \pm 2.0) \cdot 10^{-2}$
$\mathrm{Im}z$	$(0.5 \pm 1.4) \cdot 10^{-2}$
S	1.166 ± 0.019
τ_r^{Lepton}	1.00 ± 0.33
$\tau_r^{\mathrm{Kaon+KPi}}$	1.04 ± 0.13
$\tau_r^{\mathrm{Kaon+SlowPi}}$	1.27 ± 0.13
τ_r^{Other}	0.99 ± 0.22
τ_r^{Untag}	1.29 ± 0.11
$f_{Exp}^{\mathrm{Lepton}}$	0.161 ± 0.065
$f_{Exp}^{\mathrm{Kaon+KPi}}$	0.364 ± 0.049
$f_{Exp}^{\mathrm{Kaon+SlowPi}}$	0.301 ± 0.034
f_{Exp}^{Other}	0.311 ± 0.070
f_{Exp}^{Untag}	0.282 ± 0.027
$f_{outlier}$	$(4.24 \pm 0.58) \cdot 10^{-3}$
w_0^{Lepton}	$(3.23 \pm 0.33) \cdot 10^{-2}$
$w_0^{\mathrm{Kaon+KPi}}$	$(3.19 \pm 0.93) \cdot 10^{-2}$
$w_0^{\mathrm{Kaon+SlowPi}}$	0.142 ± 0.012
w_0^{Other}	0.256 ± 0.012
$w_{slope}^{\mathrm{Kaon+KPi}}$	$(9.7 \pm 1.7) \cdot 10^{-2}$
$w_{slope}^{\mathrm{Kaon+SlowPi}}$	$(9.8 \pm 1.8) \cdot 10^{-2}$
$w_{slope}^{\mathrm{Other}}$	$(8.2 \pm 1.8) \cdot 10^{-2}$
$\Delta w^{\mathrm{Lepton}}$	$(-5.8 \pm 6.1) \cdot 10^{-3}$
$\Delta w^{\mathrm{Kaon+KPi}}$	$(-0.5 \pm 5.8) \cdot 10^{-3}$
$\Delta w^{\mathrm{Kaon+SlowPi}}$	$(-2.61 \pm 0.63) \cdot 10^{-2}$
$\Delta w^{\mathrm{Other}}$	$(-3.51 \pm 0.65) \cdot 10^{-2}$
ν	$(6.3 \pm 3.9) \cdot 10^{-3}$
μ^{Lepton}	$(2.8 \pm 1.0) \cdot 10^{-2}$
$\mu^{\mathrm{Kaon+KPi}}$	$(7.2 \pm 7.9) \cdot 10^{-3}$
$\mu^{\mathrm{Kaon+SlowPi}}$	$(2.5 \pm 7.8) \cdot 10^{-3}$
μ^{Other}	$(-9.4 \pm 7.9) \cdot 10^{-3}$

Parameter	B^0 fit results (*GExp* model)
$\frac{\mathrm{Im}\lambda_{flav}}{\mid\lambda_{flav}\mid}$	-0.26 ± 0.53
$\frac{\mathrm{Im}\lambda_{flav}}{\mid\lambda_{flav}\mid}$	-0.11 ± 0.54
$\frac{\mathrm{Im}\lambda_{tag}}{\mid\lambda_{tag}\mid}$	0.76 ± 0.58
$\frac{\mathrm{Im}\lambda_{tag}}{\mid\lambda_{tag}\mid}$	0.35 ± 0.58
$f_{prompt,B_{flav}}^{\mathrm{Lepton}}$	$(0.00 \pm 0.23) \cdot 10^{-3}$
$f_{prompt,B_{flav}}^{\mathrm{Kaon+KPi}}$	$(0.00 \pm 0.14) \cdot 10^{-3}$
$f_{prompt,B_{flav}}^{\mathrm{Kaon+SlowPi}}$	$(0.00 \pm 0.31) \cdot 10^{-3}$
$f_{prompt,B_{flav}}^{\mathrm{Other}}$	$(4.9 \pm 4.3) \cdot 10^{-2}$
$f_{prompt,B_{flav}}^{\mathrm{Untag}}$	0.117 ± 0.041
S_{back}	1.312 ± 0.071
$\tau_{r,back}$	2.67 ± 0.51
$f_{back,outlier}$	$(1.17 \pm 0.39) \cdot 10^{-2}$
$w_{0,non-prompt}^{\mathrm{Lepton}}$	0.176 ± 0.022
$w_{0,non-prompt}^{\mathrm{Kaon+KPi}}$	0.219 ± 0.013
$w_{0,non-prompt}^{\mathrm{Kaon+SlowPi}}$	0.333 ± 0.012
$w_{0,non-prompt}^{\mathrm{Other}}$	0.369 ± 0.015
$\tau_{non-prompt}$	1.284 ± 0.035
$\tau_{non-prompt}$	1.284 ± 0.035
$\tau_{non-prompt,B_{CPK_S^0}}$	1.84 ± 0.16
$f_{prompt,J/\psi K_S(\pi^+\pi^-)}$	0.125 ± 0.078
$f_{prompt,J/\psi K_S(\pi^0\pi^0)}$	0.306 ± 0.098
$f_{prompt,\psi(2S)K_S}$	0.15 ± 0.21
$f_{prompt,\chi_{c1}K_S}$	0.28 ± 0.14

Table 41: Analysis 2 results, *GExp* resolution model for the standard full Monte Carlo sample (inclusive charmonium).

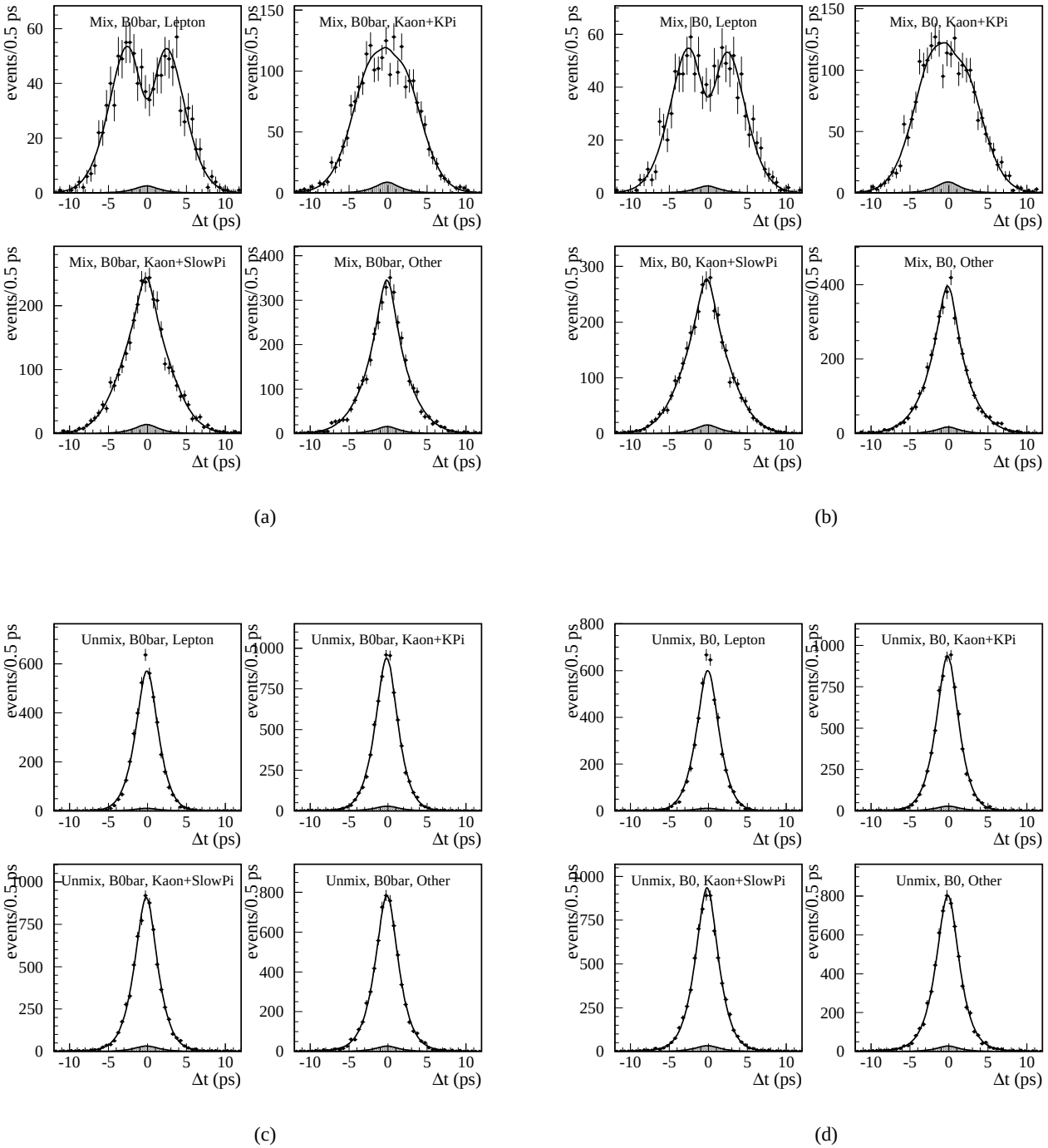

Figure 47: Δt projections of the nominal fit (Analysis 2) for the B_{flav} standard Monte Carlo sample: (a) mixed $\overline{B}^0$ tagged, (b) mixed B^0 tagged, (c) unmixed $\overline{B}^0$ tagged and (d) unmixed B^0 tagged (GG model), for each tagging category.

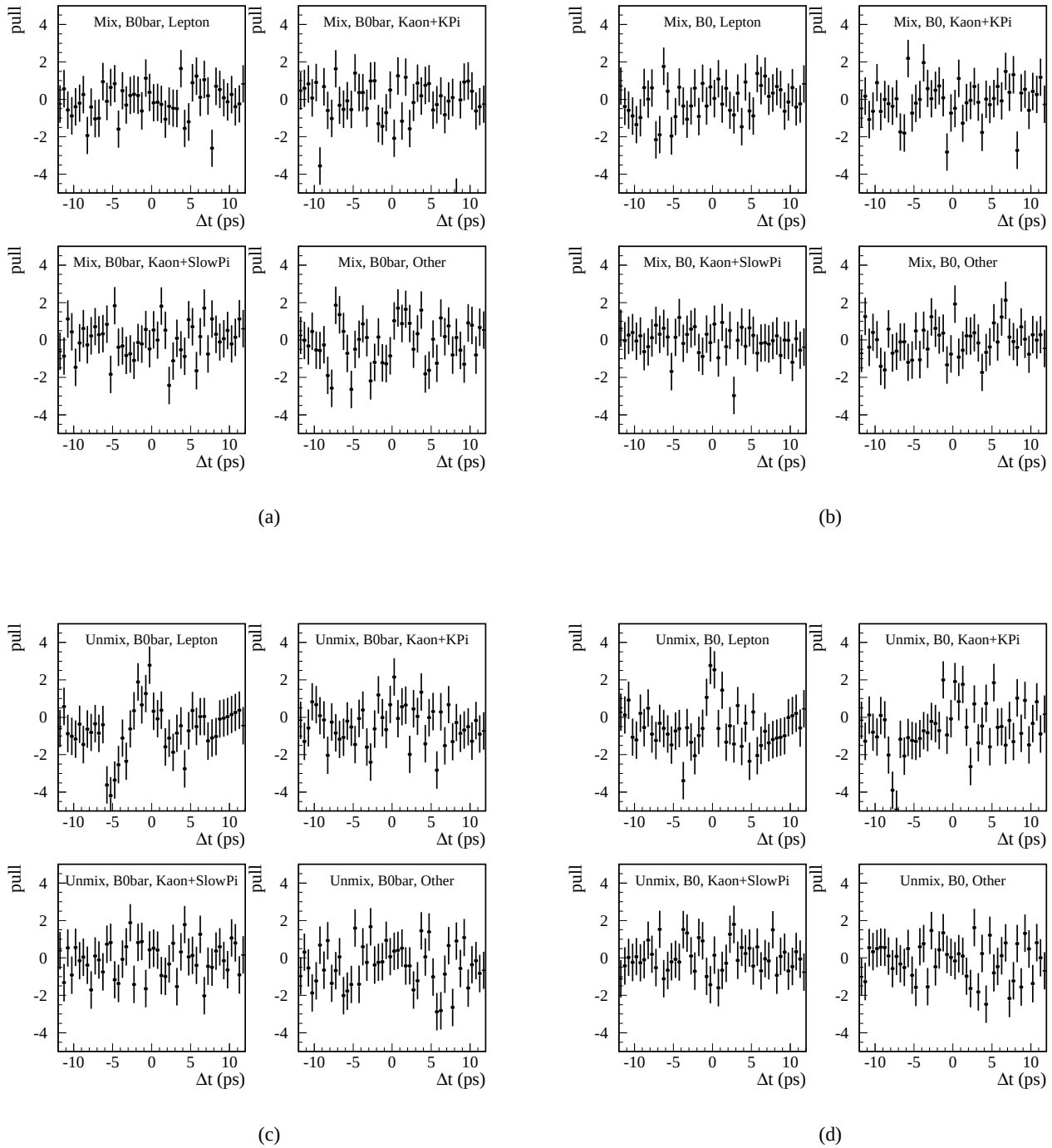

Figure 48: Normalized residuals of the Δt projections of the nominal fit (Analysis 2) for the B_{flav} standard Monte Carlo sample: (a) mixed $\overline{B}^0$ tagged, (b) mixed B^0 tagged, (c) unmixed $\overline{B}^0$ tagged and (d) unmixed B^0 tagged (*GG* model), for each tagging category.

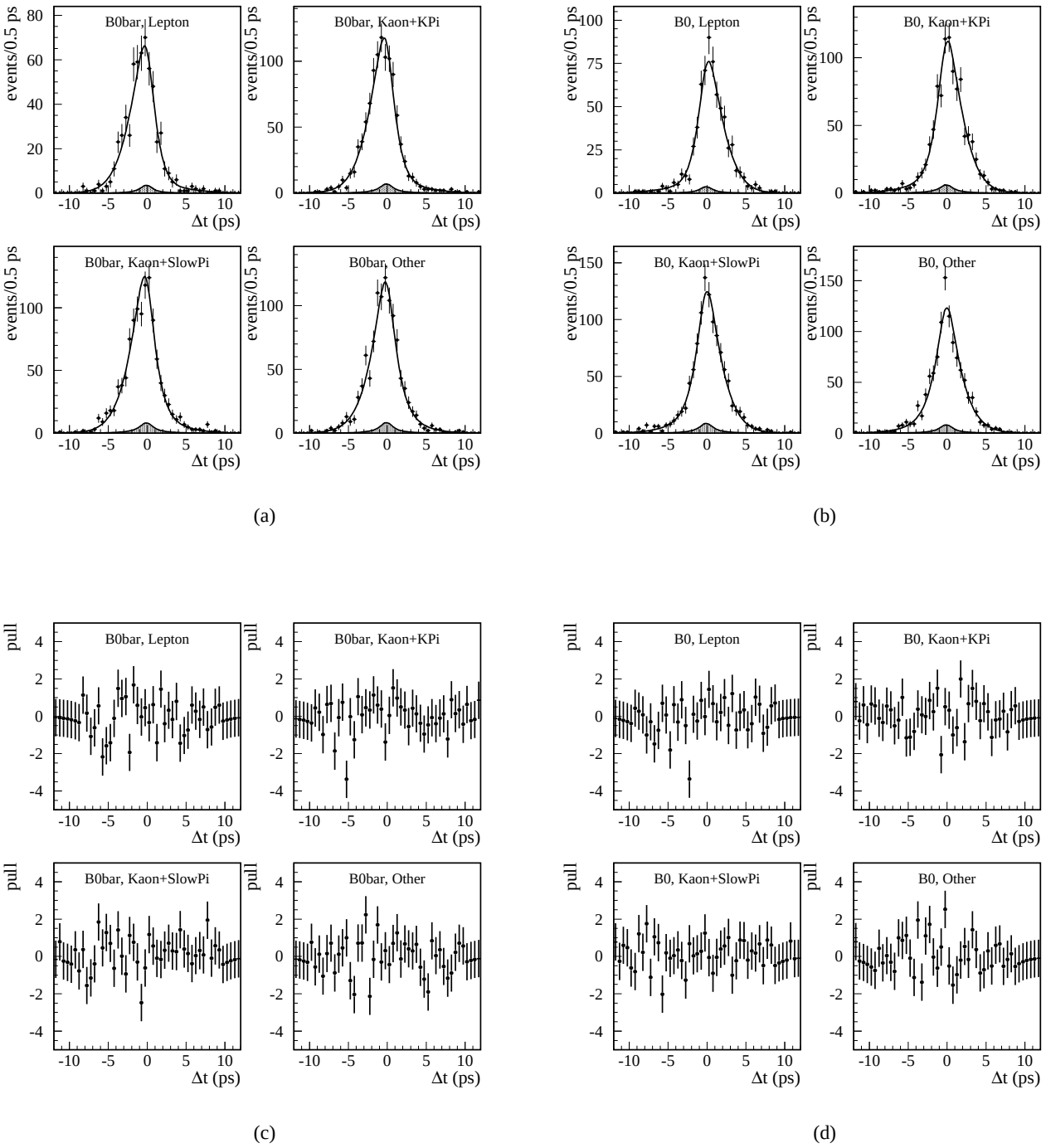

Figure 49: Δt projections and normalized residuals of the nominal fit (Analysis 2) for the $B_{CPK^0_S}$ standard inclusive Monte Carlo sample: (a)(c) $\bar{B}^0$ tagged, (b)(d) B^0 tagged (*GG* model), for each tagging category.

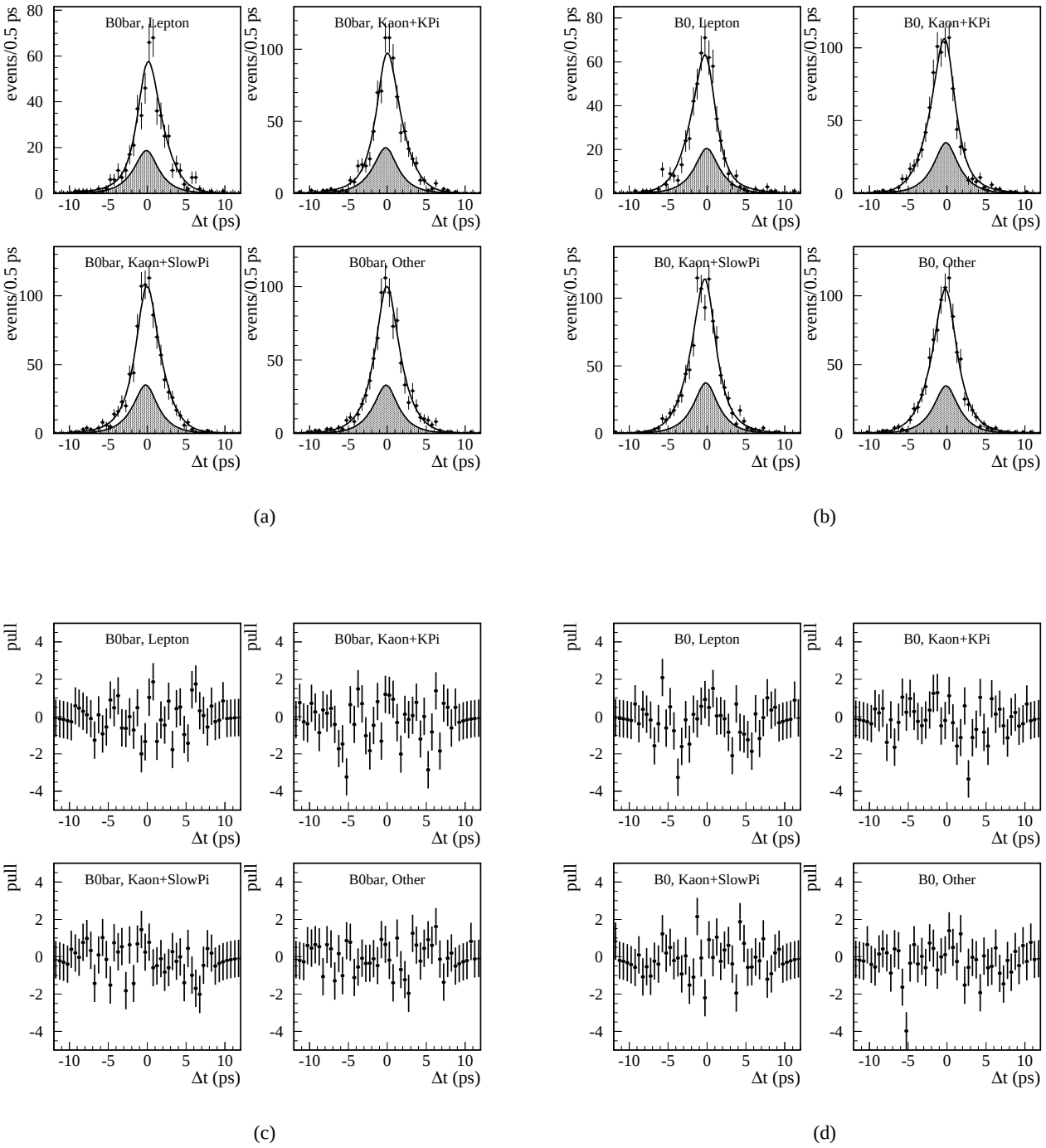

Figure 50: Δt projections and normalized residuals of the nominal fit (Analysis 2) for the $B_{CPK^0_L}$ standard inclusive Monte Carlo sample: (a)(c) $\overline{B}^0$ tagged, (b)(d) B^0 tagged (*GG* model), for each tagging category.

Parameter	incl. charmonium all CP	incl. charmonium $B_{CPK_S^0}$	incl. charmonium $B_{CPK_L^0}$
Δm	0.4815 ± 0.0038	0.4821 ± 0.0038	0.4816 ± 0.0038
$\Delta\Gamma/\Gamma$	$(-1.4 \pm 1.7) \cdot 10^{-2}$	$(-2.0 \pm 2.0) \cdot 10^{-2}$	$(-0.6 \pm 3.1) \cdot 10^{-2}$
$\mid q/p \mid$	1.0058 ± 0.0065	1.0041 ± 0.0067	1.0048 ± 0.0067
$\frac{\mathrm{Im}\lambda_{CP}}{\mid\lambda_{CP}\mid}$	0.674 ± 0.026	0.676 ± 0.031	0.667 ± 0.051
$\frac{\mathrm{Re}\lambda_{CP}}{\mid\lambda_{CP}\mid}\mathrm{Re}z$	$(-0.7 \pm 1.9) \cdot 10^{-2}$	$(-0.1 \pm 2.1) \cdot 10^{-2}$	$(-1.2 \pm 2.6) \cdot 10^{-2}$
$\mathrm{Im}z$	$(0.5 \pm 1.4) \cdot 10^{-2}$	$(0.6 \pm 1.5) \cdot 10^{-2}$	$(0.6 \pm 1.5) \cdot 10^{-2}$

Table 42: Analysis 2 results, limited to physics parameters, *GG* resolution model, for the standard full Monte Carlo sample (inclusive charmonium) using both the CP samples, $B_{CPK_S^0}$ and $B_{CPK_L^0}$ samples.

Parameter	Fit result
τ_B	1.542 ± 0.005
Δm	0.4748 ± 0.0018
$\Delta\Gamma/\Gamma$	0.205 ± 0.008
$\mid q/p \mid$	1.033 ± 0.004
$\frac{\mathrm{Im}\lambda_{CP}}{\mid\lambda_{CP}\mid}$	0.681 ± 0.009
$\frac{\mathrm{Re}\lambda_{CP}}{\mid\lambda_{CP}\mid}\mathrm{Re}z$	-0.003 ± 0.006
$\mathrm{Im}z$	0.005 ± 0.005

Table 43: Results from maximum likelihood fits to the MC truth information (perfect resolution, perfect tag) in the dedicated full Monte Carlo prodution.

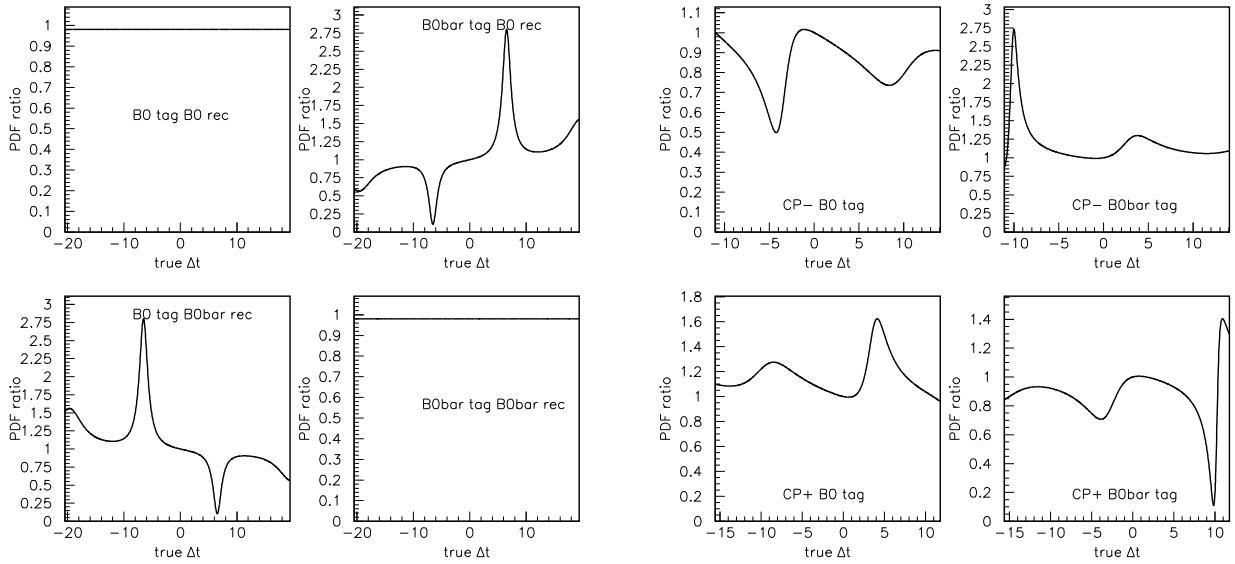

Figure 51: Reweighting functions for B_{flav} (left hand) and CP (right hand) events, corresponding to the CPT reweighted configuration with parameter values given in table 48.

Parameter	B^0 fit results (*GG* model)
Δm	0.4808 ± 0.0044
$\Delta\Gamma/\Gamma$	0.183 ± 0.014
$\mid q/p \mid$	1.0430 ± 0.0075
$\frac{\mathrm{Im}\lambda_{CP}}{\lvert\lambda_{CP}\rvert}$	0.708 ± 0.022
S_{core}	1.205 ± 0.040
$\delta_{core}^{\mathsf{Lepton}}$	-0.155 ± 0.041
$\delta_{core}^{\mathsf{Kaon+KPi}}$	-0.289 ± 0.032
$\delta_{core}^{\mathsf{Kaon+SlowPi}}$	-0.274 ± 0.030
$\delta_{core}^{\mathsf{Other}}$	-0.180 ± 0.031
$\delta_{core}^{\mathsf{Untag}}$	-0.225 ± 0.026
f_{tail}	$(8.0 \pm 2.4) \cdot 10^{-2}$
S_{tail}	3.35 ± 0.38
δ_{tail}	-1.52 ± 0.32
$f_{outlier}$	$(3.12 \pm 0.67) \cdot 10^{-3}$

Parameter	B^0 fit results (*GG* model)
w_0^{Lepton}	$(2.65 \pm 0.36) \cdot 10^{-2}$
$w_0^{\mathsf{Kaon+KPi}}$	$(3.5 \pm 1.1) \cdot 10^{-2}$
$w_0^{\mathsf{Kaon+SlowPi}}$	0.141 ± 0.013
w_0^{Other}	0.275 ± 0.013
$w_{slope}^{\mathsf{Kaon+KPi}}$	$(9.9 \pm 1.9) \cdot 10^{-2}$
$w_{slope}^{\mathsf{Kaon+SlowPi}}$	0.115 ± 0.020
$w_{slope}^{\mathsf{Other}}$	$(4.6 \pm 2.0) \cdot 10^{-2}$
$\Delta w^{\mathsf{Lepton}}$	$(-1.12 \pm 0.68) \cdot 10^{-2}$
$\Delta w^{\mathsf{Kaon+KPi}}$	$(-3.4 \pm 6.5) \cdot 10^{-3}$
$\Delta w^{\mathsf{Kaon+SlowPi}}$	$(-2.08 \pm 0.71) \cdot 10^{-2}$
$\Delta w^{\mathsf{Other}}$	$(-3.32 \pm 0.72) \cdot 10^{-2}$
ν	$(1.27 \pm 0.44) \cdot 10^{-2}$
μ^{Lepton}	$(1.4 \pm 1.1) \cdot 10^{-2}$
$\mu^{\mathsf{Kaon+KPi}}$	$(1.94 \pm 0.88) \cdot 10^{-2}$
$\mu^{\mathsf{Kaon+SlowPi}}$	$(4.6 \pm 8.8) \cdot 10^{-3}$
μ^{Other}	$(-1.97 \pm 0.90) \cdot 10^{-2}$
$\frac{\mathrm{Im}\lambda_{flav}}{\lvert\lambda_{flav}\rvert}$	-0.78 ± 0.48
$\frac{\mathrm{Im}\lambda_{flav}}{\lvert\lambda_{flav}\rvert}$	-0.67 ± 0.50
$\frac{\mathrm{Im}\lambda_{tag}}{\lvert\lambda_{tag}\rvert}$	-0.14 ± 0.48
$\frac{\mathrm{Im}\lambda_{tag}}{\lvert\lambda_{tag}\rvert}$	0.43 ± 0.50

Table 44: Results from dedicated full Monte Carlo, Analysis 1 fit, *GG* resolution function.

8.10.3 Results from nominal fits

The fit results corresponding to the Analysis 2 fits from the CPT reweighted samples, for the *GG* and *GExp* resolution models, are given in tables 50 and 51. Tables 52 and 53 show the fit results, again for Analysis 2 and 1 respectively, from the DCKM reweighted samples. In all cases the fitted values are consistent with the generated ones.

8.11 Alternative tagging configuration

The nominal fits were also performed using the Elba Tagger [22] , for data and the standard full Monte Carlo (inclusive charmonium). The results and the comparison to the default Moriond Tagger are summarized in tables 54, 55, 56, 57, 58 and 59.

8.12 Alternative vertexing configurations

Tables from 60 to 68 summarize the differences of the results for the physics parameters (Analysis 1 and Analysis 2) for different alternative vertexing configurations with respect to the nominal configuration. In order to avoid additional statistical uncertainties from events moving around only those common to the nominal and the modified configurations are used. The errors on the differences are estimated from the quadratic difference

Parameter	B^0 fit results (*GG* model)
Δm	0.4808 ± 0.0044
$\Delta\Gamma/\Gamma$	0.184 ± 0.014
$\mid q/p \mid$	1.0433 ± 0.0075
$\frac{\mathrm{Im}\lambda_{CP}}{\mid\lambda_{CP}\mid}$	0.707 ± 0.022
$\frac{\mathrm{Re}\lambda_{CP}}{\mid\lambda_{CP}\mid}\mathrm{Re}z$	$(-0.8 \pm 1.5) \cdot 10^{-2}$
$\mathrm{Im}z$	$(-0.1 \pm 1.6) \cdot 10^{-2}$
S_{core}	1.204 ± 0.040
$\delta_{core}^{\mathrm{Lepton}}$	-0.154 ± 0.041
$\delta_{core}^{\mathrm{Kaon+KPi}}$	-0.289 ± 0.032
$\delta_{core}^{\mathrm{Kaon+SlowPi}}$	-0.273 ± 0.030
$\delta_{core}^{\mathrm{Other}}$	-0.180 ± 0.031
$\delta_{core}^{\mathrm{Untag}}$	-0.224 ± 0.026
f_{tail}	$(8.1 \pm 2.5) \cdot 10^{-2}$
S_{tail}	3.34 ± 0.38
δ_{tail}	-1.51 ± 0.32
$f_{outlier}$	$(3.13 \pm 0.67) \cdot 10^{-3}$

Parameter	B^0 fit results (*GG* model)
w_0^{Lepton}	$(2.65 \pm 0.36) \cdot 10^{-2}$
$w_0^{\mathrm{Kaon+KPi}}$	$(3.5 \pm 1.1) \cdot 10^{-2}$
$w_0^{\mathrm{Kaon+SlowPi}}$	0.141 ± 0.013
w_0^{Other}	0.275 ± 0.013
$w_{slope}^{\mathrm{Kaon+KPi}}$	$(9.9 \pm 1.9) \cdot 10^{-2}$
$w_{slope}^{\mathrm{Kaon+SlowPi}}$	0.115 ± 0.020
$w_{slope}^{\mathrm{Other}}$	$(4.6 \pm 2.0) \cdot 10^{-2}$
$\Delta w^{\mathrm{Lepton}}$	$(-1.11 \pm 0.68) \cdot 10^{-2}$
$\Delta w^{\mathrm{Kaon+KPi}}$	$(-3.2 \pm 6.5) \cdot 10^{-3}$
$\Delta w^{\mathrm{Kaon+SlowPi}}$	$(-2.08 \pm 0.71) \cdot 10^{-2}$
$\Delta w^{\mathrm{Other}}$	$(-3.31 \pm 0.72) \cdot 10^{-2}$
ν	$(1.29 \pm 0.44) \cdot 10^{-2}$
μ^{Lepton}	$(1.4 \pm 1.1) \cdot 10^{-2}$
$\mu^{\mathrm{Kaon+KPi}}$	$(1.94 \pm 0.88) \cdot 10^{-2}$
$\mu^{\mathrm{Kaon+SlowPi}}$	$(4.5 \pm 8.8) \cdot 10^{-3}$
μ^{Other}	$(-1.96 \pm 0.90) \cdot 10^{-2}$
$\frac{\mathrm{Im}\lambda_{flav}}{\mid\lambda_{flav}\mid}$	-0.85 ± 0.58
$\frac{\mathrm{Im}\lambda_{flav}}{\mid\lambda_{flav}\mid}$	-0.59 ± 0.59
$\frac{\mathrm{Im}\lambda_{tag}}{\mid\lambda_{tag}\mid}$	-0.21 ± 0.61
$\frac{\mathrm{Im}\lambda_{tag}}{\mid\lambda_{tag}\mid}$	0.51 ± 0.63

Table 45: Results from dedicated full Monte Carlo, Analysis 2 fit, *GG* resolution function.

of the statistical Gaussian errors. Nevertheless, this procedure to estimate the error on the difference does not take completely into account statistical differences due to quantities changing within the common events, for example a different value of Δt and/or $\sigma_{\Delta t}$. The configurations are:

- J/ψ mass constraint imposed for the *CP* vertex (table 60);
- use charmonium (J/ψ or $\psi(2S)$) vertex for the *CP* vertex (table 61);
- remove K_S^0 mass constraint (table 62);
- removing photons from the *CP* vertex (table 63);
- do not use the constraints from the beam (table 64);
- use only the constraint from the beam spot (table 65);
- remove the V^0 veto for the tag vertex (table 66);
- use the *average boost approximation* instead of the *average-τ_B approximation* for the $\Delta z \to \Delta t$ conversion [27] (table 67);
- use `FvtCluster` instead of the default `BtaSelFit` [27] (table 68).

Parameter	B^0 fit results (*GExp* model)
Δm	0.4766 ± 0.0045
$\Delta\Gamma/\Gamma$	0.196 ± 0.014
$\mid q/p \mid$	1.0446 ± 0.0075
$\frac{\mathrm{Im}\lambda_{CP}}{\lvert\lambda_{CP}\rvert}$	0.712 ± 0.022
S	1.155 ± 0.020
τ_r^{Lepton}	1.21 ± 0.29
$\tau_r^{\mathsf{Kaon+KPi}}$	1.10 ± 0.16
$\tau_r^{\mathsf{Kaon+SlowPi}}$	1.58 ± 0.13
τ_r^{Other}	1.51 ± 0.20
τ_r^{Untag}	1.66 ± 0.16
$f_{Exp}^{\mathsf{Lepton}}$	0.210 ± 0.061
$f_{Exp}^{\mathsf{Kaon+KPi}}$	0.348 ± 0.056
$f_{Exp}^{\mathsf{Kaon+SlowPi}}$	0.254 ± 0.026
f_{Exp}^{Other}	0.194 ± 0.030
f_{Exp}^{Untag}	0.205 ± 0.023
$f_{outlier}$	$(3.31 \pm 0.65) \cdot 10^{-3}$

Parameter	B^0 fit results (*GExp* model)
w_0^{Lepton}	$(2.85 \pm 0.36) \cdot 10^{-2}$
$w_0^{\mathsf{Kaon+KPi}}$	$(3.5 \pm 1.1) \cdot 10^{-2}$
$w_0^{\mathsf{Kaon+SlowPi}}$	0.140 ± 0.013
w_0^{Other}	0.276 ± 0.013
$w_{slope}^{\mathsf{Kaon+KPi}}$	0.103 ± 0.019
$w_{slope}^{\mathsf{Kaon+SlowPi}}$	0.116 ± 0.020
$w_{slope}^{\mathsf{Other}}$	$(4.6 \pm 2.0) \cdot 10^{-2}$
$\Delta w^{\mathsf{Lepton}}$	$(-1.16 \pm 0.68) \cdot 10^{-2}$
$\Delta w^{\mathsf{Kaon+KPi}}$	$(-4.0 \pm 6.5) \cdot 10^{-3}$
$\Delta w^{\mathsf{Kaon+SlowPi}}$	$(-2.08 \pm 0.71) \cdot 10^{-2}$
$\Delta w^{\mathsf{Other}}$	$(-3.35 \pm 0.72) \cdot 10^{-2}$
ν	$(1.31 \pm 0.44) \cdot 10^{-2}$
μ^{Lepton}	$(1.5 \pm 1.1) \cdot 10^{-2}$
$\mu^{\mathsf{Kaon+KPi}}$	$(1.94 \pm 0.88) \cdot 10^{-2}$
$\mu^{\mathsf{Kaon+SlowPi}}$	$(5.3 \pm 8.7) \cdot 10^{-3}$
μ^{Other}	$(-1.98 \pm 0.89) \cdot 10^{-2}$
$\frac{\mathrm{Im}\lambda_{flav}}{\lvert\lambda_{flav}\rvert}$	-0.79 ± 0.48
$\frac{\mathrm{Im}\lambda_{flav}}{\lvert\lambda_{flav}\rvert}$	-0.69 ± 0.50
$\frac{\mathrm{Im}\lambda_{tag}}{\lvert\lambda_{tag}\rvert}$	-0.07 ± 0.47
$\frac{\mathrm{Im}\lambda_{tag}}{\lvert\lambda_{tag}\rvert}$	0.48 ± 0.50

Table 46: Results from dedicated full Monte Carlo, Analysis 1 fit, *GExp* resolution function.

Figures 52 and 53 show the same results in a graphical way. It can be seen that, overall, the shifts are consistent with zero within the statistical differences for all parameters, particularly those on which we are interested in this analysis ($\Delta\Gamma/\Gamma$, $\mid q/p \mid$ and z). The few 2-3 sigma discrepancies can be understood as statistical fluctuations combined with the underestimation of the uncertainty on the difference, as outlined above. By these reasons we did not assign any systematic uncertainty due to the changes in the vertexing configuration.

Parameter	B^0 fit results (*GExp* model)
Δm	0.4767 ± 0.0045
$\Delta\Gamma/\Gamma$	0.197 ± 0.014
$\mid q/p \mid$	1.0450 ± 0.0075
$\frac{\mathrm{Im}\lambda_{CP}}{\lvert\lambda_{CP}\rvert}$	0.710 ± 0.022
$\frac{\mathrm{Re}\lambda_{CP}}{\lvert\lambda_{CP}\rvert}\mathrm{Re}z$	$(-1.1 \pm 1.5) \cdot 10^{-2}$
$\mathrm{Im}z$	$(-0.1 \pm 1.6) \cdot 10^{-2}$
S	1.155 ± 0.020
τ_r^{Lepton}	1.19 ± 0.28
$\tau_r^{\mathrm{Kaon+KPi}}$	1.09 ± 0.16
$\tau_r^{\mathrm{Kaon+SlowPi}}$	1.58 ± 0.14
τ_r^{Other}	1.51 ± 0.20
τ_r^{Untag}	1.66 ± 0.16
$f_{Exp}^{\mathrm{Lepton}}$	0.212 ± 0.059
$f_{Exp}^{\mathrm{Kaon+KPi}}$	0.351 ± 0.057
$f_{Exp}^{\mathrm{Kaon+SlowPi}}$	0.254 ± 0.027
f_{Exp}^{Other}	0.194 ± 0.031
f_{Exp}^{Untag}	0.206 ± 0.023
$f_{outlier}$	$(3.32 \pm 0.65) \cdot 10^{-3}$

Parameter	B^0 fit results (*GExp* model)
w_0^{Lepton}	$(2.85 \pm 0.36) \cdot 10^{-2}$
$w_0^{\mathrm{Kaon+KPi}}$	$(3.5 \pm 1.1) \cdot 10^{-2}$
$w_0^{\mathrm{Kaon+SlowPi}}$	0.141 ± 0.013
w_0^{Other}	0.276 ± 0.013
$w_{slope}^{\mathrm{Kaon+KPi}}$	0.103 ± 0.019
$w_{slope}^{\mathrm{Kaon+SlowPi}}$	0.115 ± 0.020
$w_{slope}^{\mathrm{Other}}$	$(4.6 \pm 2.0) \cdot 10^{-2}$
$\Delta w^{\mathrm{Lepton}}$	$(-1.15 \pm 0.68) \cdot 10^{-2}$
$\Delta w^{\mathrm{Kaon+KPi}}$	$(-3.8 \pm 6.5) \cdot 10^{-3}$
$\Delta w^{\mathrm{Kaon+SlowPi}}$	$(-2.07 \pm 0.71) \cdot 10^{-2}$
$\Delta w^{\mathrm{Other}}$	$(-3.34 \pm 0.72) \cdot 10^{-2}$
ν	$(1.33 \pm 0.44) \cdot 10^{-2}$
μ^{Lepton}	$(1.4 \pm 1.1) \cdot 10^{-2}$
$\mu^{\mathrm{Kaon+KPi}}$	$(1.94 \pm 0.88) \cdot 10^{-2}$
$\mu^{\mathrm{Kaon+SlowPi}}$	$(5.2 \pm 8.7) \cdot 10^{-3}$
μ^{Other}	$(-1.98 \pm 0.89) \cdot 10^{-2}$
$\frac{\mathrm{Im}\lambda_{flav}}{\lvert\lambda_{flav}\rvert}$	-0.87 ± 0.57
$\frac{\mathrm{Im}\lambda_{flav}}{\lvert\lambda_{flav}\rvert}$	-0.60 ± 0.58
$\frac{\mathrm{Im}\lambda_{tag}}{\lvert\lambda_{tag}\rvert}$	-0.16 ± 0.61
$\frac{\mathrm{Im}\lambda_{tag}}{\lvert\lambda_{tag}\rvert}$	0.59 ± 0.63

Table 47: Results from dedicated full Monte Carlo, Analysis 2 fit, *GExp* resolution function.

Parameter	Original (dedicated MC)	CPT reweighted	DCKM reweighted
$\Delta\Gamma/\Gamma$	0.20	0.20	0.20
$\mid q/p \mid$	1.04	1.04	1.04
$\frac{\mathrm{Im}\lambda_{CP}}{\lvert\lambda_{CP}\rvert}$	0.70	0.70	0.70
Δm	0.472	0.472	0.472
$\frac{\mathrm{Re}\lambda_{CP}}{\lvert\lambda_{CP}\rvert}\mathrm{Re}z$	0.00	0.10	0.00
$\mathrm{Im}z$	0.00	0.02	0.00
$r_{tag}/\overline{r}_{tag}$	0.00	0.00	0.04
$\frac{\mathrm{Im}\lambda_{tag}}{\lvert\lambda_{tag}\rvert}$	0.00	0.00	-1.00
$\frac{\mathrm{Im}\lambda_{tag}}{\lvert\lambda_{tag}\rvert}$	0.00	0.00	+1.00
$r_{flav}/\overline{r}_{flav}$	0.00	0.00	0.04
$\frac{\mathrm{Im}\lambda_{flav}}{\lvert\lambda_{flav}\rvert}$	0.00	0.00	-1.00
$\frac{\mathrm{Im}\lambda_{flav}}{\lvert\lambda_{flav}\rvert}$	0.00	0.00	+1.00

Table 48: Physics parameter values of the dedicated and reweighted CPT and DCKM full Monte Carlo.

Parameter	CPT reweighted	DCKM reweighted
τ_B	1.541 ± 0.008	1.538 ± 0.006
Δm	0.4755 ± 0.0032	0.4730 ± 0.0022
$\Delta\Gamma/\Gamma$	0.193 ± 0.012	0.214 ± 0.009
$\mid q/p \mid$	1.035 ± 0.007	1.035 ± 0.005
$\frac{\mathrm{Im}\lambda_{CP}}{\mid\lambda_{CP}\mid}$	0.678 ± 0.013	0.684 ± 0.010
$\frac{\mathrm{Re}\lambda_{CP}}{\mid\lambda_{CP}\mid}\mathrm{Re}z$	0.106 ± 0.010	-0.004 ± 0.008
$\mathrm{Im}z$	0.025 ± 0.007	0.005 ± 0.006

Table 49: Results from maximum likelihood fits to the MC truth information (perfect resolution, perfect tag) in the reweighted CPT and DCKM full Monte Carlo.

Parameter	B^0 fit results (*GG* model)
Δm	0.4854 ± 0.0077
$\Delta\Gamma/\Gamma$	0.201 ± 0.023
$\mid q/p \mid$	1.048 ± 0.013
$\frac{\mathrm{Im}\lambda_{CP}}{\mid\lambda_{CP}\mid}$	0.730 ± 0.034
$\frac{\mathrm{Re}\lambda_{CP}}{\mid\lambda_{CP}\mid}\mathrm{Re}z$	$(7.5 \pm 2.3) \cdot 10^{-2}$
$\mathrm{Im}z$	$(4.6 \pm 2.6) \cdot 10^{-2}$
S_{core}	1.199 ± 0.079
$\delta_{core}^{\mathrm{Lepton}}$	-0.236 ± 0.070
$\delta_{core}^{\mathrm{Kaon+KPi}}$	-0.234 ± 0.059
$\delta_{core}^{\mathrm{Kaon+SlowPi}}$	-0.248 ± 0.058
$\delta_{core}^{\mathrm{Other}}$	$(-8.5 \pm 6.0) \cdot 10^{-2}$
$\delta_{core}^{\mathrm{Untag}}$	-0.172 ± 0.051
f_{tail}	0.106 ± 0.061
S_{tail}	2.70 ± 0.37
δ_{tail}	-1.62 ± 0.74
$f_{outlier}$	$(4.6 \pm 1.2) \cdot 10^{-3}$

Parameter	B^0 fit results (*GG* model)
w_0^{Lepton}	$(2.76 \pm 0.61) \cdot 10^{-2}$
$w_0^{\mathrm{Kaon+KPi}}$	$(2.0 \pm 1.8) \cdot 10^{-2}$
$w_0^{\mathrm{Kaon+SlowPi}}$	0.143 ± 0.023
w_0^{Other}	0.260 ± 0.023
$w_{slope}^{\mathrm{Kaon+KPi}}$	0.128 ± 0.032
$w_{slope}^{\mathrm{Kaon+SlowPi}}$	0.117 ± 0.035
$w_{slope}^{\mathrm{Other}}$	$(8.4 \pm 3.4) \cdot 10^{-2}$
$\Delta w^{\mathrm{Lepton}}$	$(-1.5 \pm 1.1) \cdot 10^{-2}$
$\Delta w^{\mathrm{Kaon+KPi}}$	$(0.8 \pm 1.1) \cdot 10^{-2}$
$\Delta w^{\mathrm{Kaon+SlowPi}}$	$(-3.7 \pm 1.2) \cdot 10^{-2}$
$\Delta w^{\mathrm{Other}}$	$(-3.9 \pm 1.2) \cdot 10^{-2}$
ν	$(1.54 \pm 0.78) \cdot 10^{-2}$
μ^{Lepton}	$(1.7 \pm 1.8) \cdot 10^{-2}$
$\mu^{\mathrm{Kaon+KPi}}$	$(3.4 \pm 1.4) \cdot 10^{-2}$
$\mu^{\mathrm{Kaon+SlowPi}}$	$(-0.5 \pm 1.5) \cdot 10^{-2}$
μ^{Other}	$(-1.9 \pm 1.5) \cdot 10^{-2}$
$\frac{\mathrm{Im}\lambda_{flav}}{\mid\lambda_{flav}\mid}$	-2.22 ± 0.92
$\frac{\mathrm{Im}\lambda_{flav}}{\mid\lambda_{flav}\mid}$	-2.34 ± 0.98
$\frac{\mathrm{Im}\lambda_{tag}}{\mid\lambda_{tag}\mid}$	-1.36 ± 0.96
$\frac{\mathrm{Im}\lambda_{tag}}{\mid\lambda_{tag}\mid}$	-1.6 ± 1.0

Table 50: Results from CPT reweighted full Monte Carlo, Analysis 2 fit, *GG* resolution function.

Parameter	B^0 fit results (*GExp* model)
Δm	0.4806 ± 0.0078
$\Delta\Gamma/\Gamma$	0.207 ± 0.023
$\mid q/p \mid$	1.049 ± 0.013
$\frac{\mathrm{Im}\lambda_{CP}}{\mid\lambda_{CP}\mid}$	0.729 ± 0.034
$\frac{\mathrm{Re}\lambda_{CP}}{\mid\lambda_{CP}\mid}\mathrm{Rez}$	$(7.3 \pm 2.3) \cdot 10^{-2}$
Imz	$(4.5 \pm 2.6) \cdot 10^{-2}$
S	1.184 ± 0.035
τ_r^{Lepton}	0.65 ± 0.33
$\tau_r^{\mathrm{Kaon+KPi}}$	0.79 ± 0.30
$\tau_r^{\mathrm{Kaon+SlowPi}}$	1.74 ± 0.20
τ_r^{Other}	1.46 ± 0.36
τ_r^{Untag}	1.48 ± 0.24
$f_{Exp}^{\mathrm{Lepton}}$	0.54 ± 0.29
$f_{Exp}^{\mathrm{Kaon+KPi}}$	0.45 ± 0.17
$f_{Exp}^{\mathrm{Kaon+SlowPi}}$	0.257 ± 0.037
f_{Exp}^{Other}	0.168 ± 0.050
f_{Exp}^{Untag}	0.224 ± 0.042
$f_{outlier}$	$(4.6 \pm 1.2) \cdot 10^{-3}$

Parameter	B^0 fit results (*GExp* model)
w_0^{Lepton}	$(2.98 \pm 0.62) \cdot 10^{-2}$
$w_0^{\mathrm{Kaon+KPi}}$	$(2.0 \pm 1.8) \cdot 10^{-2}$
$w_0^{\mathrm{Kaon+SlowPi}}$	0.140 ± 0.023
w_0^{Other}	0.260 ± 0.023
$w_{slope}^{\mathrm{Kaon+KPi}}$	0.132 ± 0.032
$w_{slope}^{\mathrm{Kaon+SlowPi}}$	0.120 ± 0.035
$w_{slope}^{\mathrm{Other}}$	$(8.5 \pm 3.4) \cdot 10^{-2}$
$\Delta w^{\mathrm{Lepton}}$	$(-1.5 \pm 1.1) \cdot 10^{-2}$
$\Delta w^{\mathrm{Kaon+KPi}}$	$(0.7 \pm 1.1) \cdot 10^{-2}$
$\Delta w^{\mathrm{Kaon+SlowPi}}$	$(-3.7 \pm 1.2) \cdot 10^{-2}$
$\Delta w^{\mathrm{Other}}$	$(-4.0 \pm 1.2) \cdot 10^{-2}$
ν	$(1.58 \pm 0.77) \cdot 10^{-2}$
μ^{Lepton}	$(1.7 \pm 1.8) \cdot 10^{-2}$
$\mu^{\mathrm{Kaon+KPi}}$	$(3.3 \pm 1.4) \cdot 10^{-2}$
$\mu^{\mathrm{Kaon+SlowPi}}$	$(-0.4 \pm 1.5) \cdot 10^{-2}$
μ^{Other}	$(-1.9 \pm 1.5) \cdot 10^{-2}$
$\frac{\mathrm{Im}\lambda_{flav}}{\mid\lambda_{flav}\mid}$	-2.16 ± 0.91
$\frac{\mathrm{Im}\lambda_{flav}}{\mid\lambda_{flav}\mid}$	-2.21 ± 0.98
$\frac{\mathrm{Im}\lambda_{tag}}{\mid\lambda_{tag}\mid}$	-1.33 ± 0.96
$\frac{\mathrm{Im}\lambda_{tag}}{\mid\lambda_{tag}\mid}$	-1.4 ± 1.0

Table 51: Results from CPT reweighted full Monte Carlo, Analysis 2 fit, *GExp* resolution function.

Parameter	B^0 fit results (*GG* model)
Δm	0.4799 ± 0.0056
$\Delta\Gamma/\Gamma$	0.177 ± 0.018
$\mid q/p \mid$	1.0532 ± 0.0093
$\frac{\mathrm{Im}\lambda_{CP}}{\lvert\lambda_{CP}\rvert}$	0.734 ± 0.028
$\frac{\mathrm{Re}\lambda_{CP}}{\lvert\lambda_{CP}\rvert}\mathrm{Re}z$	$(0.1 \pm 1.9) \cdot 10^{-2}$
Imz	$(-1.1 \pm 6.2) \cdot 10^{-2}$
S_{core}	1.264 ± 0.051
$\delta_{core}^{\mathsf{Lepton}}$	-0.180 ± 0.048
$\delta_{core}^{\mathsf{Kaon+KPi}}$	-0.297 ± 0.040
$\delta_{core}^{\mathsf{Kaon+SlowPi}}$	-0.305 ± 0.039
$\delta_{core}^{\mathsf{Other}}$	-0.204 ± 0.040
$\delta_{core}^{\mathsf{Untag}}$	-0.258 ± 0.034
f_{tail}	$(4.2 \pm 2.5) \cdot 10^{-2}$
S_{tail}	4.1 ± 1.1
δ_{tail}	-2.14 ± 0.69
$f_{outlier}$	$(2.6 \pm 1.0) \cdot 10^{-3}$

Parameter	B^0 fit results (*GG* model)
w_0^{Lepton}	$(3.07 \pm 0.72) \cdot 10^{-2}$
$w_0^{\mathsf{Kaon+KPi}}$	$(2.7 \pm 1.4) \cdot 10^{-2}$
$w_0^{\mathsf{Kaon+SlowPi}}$	0.140 ± 0.017
w_0^{Other}	0.284 ± 0.016
$w_{slope}^{\mathsf{Kaon+KPi}}$	0.116 ± 0.024
$w_{slope}^{\mathsf{Kaon+SlowPi}}$	0.122 ± 0.025
$w_{slope}^{\mathsf{Other}}$	$(3.8 \pm 2.5) \cdot 10^{-2}$
$\Delta w^{\mathsf{Lepton}}$	$(-2.24 \pm 0.89) \cdot 10^{-2}$
$\Delta w^{\mathsf{Kaon+KPi}}$	$(-1.16 \pm 0.82) \cdot 10^{-2}$
$\Delta w^{\mathsf{Kaon+SlowPi}}$	$(-2.81 \pm 0.86) \cdot 10^{-2}$
$\Delta w^{\mathsf{Other}}$	$(-2.92 \pm 0.87) \cdot 10^{-2}$
ν	$(1.82 \pm 0.59) \cdot 10^{-2}$
μ^{Lepton}	$(1.0 \pm 1.4) \cdot 10^{-2}$
$\mu^{\mathsf{Kaon+KPi}}$	$(1.2 \pm 1.1) \cdot 10^{-2}$
$\mu^{\mathsf{Kaon+SlowPi}}$	$(-0.8 \pm 1.1) \cdot 10^{-2}$
μ^{Other}	$(-0.2 \pm 1.1) \cdot 10^{-2}$
$\frac{\mathrm{Im}\lambda_{flav}}{\lvert\lambda_{flav}\rvert}$	-1.41 ± 0.81
$\frac{\mathrm{Im}\lambda_{flav}}{\lvert\lambda_{flav}\rvert}$	0.96 ± 0.89
$\frac{\mathrm{Im}\lambda_{tag}}{\lvert\lambda_{tag}\rvert}$	-1.07 ± 0.79
$\frac{\mathrm{Im}\lambda_{tag}}{\lvert\lambda_{tag}\rvert}$	1.44 ± 0.85

Table 52: Results from DCKM reweighted full Monte Carlo, Analysis 2 fit, *GG* resolution function.

Parameter	B^0 fit results (*GG* model)
Δm	0.4799 ± 0.0055
$\Delta\Gamma/\Gamma$	0.177 ± 0.018
$\mid q/p \mid$	1.0533 ± 0.0093
$\frac{\mathrm{Im}\lambda_{CP}}{\lvert\lambda_{CP}\rvert}$	0.736 ± 0.026
S_{core}	1.264 ± 0.051
$\delta_{core}^{\mathsf{Lepton}}$	-0.180 ± 0.048
$\delta_{core}^{\mathsf{Kaon+KPi}}$	-0.297 ± 0.039
$\delta_{core}^{\mathsf{Kaon+SlowPi}}$	-0.306 ± 0.038
$\delta_{core}^{\mathsf{Other}}$	-0.204 ± 0.039
$\delta_{core}^{\mathsf{Untag}}$	-0.259 ± 0.034
f_{tail}	$(4.2 \pm 2.4) \cdot 10^{-2}$
S_{tail}	4.1 ± 1.1
δ_{tail}	-2.15 ± 0.68
$f_{outlier}$	$(2.6 \pm 1.0) \cdot 10^{-3}$

Parameter	B^0 fit results (*GG* model)
w_0^{Lepton}	$(2.97 \pm 0.45) \cdot 10^{-2}$
$w_0^{\mathsf{Kaon+KPi}}$	$(2.6 \pm 1.3) \cdot 10^{-2}$
$w_0^{\mathsf{Kaon+SlowPi}}$	0.139 ± 0.016
w_0^{Other}	0.284 ± 0.016
$w_{slope}^{\mathsf{Kaon+KPi}}$	0.116 ± 0.024
$w_{slope}^{\mathsf{Kaon+SlowPi}}$	0.123 ± 0.025
$w_{slope}^{\mathsf{Other}}$	$(3.8 \pm 2.5) \cdot 10^{-2}$
$\Delta w^{\mathsf{Lepton}}$	$(-2.25 \pm 0.87) \cdot 10^{-2}$
$\Delta w^{\mathsf{Kaon+KPi}}$	$(-1.16 \pm 0.81) \cdot 10^{-2}$
$\Delta w^{\mathsf{Kaon+SlowPi}}$	$(-2.82 \pm 0.86) \cdot 10^{-2}$
$\Delta w^{\mathsf{Other}}$	$(-2.92 \pm 0.87) \cdot 10^{-2}$
ν	$(1.81 \pm 0.57) \cdot 10^{-2}$
μ^{Lepton}	$(1.0 \pm 1.4) \cdot 10^{-2}$
$\mu^{\mathsf{Kaon+KPi}}$	$(1.2 \pm 1.1) \cdot 10^{-2}$
$\mu^{\mathsf{Kaon+SlowPi}}$	$(-0.8 \pm 1.1) \cdot 10^{-2}$
μ^{Other}	$(-0.2 \pm 1.1) \cdot 10^{-2}$
$\frac{\mathrm{Im}\lambda_{flav}}{\lvert\lambda_{flav}\rvert}$	-1.27 ± 0.35
$\frac{\mathrm{Im}\lambda_{flav}}{\lvert\lambda_{flav}\rvert}$	0.82 ± 0.38
$\frac{\mathrm{Im}\lambda_{tag}}{\lvert\lambda_{tag}\rvert}$	-0.94 ± 0.29
$\frac{\mathrm{Im}\lambda_{tag}}{\lvert\lambda_{tag}\rvert}$	1.29 ± 0.32

Table 53: Results from DCKM reweighted full Monte Carlo, Analysis 1 fit, *GG* resolution function.

Parameter	B^0 fit results (*GG* model)
Δm	0.5252 ± 0.0080
$\Delta\Gamma/\Gamma$	-0.188 ± 0.035
$\mid q/p \mid$	0.926 ± 0.013
$\frac{\mathrm{Im}\lambda_{CP}}{\mid\lambda_{CP}\mid}$	0.361 ± 0.070
$\frac{\mathrm{Re}\lambda_{CP}}{\mid\lambda_{CP}\mid}\mathrm{Rez}$	-0.116 ± 0.038
Imz	0.253 ± 0.028
S_{core}	1.229 ± 0.041
δ_{core}^{lepton}	$(-2.1 \pm 6.1) \cdot 10^{-2}$
δ_{core}^{kaon}	-0.305 ± 0.035
δ_{core}^{NT1}	-0.279 ± 0.070
δ_{core}^{NT2}	-0.234 ± 0.052
δ_{core}^{Untag}	-0.283 ± 0.034
f_{tail}	$(3.9 \pm 1.1) \cdot 10^{-2}$
S_{tail}	5.40 ± 0.81
δ_{tail}	-1.53 ± 0.46
$f_{outlier}$	$(1.0 \pm 1.3) \cdot 10^{-3}$
w_0^{lepton}	$(7.29 \pm 0.78) \cdot 10^{-2}$
w_0^{kaon}	$(6.5 \pm 1.7) \cdot 10^{-2}$
w_0^{NT1}	0.227 ± 0.035
w_0^{NT2}	0.389 ± 0.031
w_{slope}^{kaon}	0.163 ± 0.027
w_{slope}^{NT1}	$(-4.7 \pm 6.0) \cdot 10^{-2}$
w_{slope}^{NT2}	$(-2.1 \pm 4.6) \cdot 10^{-2}$
Δw^{lepton}	$(0.3 \pm 1.4) \cdot 10^{-2}$
Δw^{kaon}	$(-2.63 \pm 0.99) \cdot 10^{-2}$
Δw^{NT1}	$(1.1 \pm 2.0) \cdot 10^{-2}$
Δw^{NT2}	$(-3.5 \pm 1.6) \cdot 10^{-2}$
ν	$(9.6 \pm 8.4) \cdot 10^{-3}$
μ^{lepton}	$(2.0 \pm 2.1) \cdot 10^{-2}$
μ^{kaon}	$(-1.5 \pm 1.1) \cdot 10^{-2}$
μ^{NT1}	$(0.5 \pm 2.7) \cdot 10^{-2}$
μ^{NT2}	$(2.8 \pm 2.0) \cdot 10^{-2}$

Parameter	B^0 fit results (*GG* model)
$\frac{\mathrm{Im}\lambda_{flav}}{\mid\lambda_{flav}\mid}$	1.6 ± 1.2
$\frac{\mathrm{Im}\lambda_{flav}}{\mid\lambda_{flav}\mid}$	-1.2 ± 1.2
$\frac{\mathrm{Im}\lambda_{tag}}{\mid\lambda_{tag}\mid}$	1.2 ± 1.3
$\frac{\mathrm{Im}\lambda_{tag}}{\mid\lambda_{tag}\mid}$	-0.7 ± 1.3
$f_{prompt,B_{flav}}^{lepton}$	0.371 ± 0.054
$f_{prompt,B_{flav}}^{kaon}$	0.609 ± 0.018
$f_{prompt,B_{flav}}^{NT1}$	0.600 ± 0.030
$f_{prompt,B_{flav}}^{NT2}$	0.688 ± 0.019
$f_{prompt,B_{flav}}^{Untag}$	0.701 ± 0.015
S_{back}	1.333 ± 0.014
δ_{back}	$(-3.49 \pm 0.97) \cdot 10^{-2}$
$f_{back,outlier}$	$(1.39 \pm 0.14) \cdot 10^{-2}$
$w_{0,prompt}^{lepton}$	0.118 ± 0.069
$w_{0,prompt}^{kaon}$	0.2448 ± 0.0097
$w_{0,prompt}^{NT1}$	0.330 ± 0.025
$w_{0,prompt}^{NT2}$	0.449 ± 0.013
$w_{0,non-prompt}^{lepton}$	0.422 ± 0.045
$w_{0,non-prompt}^{kaon}$	0.372 ± 0.015
$w_{0,non-prompt}^{NT1}$	0.455 ± 0.036
$w_{0,non-prompt}^{NT2}$	0.453 ± 0.025
$\tau_{non-prompt}$	1.312 ± 0.037
$\tau_{non-prompt,B_{CPK_S^0}}$	1.62 ± 0.27
$f_{prompt,J/\psi K_S(\pi^+\pi^-)}$	0.594 ± 0.077
$f_{prompt,J/\psi K_S(\pi^0\pi^0)}$	0.615 ± 0.088
$f_{prompt,\psi(2S)K_S}$	0.68 ± 0.17
$f_{prompt,\chi_{c1}K_S}$	0.22 ± 0.25

Table 54: Analysis 2 fit results, *GG* resolution function, using Elba Tagger.

Parameter	Nominal fit (Moriond tagger)	Elba Tagger
Δm	0.5254 ± 0.0076	0.5252 ± 0.0080
$\Delta\Gamma/\Gamma$	-0.189 ± 0.037	-0.188 ± 0.035
$\mid q/p \mid$	0.925 ± 0.013	0.926 ± 0.013
$\frac{\mathrm{Im}\lambda_{CP}}{\mid\lambda_{CP}\mid}$	0.327 ± 0.066	0.361 ± 0.070
$\frac{\mathrm{Re}\lambda_{CP}}{\mid\lambda_{CP}\mid}\mathrm{Rez}$	-0.120 ± 0.035	-0.116 ± 0.038
Imz	0.258 ± 0.029	0.253 ± 0.028

Table 55: Comparison of Analysis 2 fit results, *GG* resolution function, between the default Moriond Tagger and the Elba Tagger.

Parameter	Nominal fit (Moriond tagger)	Elba Tagger
Δm	0.5253 ± 0.0076	0.5252 ± 0.0079
$\Delta\Gamma/\Gamma$	-0.188 ± 0.037	-0.188 ± 0.035
$\mid q/p \mid$	0.925 ± 0.013	0.926 ± 0.013
$\frac{\mathrm{Im}\lambda_{CP}}{\mid\lambda_{CP}\mid}$	0.339 ± 0.067	0.377 ± 0.071

Table 56: Comparison of Analysis 1 fit results, *GG* resolution function, between the default Moriond Tagger and the Elba Tagger.

Parameter	B^0 fit results (*GG* model)
Δm	0.4796 ± 0.0039
$\Delta\Gamma/\Gamma$	$(-1.6 \pm 1.7) \cdot 10^{-2}$
$\mid q/p \mid$	1.0062 ± 0.0066
$\frac{\mathrm{Im}\lambda_{CP}}{\mid\lambda_{CP}\mid}$	0.678 ± 0.027
$\frac{\mathrm{Re}\lambda_{CP}}{\mid\lambda_{CP}\mid}\mathrm{Rez}$	$(-1.3 \pm 2.0) \cdot 10^{-2}$
Imz	$(0.2 \pm 1.4) \cdot 10^{-2}$
S_{core}	1.268 ± 0.023
δ_{core}^{lepton}	-0.117 ± 0.030
δ_{core}^{kaon}	-0.326 ± 0.018
δ_{core}^{NT1}	-0.203 ± 0.037
δ_{core}^{NT2}	-0.267 ± 0.026
δ_{core}^{Untag}	-0.319 ± 0.018
f_{tail}	$(3.81 \pm 0.87) \cdot 10^{-2}$
S_{tail}	4.45 ± 0.39
δ_{tail}	-1.54 ± 0.32
$f_{outlier}$	$(2.45 \pm 0.57) \cdot 10^{-3}$
w_0^{lepton}	$(6.40 \pm 0.36) \cdot 10^{-2}$
w_0^{kaon}	$(5.96 \pm 0.81) \cdot 10^{-2}$
w_0^{NT1}	0.192 ± 0.017
w_0^{NT2}	0.353 ± 0.015
w_{slope}^{kaon}	0.162 ± 0.013
w_{slope}^{NT1}	$(1.7 \pm 2.8) \cdot 10^{-2}$
w_{slope}^{NT2}	$(-2.0 \pm 2.2) \cdot 10^{-2}$
Δw^{lepton}	$(0.5 \pm 6.5) \cdot 10^{-3}$
Δw^{kaon}	$(-1.00 \pm 0.46) \cdot 10^{-2}$
Δw^{NT1}	$(0.1 \pm 1.0) \cdot 10^{-2}$
Δw^{NT2}	$(-3.18 \pm 0.78) \cdot 10^{-2}$
ν	$(6.6 \pm 3.9) \cdot 10^{-3}$
μ^{lepton}	$(1.70 \pm 0.95) \cdot 10^{-2}$
μ^{kaon}	$(8.4 \pm 5.2) \cdot 10^{-3}$
μ^{NT1}	$(-3.9 \pm 1.3) \cdot 10^{-2}$
μ^{NT2}	$(-1.35 \pm 0.99) \cdot 10^{-2}$

Parameter	B^0 fit results (*GG* model)
$\frac{\mathrm{Im}\lambda_{flav}}{\mid\lambda_{flav}\mid}$	-0.25 ± 0.55
$\frac{\mathrm{Im}\lambda_{flav}}{\mid\lambda_{flav}\mid}$	0.20 ± 0.56
$\frac{\mathrm{Im}\lambda_{tag}}{\mid\lambda_{tag}\mid}$	0.54 ± 0.59
$\frac{\mathrm{Im}\lambda_{tag}}{\mid\lambda_{tag}\mid}$	0.25 ± 0.60
$f_{prompt,B_{flav}}^{lepton}$	$(0.00 \pm 0.29) \cdot 10^{-3}$
$f_{prompt,B_{flav}}^{kaon}$	$(0.00 \pm 0.18) \cdot 10^{-3}$
$f_{prompt,B_{flav}}^{NT1}$	$(0.00 \pm 0.25) \cdot 10^{-3}$
$f_{prompt,B_{flav}}^{NT2}$	$(7.5 \pm 4.5) \cdot 10^{-2}$
$f_{prompt,B_{flav}}^{Untag}$	0.103 ± 0.040
S_{back}	1.361 ± 0.070
δ_{back}	-0.195 ± 0.033
$f_{back,outlier}$	$(1.63 \pm 0.38) \cdot 10^{-2}$
$w_{0,non-prompt}^{lepton}$	0.195 ± 0.020
$w_{0,non-prompt}^{kaon}$	0.2897 ± 0.0092
$w_{0,non-prompt}^{NT1}$	0.321 ± 0.024
$w_{0,non-prompt}^{NT2}$	0.398 ± 0.017
$\tau_{non-prompt}$	1.338 ± 0.034
$\tau_{non-prompt,B_{CPK_S^0}}$	1.87 ± 0.16
$f_{prompt,J/\psi K_S(\pi^+\pi^-)}$	0.112 ± 0.075
$f_{prompt,J/\psi K_S(\pi^0\pi^0)}$	0.301 ± 0.093
$f_{prompt,\psi(2S)K_S}$	0.16 ± 0.20
$f_{prompt,\chi_{c1}K_S}$	0.29 ± 0.14

Table 57: Analysis 2 fit results, for inclusive MC, *GG* resolution function, using Elba Tagger.

Parameter	Nominal fit (Moriond tagger)	Elba Tagger
Δm	0.4815 ± 0.0038	0.4796 ± 0.0039
$\Delta\Gamma/\Gamma$	$(-1.4 \pm 1.7) \cdot 10^{-2}$	$(-1.6 \pm 1.7) \cdot 10^{-2}$
$\mid q/p \mid$	1.0058 ± 0.0065	1.0062 ± 0.0066
$\frac{\mathrm{Im}\lambda_{CP}}{\mid\lambda_{CP}\mid}$	0.674 ± 0.026	0.678 ± 0.027
$\frac{\mathrm{Re}\lambda_{CP}}{\mid\lambda_{CP}\mid}\mathrm{Re}z$	$(-0.7 \pm 1.9) \cdot 10^{-2}$	$(-1.3 \pm 2.0) \cdot 10^{-2}$
$\mathrm{Im}z$	$(0.5 \pm 1.4) \cdot 10^{-2}$	$(0.2 \pm 1.4) \cdot 10^{-2}$

Table 58: Comparison of Analysis 2 fit results, *GG* resolution function, between the default Moriond Tagger and the Elba Tagger, for the standard inclusive Monte Carlo.

Parameter	Nominal fit (Moriond tagger)	Elba Tagger
Δm	0.4814 ± 0.0037	0.4795 ± 0.0039
$\Delta\Gamma/\Gamma$	$(-1.4 \pm 1.7) \cdot 10^{-2}$	$(-1.6 \pm 1.7) \cdot 10^{-2}$
$\mid q/p \mid$	1.0057 ± 0.0065	1.0060 ± 0.0066
$\frac{\mathrm{Im}\lambda_{CP}}{\mid\lambda_{CP}\mid}$	0.673 ± 0.026	0.677 ± 0.027

Table 59: Comparison of Analysis 1 fit results, *GG* resolution function, between the default Moriond Tagger and the Elba Tagger, for the standard inclusive Monte Carlo.

Parameter	Analysis 1	Analysis 2
Δm	$(6.9 \pm 2.6) \cdot 10^{-4}$	$(6.8 \pm 2.6) \cdot 10^{-4}$
$\Delta\Gamma/\Gamma$	$(8.9 \pm 5.6) \cdot 10^{-3}$	$(9.1 \pm 5.4) \cdot 10^{-3}$
$\mid q/p \mid$	$(2.8 \pm 4.4) \cdot 10^{-4}$	$(2.6 \pm 4.4) \cdot 10^{-4}$
$\frac{\mathrm{Im}\lambda_{CP}}{\mid\lambda_{CP}\mid}$	$(2.1 \pm 3.5) \cdot 10^{-3}$	$(1.9 \pm 3.9) \cdot 10^{-3}$
$\frac{\mathrm{Re}\lambda_{CP}}{\mid\lambda_{CP}\mid}\mathrm{Re}z$	—	$(-7.1 \pm 6.0) \cdot 10^{-4}$
$\mathrm{Im}z$	—	$(1.7 \pm 1.8) \cdot 10^{-4}$

Table 60: Differences between the standard fit and the one done imposing J/ψ mass constraint for the *CP* vertex (for technical reasons $B^0 \to J/\psi K_S^0$ ($\pi^0\pi^0$) is excluded from this comparison). The quadratic error difference is reported as well. Only common events are used here.

Parameter	Analysis 1	Analysis 2
Δm	$(9.8 \pm 7.7) \cdot 10^{-4}$	$(1.09 \pm 0.97) \cdot 10^{-3}$
$\Delta\Gamma/\Gamma$	$(3.4 \pm 4.4) \cdot 10^{-3}$	$(2.6 \pm 3.9) \cdot 10^{-3}$
$\mid q/p \mid$	$(-6.5 \pm 5.8) \cdot 10^{-4}$	$(-5.3 \pm 5.6) \cdot 10^{-4}$
$\frac{\mathrm{Im}\lambda_{CP}}{\mid\lambda_{CP}\mid}$	$(-7.1 \pm 9.3) \cdot 10^{-3}$	$(-6.9 \pm 6.8) \cdot 10^{-3}$
$\frac{\mathrm{Re}\lambda_{CP}}{\mid\lambda_{CP}\mid}\mathrm{Re}z$	—	$(5.8 \pm 2.6) \cdot 10^{-3}$
$\mathrm{Im}z$	—	$(-3.3 \pm 3.2) \cdot 10^{-3}$

Table 61: Differences between the standard fit and the one done using the charmonium vertex as *CP* vertex. The quadratic error difference is reported as well. Only common events are used here.

Parameter	Analysis 1	Analysis 2
Δm	$(-0.1 \pm 1.4) \cdot 10^{-4}$	$(-0.7 \pm 3.9) \cdot 10^{-5}$
$\Delta\Gamma/\Gamma$	$(0.6 \pm 1.8) \cdot 10^{-3}$	$(0.6 \pm 2.0) \cdot 10^{-3}$
$\mid q/p \mid$	$(-2.1 \pm 2.3) \cdot 10^{-4}$	$(-2.0 \pm 2.3) \cdot 10^{-4}$
$\frac{\mathrm{Im}\lambda_{CP}}{\mid\lambda_{CP}\mid}$	$(-2.62 \pm 0.81) \cdot 10^{-3}$	$(-2.7 \pm 1.6) \cdot 10^{-3}$
$\frac{\mathrm{Re}\lambda_{CP}}{\mid\lambda_{CP}\mid}\mathrm{Re}z$	—	$(0.2 \pm 3.2) \cdot 10^{-3}$
$\mathrm{Im}z$	—	$(-0.0 \pm 1.9) \cdot 10^{-3}$

Table 62: Differences between the standard fit and the one done removing the K_S^0 mass constraint. The quadratic error difference is reported as well. Only common events are used here.

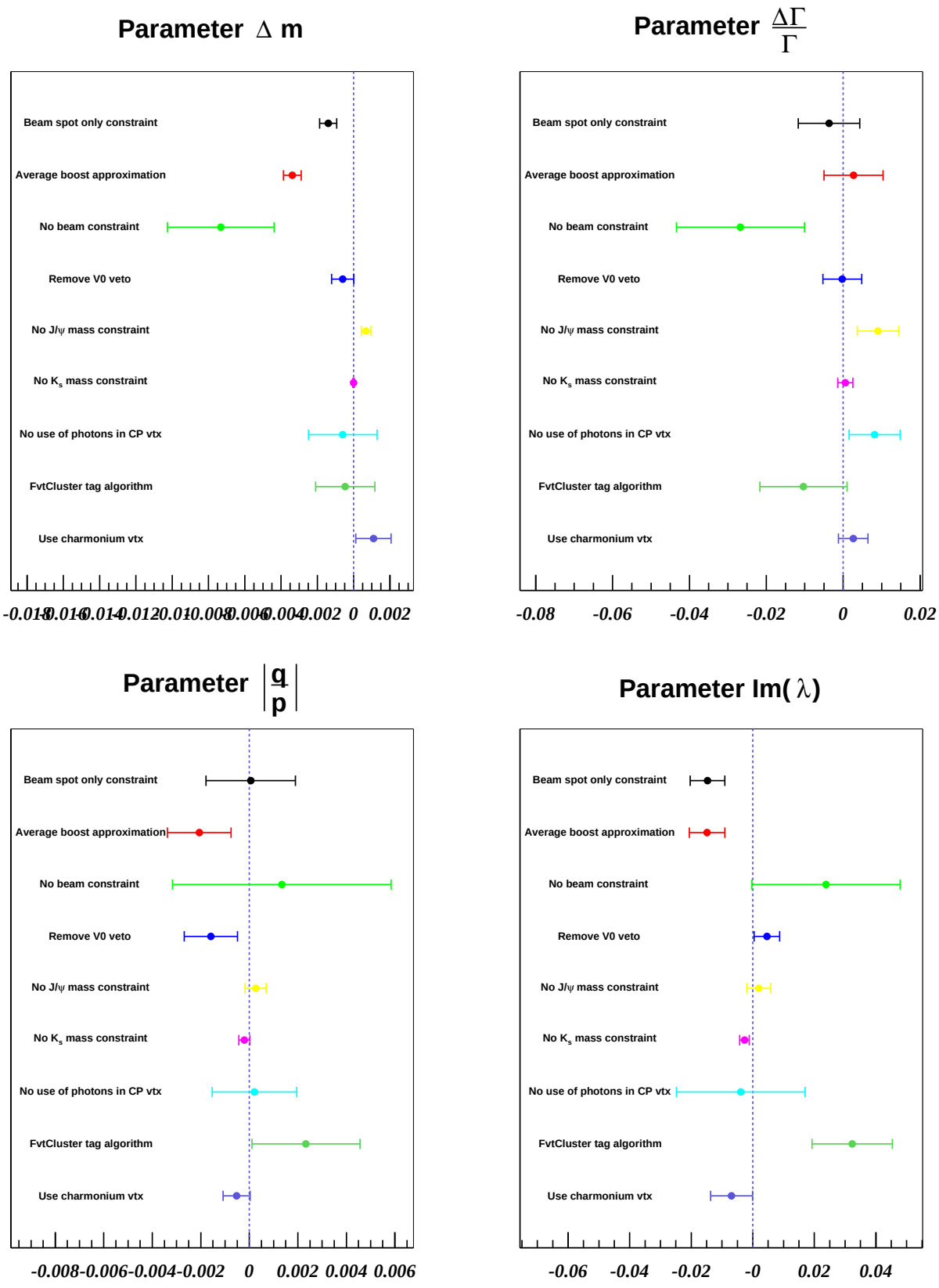

Figure 52: Graphical summary of the differences between the standard fit and the different vertexing configurations (explained in the text) from common events, for Δm, $\Delta\Gamma/\Gamma$, $|\,q/p\,|$ and $\frac{\mathrm{Im}\lambda_{CP}}{|\lambda_{CP}|}$ (Analysis 2).

Parameter	Analysis 1	Analysis 2
Δm	$(-0.7 \pm 1.8) \cdot 10^{-3}$	$(-0.6 \pm 1.9) \cdot 10^{-3}$
$\Delta\Gamma/\Gamma$	$(8.0 \pm 7.7) \cdot 10^{-3}$	$(8.2 \pm 6.6) \cdot 10^{-3}$
$\mid q/p \mid$	$(0.2 \pm 1.7) \cdot 10^{-3}$	$(0.2 \pm 1.7) \cdot 10^{-3}$
$\frac{\mathrm{Im}\lambda_{CP}}{\mid\lambda_{CP}\mid}$	$(-0.7 \pm 2.2) \cdot 10^{-2}$	$(-0.4 \pm 2.1) \cdot 10^{-2}$
$\frac{\mathrm{Re}\lambda_{CP}}{\mid\lambda_{CP}\mid}\mathrm{Re}z$	—	$(6.7 \pm 9.3) \cdot 10^{-3}$
$\mathrm{Im}z$	—	$(2.6 \pm 3.8) \cdot 10^{-3}$

Table 63: Differences between the standard fit and the one done removing the photons from the *CP* vertex. The quadratic error difference is reported as well. Only common events are used here.

Parameter	Analysis 1	Analysis 2
Δm	$(-7.6 \pm 2.8) \cdot 10^{-3}$	$(-7.3 \pm 2.9) \cdot 10^{-3}$
$\Delta\Gamma/\Gamma$	$(-2.5 \pm 1.7) \cdot 10^{-2}$	$(-2.7 \pm 1.7) \cdot 10^{-2}$
$\mid q/p \mid$	$(1.3 \pm 4.5) \cdot 10^{-3}$	$(1.3 \pm 4.5) \cdot 10^{-3}$
$\frac{\mathrm{Im}\lambda_{CP}}{\mid\lambda_{CP}\mid}$	$(2.3 \pm 2.2) \cdot 10^{-2}$	$(2.4 \pm 2.4) \cdot 10^{-2}$
$\frac{\mathrm{Re}\lambda_{CP}}{\mid\lambda_{CP}\mid}\mathrm{Re}z$	—	$(0.6 \pm 1.3) \cdot 10^{-2}$
$\mathrm{Im}z$	—	$(0.3 \pm 1.1) \cdot 10^{-2}$

Table 64: Differences between the standard fit and the one done removing the constraints from the beam. The quadratic error difference is reported as well. Only common events are used here.

Parameter	Analysis 1	Analysis 2
Δm	$(-1.48 \pm 0.25) \cdot 10^{-3}$	$(-1.40 \pm 0.47) \cdot 10^{-3}$
$\Delta\Gamma/\Gamma$	$(-3.4 \pm 5.5) \cdot 10^{-3}$	$(-3.7 \pm 8.0) \cdot 10^{-3}$
$\mid q/p \mid$	$(0.0 \pm 1.9) \cdot 10^{-3}$	$(0.1 \pm 1.8) \cdot 10^{-3}$
$\frac{\mathrm{Im}\lambda_{CP}}{\mid\lambda_{CP}\mid}$	$(-1.31 \pm 0.48) \cdot 10^{-2}$	$(-1.47 \pm 0.56) \cdot 10^{-2}$
$\frac{\mathrm{Re}\lambda_{CP}}{\mid\lambda_{CP}\mid}\mathrm{Re}z$	—	$(-3.0 \pm 4.6) \cdot 10^{-3}$
$\mathrm{Im}z$	—	$(-1.8 \pm 5.5) \cdot 10^{-3}$

Table 65: Differences between the standard fit and the one done using only the beam spot constraint. The quadratic error difference is reported as well. Only common events are used here.

Parameter	Analysis 1	Analysis 2
Δm	$(-6.3 \pm 5.7) \cdot 10^{-4}$	$(-6.1 \pm 6.1) \cdot 10^{-4}$
$\Delta\Gamma/\Gamma$	$(-0.2 \pm 4.8) \cdot 10^{-3}$	$(-0.2 \pm 5.1) \cdot 10^{-3}$
$\mid q/p \mid$	$(-1.6 \pm 1.1) \cdot 10^{-3}$	$(-1.6 \pm 1.1) \cdot 10^{-3}$
$\frac{\mathrm{Im}\lambda_{CP}}{\mid\lambda_{CP}\mid}$	$(5.0 \pm 4.4) \cdot 10^{-3}$	$(4.6 \pm 4.1) \cdot 10^{-3}$
$\frac{\mathrm{Re}\lambda_{CP}}{\mid\lambda_{CP}\mid}\mathrm{Re}z$	—	$(1.5 \pm 5.5) \cdot 10^{-3}$
$\mathrm{Im}z$	—	$(-0.6 \pm 2.2) \cdot 10^{-3}$

Table 66: Differences between the standard fit and the one done removing the V^0 veto in the tag vertex reconstructions. The quadratic error difference is reported as well. Only common events are used here.

Parameter	Analysis 1	Analysis 2
Δm	$(-3.42 \pm 0.61) \cdot 10^{-3}$	$(-3.38 \pm 0.48) \cdot 10^{-3}$
$\Delta\Gamma/\Gamma$	$(3.1 \pm 6.4) \cdot 10^{-3}$	$(2.7 \pm 7.7) \cdot 10^{-3}$
$\mid q/p \mid$	$(-2.0 \pm 1.4) \cdot 10^{-3}$	$(-2.1 \pm 1.3) \cdot 10^{-3}$
$\frac{\mathrm{Im}\lambda_{CP}}{\mid\lambda_{CP}\mid}$	$(-1.49 \pm 0.63) \cdot 10^{-2}$	$(-1.49 \pm 0.58) \cdot 10^{-2}$
$\frac{\mathrm{Re}\lambda_{CP}}{\mid\lambda_{CP}\mid}\mathrm{Re}z$	—	$(-3.6 \pm 3.2) \cdot 10^{-3}$
$\mathrm{Im}z$	—	$(-1.2 \pm 1.3) \cdot 10^{-3}$

Table 67: Differences between the standard fit and the one done using the *average boost approximation*. The quadratic error difference is reported as well. Only common events are used here.

Parameter	Analysis 1	Analysis 2
Δm	$(-0.9 \pm 1.3) \cdot 10^{-3}$	$(-0.5 \pm 1.6) \cdot 10^{-3}$
$\Delta\Gamma/\Gamma$	$(-0.9 \pm 1.0) \cdot 10^{-2}$	$(-1.0 \pm 1.1) \cdot 10^{-2}$
$\mid q/p \mid$	$(2.3 \pm 2.2) \cdot 10^{-3}$	$(2.3 \pm 2.2) \cdot 10^{-3}$
$\frac{\mathrm{Im}\lambda_{CP}}{\mid\lambda_{CP}\mid}$	$(2.67 \pm 0.90) \cdot 10^{-2}$	$(3.2 \pm 1.3) \cdot 10^{-2}$
$\frac{\mathrm{Re}\lambda_{CP}}{\mid\lambda_{CP}\mid}\mathrm{Re}z$	—	$(1.31 \pm 0.84) \cdot 10^{-2}$
$\mathrm{Im}z$	—	$(1.12 \pm 0.51) \cdot 10^{-2}$

Table 68: Differences between the standard fit and the one done using the alternative `FvtCluster` tag vertex algorithm. The quadratic error difference is reported as well. Only common events are used here.

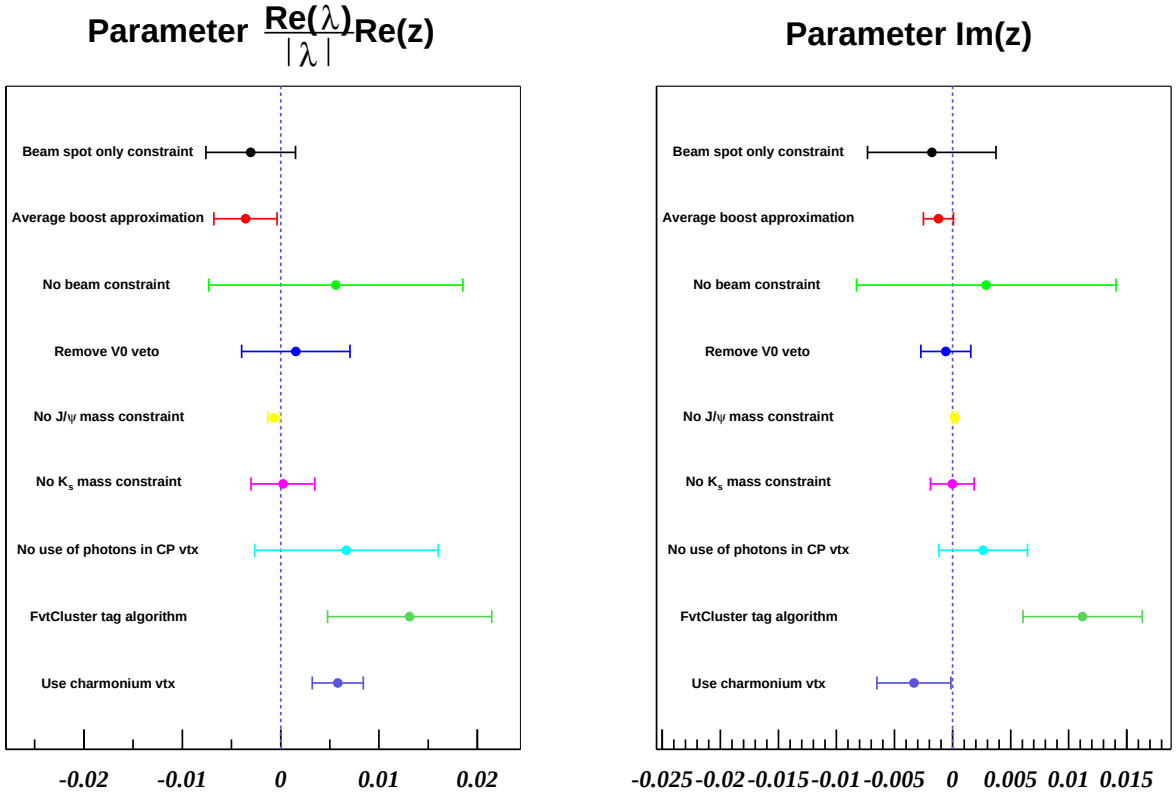

Figure 53: Graphical summary of the differences between the standard fit and the different vertexing configurations (explained in the text) from common events, for Re$z\frac{\mathrm{Re}\lambda_{CP}}{|\lambda_{CP}|}$ and Imz (Analysis 2).

8.13 $B^0\bar{B}^0$ differences in reconstruction and tagging efficiencies

As discussed in appendix A, $B^0\bar{B}^0$ differences in reconstruction and tagging efficiencies, parameterized by ν and μ^α, can be extracted using two alternative approaches. In the Alternative method, the detector charge asymmetries are extracted with a counting-based approach, exploiting the time-integrated information contained in the tagged and untagged events. On the contrary, in the Tagged only method the untagged events are not used at all and the precision that the estimate of ν and μ^α can reach is completely dominated by the large error in the measurement of $\mid q/p \mid$, since in this case $\mid q/p \mid$ can only be measured with CP events. Tables 69 and 70 show the physics and ν and μ^α parameters extracted with the two methods, to be compared to the nominal fit configuration (All Events method), shown in tables 16 and 20. To note: i) overall, the statistical error for all physics parameters is better for the nominal fit configuration (a fully time-dependent analysis exploiting tagged and untagged events provides the smaller variance), and as discussed in appendix A, the improvement is large for $\Delta\Gamma/\Gamma$; ii) there is an excellent agreement between the All Events (nominal) and Alternative methods in the extracted values of ν and μ^α; iii) very large error on $\mid q/p \mid$ with the Tagged only method, since this parameter is in this case measured with CP events only.

Parameter	Analysis 1	Analysis 2
Δm	0.5266 ± 0.0079	0.5267 ± 0.0079
$\Delta\Gamma/\Gamma$	-0.183 ± 0.046	-0.186 ± 0.046
$\mid q/p \mid$	0.924 ± 0.015	0.925 ± 0.015
$\frac{\mathrm{Im}\lambda_{CP}}{\mid\lambda_{CP}\mid}$	0.335 ± 0.067	0.323 ± 0.066
$\frac{\mathrm{Re}\lambda_{CP}}{\mid\lambda_{CP}\mid}\mathrm{Re}z$	—	-0.120 ± 0.036
$\mathrm{Im}z$	—	0.258 ± 0.029
ν	$(0.7 \pm 0.8) \cdot 10^{-2}$	$(0.7 \pm 0.8) \cdot 10^{-2}$
μ^{Lepton}	$(2.9 \pm 4.2) \cdot 10^{-2}$	$(2.9 \pm 4.2) \cdot 10^{-2}$
$\mu^{\mathrm{Kaon+KPi}}$	$(-2.2 \pm 2.9) \cdot 10^{-2}$	$(-2.2 \pm 2.9) \cdot 10^{-2}$
$\mu^{\mathrm{Kaon+SlowPi}}$	$(0.4 \pm 2.7) \cdot 10^{-2}$	$(0.4 \pm 2.7) \cdot 10^{-2}$
μ^{Other}	$(2.6 \pm 2.7) \cdot 10^{-2}$	$(2.5 \pm 2.7) \cdot 10^{-2}$

Table 69: Physics and ν and μ^α parameters as extracted using the Alternative method (see appendix A). In this method the $B^0\bar{B}^0$ detector asymmetries are extracted using time-integrated rates. These results must be compared to those obtained with the nominal fit (All Events method in appendix A), tables 16 and 20.

8.14 Results by run period

The fit was also performed for four different data taking periods: Run 1, Run 2a, Run 2b, Run2c-d. Run 2d is joined to Run 2c since the low statistics ($\sim 2\,\mathrm{fb}^{-1}$). See section 3 for the corresponding run numbers and integrated luminosity. The results are given in table 71.

8.15 Splitting of B_{flav} sample

As a cross-check of the DCKM effects in the reconstructed side (B_{flav} sample), the B_{flav} sample was splitted in two sub-samples: $B^0 \to \mathrm{D}^{(*)}\pi(\rho, \mathrm{a}_1)$ and $B^0 \to J/\psi K^{*0}$, the latter free of DCKM contributions in the reco'd side. The test was performed running the nominal fit separately for $B^0 \to \mathrm{D}^{(*)}\pi(\rho, \mathrm{a}_1)$ and $B^0 \to J/\psi K^{*0}$. $B_{CPK^0_S}$ and $B_{CPK^0_L}$ samples are unchanged with respect to nominal fit. When fitting the $B^0 \to J/\psi K^{*0}$ sample, $\frac{\mathrm{Im}\lambda_{flav}}{\mid\lambda_{flav}\mid}$ and

Parameter	Analysis 1	Analysis 2
Δm	0.5268 ± 0.0079	0.5268 ± 0.0079
$\Delta\Gamma/\Gamma$	-0.185 ± 0.046	-0.187 ± 0.046
$\mid q/p \mid$	0.969 ± 0.046	0.969 ± 0.046
$\frac{\mathrm{Im}\lambda_{CP}}{\mid\lambda_{CP}\mid}$	0.333 ± 0.067	0.320 ± 0.066
$\frac{\mathrm{Re}\lambda_{CP}}{\mid\lambda_{CP}\mid}\mathrm{Re}z$	—	-0.120 ± 0.036
$\mathrm{Im}z$	—	0.257 ± 0.030
ν	$(-3.7 \pm 4.7) \cdot 10^{-2}$	$(-3.6 \pm 4.7) \cdot 10^{-2}$
μ^{Lepton}	$(-2.1 \pm 4.9) \cdot 10^{-2}$	$(-2.1 \pm 4.9) \cdot 10^{-2}$
$\mu^{\mathrm{Kaon+KPi}}$	$(-6.8 \pm 4.9) \cdot 10^{-2}$	$(-6.9 \pm 4.8) \cdot 10^{-2}$
$\mu^{\mathrm{Kaon+SlowPi}}$	$(-3.4 \pm 5.0) \cdot 10^{-2}$	$(-3.4 \pm 4.9) \cdot 10^{-2}$
μ^{Other}	$(-3.3 \pm 5.0) \cdot 10^{-2}$	$(-3.4 \pm 5.0) \cdot 10^{-2}$

Table 70: Physics and ν and μ^{α} parameters as extracted using the Tagged only method (see appendix A). In this method the untagged events are not used at all. These results must be compared to those obtained with the nominal fit All Events method in appendix A), tables 16 and 20.

Parameter	Run 1	Run 2a	Run 2b	Run 2c+2d
Δm	0.514 ± 0.016	0.555 ± 0.021	0.525 ± 0.013	0.526 ± 0.014
$\Delta\Gamma/\Gamma$	-0.240 ± 0.075	-0.23 ± 0.12	-0.124 ± 0.065	-0.181 ± 0.059
$\mid q/p \mid$	0.933 ± 0.025	0.959 ± 0.033	0.930 ± 0.022	0.897 ± 0.024
$\frac{\mathrm{Im}\lambda_{CP}}{\mid\lambda_{CP}\mid}$	0.46 ± 0.14	0.19 ± 0.16	0.31 ± 0.11	0.33 ± 0.12

Parameter	Run 1	Run 2a	Run 2b	Run 2c+2d
Δm	0.527 ± 0.019	0.556 ± 0.021	0.525 ± 0.013	0.527 ± 0.014
$\Delta\Gamma/\Gamma$	-0.238 ± 0.057	-0.23 ± 0.13	-0.124 ± 0.066	-0.182 ± 0.060
$\mid q/p \mid$	0.935 ± 0.026	0.959 ± 0.032	0.930 ± 0.022	0.897 ± 0.024
$\frac{\mathrm{Im}\lambda_{CP}}{\mid\lambda_{CP}\mid}$	0.45 ± 0.13	0.15 ± 0.14	0.31 ± 0.11	0.31 ± 0.12
$\frac{\mathrm{Re}\lambda_{CP}}{\mid\lambda_{CP}\mid}\mathrm{Re}z$	$(1.9 \pm 7.0) \cdot 10^{-2}$	-0.135 ± 0.044	-0.131 ± 0.048	-0.140 ± 0.073
$\mathrm{Im}z$	0.265 ± 0.058	0.126 ± 0.092	0.289 ± 0.050	0.266 ± 0.057

Table 71: Fit results by run period for Analysis 1 (top) and 2 (bottom).

$\frac{\mathrm{Im}\bar{\lambda}_{flav}}{\mid\lambda_{flav}\mid}$ were fixed to zero. The complete fit results from both these fits are given in table 72.

8.16 Results from alternative minimization algorithm

The nominal fits for Analysis 1 and Analysis 2 were performed using `Minuit` instead of the default `NAG` option in `cptNagFit`. The results are reported in tables 73 and 74, for Analysis 1 and 2 respectively. The agreement with the nominal fits, tables 16 and 20, is excellent. This cross-check for data fits using two completely different minimization libraries was very important to verify the robustness of the final result.

8.17 Results from charged B's

As an additional control check, the nominal fit was applied to the charged B sample. As flavor sample in this case we used the open charm charged B sample described in section 7.1.1 as B_{flav} sample, and as CP sample we used the charmonium B^+ sample. Due to the absence of mixing and CP violation in these samples, it was not possible to perform a simulatenous fit to all the parameters. The check was then performed by fixing Δm=0 and $\mid q/p \mid$=1 in the B_{flav} sample, and Δm=0.472 ps^{-1} and $\frac{\mathrm{Im}\lambda_{CP}}{|\lambda_{CP}|}$=0 in the B_{CP} samples, fitting only for $\Delta\Gamma/\Gamma$, Rez and Imz. The results are given in table 75. No statistically significant deviations from 0 are observed.

Figure 54 summarizes graphically the differences to the nominal fit in the data for the different cross-check configurations described in this section.

8.18 Resolution function dependence with tagging category

We assumed in the nominal fit common resolution function parameters for all tagging categories (f_{tail}, δ_{tail}, σ_{core}, σ_{tail} and f_{out}, only δ_{core} is different for each category). From the inspection of the normalized residual distributions of the high statistics inclusive Monte Carlo fits, section 8.8, there is evidence of small differences between `Lepton` and `non-Lepton` categories, seen as a small Δt structure in the residual distribution for unmixed events, figure 48. The B_{flav} data sample, about 4 times smaller in size than the Monte Carlo, does not show such a structure (figure 25). To check the impact of the asumption of common resolution function parameters for all tags, we performed dedicated fits for data and inclusive Monte Carlo, using a different resolution function for `Lepton` and `non-Lepton` tags (a different set of parameters f_{tail}, δ_{tail}, σ_{core} and σ_{tail}, but with a common f_{out}). Despite a sizeable difference in the fitted resolution function parameters, the change in the physical parameters remains negligible, as seen in tables 76 and 77.

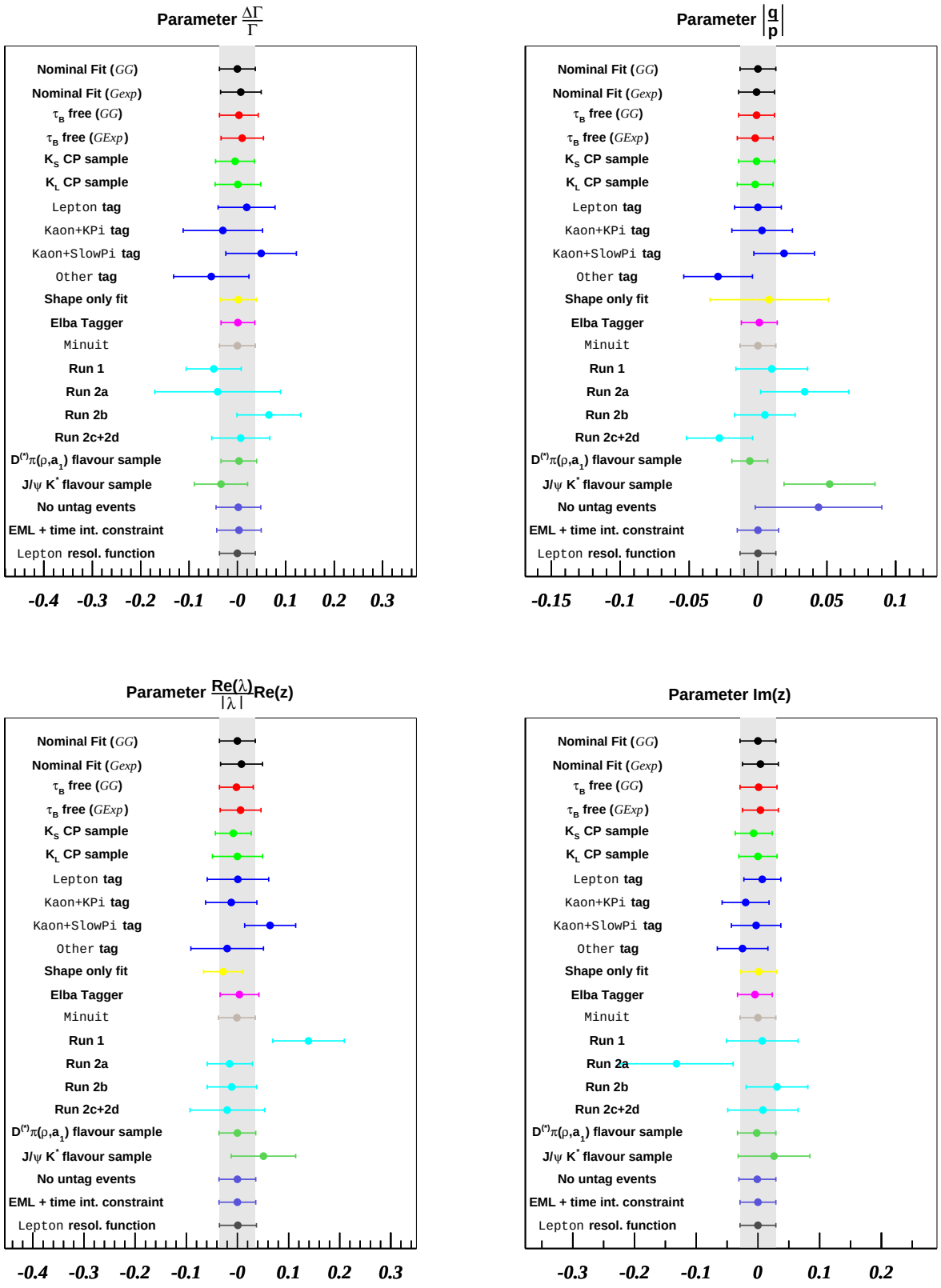

Figure 54: Graphical summary of the differences between the standard data fit and the different cross-check configurations described in this section for $\Delta\Gamma/\Gamma$, $|\,q/p\,|$, $\frac{\mathrm{Re}\lambda_{CP}}{|\lambda_{CP}|}$Rez and Imz (Analysis 2).

Parameter	Standard B_{flav}	Using D$^*X$	Using J/ψK^*
Δm	0.5254 ± 0.0076	0.5258 ± 0.0078	0.514 ± 0.023
$\Delta\Gamma/\Gamma$	-0.189 ± 0.037	-0.186 ± 0.037	-0.223 ± 0.055
$\mid q/p \mid$	0.925 ± 0.013	0.919 ± 0.013	0.977 ± 0.033
$\frac{\mathrm{Im}\lambda_{CP}}{\mid\lambda_{CP}\mid}$	0.327 ± 0.066	0.331 ± 0.066	0.291 ± 0.079
$\frac{\mathrm{Re}\lambda_{CP}}{\mid\lambda_{CP}\mid}$Rez	-0.120 ± 0.035	-0.120 ± 0.036	$(-6.9 \pm 6.3) \cdot 10^{-2}$
Imz	0.258 ± 0.029	0.256 ± 0.031	0.284 ± 0.058
ν	$(1.11 \pm 0.84) \cdot 10^{-2}$	$(1.18 \pm 0.89) \cdot 10^{-2}$	$(1.3 \pm 2.5) \cdot 10^{-2}$
μ^{Lepton}	$(2.4 \pm 2.2) \cdot 10^{-2}$	$(2.6 \pm 2.3) \cdot 10^{-2}$	$(3.3 \pm 6.6) \cdot 10^{-2}$
$\mu^{\mathrm{Kaon+KPi}}$	$(-2.2 \pm 1.7) \cdot 10^{-2}$	$(-3.3 \pm 1.8) \cdot 10^{-2}$	$(3.2 \pm 4.7) \cdot 10^{-2}$
$\mu^{\mathrm{Kaon+SlowPi}}$	$(1.4 \pm 1.6) \cdot 10^{-2}$	$(0.5 \pm 1.7) \cdot 10^{-2}$	0.123 ± 0.045
μ^{Other}	$(1.4 \pm 1.6) \cdot 10^{-2}$	$(2.8 \pm 1.7) \cdot 10^{-2}$	-0.144 ± 0.049
$\frac{\mathrm{Im}\lambda_{flav}}{\mid\lambda_{flav}\mid}$	2.3 ± 1.1	2.7 ± 1.2	
$\frac{\mathrm{Im}\bar{\lambda}_{flav}}{\mid\lambda_{flav}\mid}$	-0.6 ± 1.1	-0.6 ± 1.2	
$\frac{\mathrm{Im}\lambda_{tag}}{\mid\lambda_{tag}\mid}$	1.5 ± 1.2	1.9 ± 1.3	1.5 ± 2.2
$\frac{\mathrm{Im}\bar{\lambda}_{tag}}{\mid\lambda_{tag}\mid}$	-0.1 ± 1.2	0.0 ± 1.3	2.7 ± 2.3
S_{core}	1.245 ± 0.039	1.234 ± 0.040	1.352 ± 0.083
$\delta_{core}^{\mathrm{Lepton}}$	$(2.3 \pm 6.5) \cdot 10^{-2}$	$(6.7 \pm 6.6) \cdot 10^{-2}$	-0.11 ± 0.16
$\delta_{core}^{\mathrm{Kaon+KPi}}$	-0.273 ± 0.048	-0.280 ± 0.049	-0.31 ± 0.12
$\delta_{core}^{\mathrm{Kaon+SlowPi}}$	-0.322 ± 0.042	-0.318 ± 0.044	-0.34 ± 0.10
$\delta_{core}^{\mathrm{Other}}$	-0.295 ± 0.043	-0.301 ± 0.045	-0.38 ± 0.11
$\delta_{core}^{\mathrm{Untag}}$	-0.277 ± 0.033	-0.283 ± 0.034	-0.251 ± 0.079
f_{tail}	$(3.40 \pm 0.98) \cdot 10^{-2}$	$(3.30 \pm 0.99) \cdot 10^{-2}$	$(1.7 \pm 1.2) \cdot 10^{-2}$
S_{tail}	5.65 ± 0.80	5.64 ± 0.84	7.5 ± 2.0
δ_{tail}	-1.45 ± 0.49	-1.49 ± 0.53	-0.6 ± 1.9
$f_{outlier}$	$(0.8 \pm 1.2) \cdot 10^{-3}$	$(1.1 \pm 1.3) \cdot 10^{-3}$	$(0.0 \pm 6.9) \cdot 10^{-5}$
w_0^{Lepton}	$(2.59 \pm 0.65) \cdot 10^{-2}$	$(2.59 \pm 0.67) \cdot 10^{-2}$	$(4.7 \pm 2.8) \cdot 10^{-2}$
$w_0^{\mathrm{Kaon+KPi}}$	$(2.0 \pm 2.0) \cdot 10^{-2}$	$(2.2 \pm 2.1) \cdot 10^{-2}$	$(0.0 \pm 5.1) \cdot 10^{-4}$
$w_0^{\mathrm{Kaon+SlowPi}}$	0.159 ± 0.024	0.153 ± 0.025	0.212 ± 0.068
w_0^{Other}	0.265 ± 0.025	0.262 ± 0.026	0.262 ± 0.070
$w_{slope}^{\mathrm{Kaon+KPi}}$	0.133 ± 0.036	0.120 ± 0.037	0.237 ± 0.043
$w_{slope}^{\mathrm{Kaon+SlowPi}}$	$(7.1 \pm 3.6) \cdot 10^{-2}$	$(7.6 \pm 3.8) \cdot 10^{-2}$	0.03 ± 0.11
$w_{slope}^{\mathrm{Other}}$	$(7.4 \pm 3.8) \cdot 10^{-2}$	$(8.3 \pm 4.0) \cdot 10^{-2}$	0.05 ± 0.11
$\Delta w^{\mathrm{Lepton}}$	$(-1.2 \pm 1.2) \cdot 10^{-2}$	$(-1.4 \pm 1.3) \cdot 10^{-2}$	$(3.3 \pm 4.9) \cdot 10^{-2}$
$\Delta w^{\mathrm{Kaon+KPi}}$	$(-2.7 \pm 1.3) \cdot 10^{-2}$	$(-3.3 \pm 1.3) \cdot 10^{-2}$	$(0.5 \pm 3.6) \cdot 10^{-2}$
$\Delta w^{\mathrm{Kaon+SlowPi}}$	$(-4.2 \pm 1.3) \cdot 10^{-2}$	$(-5.0 \pm 1.4) \cdot 10^{-2}$	$(3.0 \pm 3.5) \cdot 10^{-2}$
$\Delta w^{\mathrm{Other}}$	$(-2.9 \pm 1.3) \cdot 10^{-2}$	$(-2.9 \pm 1.4) \cdot 10^{-2}$	$(-6.8 \pm 3.6) \cdot 10^{-2}$
$f_{prompt,B_{flav}}^{\mathrm{Lepton}}$	0.252 ± 0.065	0.254 ± 0.066	0.134 ± 0.089
$f_{prompt,B_{flav}}^{\mathrm{Kaon+KPi}}$	0.601 ± 0.022	0.600 ± 0.022	0.45 ± 0.15
$f_{prompt,B_{flav}}^{\mathrm{Kaon+SlowPi}}$	0.622 ± 0.020	0.626 ± 0.020	0.20 ± 0.17
$f_{prompt,B_{flav}}^{\mathrm{Other}}$	0.651 ± 0.019	0.655 ± 0.019	0.28 ± 0.16
$f_{prompt,B_{flav}}^{\mathrm{Untag}}$	0.704 ± 0.015	0.708 ± 0.015	0.25 ± 0.13
S_{back}	1.334 ± 0.014	1.334 ± 0.014	1.20 ± 0.13
δ_{back}	$(-3.41 \pm 0.97) \cdot 10^{-2}$	$(-3.41 \pm 0.97) \cdot 10^{-2}$	$(1.0 \pm 6.8) \cdot 10^{-2}$
$f_{back,outlier}$	$(1.40 \pm 0.14) \cdot 10^{-2}$	$(1.38 \pm 0.14) \cdot 10^{-2}$	$(3.6 \pm 1.3) \cdot 10^{-2}$
$w_{0,prompt}^{\mathrm{Lepton}}$	-0.21 ± 0.14	-0.20 ± 0.14	-1.0000 ± 0.0055
$w_{0,prompt}^{\mathrm{Kaon+KPi}}$	0.173 ± 0.015	0.167 ± 0.015	0.63 ± 0.20
$w_{0,prompt}^{\mathrm{Kaon+SlowPi}}$	0.304 ± 0.012	0.303 ± 0.012	0.35 ± 0.32
$w_{0,prompt}^{\mathrm{Other}}$	0.419 ± 0.012	0.416 ± 0.012	0.84 ± 0.31
$w_{0,non-prompt}^{\mathrm{Lepton}}$	0.397 ± 0.047	0.391 ± 0.048	0.50 ± 0.19
$w_{0,non-prompt}^{\mathrm{Kaon+KPi}}$	0.352 ± 0.022	0.357 ± 0.022	0.21 ± 0.13
$w_{0,non-prompt}^{\mathrm{Kaon+SlowPi}}$	0.342 ± 0.019	0.343 ± 0.020	0.305 ± 0.092
$w_{0,non-prompt}^{\mathrm{Other}}$	0.465 ± 0.021	0.469 ± 0.022	0.37 ± 0.10
$\tau_{non-prompt}$	1.313 ± 0.037	1.307 ± 0.037	1.48 ± 0.19
$\tau_{non-prompt,B_{CPK_S^0}}$	1.63 ± 0.27	1.63 ± 0.27	1.23 ± 0.19
$f_{prompt,J/\psi K_S(\pi^+\pi^-)}$	0.587 ± 0.077	0.587 ± 0.077	0.47 ± 0.12
$f_{prompt,J/\psi K_S(\pi^0\pi^0)}$	0.622 ± 0.087	0.623 ± 0.087	0.51 ± 0.12
$f_{prompt,\psi(2S)K_S}$	0.69 ± 0.17	0.69 ± 0.17	0.49 ± 0.25
$f_{prompt,\chi_{c1}K_S}$	0.22 ± 0.25	0.22 ± 0.25	$(0.0 \pm 5.8) \cdot 10^{-3}$

Table 72: Comparison of Analysis 2 fit results using $B^0 \to \mathrm{D}^{(*)}\pi(\rho, a_1)$ or $B^0 \to J/\psi K^{*0}$ alone as B_{flav} sample. $\frac{\mathrm{Im}\lambda_{flav}}{\mid\lambda_{flav}\mid}$ and $\frac{\mathrm{Im}\bar{\lambda}_{flav}}{\mid\lambda_{flav}\mid}$ were fixed to zero for the latter.

Parameter	B^0 fit results (*GG* model)
Δm	0.5253 ± 0.0077
$\Delta\Gamma/\Gamma$	-0.188 ± 0.037
$\mid q/p \mid$	0.925 ± 0.013
$\frac{\mathrm{Im}\lambda_{CP}}{\lvert\lambda_{CP}\rvert}$	0.338 ± 0.067
S_{core}	1.245 ± 0.046
$\delta_{core}^{\mathsf{Lepton}}$	$(2.3 \pm 6.5) \cdot 10^{-2}$
$\delta_{core}^{\mathsf{Kaon+KPi}}$	-0.273 ± 0.048
$\delta_{core}^{\mathsf{Kaon+SlowPi}}$	-0.322 ± 0.043
$\delta_{core}^{\mathsf{Other}}$	-0.295 ± 0.044
$\delta_{core}^{\mathsf{Untag}}$	-0.277 ± 0.034
f_{tail}	$(3.4 \pm 1.4) \cdot 10^{-2}$
S_{tail}	5.7 ± 1.1
δ_{tail}	-1.46 ± 0.49
$f_{outlier}$	$(0.8 \pm 1.3) \cdot 10^{-3}$
w_0^{Lepton}	$(2.59 \pm 0.65) \cdot 10^{-2}$
$w_0^{\mathsf{Kaon+KPi}}$	$(1.9 \pm 2.1) \cdot 10^{-2}$
$w_0^{\mathsf{Kaon+SlowPi}}$	0.160 ± 0.023
w_0^{Other}	0.265 ± 0.024
$w_{slope}^{\mathsf{Kaon+KPi}}$	0.132 ± 0.038
$w_{slope}^{\mathsf{Kaon+SlowPi}}$	$(6.9 \pm 3.4) \cdot 10^{-2}$
$w_{slope}^{\mathsf{Other}}$	$(7.3 \pm 3.7) \cdot 10^{-2}$
$\Delta w^{\mathsf{Lepton}}$	$(-1.2 \pm 1.2) \cdot 10^{-2}$
$\Delta w^{\mathsf{Kaon+KPi}}$	$(-2.6 \pm 1.2) \cdot 10^{-2}$
$\Delta w^{\mathsf{Kaon+SlowPi}}$	$(-4.0 \pm 1.3) \cdot 10^{-2}$
$\Delta w^{\mathsf{Other}}$	$(-2.8 \pm 1.3) \cdot 10^{-2}$
ν	$(10.0 \pm 8.3) \cdot 10^{-3}$
μ^{Lepton}	$(2.3 \pm 2.2) \cdot 10^{-2}$
$\mu^{\mathsf{Kaon+KPi}}$	$(-2.3 \pm 1.7) \cdot 10^{-2}$
$\mu^{\mathsf{Kaon+SlowPi}}$	$(1.4 \pm 1.6) \cdot 10^{-2}$
μ^{Other}	$(1.4 \pm 1.6) \cdot 10^{-2}$

Parameter	B^0 fit results (*GG* model)
$\frac{\mathrm{Im}\lambda_{flav}}{\lvert\lambda_{flav}\rvert}$	1.43 ± 0.94
$\frac{\mathrm{Im}\lambda_{flav}}{\lvert\lambda_{flav}\rvert}$	0.15 ± 0.94
$\frac{\mathrm{Im}\lambda_{tag}}{\lvert\lambda_{tag}\rvert}$	0.46 ± 0.98
$\frac{\mathrm{Im}\lambda_{tag}}{\lvert\lambda_{tag}\rvert}$	0.8 ± 1.0
$f_{prompt,B_{flav}}^{\mathsf{Lepton}}$	0.253 ± 0.064
$f_{prompt,B_{flav}}^{\mathsf{Kaon+KPi}}$	0.601 ± 0.022
$f_{prompt,B_{flav}}^{\mathsf{Kaon+SlowPi}}$	0.623 ± 0.020
$f_{prompt,B_{flav}}^{\mathsf{Other}}$	0.652 ± 0.019
$f_{prompt,B_{flav}}^{\mathsf{Untag}}$	0.704 ± 0.015
S_{back}	1.334 ± 0.014
δ_{back}	$(-3.42 \pm 0.97) \cdot 10^{-2}$
$f_{back,outlier}$	$(1.40 \pm 0.14) \cdot 10^{-2}$
$w_{0,prompt}^{\mathsf{Lepton}}$	-0.21 ± 0.13
$w_{0,prompt}^{\mathsf{Kaon+KPi}}$	0.173 ± 0.015
$w_{0,prompt}^{\mathsf{Kaon+SlowPi}}$	0.304 ± 0.012
$w_{0,prompt}^{\mathsf{Other}}$	0.419 ± 0.012
$w_{0,non-prompt}^{\mathsf{Lepton}}$	0.397 ± 0.045
$w_{0,non-prompt}^{\mathsf{Kaon+KPi}}$	0.352 ± 0.022
$w_{0,non-prompt}^{\mathsf{Kaon+SlowPi}}$	0.343 ± 0.019
$w_{0,non-prompt}^{\mathsf{Other}}$	0.466 ± 0.021
$\tau_{non-prompt}$	1.314 ± 0.037
$\tau_{non-prompt,B_{CPK_S^0}}$	1.63 ± 0.26
$f_{prompt,J/\psi K_S(\pi^+\pi^-)}$	0.586 ± 0.076
$f_{prompt,J/\psi K_S(\pi^0\pi^0)}$	0.622 ± 0.086
$f_{prompt,\psi(2S)K_S}$	0.68 ± 0.17
$f_{prompt,\chi_{c1}K_S}$	0.22 ± 0.25

Table 73: Analysis 1 results from `Minuit`, *GG* resolution model.

Parameter	B^0 fit results (*GG* model)
Δm	0.5253 ± 0.0077
$\Delta\Gamma/\Gamma$	-0.189 ± 0.037
$\mid q/p \mid$	0.925 ± 0.013
$\frac{\mathrm{Im}\lambda_{CP}}{\mid\lambda_{CP}\mid}$	0.326 ± 0.066
$\frac{\mathrm{Re}\lambda_{CP}}{\mid\lambda_{CP}\mid}\mathrm{Rez}$	-0.121 ± 0.036
Imz	0.258 ± 0.029
S_{core}	1.245 ± 0.046
$\delta_{core}^{\mathsf{Lepton}}$	$(2.2 \pm 6.5) \cdot 10^{-2}$
$\delta_{core}^{\mathsf{Kaon+KPi}}$	-0.273 ± 0.048
$\delta_{core}^{\mathsf{Kaon+SlowPi}}$	-0.322 ± 0.043
$\delta_{core}^{\mathsf{Other}}$	-0.296 ± 0.044
$\delta_{core}^{\mathsf{Untag}}$	-0.277 ± 0.034
f_{tail}	$(3.4 \pm 1.3) \cdot 10^{-2}$
S_{tail}	5.7 ± 1.1
δ_{tail}	-1.43 ± 0.49
$f_{outlier}$	$(0.8 \pm 1.3) \cdot 10^{-3}$
w_0^{Lepton}	$(2.59 \pm 0.65) \cdot 10^{-2}$
$w_0^{\mathsf{Kaon+KPi}}$	$(1.9 \pm 2.1) \cdot 10^{-2}$
$w_0^{\mathsf{Kaon+SlowPi}}$	0.160 ± 0.023
w_0^{Other}	0.265 ± 0.024
$w_{slope}^{\mathsf{Kaon+KPi}}$	0.133 ± 0.037
$w_{slope}^{\mathsf{Kaon+SlowPi}}$	$(7.0 \pm 3.4) \cdot 10^{-2}$
$w_{slope}^{\mathsf{Other}}$	$(7.4 \pm 3.6) \cdot 10^{-2}$
$\Delta w^{\mathsf{Lepton}}$	$(-1.2 \pm 1.2) \cdot 10^{-2}$
$\Delta w^{\mathsf{Kaon+KPi}}$	$(-2.7 \pm 1.3) \cdot 10^{-2}$
$\Delta w^{\mathsf{Kaon+SlowPi}}$	$(-4.2 \pm 1.3) \cdot 10^{-2}$
$\Delta w^{\mathsf{Other}}$	$(-2.9 \pm 1.3) \cdot 10^{-2}$
ν	$(1.10 \pm 0.84) \cdot 10^{-2}$
μ^{Lepton}	$(2.4 \pm 2.2) \cdot 10^{-2}$
$\mu^{\mathsf{Kaon+KPi}}$	$(-2.3 \pm 1.7) \cdot 10^{-2}$
$\mu^{\mathsf{Kaon+SlowPi}}$	$(1.4 \pm 1.6) \cdot 10^{-2}$
μ^{Other}	$(1.5 \pm 1.6) \cdot 10^{-2}$

Parameter	B^0 fit results (*GG* model)
$\frac{\mathrm{Im}\lambda_{flav}}{\mid\lambda_{flav}\mid}$	2.3 ± 1.1
$\frac{\mathrm{Im}\lambda_{flav}}{\mid\lambda_{flav}\mid}$	-0.6 ± 1.1
$\frac{\mathrm{Im}\lambda_{tag}}{\mid\lambda_{tag}\mid}$	1.5 ± 1.2
$\frac{\mathrm{Im}\lambda_{tag}}{\mid\lambda_{tag}\mid}$	-0.1 ± 1.2
$f_{prompt,B_{flav}}^{\mathsf{Lepton}}$	0.252 ± 0.065
$f_{prompt,B_{flav}}^{\mathsf{Kaon+KPi}}$	0.601 ± 0.022
$f_{prompt,B_{flav}}^{\mathsf{Kaon+SlowPi}}$	0.622 ± 0.020
$f_{prompt,B_{flav}}^{\mathsf{Other}}$	0.652 ± 0.019
$f_{prompt,B_{flav}}^{\mathsf{Untag}}$	0.704 ± 0.015
S_{back}	1.334 ± 0.014
δ_{back}	$(-3.41 \pm 0.97) \cdot 10^{-2}$
$f_{back,outlier}$	$(1.40 \pm 0.14) \cdot 10^{-2}$
$w_{0,prompt}^{\mathsf{Lepton}}$	-0.21 ± 0.13
$w_{0,prompt}^{\mathsf{Kaon+KPi}}$	0.173 ± 0.015
$w_{0,prompt}^{\mathsf{Kaon+SlowPi}}$	0.304 ± 0.012
$w_{0,prompt}^{\mathsf{Other}}$	0.419 ± 0.012
$w_{0,non-prompt}^{\mathsf{Lepton}}$	0.398 ± 0.045
$w_{0,non-prompt}^{\mathsf{Kaon+KPi}}$	0.352 ± 0.022
$w_{0,non-prompt}^{\mathsf{Kaon+SlowPi}}$	0.342 ± 0.019
$w_{0,non-prompt}^{\mathsf{Other}}$	0.465 ± 0.021
$\tau_{non-prompt}$	1.313 ± 0.037
$\tau_{non-prompt,B_{CPK_S^0}}$	1.63 ± 0.26
$f_{prompt,J/\psi K_S(\pi^+\pi^-)}$	0.586 ± 0.076
$f_{prompt,J/\psi K_S(\pi^0\pi^0)}$	0.622 ± 0.086
$f_{prompt,\psi(2S)K_S}$	0.68 ± 0.17
$f_{prompt,\chi_{c1}K_S}$	0.21 ± 0.25

Table 74: Analysis 2 results from `Minuit`, *GG* resolution model.

Parameter	B^+ fit results (GG model)
$\Delta\Gamma/\Gamma$	$(-3.0 \pm 1.8) \cdot 10^{-2}$
$\frac{\mathrm{Re}\lambda_{CP}}{\lvert\lambda_{CP}\rvert}$Rez	$(-0.3 \pm 3.3) \cdot 10^{-2}$
Imz	$(-2.8 \pm 3.4) \cdot 10^{-2}$
S_{core}	1.148 ± 0.071
$\delta_{core}^{\mathsf{Lepton}}$	-0.172 ± 0.082
$\delta_{core}^{\mathsf{Kaon1}}$	-0.257 ± 0.064
$\delta_{core}^{\mathsf{Kaon+SlowPi}}$	-0.270 ± 0.058
$\delta_{core}^{\mathsf{Other}}$	-0.161 ± 0.060
$\delta_{core}^{\mathsf{Untag}}$	-0.264 ± 0.046
f_{tail}	$(3.3 \pm 3.2) \cdot 10^{-2}$
δ_{tail}	-0.1 ± 1.2
$f_{outlier}$	$(2.9 \pm 1.3) \cdot 10^{-3}$
w_0^{Lepton}	$(9.5 \pm 2.9) \cdot 10^{-3}$
$w_0^{\mathsf{Kaon+KPi}}$	$(1.4 \pm 1.5) \cdot 10^{-2}$
$w_0^{\mathsf{Kaon+SlowPi}}$	0.111 ± 0.019
w_0^{Other}	0.205 ± 0.022
$w_{slope}^{\mathsf{Kaon+KPi}}$	0.115 ± 0.028
$w_{slope}^{\mathsf{Kaon+SlowPi}}$	$(9.6 \pm 3.0) \cdot 10^{-2}$
$w_{slope}^{\mathsf{Other}}$	0.118 ± 0.035
$\Delta w^{\mathsf{Lepton}}$	$(6.5 \pm 5.5) \cdot 10^{-3}$
$\Delta w^{\mathsf{Kaon+KPi}}$	$(-3.1 \pm 9.0) \cdot 10^{-3}$
$\Delta w^{\mathsf{Kaon+SlowPi}}$	$(-2.4 \pm 1.2) \cdot 10^{-2}$
$\Delta w^{\mathsf{Other}}$	$(-3.0 \pm 1.4) \cdot 10^{-2}$

Parameter	B^+ fit results (GG model)
ν	$(1.14 \pm 0.76) \cdot 10^{-2}$
μ^{Lepton}	$(1.8 \pm 2.0) \cdot 10^{-2}$
$\mu^{\mathsf{Kaon+KPi}}$	$(1.5 \pm 1.5) \cdot 10^{-2}$
$\mu^{\mathsf{Kaon+SlowPi}}$	$(1.4 \pm 1.4) \cdot 10^{-2}$
μ^{Other}	$(-1.9 \pm 1.5) \cdot 10^{-2}$
$f_{prompt,B_{flav}}^{\mathsf{Lepton}}$	0.125 ± 0.088
$f_{prompt,B_{flav}}^{\mathsf{Kaon+KPi}}$	0.625 ± 0.027
$f_{prompt,B_{flav}}^{\mathsf{Kaon+SlowPi}}$	0.655 ± 0.024
$f_{prompt,B_{flav}}^{\mathsf{Other}}$	0.713 ± 0.022
$f_{prompt,B_{flav}}^{\mathsf{Untag}}$	0.786 ± 0.016
S_{back}	1.327 ± 0.016
δ_{back}	$(-0.7 \pm 1.2) \cdot 10^{-2}$
$f_{back,outlier}$	$(1.46 \pm 0.18) \cdot 10^{-2}$
$w_{0,prompt}^{\mathsf{Lepton}}$	0.08 ± 0.20
$w_{0,prompt}^{\mathsf{Kaon+KPi}}$	0.113 ± 0.014
$w_{0,prompt}^{\mathsf{Kaon+SlowPi}}$	0.220 ± 0.014
$w_{0,prompt}^{\mathsf{Other}}$	0.352 ± 0.015
$w_{0,non-prompt}^{\mathsf{Lepton}}$	0.157 ± 0.041
$w_{0,non-prompt}^{\mathsf{Kaon+KPi}}$	0.185 ± 0.022
$w_{0,non-prompt}^{\mathsf{Kaon+SlowPi}}$	0.260 ± 0.025
$w_{0,non-prompt}^{\mathsf{Other}}$	0.381 ± 0.031
$\tau_{non-prompt}$	1.324 ± 0.052

Table 75: Results from the fit to the B^+ control sample.

Parameter	Analysis 1	Analysis 2
Δm	0.5257 ± 0.0076	0.5257 ± 0.0076
$\Delta\Gamma/\Gamma$	-0.188 ± 0.037	-0.189 ± 0.037
$\lvert q/p \rvert$	0.925 ± 0.013	0.925 ± 0.013
$\frac{\mathrm{Im}\lambda_{CP}}{\lvert\lambda_{CP}\rvert}$	0.338 ± 0.067	0.326 ± 0.066
$\frac{\mathrm{Re}\lambda_{CP}}{\lvert\lambda_{CP}\rvert}$Rez	—	-0.119 ± 0.036
Imz	—	0.258 ± 0.029

Table 76: Fit to full data sample using separate resolution function parameters for `Lepton` and `non-Lepton` categories.

Parameter	Analysis 1	Analysis 2
Δm	0.4800 ± 0.0038	0.4800 ± 0.0038
$\Delta\Gamma/\Gamma$	$(-1.5 \pm 1.7) \cdot 10^{-2}$	$(-1.4 \pm 1.7) \cdot 10^{-2}$
$\mid q/p \mid$	1.0058 ± 0.0066	1.0059 ± 0.0066
$\frac{\mathrm{Im}\lambda_{CP}}{\mid\lambda_{CP}\mid}$	0.670 ± 0.026	0.672 ± 0.026
$\frac{\mathrm{Re}\lambda_{CP}}{\mid\lambda_{CP}\mid}\mathrm{Re}z$	—	$(-0.9 \pm 1.9) \cdot 10^{-2}$
$\mathrm{Im}z$	—	$(0.5 \pm 1.4) \cdot 10^{-2}$

Table 77: Fit to inclusive Monte Carlo sample using separate resolution function parameters for `Lepton` and `non-Lepton` categories.

9 Systematic uncertainties

9.1 Signal probability of B_{flav} and $B_{CPK^0_S}$ samples

The event-by-event probability for B_{flav} and $B_{CPK^0_S}$ samples was fixed to the values obtained from the previous m_{ES} fits. We compared the fit results from the nominal fits to the values obtained by changing one sigma up and down all the m_{ES} distribution parameters, taking into account their correlations. This is performed simultaneously for all tagging categories, and independently for the B_{flav} and $B_{CPK^0_S}$ samples. The resulting variations of physical parameters are given in table 78.

Parameter	Analysis 1	Analysis 2
$\Delta\Gamma/\Gamma$	$^{-4.6\cdot10^{-4}}_{+4.6\cdot10^{-4}}$	$^{-5.0\cdot10^{-4}}_{+4.9\cdot10^{-4}}$
$\mid q/p \mid$	$^{+1.1\cdot10^{-4}}_{-1.0\cdot10^{-4}}$	$^{+1.1\cdot10^{-4}}_{-1.0\cdot10^{-4}}$
$\frac{\mathrm{Re}\lambda_{CP}}{\lvert\lambda_{CP}\rvert}$Rez	—	$^{+3.5\cdot10^{-4}}_{-3.3\cdot10^{-4}}$
Imz	—	$^{-2.6\cdot10^{-4}}_{+2.5\cdot10^{-4}}$

Parameter	Analysis 1	Analysis 2
$\Delta\Gamma/\Gamma$	$^{+3.8\cdot10^{-3}}_{-3.7\cdot10^{-3}}$	$^{+3.5\cdot10^{-3}}_{-3.5\cdot10^{-3}}$
$\mid q/p \mid$	$^{+2.5\cdot10^{-4}}_{-2.3\cdot10^{-4}}$	$^{+2.9\cdot10^{-4}}_{-2.6\cdot10^{-4}}$
$\frac{\mathrm{Re}\lambda_{CP}}{\lvert\lambda_{CP}\rvert}$Rez	—	$^{+1.7\cdot10^{-3}}_{-1.9\cdot10^{-3}}$
Imz	—	$^{-6.5\cdot10^{-4}}_{+5.6\cdot10^{-4}}$

Table 78: Signal probability systematics, B_{flav}(left) and $B_{CPK^0_S}$(right) sample.

We adopted also an alternative approach assuming a flat signal probability distribution: the events belonging to the sideband region (m_{ES}<5.27 GeV/c^2) are assigned a signal probability of zero, while we gave a signal probability equal to the purity of the corresponding sample to signal region events (m_{ES}>5.27 GeV/c^2). The differences among fitted physical parameters with respect to standard approach are given in table 79. Results are consistent. We extracted the systematics due to this parameterization just varying up and down the signal probability by the purity statistical error, as shown in table 80.

We finally assigned as systematics the larger one sigma variation between the two methods.

Parameter	Analysis 1	Analysis 2
$\Delta\Gamma/\Gamma$	$(0.70\pm0.33)\cdot10^{-2}$	$(6.6\pm2.9)\cdot10^{-3}$
$\mid q/p \mid$	$(-4.6\pm2.9)\cdot10^{-3}$	$(-4.5\pm2.9)\cdot10^{-3}$
$\frac{\mathrm{Re}\lambda_{CP}}{\lvert\lambda_{CP}\rvert}$Rez	—	$(4.8\pm4.3)\cdot10^{-3}$
Imz	—	$(-2.4\pm2.3)\cdot10^{-3}$

Table 79: Differences of the parameters using signal probability flat distribution instead of standard ARGUS. The errors are the quadratic statistical differences among the two measurements.

In addition, we changed the m_{ES} endpoint in the m_{ES} fit (by default is fixed to 5.291 GeV/c^2) by $\pm$0.002 GeV/c^2. The change on the parameters is given in table 81.

9.2 Resolution function

Two difference sources of systematics from the resolution function are considered.

Parameter	Analysis 1	Analysis 2
$\Delta\Gamma/\Gamma$	$^{-7.7\cdot10^{-4}}_{+7.9\cdot10^{-4}}$	$^{-8.0\cdot10^{-4}}_{+8.2\cdot10^{-4}}$
$\mid q/p \mid$	$^{+2.2\cdot10^{-4}}_{-2.2\cdot10^{-4}}$	$^{+2.2\cdot10^{-4}}_{-2.2\cdot10^{-4}}$
$\frac{\mathrm{Re}\lambda_{CP}}{\lvert\lambda_{CP}\rvert}$Rez	—	$^{+4.5\cdot10^{-4}}_{-4.3\cdot10^{-4}}$
Imz	—	$^{+1.0\cdot10^{-4}}_{-9.6\cdot10^{-5}}$

Parameter	Analysis 1	Analysis 2
$\Delta\Gamma/\Gamma$	$^{+1.9\cdot10^{-3}}_{-1.7\cdot10^{-3}}$	$^{+1.7\cdot10^{-3}}_{-1.6\cdot10^{-3}}$
$\mid q/p \mid$	$^{+2.9\cdot10^{-4}}_{-2.7\cdot10^{-4}}$	$^{+3.3\cdot10^{-4}}_{-3.1\cdot10^{-4}}$
$\frac{\mathrm{Re}\lambda_{CP}}{\lvert\lambda_{CP}\rvert}$Rez	—	$^{+6.5\cdot10^{-5}}_{-1.9\cdot10^{-4}}$
Imz	—	$^{-6.1\cdot10^{-4}}_{+5.7\cdot10^{-4}}$

Table 80: Signal probability systematics using signal probability flat distribution, for $B_{CPK^0_S}$(left) and B_{flav}(right) sample.

Parameter	Analysis 1	Analysis 2
$\Delta\Gamma/\Gamma$	$^{+6.2\cdot10^{-6}}_{-2.3\cdot10^{-4}}$	$^{-1.5\cdot10^{-5}}_{-4.3\cdot10^{-4}}$
$\mid q/p \mid$	$^{+5.9\cdot10^{-5}}_{+4.9\cdot10^{-4}}$	$^{+6.2\cdot10^{-5}}_{+4.9\cdot10^{-4}}$
$\frac{\mathrm{Re}\lambda_{CP}}{\lvert\lambda_{CP}\rvert}$Rez	—	$^{+9.9\cdot10^{-5}}_{+1.9\cdot10^{-3}}$
Imz	—	$^{-4.2\cdot10^{-5}}_{-3.5\cdot10^{-5}}$

Table 81: m_{ES} endpoint systematics.

The first one is due to its parameterization, for signal and combinatorial background. This is estimated from the difference between the (*GG* vs *GExp*) resolution models. The differences are reported in table 82.

The second source contributing to the systematics from the resolution function is due to the parameters of the outlier component (width and bias), fixed, respectively, to 8.0 and 0.0 ps. The uncertainty was estimated in this case by assuming a flat outlier Gaussian, using asymptotic (table 83) and finite (table 84) normalization. Differences have been done with respect to the nominal fit with the same (asymptotic or finite) normalization. We take the largest variation for each parameter as systematic error. The impact on the different parameters due to the use of asymptotic normalization was extensively investigated using toy Monte Carlo in reference [12] (section 4.1.8). The conclusion from the study was that the asymptotic normalization is not a source of concern except in the limit of large values of $\Delta\Gamma/\Gamma$ (range 0.2-0.3), in which case the finite normalization turns out to be more appropiate. Assigning a systematics as done above (largest difference among the asymptotic and finite normalization assuming an outlier width of 8.0 and a flat outlier component) accounts for any possible bias due to the use of the asymptotic normalization. An additional contribution was estimated by varying +4 ps/-2 ps the width, and $\pm$5 ps the bias. The results from this variation are summarized in tables 85 and 86.

9.3 Beam spot

The beam spot position and width are used in the vertexing algorithm of the tagging *B* [27]. For this reason is important to determine the systematic contribution coming from the determination of its parameters. We performed Analysis 1 and 2 data fits moving the beam spot by 20 and 40 μm in the *y* direction (the one along

Parameter	Analysis 1	Analysis 2
$\Delta\Gamma/\Gamma$	$+7.7\cdot10^{-3}$	$+7.3\cdot10^{-3}$
$\mid q/p \mid$	$-1.3\cdot10^{-3}$	$-1.1\cdot10^{-3}$
$\frac{\mathrm{Re}\lambda_{CP}}{\mid\lambda_{CP}\mid}$Rez	—	$+8.0\cdot10^{-3}$
Imz	—	$+3.2\cdot10^{-3}$

Table 82: Resolution function parameterization systematics.

Parameter	Analysis 1	Analysis 2
$\Delta\Gamma/\Gamma$	$-9.6\cdot10^{-4}$	$-1.1\cdot10^{-3}$
$\mid q/p \mid$	$+3.4\cdot10^{-4}$	$+3.4\cdot10^{-4}$
$\frac{\mathrm{Re}\lambda_{CP}}{\mid\lambda_{CP}\mid}$Rez	—	$-3.8\cdot10^{-5}$
Imz	—	$+6.4\cdot10^{-5}$

Table 83: Systematic shift due to a flat outlier component ($\sigma_{outlier}$ fixed to 20 ps).

Parameter	Analysis 1	Analysis 2
$\Delta\Gamma/\Gamma$	$+1.7\cdot10^{-3}$	$+1.9\cdot10^{-3}$
$\mid q/p \mid$	$-2.0\cdot10^{-4}$	$-2.0\cdot10^{-4}$
$\frac{\mathrm{Re}\lambda_{CP}}{\mid\lambda_{CP}\mid}$Rez	—	$+7.4\cdot10^{-4}$
Imz	—	$-6.6\cdot10^{-5}$

Table 84: Systematic shift due to a flat outlier component ($\sigma_{outlier}$ fixed to 20 ps). Finite normalization is used and differences are calculated with respect to finite normalization.

which is best determined the width) and increasing the width by 30 and 60 μm. Since the sample composition of the reconstructed events can differ when the beam spots parameters are changed, we used the events common to the two samples to perform a fit in the standard configuration and in the one where we introduced the systematic effect. The differences among the fitted values are reported in tables 87 and 88. The largest differences are used to assign the systematic error.

9.4 Absolute *z* scale and boost uncertainty

The uncertainty in the scale of the Δz measurement has been estimated to be about $\pm0.3\%$ [28]. As this estimate corresponds to the beampipe, the uncertainty has been conservatively increased by a factor 2 to account for possible mistakes in the extrapolation to the beamspot. On the other hand, the boost is known with a relative precision of $\pm0.1\%$ [30]. The effect of the uncertainty on the absolute z scale and boost can then be evaluated scaling the measured Δt and its error by 0.6% in the data sample. The effect on the physical parameters is shown in table 89.

Parameter	Analysis 1	Analysis 2
$\Delta\Gamma/\Gamma$	$^{-1.8\cdot10^{-4}}_{+2.2\cdot10^{-3}}$	$^{-2.5\cdot10^{-4}}_{-3.7\cdot10^{-4}}$
$\mid q/p \mid$	$^{+1.4\cdot10^{-4}}_{-1.2\cdot10^{-4}}$	$^{+1.4\cdot10^{-4}}_{+1.9\cdot10^{-4}}$
$\frac{\mathrm{Re}\lambda_{CP}}{\mid\lambda_{CP}\mid}$Rez	—	$^{+9.1\cdot10^{-5}}_{-1.1\cdot10^{-4}}$
Imz	—	$^{-9.8\cdot10^{-5}}_{+2.1\cdot10^{-4}}$

Table 85: Systematic shift corresponding to the variation of $\sigma_{outlier}$ of +4 / -2 ps around the value fixed in the standard fit (8 ps).

Parameter	Analysis 1	Analysis 2
$\Delta\Gamma/\Gamma$	$^{-3.9\cdot10^{-4}}_{-1.1\cdot10^{-3}}$	$^{-4.1\cdot10^{-4}}_{-1.2\cdot10^{-3}}$
$\mid q/p \mid$	$^{+2.3\cdot10^{-4}}_{+3.6\cdot10^{-4}}$	$^{+2.3\cdot10^{-4}}_{+3.6\cdot10^{-4}}$
$\frac{\mathrm{Re}\lambda_{CP}}{\mid\lambda_{CP}\mid}$Rez	—	$^{+1.1\cdot10^{-4}}_{+5.7\cdot10^{-5}}$
Imz	—	$^{+9.0\cdot10^{-5}}_{+1.6\cdot10^{-4}}$

Table 86: Systematic shift corresponding to the variation of $\delta_{outlier}$ of ±5 ps around zero (standard fit).

Parameter	Analysis 1	Analysis 2
$\Delta\Gamma/\Gamma$	$-2.1\cdot10^{-3}$	$-2.2\cdot10^{-3}$
$\mid q/p \mid$	$-2.6\cdot10^{-4}$	$-2.4\cdot10^{-4}$
$\frac{\mathrm{Re}\lambda_{CP}}{\mid\lambda_{CP}\mid}$Rez	—	$+4.0\cdot10^{-4}$
Imz	—	$+3.8\cdot10^{-3}$

Parameter	Analysis 1	Analysis 2
$\Delta\Gamma/\Gamma$	$-4.1\cdot10^{-4}$	$-9.4\cdot10^{-4}$
$\mid q/p \mid$	$+1.2\cdot10^{-3}$	$+1.2\cdot10^{-3}$
$\frac{\mathrm{Re}\lambda_{CP}}{\mid\lambda_{CP}\mid}$Rez	—	$+1.0\cdot10^{-3}$
Imz	—	$+1.1\cdot10^{-2}$

Table 87: Variation of the fitted physical parameters, when the beam spot position is moved of 20 μm (left table) and 40 μm (right table) in the positive y direction.

Parameter	Analysis 1	Analysis 2
$\Delta\Gamma/\Gamma$	$-2.5\cdot10^{-3}$	$-2.4\cdot10^{-3}$
$\mid q/p \mid$	$+1.9\cdot10^{-4}$	$+2.4\cdot10^{-4}$
$\frac{\mathrm{Re}\lambda_{CP}}{\mid\lambda_{CP}\mid}$Rez	—	$+3.9\cdot10^{-4}$
Imz	—	$+6.2\cdot10^{-4}$

Parameter	Analysis 1	Analysis 2
$\Delta\Gamma/\Gamma$	$+6.5\cdot10^{-3}$	$+7.3\cdot10^{-3}$
$\mid q/p \mid$	$-9.3\cdot10^{-4}$	$-8.8\cdot10^{-4}$
$\frac{\mathrm{Re}\lambda_{CP}}{\mid\lambda_{CP}\mid}$Rez	—	$+4.1\cdot10^{-4}$
Imz	—	$+1.7\cdot10^{-3}$

Table 88: Variation of the fitted physical parameters, when the beam spot width is expanded of 30 μm (left table) and 60 μm (right table) in the y direction.

Parameter	Analysis 1	Analysis 2
$\Delta\Gamma/\Gamma$	$+2.9\cdot10^{-3}$ $+2.9\cdot10^{-3}$	$+3.2\cdot10^{-3}$ $+3.2\cdot10^{-3}$
$\mid q/p \mid$	$-6.0\cdot10^{-4}$ $-6.0\cdot10^{-4}$	$-6.2\cdot10^{-4}$ $-6.2\cdot10^{-4}$
$\frac{\mathrm{Re}\lambda_{CP}}{\mid\lambda_{CP}\mid}$Rez	—	$-1.5\cdot10^{-3}$ $-1.5\cdot10^{-3}$
Imz	—	$+2.4\cdot10^{-4}$ $+2.4\cdot10^{-4}$

Table 89: Variation of the physics parameters by scaling the measured Δt and its error by $\pm0.6\%$.

9.5 SVT misalignment

In table 90 are reported the differences among the fitted values of the same Monte Carlo sample with perfect and `diffEL` alignments. `diffEL` (difference between the E and L alignment sets) is considered an extreme and unrealistic representation of the real misalignment. Conservatively, we use it to estimate the systematic error from the SVT internal misalignment [9].

Parameter	Analysis 1	Analysis 2
$\Delta\Gamma/\Gamma$	$+5.2\cdot10^{-3}$	$+6.1\cdot10^{-3}$
$\mid q/p \mid$	$-1.0\cdot10^{-3}$	$-1.2\cdot10^{-3}$
$\frac{\mathrm{Re}\lambda_{CP}}{\mid\lambda_{CP}\mid}$Rez	—	$-1.4\cdot10^{-3}$
Imz	—	$-1.1\cdot10^{-2}$

Table 90: Systematic contribution coming from SVT alignment. The values reported are the differences among perfect and `diffEL` alignments using the same MC sample.

9.6 Average B^0 lifetime

As discussed in section 8.1, the average B^0 lifetime was varied by twice the PDG2002 error [26], ± 0.016, to assign the systematic error due to the fact that it was fixed in the nominal fit configuration. The effect on the physical parameters is reported in table 91.

Parameter	Analysis 1	Analysis 2
$\Delta\Gamma/\Gamma$	$^{-2.8\cdot10^{-3}}_{+3.4\cdot10^{-3}}$	$^{-3.0\cdot10^{-3}}_{+3.6\cdot10^{-3}}$
$\mid q/p \mid$	$^{+1.2\cdot10^{-3}}_{-1.2\cdot10^{-3}}$	$^{+1.2\cdot10^{-3}}_{-1.2\cdot10^{-3}}$
$\frac{\mathrm{Re}\lambda_{CP}}{\lvert\lambda_{CP}\rvert}\mathrm{Re}z$	—	$^{+3.6\cdot10^{-3}}_{-3.0\cdot10^{-3}}$
Imz	—	$^{-3.6\cdot10^{-4}}_{+4.2\cdot10^{-4}}$

Table 91: Systematics from the variation of the average B^0 lifetime by $\pm 2 \times 0.016$ ps.

9.7 B^+ lifetime

The B^+ lifetime (used in the peaking background of the B_{flav} sample) was varied by ± 0.018 ps [26]. The effect of the variation can be found in table 92. Let us note that there is no effect propagated via the B^+ mistags since in the charged B sample fit used to extract the mistag parameters the B^+ lifetime was left free.

9.8 B^+ mistags

Change by $\pm\sigma$ the B^+ mistags (only the average mistag at $\sigma_{\Delta t} = 0$; the slope and $B^0\bar{B}^0$ differences were not varied). All the mistags were moved simultaneously one σ up and down. The variation of the physics parameters is given in table 93.

Parameter	Analysis 1	Analysis 2
$\Delta\Gamma/\Gamma$	$^{+1.2\cdot10^{-5}}_{-1.1\cdot10^{-5}}$	$^{+2.0\cdot10^{-5}}_{-1.9\cdot10^{-5}}$
$\mid q/p \mid$	$^{0.0}_{0.0}$	$^{-1.3\cdot10^{-6}}_{+1.3\cdot10^{-6}}$
$\frac{\mathrm{Re}\lambda_{CP}}{\lvert\lambda_{CP}\rvert}\mathrm{Re}z$	—	$^{-5.2\cdot10^{-5}}_{+5.2\cdot10^{-5}}$
Imz	—	$^{+2.2\cdot10^{-5}}_{-2.1\cdot10^{-5}}$

Table 92: Systematics the the variation of the B^+ lifetime by ± 0.018 ps.

Parameter	Analysis 1	Analysis 2
$\Delta\Gamma/\Gamma$	$^{-3.9\cdot10^{-6}}_{+3.8\cdot10^{-6}}$	$^{-1.4\cdot10^{-5}}_{+1.3\cdot10^{-5}}$
$\mid q/p \mid$	$^{-8.7\cdot10^{-6}}_{+8.9\cdot10^{-6}}$	$^{-7.2\cdot10^{-6}}_{+7.0\cdot10^{-6}}$
$\frac{\mathrm{Re}\lambda_{CP}}{\lvert\lambda_{CP}\rvert}\mathrm{Re}z$	—	$^{+1.3\cdot10^{-4}}_{-1.2\cdot10^{-4}}$
Imz	—	$^{+3.5\cdot10^{-6}}_{-3.3\cdot10^{-6}}$

Table 93: Systematic uncertainties due to the variation of one σ variation of the B^+ mistag rates. Central values are varied simultaneously for all the tagging categories in the same direction.

9.9 $B^0\overline{B}^0$ differences in reconstruction and tagging efficiencies

Charge asymmetries induced by a difference in the detector response for positive and negative tracks and any possible direct CP violation in the decay of flavor eigenstate B mesons (tagging B's and reconstructed B's in the flavor eigenstate sample) are included in the PDF and extracted together with the other parameters from the time-dependent analysis. By this reason no significant systematic effects are expected from this source. However, in order to account for any possible and residual effect, we assigned a systematic uncertainty as follows. We rerun the B reconstruction, vertexing and tagging code after killing randomly and uniformly (no p, θ, ϕ dependencies) 5% of positive and negative tracks in the large statistics dedicated full Monte Carlo sample. This 5% is on average more than a factor three larger than the precision with which it has been verified on the data that there are no statistically significant asymmetries (as shown in tables 16 and 20). The results from standard fits, for the Analysis 1 and Analysis 2 fits, are shown in table 94 (should be compared to the results with no killing, tables 44 and 45). The half difference between the results obtained for positive and negative tracks is assigned as systematics, as shown in table 95.

Parameter	An. 1 - positive	An. 1 - negative	An. 2 - positive	An. 2 - negative
Δm	0.4814 ± 0.0047	0.4803 ± 0.0048	0.4814 ± 0.0047	0.4804 ± 0.0048
$\Delta\Gamma/\Gamma$	0.189 ± 0.014	0.183 ± 0.015	0.189 ± 0.015	0.184 ± 0.016
$\mid q/p \mid$	1.0435 ± 0.0080	1.0376 ± 0.0080	1.0437 ± 0.0080	1.0379 ± 0.0080
$\frac{\mathrm{Im}\lambda_{CP}}{\mid\lambda_{CP}\mid}$	0.706 ± 0.023	0.721 ± 0.023	0.705 ± 0.024	0.722 ± 0.024
$\frac{\mathrm{Re}\lambda_{CP}}{\mid\lambda_{CP}\mid}\mathrm{Re}z$	—	—	$(-0.4 \pm 1.6) \cdot 10^{-2}$	$(-0.8 \pm 1.6) \cdot 10^{-2}$
$\mathrm{Im}z$	—	—	$(-0.2 \pm 1.7) \cdot 10^{-2}$	$(0.4 \pm 1.7) \cdot 10^{-2}$

Table 94: Results from dedicated full Monte Carlo, Analysis 2 fit, killing 5% of positive and negative tracks. *GG* resolution function is used.

Parameter	Analysis 1	Analysis 2
$\Delta\Gamma/\Gamma$	$-5.6 \cdot 10^{-3}$	$-5.0 \cdot 10^{-3}$
$\mid q/p \mid$	$-5.9 \cdot 10^{-3}$	$-5.8 \cdot 10^{-3}$
$\frac{\mathrm{Re}\lambda_{CP}}{\mid\lambda_{CP}\mid}\mathrm{Re}z$	—	$-3.9 \cdot 10^{-3}$
$\mathrm{Im}z$	—	$+5.9 \cdot 10^{-3}$

Table 95: Systematics from residual charge asymmetries.

Another source of residual charge asymmetries is due to the fact that the $B^0\overline{B}^0$ differences in tagging and reconstruction efficiencies for combinatorial background components were fixed to zero in the nominal fit. The effect from this assumption can be tested adding a new set of charge asymmetry parameters for the combinatorial background components. The measured values of ν and μ^α are well compatible with zero and the variation of the physical parameters with respect to the nominal fit is shown in table 96.

9.10 Tagging efficiency

Since the value of tagging efficiency is fixed in the nominal fit, we made a set of fits varying up and down each tagging category efficiency, according to Poisson errors. As systematic uncertainty, shown in table 97, we quote the quadratic sum of the contributions from all tagging categories. The contribution is found to be negligible.

Parameter	Analysis 1	Analysis 2
$\Delta\Gamma/\Gamma$	$-3.1\cdot10^{-4}$	$-3.1\cdot10^{-4}$
$\mid q/p \mid$	$+9.9\cdot10^{-4}$	$+9.9\cdot10^{-4}$
$\frac{\mathrm{Re}\lambda_{CP}}{\mid\lambda_{CP}\mid}$Rez	—	$-4.2\cdot10^{-5}$
Imz	—	$-7.9\cdot10^{-5}$

Table 96: Systematics due to residual charge asymmetries in combinatorial background.

Parameter	Analysis 1	Analysis 2
$\Delta\Gamma/\Gamma$	$+1.7\cdot10^{-6}$	$+1.4\cdot10^{-6}$
$\mid q/p \mid$	$+8.9\cdot10^{-5}$	$+8.9\cdot10^{-5}$
$\frac{\mathrm{Re}\lambda_{CP}}{\mid\lambda_{CP}\mid}$Rez	—	$+6.2\cdot10^{-7}$
Imz	—	$+1.9\cdot10^{-6}$

Table 97: Systematic uncertainty from fixing the tagging efficiencies. Tagging efficiencies have been varied separately up and down for each category, according to Poisson errors. The quadratic sum of the contributions from each category is quoted as uncertainty.

9.11 CP violation in the decay

We changed by $\pm10\%$ the ratio of conjugate decay amplitudes for CP eigenstates, $r_{CP,CP}$. The impact on the physics parameters is given in table 98. No systematics is assigned to possible direct CP violation effects in the tagging and flavor eigenstate B samples since these effects are included in the PDF and are part of the charge asymetries, parameters ν and μ^{α}, equations (101) and (100).

Parameter	Analysis 1	Analysis 2
$\Delta\Gamma/\Gamma$	$^{+1.7\cdot10^{-3}}_{-1.4\cdot10^{-3}}$	$^{+1.8\cdot10^{-3}}_{-1.6\cdot10^{-3}}$
$\mid q/p \mid$	$^{+3.9\cdot10^{-3}}_{-4.3\cdot10^{-3}}$	$^{+3.9\cdot10^{-3}}_{-4.3\cdot10^{-3}}$
$\frac{\mathrm{Re}\lambda_{CP}}{\mid\lambda_{CP}\mid}$Rez	—	$^{+6.8\cdot10^{-4}}_{-3.3\cdot10^{-4}}$
Imz	—	$^{+2.7\cdot10^{-3}}_{-4.3\cdot10^{-4}}$

Table 98: Variation in the physics parameters due to a $\pm10\%$ direct CP violation in the CP eigenstate sample ($r_{CP,CP}$ parameter).

9.12 Doubly-CKM-Suppressed decays

Systematics from Doubly-CKM-Suppressed decays arise due to uncertainties in $r_{tag}\frac{\mathrm{Re}\lambda_{tag}}{\mid\lambda_{tag}\mid}$, $\bar{r}_{tag}\frac{\mathrm{Re}\bar{\lambda}_{tag}}{\mid\bar{\lambda}_{tag}\mid}$, $r_{flav}\frac{\mathrm{Re}\lambda_{flav}}{\mid\lambda_{flav}\mid}$ and $\bar{r}_{tag}\frac{\mathrm{Re}\bar{\lambda}_{flav}}{\mid\lambda_{flav}\mid}$. Uncertainties from r_k and $\bar{r}_k$ via the DCKM sine terms are taken into account via the rescaling of $\frac{\mathrm{Im}\lambda_{tag}}{\mid\lambda_{tag}\mid}$, $\frac{\mathrm{Im}\bar{\lambda}_{tag}}{\mid\bar{\lambda}_{tag}\mid}$, $\frac{\mathrm{Im}\lambda_{flav}}{\mid\lambda_{flav}\mid}$ and $\frac{\mathrm{Im}\bar{\lambda}_{flav}}{\mid\bar{\lambda}_{flav}\mid}$, as discussed in section 2.10. To evaluate the systematics, toy Monte Carlo

samples scanning all possible values of the DCKM phases which give different values of the cosines, for B^0 and $\overline{B}^0$ independently (81 combinations), were generated. The generation used a single channel since, as discussed in 2.10 and proved in B.3, this corresponds to the worse situation. In the nominal fit we assumed the central value of r_{tag} and r_{flav} to be 0.02, estimated assuming that the amplitudes are dominated by the Standard Model $b \to c$ and $b \to c$ transitions for the favored and suppressed decays, respectively (see figure 1), taking the values of the CKM matrix elements from [26] and neglecting corrections due to the ratio of the suppressed to the allowed decay constants. In an attempt to account for potential additional diagrams (due to New Physics), effects from decays constants ([36]) and $B^0\overline{B}^0$ differences, we assign an uncertainty of 100%, which gives a maximum value of 0.04. This is the value used in the generation. The samples were then fitted with the nominal fit, including all the experimental effects except backgrounds. From about 150 times the data statistics, the largest offset among the 81 different DCKM phase configurations for each physical parameter independently is evaluated, as reported (together with their statistical uncertainty) in table 99, for Analysis 1 and Analysis 2, respectively. The largest between the bias and its statistical uncertainty is used to assign the systematics from Doubly-CKM-Suppressed decays, as given in table 100.

Parameter	Analysis 1	Analysis 2
Δm	0.0011 ± 0.0003	0.0033 ± 0.0005
$\Delta\Gamma/\Gamma$	0.0057 ± 0.0026	0.008 ± 0.003
$\mid q/p \mid$	0.0031 ± 0.0009	0.0035 ± 0.0007
$\frac{\mathrm{Im}\lambda_{CP}}{\mid\lambda_{CP}\mid}$	0.020 ± 0.005	0.028 ± 0.006
$\frac{\mathrm{Re}\lambda_{CP}}{\mid\lambda_{CP}\mid}$Rez	–	0.0325 ± 0.0021
Imz	–	0.0062 ± 0.0018

Table 99: Largest offset among the 81 different DCKM phase configurations for each physical parameter, for Analysis 1 and Analysis 2. Estimated from ≈ 150 times the data statistics.

Moreover, the dependence of the central value and the statistical error of each parameter was evaluated in a wide range of r_{tag}=r_{flav} (between 0.005 and 0.055). The stability was remarkable, as shown in figure 55. This stability is expected since the sine terms of the DCKM phases are free parameters, therefore absorbing r_{tag},r_{flav} effects (see section 2.10), while the cosine terms are fixed to zero.

Parameter	Analysis 1	Analysis 2
$\Delta\Gamma/\Gamma$	0.0057	0.0077
$\mid q/p \mid$	0.0031	0.0035
$\frac{\mathrm{Re}\lambda_{CP}}{\mid\lambda_{CP}\mid}$Rez	–	0.0325
Imz	–	0.0062

Table 100: Systematics from Doubly-CKM-Suppressed decays.

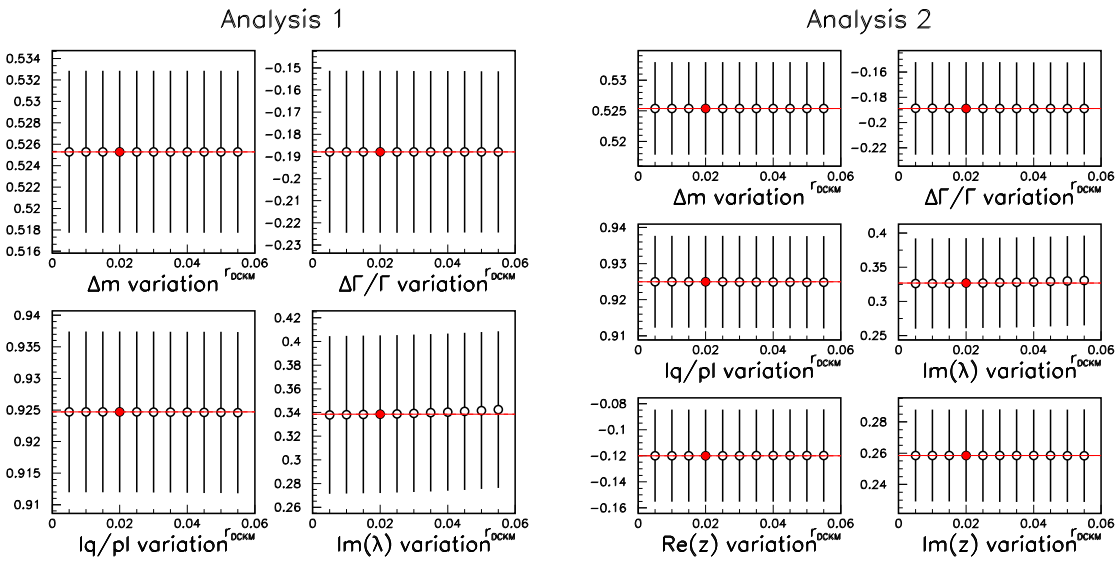

Figure 55: Variation of the central value and statistical error of the different parameters as a function of r_{tag}=r_{flav}.

9.13 PDF asymptotic normalization

The PDF in the nominal fit was normalized asymptotically. The effect from this assumption was evaluated by normalizing in the finite range defined by the Δt cuts ($[-20,20]$ ps), according to equation (105). The effect on the different parameters is summarized in table 101.

Parameter	Analysis 1	Analysis 2
$\Delta\Gamma/\Gamma$	$-3.8\cdot10^{-4}$	$-4.1\cdot10^{-4}$
$\mid q/p \mid$	$+5.1\cdot10^{-5}$	$+5.2\cdot10^{-5}$
$\frac{\mathrm{Re}\lambda_{CP}}{\lvert\lambda_{CP}\rvert}$Rez	—	$-5.8\cdot10^{-5}$
Imz	—	$+1.3\cdot10^{-4}$

Table 101: Systematic contribution from the usage of PDF asymptotic normalization.

9.14 Likelihood fit

The precision on which we have verified from toy Monte Carlo (section 7.5) that the fitting procedure provides an unbiassed estimation of all the physics parameters is assigned as systematic error due to the fitting procedure. More specifically, we take as systematic error due to this source the largest between the observed bias (mean value of the residual distributions) and its statistical error due to the limited amount of toy Monte Carlo experiments. The values can be found in table 102.

Parameter	Analysis 1	Analysis 2
$\Delta\Gamma/\Gamma$	$8.4\cdot10^{-3}$	$3.1\cdot10^{-3}$
$\mid q/p \mid$	$1.4\cdot10^{-3}$	$7.3\cdot10^{-4}$
$\frac{\mathrm{Re}\lambda_{CP}}{\lvert\lambda_{CP}\rvert}$Rez	—	$2.8\cdot10^{-3}$
Imz	—	$2.9\cdot10^{-3}$

Table 102: Likelihood fit systematics from fitting procedure.

Another source of uncertainty contributing to the likelihood fit systematics was estimated using the full *BABAR* Monte Carlo. To evaluate this contribution we split the exclusive standard Monte Carlo sample into data-sized samples, keeping the relative sizes of signal B_{flav}, $B_{CPK^0_S}$ and $B_{CPK^0_L}$ samples as observed in the data. The dedicated B_{flav} Monte Carlo was also used after reweighting it to the values of the standard sample. The nominal fit (signal only) was then applied to the samples. The small combinatorial background in these exclusive samples was rejected by using only events in the signal region ($m_{ES} > 5.25$ GeV/c^2 for B_{flav}, $B_{CPK^0_S}$ $\mid \Delta E \mid < 10$ MeV for $B_{CPK^0_L}$). The total available statistics after applying this procedure was 6 times the B_{flav} sample and 84 times the $B_{CPK^0_S}$ and $B_{CPK^0_L}$ samples. To take profit of the much larger B_{CP} statistics, we performed the fit for all possible combinations of B_{CP} and B_{flav} samples (6 fits). For B_{CP} dominated measurements ($\Delta\Gamma/\Gamma$, $\frac{\mathrm{Re}\lambda_{CP}}{\lvert\lambda_{CP}\rvert}$Rez), we evaluated the mean bias from the 6×84 fits, and the error from the combination of 84 fits (6) with the largest RMS. For B_{flav} dominated measurements ($\mid q/p \mid$, Imz), the mean bias and RMS was estimated from 6 random B_{CP} samples (as expected, no sizeable changes were observed by selecting a different set of B_{CP} samples). The results obtained with this procedure are reported in table 103. We assigned as systematics the largest between the mean residual and its uncertainty, as given in table 104. No corrections were applied to the central values extracted from the data since no biases are observed. We should note that this contribution takes into account possible missing or not accurate enough assumptions reproduced by the

BABAR Monte Carlo, included possible correlations among them. Specific contributions are the assumption of a common Δt resolution function and mistags for all samples, as well as the common resolution function parameters for right and wrong tags and for all tagging categories. The small deviation from the linear model of the tagging-vertexing correlation (see figure 18) is also accounted for with this source of uncertainty.

Parameter	Analysis 1	Analysis 2
Δm	0.0045 ± 0.0019	0.0047 ± 0.0020
$\Delta\Gamma/\Gamma$	-0.0028 ± 0.0051	-0.0028 ± 0.0051
$\mid q/p \mid$	0.0074 ± 0.0063	0.0074 ± 0.0063
$\frac{\mathrm{Im}\lambda_{CP}}{\mid\lambda_{CP}\mid}$	0.0089 ± 0.0071	0.0097 ± 0.0071
$\frac{\mathrm{Re}\lambda_{CP}}{\mid\lambda_{CP}\mid}\mathrm{Rez}$	—	-0.0038 ± 0.0037
Imz	—	0.0034 ± 0.0157

Table 103: Mean residuals with error from the data-sized full Monte Carlo fits.

Parameter	Analysis 1	Analysis 2
$\Delta\Gamma/\Gamma$	0.0051	0.0051
$\mid q/p \mid$	0.0074	0.0074
$\frac{\mathrm{Re}\lambda_{CP}}{\mid\lambda_{CP}\mid}\mathrm{Rez}$	—	0.0038
Imz	—	0.0157

Table 104: Likelihood fit systematics from common mistags and Δt resolution.

9.15 Peaking background fractions

The effect due to the uncertainty on the amount of charged B background that peaks in the m_{ES} B_{flav} distribution was estimated by changing the fraction of peaking background, f^{α}_{peak}, by $\pm 0.6\%$. In the case of the $B_{CPK^0_S}$ sample, it was changed according to the errors reported in table 12, adding in quadrature the contribution from each subsample. The impact on the physics parameters is given in table 105.

Parameter	Analysis 1	Analysis 2
$\Delta\Gamma/\Gamma$	$^{-3.5\cdot10^{-5}}_{+4.4\cdot10^{-5}}$	$^{+4.4\cdot10^{-5}}_{-5.3\cdot10^{-5}}$
$\mid q/p \mid$	$^{-5.7\cdot10^{-5}}_{+5.8\cdot10^{-5}}$	$^{-6.7\cdot10^{-5}}_{+7.0\cdot10^{-5}}$
$\frac{\mathrm{Re}\lambda_{CP}}{\mid\lambda_{CP}\mid}\mathrm{Rez}$	—	$^{-1.1\cdot10^{-3}}_{+1.3\cdot10^{-3}}$
Imz	—	$^{-1.3\cdot10^{-4}}_{+1.2\cdot10^{-4}}$

Parameter	Analysis 1	Analysis 2
$\Delta\Gamma/\Gamma$	$^{-2.2\cdot10^{-4}}_{+8.3\cdot10^{-5}}$	$^{-1.9\cdot10^{-4}}_{+6.9\cdot10^{-5}}$
$\mid q/p \mid$	$^{-9.8\cdot10^{-6}}_{+4.3\cdot10^{-6}}$	$^{-1.6\cdot10^{-5}}_{+7.0\cdot10^{-6}}$
$\frac{\mathrm{Re}\lambda_{CP}}{\mid\lambda_{CP}\mid}\mathrm{Rez}$	—	$^{-5.6\cdot10^{-4}}_{+2.1\cdot10^{-4}}$
Imz	—	$^{+3.1\cdot10^{-5}}_{-5.7\cdot10^{-5}}$

Table 105: Peaking background systematics (left: B_{flav} sample; right: $B_{CPK^0_S}$ sample).

9.16 CP content in $B_{CPK_S^0}$ peaking background

The nominal fit assumes that the effective η_{CP} of the peaking background for the $B_{CPK_S^0}$ sample is zero. The resolution function, mistags and physics parameters are assumed to be the same as for the signal. We varied the the effective η_{CP} between $+1$ and -1, and we assigned as systematic error from this source the difference to the nominal fit. The results are given in table 106.

Parameter	Analysis 1	Analysis 2
$\Delta\Gamma/\Gamma$	$-4.9\cdot10^{-5}$ $+4.7\cdot10^{-5}$	$-3.1\cdot10^{-5}$ $+2.8\cdot10^{-5}$
$\mid q/p \mid$	$-5.6\cdot10^{-6}$ $+5.6\cdot10^{-6}$	$-9.1\cdot10^{-6}$ $+9.2\cdot10^{-6}$
$\frac{\mathrm{Re}\lambda_{CP}}{\lvert\lambda_{CP}\rvert}$Rez	—	$-1.8\cdot10^{-4}$ $+1.9\cdot10^{-4}$
Imz	—	$+1.8\cdot10^{-4}$ $-1.7\cdot10^{-4}$

Table 106: Systematics due to the CP content of the peaking background component in the $B_{CPK_S^0}$ sample.

9.17 Δt structure in combinatorial background

Another source of systematic uncertainty originates from the assumption that the temporal structure of the combinatorial background in the side band region is a good description of the one in the signal region. We varied the lower edge of m_{ES} distribution from 5.20 GeV/c^2 to 5.27 GeV/c^2, simultaneously for the B_{flav} and $B_{CPK_S^0}$ samples. The variations of the fitted parameters with respect to the nominal fit are shown in figure 56.

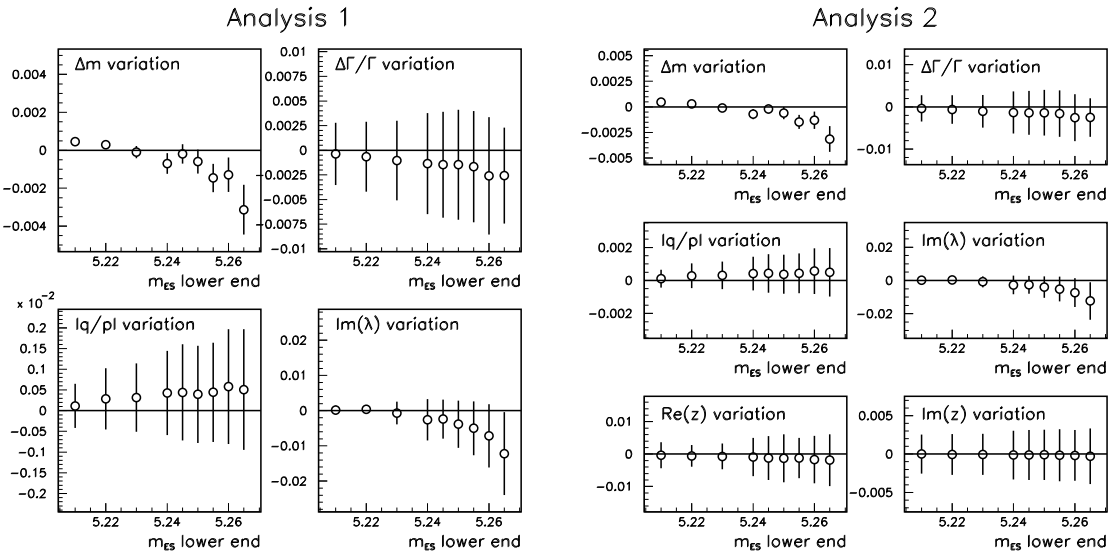

Figure 56: Variation of the fitted physical parameters for Analysis 1 and 2 with respect to the nominal fit for different values of the lower edge of the m_{ES} distribution (nominal value is 5.2 GeV/c^2).

We also split the sideband region in seven equal slices each 10 MeV/c^2 wide, simultaneously for the B_{flav} and $B_{CPK^0_S}$ samples, and used each of these ranges, in a standard fit. The results are shown in figure 57, where we indicated also the extrapolation to signal region. We estimate as systematic uncertainty the quadratic sum of the extrapolation and the error on it. Results are reported in table 107.

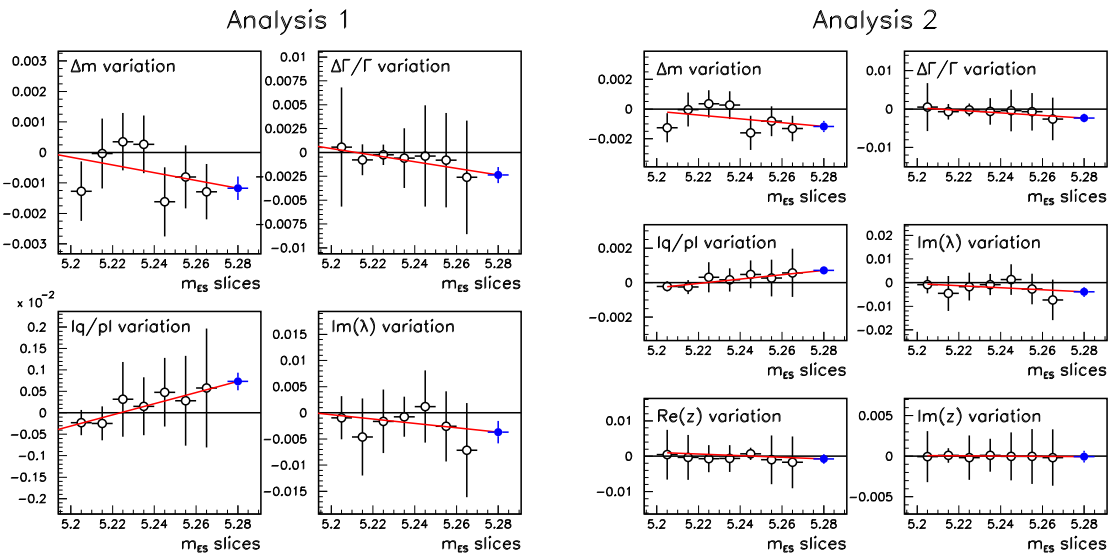

Figure 57: Variation of the fitted physical parameters for Analysis 1 and 2 with respect to the nominal fit using different "slices" of events in the m_{ES} sideband region. The extrapolation to the signal region (blue solid circle) from a linear fit is indicated as well.

Parameter	Analysis 1	Analysis 2
$\Delta\Gamma/\Gamma$	$1.7 \cdot 10^{-3}$	$1.8 \cdot 10^{-3}$
$\mid q/p \mid$	$5.4 \cdot 10^{-4}$	$5.3 \cdot 10^{-4}$
$\frac{\mathrm{Re}\lambda_{CP}}{\lvert\lambda_{CP}\rvert}$Rez	—	$1.1 \cdot 10^{-3}$
Imz	—	$5.1 \cdot 10^{-4}$

Table 107: Systematic error due to the assumption of a common temporal structure for sideband and signal events in the m_{ES} distribution. See text and figure 57 for details.

9.18 Peaking background composition of B_{flav} sample

The nominal fit assumes that the peaking background of the B_{flav} sample comes exclusively from B^+ decays, neglecting the small B^0 component [29], which potentially has a $\Delta\Gamma$, CPT/CP/T, mixing and DCKM structure. In order to evaluate conservatively a systematic error from this assumption, the complete peaking background component was assumed to come from B^0 decays (i.e. same structure as the signal). The variation with respect to the nominal configuration is shown in table 108.

Parameter	Analysis 1	Analysis 2
$\Delta\Gamma/\Gamma$	$+5.1\cdot10^{-6}$	$-2.9\cdot10^{-4}$
$\mid q/p \mid$	$+1.2\cdot10^{-4}$	$+1.8\cdot10^{-4}$
$\frac{\mathrm{Re}\lambda_{CP}}{\mid\lambda_{CP}\mid}$Rez	—	$+3.5\cdot10^{-3}$
Imz	—	$+1.9\cdot10^{-4}$

Table 108: Systematics due to B^0 peaking background instead of B^+.

9.19 $\Delta\Gamma$/CPT/CP/T/Mixing/DCKM content in combinatorial backgrounds

The nominal fit assumes that there is no $\Delta\Gamma$, CPT/CP/T, mixing and DCKM structure in the combinatorial background components (B_{flav} and $B_{CPK^0_S}$ samples) and in the non-J/ψ background ($B_{CPK^0_L}$ sample). To evaluate the effect from this assumption we repeated the fit but now assumming non-zero $\Delta\Gamma$, CPT/CP/T and mixing effects. This check was performed by introducing in the PDF an independent set of physics parameters to those of the signal, assuming maximal mixing and CP violation (Δm and $\frac{\mathrm{Im}\lambda_{CP}}{\mid\lambda_{CP}\mid}$ were fixed to 0.489 ps^{-1} and 0.75, respectively [26]). DCKM effects were incorporated assuming the maximal value of r_{tag}=r_{flav} (0.04) and scanning all the possible values of the B^0 and $\bar{B}^0$ phases, assuming to be the same for the tagging and reconstructed flavor sides (16 combinations). The largest difference among the 16 DCKM phase combinations with respect to the nominal fit is assigned as systematic uncertainty from this source, and are shown in table 109. In order to evaluate this systematics we assumed $\eta_{CP}=-1$ for the $B_{CPK^0_S}$ sample (taking $\eta_{CP}=+1$ would just change the sign of some of the background physics parameters).

Parameter	Analysis 1	Analysis 2
$\Delta\Gamma/\Gamma$	$\pm4.0\cdot10^{-3}$	$\mp1.4\cdot10^{-3}$
$\mid q/p \mid$	$\mp2.2\cdot10^{-3}$	$\pm1.7\cdot10^{-3}$
$\frac{\mathrm{Re}\lambda_{CP}}{\mid\lambda_{CP}\mid}$Rez	—	$\mp1.5\cdot10^{-3}$
Imz	—	$\mp2.6\cdot10^{-4}$

Table 109: Systematics due to the $\Delta\Gamma$/CPT/T/CP/Mixing content of the combinatorial background components in the B_{flav} and $B_{CPK^0_S}$ samples, including doubly CKM suppressed decays effects. The variations refer to $\eta_{CP}=\mp1$

9.20 Charm content

Charm meson effects in the inclusively reconstructed tagging B are mostly parameterized in the PDF via the bias of the resolution function and the correlation of the mistag fractions with the reconstructed Δt error. Residual effects were extensively investigated in the hadronic B mixing analysis [23] (the studies neglected tagging-vertexing correlations). The impact on the Δm measurement due to uncertainties on the relative amounts of charm meason specifies and their lifetimes was found very small or negligible. By this reason, no systematic error has been explicitely evaluated and assigned due to this source.

9.21 $J/\psi K^0_L$ specific systematics

The $B_{CPK^0_L}$ specific systematics is evaluated as detailed in [20]. In the following all the sources of systematics are listed and their contribution reported. For a summary of the different contributions, see tables 123 and 124.

9.21.1 CP content of background

The CP eigenvalue of most of the components in the fit is known. The cases where it is not known:

- $B^0 \to J/\psi K^{*0}$, $K^{*0} \to K^0_L \pi^0$: Change the nominal value (-0.68) by ± 0.07. The effect of the variation is shown in table 110;
- non-itemized inclusive J/ψ background: change the nominal net CP ($+0.21$ in the EMC and $+0.24$ in the IFR) from 0.15 to 0.33 in the EMC and from 0.18 to 0.38 for the IFR. The effect of this variation is shown in table 111;
- non-J/ψ background: the same procedure as described in section 9.19 was used here, varying the net CP (nominal is 0) by ± 1. The systematics was evaluated together with the equivalent effect in the combinatorial background of the B_{flav} and $B_{CPK^0_S}$ samples, and is already included in table 109.

Parameter	Analysis 1	Analysis 2
$\Delta\Gamma/\Gamma$	$^{-3.4\cdot10^{-5}}_{+3.4\cdot10^{-5}}$	$^{-2.4\cdot10^{-5}}_{+2.4\cdot10^{-5}}$
$\mid q/p \mid$	$^{+1.7\cdot10^{-6}}_{-1.6\cdot10^{-6}}$	$^{+1.2\cdot10^{-6}}_{-1.4\cdot10^{-6}}$
$\frac{\mathrm{Re}\lambda_{CP}}{\lvert\lambda_{CP}\rvert}\mathrm{Re}z$	—	$^{+3.8\cdot10^{-5}}_{-3.8\cdot10^{-5}}$
Imz	—	$^{+3.5\cdot10^{-4}}_{-3.5\cdot10^{-4}}$

Table 110: $J/\psi K^0_L$ specific systematics: assumed CP eigenvalue of the $B^0 \to J/\psi K^{*0}$, $K^{*0} \to K^0_L \pi^0$ background.

Parameter	Analysis 1	Analysis 2
$\Delta\Gamma/\Gamma$	$^{-3.4\cdot10^{-4}}_{+1.5\cdot10^{-4}}$	$^{-2.9\cdot10^{-4}}_{+1.3\cdot10^{-4}}$
$\mid q/p \mid$	$^{-3.0\cdot10^{-7}}_{+1.0\cdot10^{-6}}$	$^{-5.0\cdot10^{-7}}_{+1.0\cdot10^{-6}}$
$\frac{\mathrm{Re}\lambda_{CP}}{\lvert\lambda_{CP}\rvert}\mathrm{Re}z$	—	$^{+8.1\cdot10^{-5}}_{-4.1\cdot10^{-5}}$
Imz	—	$^{+8.3\cdot10^{-4}}_{-3.8\cdot10^{-4}}$

Table 111: $J/\psi K^0_L$ specific systematics: assumed net CP eigenvalue of the non-itemized inclusive J/ψ background.

9.21.2 Prompt fraction and lifetime of non-J/ψ background

The fraction of the prompt component and the lifetime of the non-prompt of the non-J/ψ background were varied according with the errors from the external fit to the sideband events, ± 0.08 and ± 0.3, respectively. The effects of these variations are reported in tables 112 and 113.

9.21.3 IFR K^0_L angular resolution

The same prescription as in [20] has been used to estimate the systematics due to the difference between data and Monte Carlo in the K^0_L angular resolution. The nominal ΔE fit has added angular resolution smearing

Parameter	Analysis 1	Analysis 2
$\Delta\Gamma/\Gamma$	$^{-8.5\cdot10^{-5}}_{+7.7\cdot10^{-5}}$	$^{-1.0\cdot10^{-4}}_{+9.3\cdot10^{-5}}$
$\mid q/p \mid$	$^{+1.1\cdot10^{-5}}_{-1.2\cdot10^{-5}}$	$^{+1.5\cdot10^{-5}}_{-1.5\cdot10^{-5}}$
$\frac{\mathrm{Re}\lambda_{CP}}{\lvert\lambda_{CP}\rvert}$Rez	—	$^{-1.6\cdot10^{-5}}_{+1.9\cdot10^{-5}}$
Imz	—	$^{+1.5\cdot10^{-4}}_{-1.4\cdot10^{-4}}$

Table 112: $J/\psi K_L^0$ specific systematics: prompt fraction of non-J/ψ background.

Parameter	Analysis 1	Analysis 2
$\Delta\Gamma/\Gamma$	$^{+2.9\cdot10^{-4}}_{-2.0\cdot10^{-4}}$	$^{+3.0\cdot10^{-4}}_{-2.1\cdot10^{-4}}$
$\mid q/p \mid$	$^{-1.3\cdot10^{-5}}_{+10.0\cdot10^{-6}}$	$^{-1.6\cdot10^{-5}}_{+1.3\cdot10^{-5}}$
$\frac{\mathrm{Re}\lambda_{CP}}{\lvert\lambda_{CP}\rvert}$Rez	—	$^{-5.8\cdot10^{-5}}_{+4.9\cdot10^{-5}}$
Imz	—	$^{+7.8\cdot10^{-6}}_{+1.6\cdot10^{-5}}$

Table 113: $J/\psi K_L^0$ specific systematics: lifetime of non-J/ψ background.

for IFR K_L^0 events. The fit was also done ignoring the angular resolution smearing, and the difference to the nominal fit was assigned as systematic error. The effect on the parameters is reported in table 114.

Parameter	Analysis 1	Analysis 2
$\Delta\Gamma/\Gamma$	$-9.7\cdot10^{-6}$	$-8.0\cdot10^{-7}$
$\mid q/p \mid$	$+2.4\cdot10^{-6}$	$+3.6\cdot10^{-6}$
$\frac{\mathrm{Re}\lambda_{CP}}{\lvert\lambda_{CP}\rvert}$Rez	—	$+1.3\cdot10^{-4}$
Imz	—	$+5.1\cdot10^{-4}$

Table 114: $J/\psi K_L^0$ specific systematics: K_L^0 angular resolution.

9.21.4 Shape of ΔE distributions

The ΔE distributions used to help to discriminate between signal and background are taken from Monte Carlo. To have good agreement with the data, the Monte Carlo was shifted by -0.5 MeV and smeared by 0.85 MeV. The sensitivity to the uncertainties on the ΔE shape were evaluated by applying an additional shift of ±0.25 MeV and an additional smearing of 0.45 MeV. The impact of the physics parameters is shown in tables 115 and 116.

Parameter	Analysis 1	Analysis 2
$\Delta\Gamma/\Gamma$	$^{+6.9\cdot10^{-5}}_{+8.6\cdot10^{-5}}$	$^{+7.5\cdot10^{-5}}_{+8.5\cdot10^{-5}}$
$\mid q/p \mid$	$^{+4.7\cdot10^{-6}}_{+4.7\cdot10^{-6}}$	$^{+5.5\cdot10^{-6}}_{+5.0\cdot10^{-6}}$
$\frac{\mathrm{Re}\lambda_{CP}}{\lvert\lambda_{CP}\rvert}$Rez	—	$^{+1.3\cdot10^{-4}}_{+2.8\cdot10^{-5}}$
Imz	—	$^{+4.5\cdot10^{-4}}_{+1.2\cdot10^{-4}}$

Table 115: $J/\psi K_L^0$ specific systematics: ΔE shape (ΔE shift).

Parameter	Analysis 1	Analysis 2
$\Delta\Gamma/\Gamma$	$+1.7\cdot10^{-4}$	$+1.6\cdot10^{-4}$
$\mid q/p \mid$	$+8.4\cdot10^{-6}$	$+8.4\cdot10^{-6}$
$\frac{\mathrm{Re}\lambda_{CP}}{\mid\lambda_{CP}\mid}$Rez	—	$+1.8\cdot10^{-5}$
Imz	—	$+4.5\cdot10^{-5}$

Table 116: $J/\psi K_L^0$ specific systematics: ΔE shape (additional ΔE smearing).

9.21.5 Measured sample composition from ΔE fit

The relative amount of signal, inclusive J/ψ background, and non J/ψ background is determined from a three component fit of the ΔE spectrum, which is described in reference [19]. The fitted fractions for IFR and EMC samples are variated randomly accordingly to the covariance matrix from the ΔE fit and the global fit is performed for each of the configurations. In figure 58 we report the distributions of the fitted values for 150 random configurations. The width of a Gaussian fit to these distributions are quoted as the systematic contribution for each variable.

Parameter	Analysis 1	Analysis 2
$\Delta\Gamma/\Gamma$	$8.7\cdot10^{-4}$	$9.1\cdot10^{-4}$
$\mid q/p \mid$	$3.9\cdot10^{-5}$	$4.1\cdot10^{-5}$
$\frac{\mathrm{Re}\lambda_{CP}}{\mid\lambda_{CP}\mid}$Rez	—	$7.0\cdot10^{-4}$
Imz	—	$2.2\cdot10^{-3}$

Table 117: $J/\psi K_L^0$ specific systematics: uncertainties from the variation of the sample composition. .

9.21.6 Branching fractions

One of the inputs of the sample composition fit are the branching fractions of the various $J/\psi X$ modes. We varied these numbers by either their measured errors or conservative estimates, as in [20]. After each variation the ΔE fit for the sample composition is recomputed. The difference among the results of the subsequent global fit and the nominal case are taken as the sytematic error.

Parameter	Analysis 1	Analysis 2
$\Delta\Gamma/\Gamma$	$^{-4.8\cdot10^{-6}}_{-7.5\cdot10^{-6}}$	$^{-5.5\cdot10^{-6}}_{-6.1\cdot10^{-6}}$
$\mid q/p \mid$	$^{-3.0\cdot10^{-7}}_{-6.0\cdot10^{-7}}$	$^{-5.0\cdot10^{-7}}_{-10.0\cdot10^{-7}}$
$\frac{\mathrm{Re}\lambda_{CP}}{\mid\lambda_{CP}\mid}$Rez	—	$^{-1.0\cdot10^{-7}}_{+5.2\cdot10^{-6}}$
Imz	—	$^{-8.8\cdot10^{-6}}_{+1.4\cdot10^{-5}}$

Parameter	Analysis 1	Analysis 2
$\Delta\Gamma/\Gamma$	$^{+1.8\cdot10^{-5}}_{-9.9\cdot10^{-6}}$	$^{+1.6\cdot10^{-5}}_{-3.6\cdot10^{-3}}$
$\mid q/p \mid$	$^{+2.0\cdot10^{-7}}_{-4.0\cdot10^{-7}}$	$^{0.0}_{+1.8\cdot10^{-4}}$
$\frac{\mathrm{Re}\lambda_{CP}}{\mid\lambda_{CP}\mid}$Rez	—	$^{-1.9\cdot10^{-5}}_{+3.4\cdot10^{-3}}$
Imz	—	$^{-8.0\cdot10^{-5}}_{+1.9\cdot10^{-3}}$

Table 118: $J/\psi K_L^0$ specific systematics: $\pm10\%$ variation of $B\to J/\psi K^*$ branching fraction (left); $\pm10\%$ variation of $B^0\to J/\psi K_S^0$ branching fraction (right).

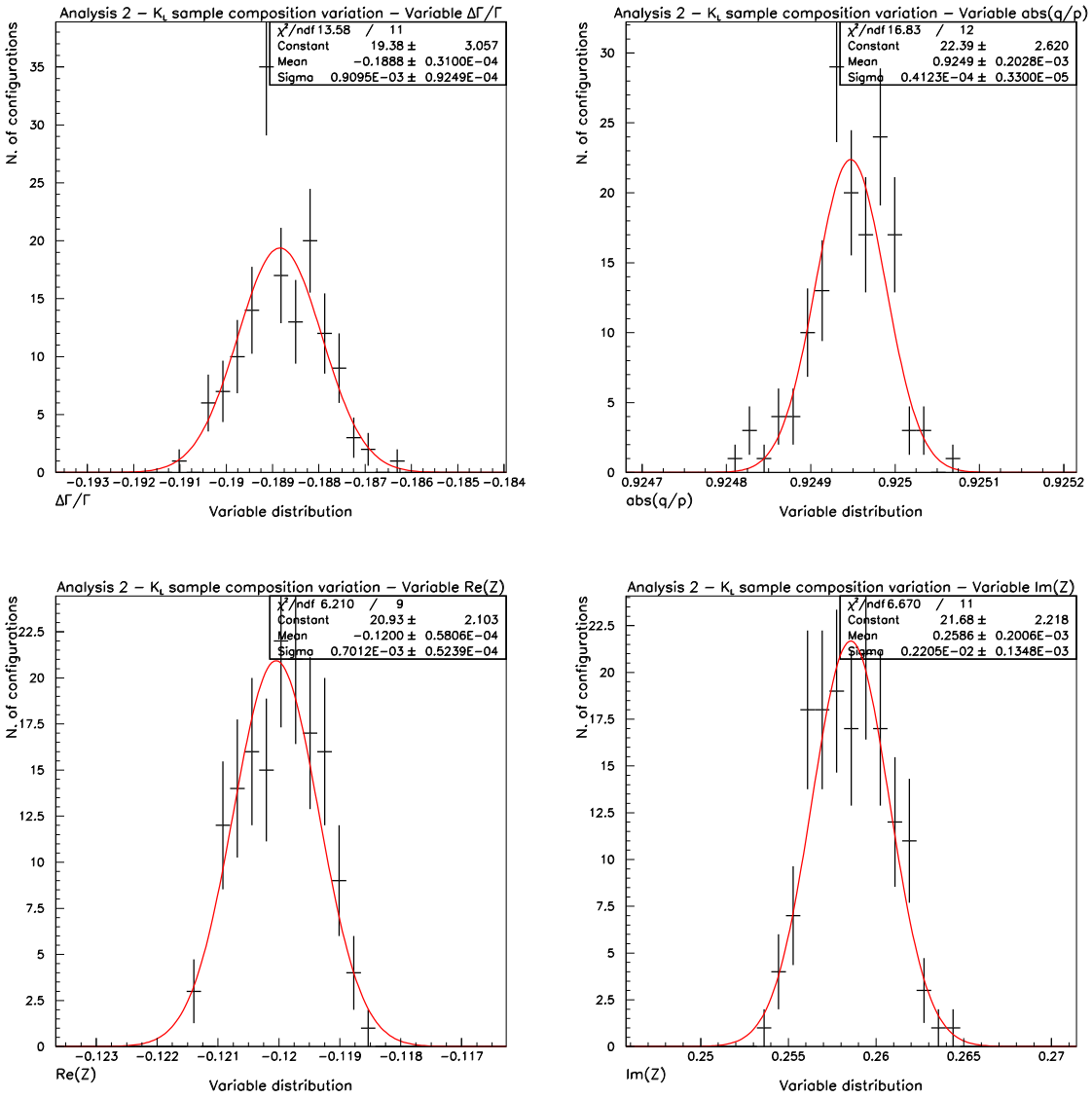

Figure 58: Distribution of the (BLIND) fitted parameters from Analysis 2 varying the sample composition extracted from ΔE fit. The widths of the fitted gaussians are taken as the systematic uncertainties.

9.21.7 `Lepton` tag signal fraction correction

Since there is an observed significative difference on flavor tag of `Lepton` and `non-lepton` in the J/ψ events, a correction for this effect is applied to the fractions of J/ψ events ([20]), that are an input of the standard fit. We performed a fit without this correction in order to evaluate the systematic effect due to this correction. Results are shown in table 121.

Parameter	Analysis 1	Analysis 2
$\Delta\Gamma/\Gamma$	$^{+1.3\cdot10^{-5}}_{-1.5\cdot10^{-5}}$	$^{+1.3\cdot10^{-5}}_{-1.4\cdot10^{-5}}$
$\mid q/p \mid$	$^{+6.0\cdot10^{-7}}_{-1.3\cdot10^{-6}}$	$^{+5.0\cdot10^{-7}}_{-1.5\cdot10^{-6}}$
$\frac{\mathrm{Re}\lambda_{CP}}{\lvert\lambda_{CP}\rvert}$Rez	—	$^{+9.4\cdot10^{-6}}_{-9.0\cdot10^{-6}}$
Imz	—	$^{+2.9\cdot10^{-5}}_{-3.2\cdot10^{-5}}$

Parameter	Analysis 1	Analysis 2
$\Delta\Gamma/\Gamma$	$^{+5.0\cdot10^{-5}}_{-5.6\cdot10^{-5}}$	$^{+4.7\cdot10^{-5}}_{-5.3\cdot10^{-5}}$
$\mid q/p \mid$	$^{+2.0\cdot10^{-6}}_{-3.1\cdot10^{-6}}$	$^{+1.9\cdot10^{-6}}_{-3.3\cdot10^{-6}}$
$\frac{\mathrm{Re}\lambda_{CP}}{\lvert\lambda_{CP}\rvert}$Rez	—	$^{-8.0\cdot10^{-7}}_{+9.9\cdot10^{-6}}$
Imz	—	$^{-1.3\cdot10^{-5}}_{+1.7\cdot10^{-5}}$

Table 119: $J/\psi K_L^0$ specific systematics: $\pm$50% variation of $B \to J/\psi K_L \pi$ branching fraction (left); $\pm$50% variation of $B^0 \to \chi_c K_L$ branching fraction (right).

Parameter	Analysis 1	Analysis 2
$\Delta\Gamma/\Gamma$	$^{-4.8\cdot10^{-6}}_{-7.5\cdot10^{-6}}$	$^{-5.5\cdot10^{-6}}_{-6.1\cdot10^{-6}}$
$\mid q/p \mid$	$^{-3.0\cdot10^{-7}}_{-6.0\cdot10^{-7}}$	$^{-5.0\cdot10^{-7}}_{-10.0\cdot10^{-7}}$
$\frac{\mathrm{Re}\lambda_{CP}}{\lvert\lambda_{CP}\rvert}$Rez	—	$^{-1.0\cdot10^{-7}}_{+5.2\cdot10^{-6}}$
Imz	—	$^{-8.8\cdot10^{-6}}_{+1.4\cdot10^{-5}}$

Table 120: $J/\psi K_L^0$ specific systematics: $\pm$50% variation of $B \to J/\psi X$ residual branching fraction.

Parameter	Analysis 1	Analysis 2
$\Delta\Gamma/\Gamma$	$+3.8\cdot10^{-4}$	$+3.9\cdot10^{-4}$
$\mid q/p \mid$	$-4.0\cdot10^{-5}$	$-3.6\cdot10^{-5}$
$\frac{\mathrm{Re}\lambda_{CP}}{\lvert\lambda_{CP}\rvert}$Rez	—	$+2.2\cdot10^{-5}$
Imz	—	$+6.0\cdot10^{-4}$

Table 121: $J/\psi K_L^0$ specific systematics: effect of the removal of `Lepton` fractions correction due to tagging efficiency differences in sideband J/ψ events.

9.21.8 Reweighting of Monte Carlo events

According to Monte Carlo, the ratio of reconstructed $B^0 \to J/\psi K_L^0$ events reconstructed in the EMC compared to the IFR is 1.29 ± 0.03 (see [20]), while the fit to the entire data sample returns a value of 0.95 ± 0.07. This indicates that K_L^0 efficiencies are not correctly modeled in the detector. We correct for this difference reducing by a factor 0.74 Monte Carlo K_L^0 events in the EMC. We used the difference among standard fit and the one using the corrected Monte Carlo distribution to estimate the systematics contribution, as shown in table 122.

Parameter	Analysis 1	Analysis 2
$\Delta\Gamma/\Gamma$	$-3.0\cdot10^{-7}$	$-1.0\cdot10^{-7}$
$\mid q/p \mid$	$+10.0\cdot10^{-8}$	0.0
$\frac{\mathrm{Re}\lambda_{CP}}{\mid\lambda_{CP}\mid}$Rez	—	$-1.0\cdot10^{-7}$
Imz	—	$-6.0\cdot10^{-7}$

Table 122: $J/\psi K_L^0$ specific systematics: reweighting of Monte Carlo K_L^0 events in the EMC.

Systematics	$\Delta\Gamma/\Gamma$	$\mid q/p \mid$
η_{CP} of K^* bkg	$3.4\cdot10^{-5}$	$1.7\cdot10^{-6}$
η_{CP} of non itemized J/ψ bkg	$3.4\cdot10^{-4}$	$1.0\cdot10^{-6}$
η_{CP} non-J/ψ bkg	$1.0\cdot10^{-7}$	$1.0\cdot10^{-7}$
prompt fraction of non-J/ψ bkg	$8.5\cdot10^{-5}$	$1.2\cdot10^{-5}$
lifetime of non-J/ψ bkg	$2.9\cdot10^{-4}$	$1.3\cdot10^{-5}$
angular resolution	$9.7\cdot10^{-6}$	$1.3\cdot10^{-5}$
ΔE shape (shift)	$8.6\cdot10^{-5}$	$4.7\cdot10^{-6}$
ΔE shape (additional smearing)	$1.7\cdot10^{-4}$	$8.4\cdot10^{-6}$
Measured sample composition	$8.7\cdot10^{-4}$	$3.9\cdot10^{-5}$
Branching fraction: $J/\psi K^*$	$7.5\cdot10^{-6}$	$6.0\cdot10^{-7}$
Branching fraction: $J/\psi K_S$	$1.8\cdot10^{-5}$	$4.0\cdot10^{-7}$
Branching fraction: $J/\psi K_L\pi$	$1.5\cdot10^{-5}$	$1.3\cdot10^{-6}$
Branching fraction: $\chi_c K_L$	$5.6\cdot10^{-5}$	$3.1\cdot10^{-6}$
Branching fraction: $J/\psi X$ other	$7.5\cdot10^{-6}$	$6.0\cdot10^{-7}$
`Lepton` fraction correction	$3.8\cdot10^{-4}$	$4.0\cdot10^{-5}$
MC reweighting	$3.0\cdot10^{-7}$	$1.0\cdot10^{-7}$
Total	**0.0011**	**0.000061**

Table 123: Analysis 1 K_L^0 specific systematics summary.

9.22 Summary of systematic uncertainties

All the systematic uncertainties have been added in quadrature. When there is a positive and negative variation we always take the largest value. The final break-down of the systematic error for the two analyses is given in tables 125 and 126.

9.23 Setting limits procedure

The method used to estimate 90% two-side confidence intervals was the following. We first used toy Monte Carlo tunned to the parameters found in the data to determine whether the coverage given by a variation in the log-likelihood of $1.64^2/2 = 1.345$ was correct, and if it scales as 1.64 with the usual 68% intervals. To speed

Systematics	$\Delta\Gamma/\Gamma$	$\mid q/p \mid$	$\frac{\mathrm{Re}\lambda_{CP}}{\mid\lambda_{CP}\mid}$Rez	Imz
η_{CP} of K^* bkg	$2.4\cdot10^{-5}$	$1.4\cdot10^{-6}$	$3.8\cdot10^{-5}$	$3.5\cdot10^{-4}$
η_{CP} of non itemized J/ψ bkg	$2.9\cdot10^{-4}$	$1.0\cdot10^{-6}$	$8.1\cdot10^{-5}$	$8.3\cdot10^{-4}$
η_{CP} non-J/ψ bkg	$1.0\cdot10^{-7}$	$0.0\cdot10^{-7}$	$3.0\cdot10^{-7}$	$1.0\cdot10^{-7}$
prompt fraction of non-J/ψ bkg	$1.0\cdot10^{-4}$	$1.5\cdot10^{-5}$	$1.9\cdot10^{-5}$	$1.5\cdot10^{-4}$
lifetime of non-J/ψ bkg	$3.0\cdot10^{-4}$	$1.6\cdot10^{-5}$	$5.8\cdot10^{-5}$	$1.6\cdot10^{-5}$
angular resolution	$8.0\cdot10^{-7}$	$3.6\cdot10^{-6}$	$1.3\cdot10^{-4}$	$5.1\cdot10^{-4}$
ΔE shape (shift)	$8.5\cdot10^{-5}$	$5.5\cdot10^{-6}$	$1.3\cdot10^{-4}$	$4.5\cdot10^{-4}$
ΔE shape (additional smearing)	$1.6\cdot10^{-4}$	$8.4\cdot10^{-6}$	$1.8\cdot10^{-5}$	$4.5\cdot10^{-5}$
Measured sample composition	$9.1\cdot10^{-4}$	$4.1\cdot10^{-5}$	$7.0\cdot10^{-4}$	$2.2\cdot10^{-3}$
Branching fraction: $J/\psi K^*$	$6.1\cdot10^{-6}$	$1.0\cdot10^{-6}$	$5.2\cdot10^{-6}$	$1.4\cdot10^{-5}$
Branching fraction: $J/\psi K_S$	$3.6\cdot10^{-3}$	$1.8\cdot10^{-4}$	$3.4\cdot10^{-3}$	$1.9\cdot10^{-3}$
Branching fraction: $J/\psi K_L\pi$	$1.4\cdot10^{-5}$	$1.5\cdot10^{-6}$	$9.4\cdot10^{-6}$	$3.2\cdot10^{-5}$
Branching fraction: $\chi_c K_L$	$5.3\cdot10^{-5}$	$3.3\cdot10^{-6}$	$9.9\cdot10^{-6}$	$1.7\cdot10^{-5}$
Branching fraction: $J/\psi X$ other	$6.1\cdot10^{-6}$	$1.0\cdot10^{-6}$	$5.2\cdot10^{-6}$	$1.4\cdot10^{-5}$
`Lepton` fraction correction	$3.9\cdot10^{-4}$	$3.6\cdot10^{-5}$	$2.2\cdot10^{-5}$	$6.0\cdot10^{-4}$
MC reweighting	$1.0\cdot10^{-7}$	$0.0\cdot10^{-7}$	$1.0\cdot10^{-7}$	$6.0\cdot10^{-7}$
Total	**0.0038**	**0.00019**	**0.0035**	**0.0032**

Table 124: Analysis 2 K_L^0 specific systematics summary.

up the test, we used signal only fits and the total statistics of the B_{flav} sample was divided by a factor 2. From more than 300 experiments the 90% coverage was confirmed. Using these experiments we also compared the 90% asymmetric (MINOS) errors with the corresponding symmetric (Gaussian) errors, and the agreement was found to be satisfactory, within 10%, as for the 68% intervals. This was a new check of the Gaussian behavior of the statistical errors.

Second, we ran the nominal data fits with error calculation at 90% confidence level. The errors (Gaussian and asymmetric) were found to scale with the 68% errors as expected and confirmed above with the toy Monte Carlo experiments. Again, the Gaussian behavior is confirmed.

Third, we calculated possible multiplicative systematic errors by reevaluating the statistical errors at one sigma variation of different systematic sources. For each indivial contribution we evaluated the factor $f = 1-\sigma'/\sigma$, where σ' is the statistical error at the one sigma systematics variation while σ is the statistical error at central value (nominal fit configuration). The values obtained for all contributions studied are shown in tables 127 and 128, for Analysis 1 and Analysis 2 respectively. Conservatively, the total factor has been obtained using only negative contributions. As seen, there are no significant contributions. The largest contribution, due to the resolution function parameterization, is not indeed a multiplicative contribution since it is due to its difference in statistical error to the nominal model, accounting for the observed difference in central value. Conservatively we include it as multiplicative error. The 90% intervals are finally obtained adding in quadrature the 90% statistical error multiplied by the previous total multiplicative factor $(1+f)$ to the total additive systematic error multiplied by 1.64.

Systematics	$\Delta\Gamma/\Gamma$	$\mid q/p \mid$
Signal probability (B_{flav})	$7.9 \cdot 10^{-4}$	$2.2 \cdot 10^{-4}$
Signal probability ($B_{CPK^0_S}$)	$3.8 \cdot 10^{-3}$	$2.9 \cdot 10^{-4}$
m_{ES} endpoint	$2.3 \cdot 10^{-4}$	$4.9 \cdot 10^{-4}$
Resolut. function param.	$7.7 \cdot 10^{-3}$	$1.3 \cdot 10^{-3}$
Flat outlier component	$1.0 \cdot 10^{-3}$	$3.4 \cdot 10^{-4}$
$\sigma_{outlier}$ variation	$2.2 \cdot 10^{-3}$	$1.2 \cdot 10^{-4}$
$\delta_{outlier}$ variation	$1.1 \cdot 10^{-3}$	$3.6 \cdot 10^{-4}$
Beam spot position	$2.1 \cdot 10^{-3}$	$1.2 \cdot 10^{-3}$
Beam spot expansion	$6.5 \cdot 10^{-3}$	$9.3 \cdot 10^{-4}$
SVT alignment	$5.2 \cdot 10^{-3}$	$1.0 \cdot 10^{-3}$
z scale and boost	$2.9 \cdot 10^{-3}$	$6.0 \cdot 10^{-4}$
Average B^0 lifetime	$3.4 \cdot 10^{-3}$	$1.2 \cdot 10^{-3}$
Average B^+ lifetime	$1.2 \cdot 10^{-5}$	$< 10^{-6}$
B^+ mistag rates	$3.9 \cdot 10^{-6}$	$8.9 \cdot 10^{-6}$
Residual charge asymmetry (sig)	$5.6 \cdot 10^{-3}$	$5.9 \cdot 10^{-3}$
Residual charge asymmetry (comb bkg)	$3.1 \cdot 10^{-4}$	$9.9 \cdot 10^{-4}$
Fixed tagging efficiency	$1.7 \cdot 10^{-6}$	$8.9 \cdot 10^{-5}$
Direct CP violation	$1.7 \cdot 10^{-3}$	$4.3 \cdot 10^{-3}$
Doubly CKM suppressed decays systematics	$5.7 \cdot 10^{-3}$	$3.1 \cdot 10^{-3}$
PDF asymptotic normalization	$3.8 \cdot 10^{-4}$	$5.1 \cdot 10^{-5}$
Fitting procedure	$8.4 \cdot 10^{-3}$	$1.4 \cdot 10^{-3}$
MC statistics	$5.1 \cdot 10^{-3}$	$7.4 \cdot 10^{-3}$
Fraction of peaking bg (B_{flav})	$4.4 \cdot 10^{-5}$	$5.8 \cdot 10^{-5}$
Fraction of peaking bg ($B_{CPK^0_S}$)	$2.2 \cdot 10^{-4}$	$9.8 \cdot 10^{-6}$
CP content of peaking bg	$4.9 \cdot 10^{-5}$	$5.6 \cdot 10^{-6}$
B^0 peaking background	$5.1 \cdot 10^{-6}$	$1.2 \cdot 10^{-4}$
Δt structure in combinatorial background	$1.7 \cdot 10^{-3}$	$5.4 \cdot 10^{-4}$
$\Delta\Gamma$/CP/T/Mixing/DCKM content in combinatorial bkg	$4.0 \cdot 10^{-3}$	$2.2 \cdot 10^{-3}$
K^0_L specific systematics	$1.1 \cdot 10^{-3}$	$6.1 \cdot 10^{-5}$
Total	**0.019**	**0.011**

Table 125: Analysis 1 systematics break-down.

10 Summary

We described in this document that from a precision analysis of the time evolution of the decay of $B^0_d\bar{B}^0_d$ mesons we can provide the first measurement of the width difference $\Delta\Gamma$ between the B^0_d mass eigenstates

Systematics	$\Delta\Gamma/\Gamma$	$\mid q/p \mid$	$\frac{\mathrm{Re}\lambda_{CP}}{\lvert\lambda_{CP}\rvert}$Rez	Imz
Signal probability (B_{flav})	$8.2\cdot10^{-4}$	$2.2\cdot10^{-4}$	$4.5\cdot10^{-4}$	$2.6\cdot10^{-4}$
Signal probability ($B_{CPK^0_S}$)	$3.5\cdot10^{-3}$	$3.3\cdot10^{-4}$	$1.9\cdot10^{-3}$	$6.5\cdot10^{-4}$
m_{ES} endpoint	$4.3\cdot10^{-4}$	$4.9\cdot10^{-4}$	$1.9\cdot10^{-3}$	$4.2\cdot10^{-5}$
Resolut. function param.	$7.3\cdot10^{-3}$	$1.1\cdot10^{-3}$	$8.0\cdot10^{-3}$	$3.2\cdot10^{-3}$
Flat outlier component	$1.1\cdot10^{-3}$	$3.4\cdot10^{-4}$	$3.8\cdot10^{-5}$	$6.4\cdot10^{-5}$
$\sigma_{outlier}$ variation	$1.9\cdot10^{-3}$	$2.0\cdot10^{-4}$	$7.4\cdot10^{-4}$	$2.1\cdot10^{-4}$
$\delta_{outlier}$ variation	$1.2\cdot10^{-3}$	$3.6\cdot10^{-4}$	$1.1\cdot10^{-4}$	$1.6\cdot10^{-4}$
Beam spot position	$2.2\cdot10^{-3}$	$1.2\cdot10^{-3}$	$1.0\cdot10^{-3}$	$1.1\cdot10^{-2}$
Beam spot expansion	$7.3\cdot10^{-3}$	$8.8\cdot10^{-4}$	$4.1\cdot10^{-4}$	$1.7\cdot10^{-3}$
SVT alignment	$6.1\cdot10^{-3}$	$1.2\cdot10^{-3}$	$1.4\cdot10^{-3}$	$1.1\cdot10^{-2}$
z scale and boost	$3.2\cdot10^{-3}$	$6.2\cdot10^{-4}$	$1.5\cdot10^{-3}$	$2.4\cdot10^{-4}$
Average B^0 lifetime	$3.6\cdot10^{-3}$	$1.2\cdot10^{-3}$	$3.6\cdot10^{-3}$	$4.2\cdot10^{-4}$
Average B^+ lifetime	$2.0\cdot10^{-5}$	$1.3\cdot10^{-6}$	$5.2\cdot10^{-5}$	$2.2\cdot10^{-5}$
B^+ mistag rates	$1.4\cdot10^{-5}$	$7.2\cdot10^{-6}$	$1.3\cdot10^{-4}$	$3.5\cdot10^{-6}$
Residual charge asymmetry (sig)	$5.0\cdot10^{-3}$	$5.8\cdot10^{-3}$	$3.9\cdot10^{-3}$	$5.9\cdot10^{-3}$
Residual charge asymmetry (comb bkg)	$3.1\cdot10^{-4}$	$9.9\cdot10^{-4}$	$4.2\cdot10^{-5}$	$7.9\cdot10^{-5}$
Fixed tagging efficiency	$1.4\cdot10^{-6}$	$8.9\cdot10^{-5}$	$6.2\cdot10^{-7}$	$1.9\cdot10^{-6}$
Direct CP violation	$1.8\cdot10^{-3}$	$4.3\cdot10^{-3}$	$6.8\cdot10^{-4}$	$2.7\cdot10^{-3}$
Doubly CKM suppressed decays systematics	$7.7\cdot10^{-3}$	$3.5\cdot10^{-3}$	$3.2\cdot10^{-2}$	$6.2\cdot10^{-3}$
PDF asympotic normalization	$4.1\cdot10^{-4}$	$5.2\cdot10^{-5}$	$5.8\cdot10^{-5}$	$1.3\cdot10^{-4}$
Fitting procedure	$3.1\cdot10^{-3}$	$7.3\cdot10^{-4}$	$2.8\cdot10^{-3}$	$2.9\cdot10^{-3}$
MC statistics	$5.1\cdot10^{-3}$	$7.4\cdot10^{-3}$	$3.8\cdot10^{-3}$	$1.6\cdot10^{-2}$
Fraction of peaking bg (B_{flav})	$5.3\cdot10^{-5}$	$7.0\cdot10^{-5}$	$1.3\cdot10^{-3}$	$1.3\cdot10^{-4}$
Fraction of peaking bg ($B_{CPK^0_S}$)	$1.9\cdot10^{-4}$	$1.6\cdot10^{-5}$	$5.6\cdot10^{-4}$	$5.7\cdot10^{-5}$
CP content of peaking bg	$3.1\cdot10^{-5}$	$9.2\cdot10^{-6}$	$1.9\cdot10^{-4}$	$1.8\cdot10^{-4}$
B^0 peaking background	$2.9\cdot10^{-4}$	$1.8\cdot10^{-4}$	$3.5\cdot10^{-3}$	$1.9\cdot10^{-4}$
Δt structure in combinatorial background	$1.8\cdot10^{-3}$	$5.3\cdot10^{-4}$	$1.1\cdot10^{-3}$	$5.1\cdot10^{-4}$
$\Delta\Gamma$/CP/T/Mixing/DCKM content in combinatorial bkg	$1.4\cdot10^{-3}$	$1.7\cdot10^{-3}$	$1.5\cdot10^{-3}$	$2.6\cdot10^{-4}$
K^0_L specific systematics	$3.8\cdot10^{-3}$	$1.9\cdot10^{-4}$	$3.5\cdot10^{-3}$	$3.2\cdot10^{-3}$
Total	**0.018**	**0.011**	**0.034**	**0.025**

Table 126: Analysis 2 systematics break-down.

together with a stringent test of the CPT invariance in the neutral B^0_d meson system, the first to date sensitive to both the dispersive and the absortive parts of the effective Hamiltonian of evolution. The analysis provides also a competitive test of T violation in mixing based on fully hadronic events, complementary to the standard dilepton approach. All these measurements provide a new way for exploring new physics.

Systematics	$1-\frac{\sigma'}{\sigma}$ factor $\Delta\Gamma/\Gamma$	$\mid q/p \mid$
Resolut. function param.	-0.12	-0.0049
Flat outlier component	-0.015	-0.0013
$\sigma_{outlier}$ variation	-0.089	-0.00078
$\delta_{outlier}$ variation	-0.029	0.092
Beam spot position	0.0012	-0.0036
Beam spot expansion	-0.049	-0.0022
z scale and boost	-0.030	-0.0074
Average B^0 lifetime	-0.056	-0.012
Average B^+ lifetime	0.00080	-0.00012
B^+ mistag rates	0.00037	-0.00020
Direct CP violation	-0.0026	-0.0044
Doubly CKM suppressed decays systematics	0.022	-0.018
PDF asymptotic normalization	0.014	$9.4\cdot10^{-5}$
Total	0.173	0.024

Table 127: Scaling factor of multiplicative systematic errors, Analysis 1.

Systematics	$1-\frac{\sigma'}{\sigma}$ factor $\Delta\Gamma/\Gamma$	$\mid q/p \mid$	$\frac{\mathrm{Re}\lambda_{CP}}{\lvert\lambda_{CP}\rvert}$Rez	Imz
Resolut. function param.	-0.15	-0.0065	-0.15	0.021
Flat outlier component	-0.013	-0.0013	-0.020	$-7.5\cdot10^{-5}$
$\sigma_{outlier}$ variation	-0.0038	$-9.4\cdot10^{-5}$	0.0020	$8.2\cdot10^{-5}$
$\delta_{outlier}$ variation	-0.030	0.090	0.0050	0.073
Beam spot position	-0.0011	-0.0023	0.057	-0.010
Beam spot expansion	-0.011	-0.0020	-0.039	-0.013
z scale and boost	-0.031	-0.0073	0.025	-0.00091
Average B^0 lifetime	-0.057	-0.013	-0.053	-0.080
Average B^+ lifetime	0.00084	-0.00011	-0.0013	-0.00028
B^+ mistag rates	0.00039	-0.00020	-0.0037	0.0013
Direct CP violation	-0.0026	-0.0043	-0.0077	0.0024
DCKM suppressed decays	0.0077	-0.018	0.062	0.021
PDF asympotic normalization	0.013	$9.4\cdot10^{-5}$	0.0022	$-2.7\cdot10^{-5}$
Total	0.167	0.025	0.167	0.082

Table 128: Scaling factor ultiplicative systematic errors, Analysis 2.

The analysis uses 81 fb^{-1} of *BABAR* data collected from 1999 to 2002, selecting samples of $B^0\to J/\psi$(or

$\psi(2S)$, χ_{c1}) K^0_Sdecays ($\eta_{CP}=-1$), $B^0\to J/\psi K^0_L(\eta_{CP}=+1)$ and $B^0\to D^{(*)}\pi(\rho,a_1)$ and $B^0\to J/\psi K^{*0}$(flavor eigenstates). One B meson is fully reconstructed while in the opposite B inclusive methods are used to identify the flavor and reconstruct the decay vertex.

A global unbinned maximum likelihood fit to the tagged and untagged time distributions of the CP and flavor eigenstate samples is performed (58 free parameters in total). All the oscillation and CPT/CP/T violation parameters (6 in total) are floated simultaneously (**Analysis 2**), while the average B^0_d lifetime is fixed to its world average. The *BABAR* standard $\{\mid q/p \mid,\lambda\}$ phase-convention independent formalism has been generalized to allow for CPT violation and non-zero $\Delta\Gamma$ values. The choice of 6 independent phase-convention independent parameters is:

- Re$z\frac{\mathrm{Re}\lambda_{CP}}{|\lambda_{CP}|}$ and Imz, which parameterize CPT violation. Rez is primarily connected to the dispersive (δM) part of the Hamiltonian, while Imz is porportional to the absortive ($\delta\Gamma$) part, so the measurement of Rez is in principle more interesting than Imz. As the CPT asymmetries turn out to be proportional to Re$z\frac{\mathrm{Re}\lambda_{CP}}{|\lambda_{CP}|}$, this is the parameter which is actually measured. This also removes sign ambiguities;
- $\frac{\mathrm{Im}\lambda_{CP}}{|\lambda_{CP}|}$ and $\mid q/p \mid$, the standard CP/T violation parameters;
- $sign(\frac{\mathrm{Re}\lambda_{CP}}{|\lambda_{CP}|})\Delta\Gamma/\Gamma$. The product of $\Delta\Gamma/\Gamma$ by $sign(\frac{\mathrm{Re}\lambda_{CP}}{|\lambda_{CP}|})$ is needed to remove discrete symmetries (the same as for Rez);
- Δm, the well-know mixing frequency parameter.

Although Δm and $\frac{\mathrm{Im}\lambda_{CP}}{|\lambda_{CP}|}$ are floated in the nominal fit, they are used as cross-check with other analyses, as well as τ_B when it is floated as a cross-check.

The combined use of flavor and CP samples provides maximal sensitivity to all the physics parameters, with small correlations, since they are determined either from different samples, or from different Δt dependencies:

- the $\Delta\Gamma$ dependence for flavor eigenstates appears to be at second order in $\Delta\Gamma$, while it is to first order for CP eigenstates. This implies that the estimation of $\Delta\Gamma$ is dominated, for small values of $\Delta\Gamma$, by the CP sample;
- the dependence with Rez (even in Δt) is suppressed by terms linear in $\Delta\Gamma$ for flavor eigenstates. This implies, again, that for small values of $\Delta\Gamma$ and in the presence of CP violation, the CP eigenstate sample largely dominates the determination of Rez;
- the dependence with $\mathrm{Im}\lambda_{CP}$ (CP eigenstates) appears to be odd in Δt, and therefore can be resolved from the even dependence with Rez;
- the determination of $\mid q/p \mid$, Imz and Δm is dominated by the high statistics flavor sample due to the absence of suppression factors.

Results have been also provided with Rez and Imz fixed to zero, i.e. under the assumption that CPT is conserved (**Analysis 1**).

Many experimental effects have been accounted for:

- Δt limited resolution. We use two different resolution models to parameterize the core and tail Δt distributions: a two Gaussians model (GG) and a Gaussian plus the same Gaussian convoluted with an

exponential. An additional Gaussian is added to model outliers. The GG model is adopted for the nominal fit configuration, while the GExp approach is used to assign systematics from resolution model parameterization;

- mistag rates and their correlation with the reconstructed Δt error as well as $B^0\bar{B}^0$ differences in the mistags;
- $B^0\bar{B}^0$ differences in reconstruction and tagging efficiencies due to a different answer of the detector to positive and negative particles (ν and μ^α parameters). A key tool to extract these asymmetries together with the physics parameters (mainly $|\,q/p\,|$) is the time-integrated information contained in the untagged events. This analysis makes use of untagged events in a fully time-dependent approach, providing also additional sensitivity to the determination of $\Delta\Gamma/\Gamma$;
- backgrounds. A total of 22 background parameters are floated in the nominal fit (section 6), while many other are fixed either from prior fits to the data (mistags rates and detector charge asymmetries of B^+ background, event-by-event signal probability, etc) or from Monte Carlo studies (peaking background fractions, $B_{CPK^0_L}$ background composition, etc), therefore contributing to the systematic uncertainty.

One of the most delicate effects that this analysis revealed for the first time was the non-negligible impact from the assumption that the flavor eigenstate B's as well as the tagging B's are perfect tagging states. Doubly-CKM-Suppressed decays make this assumption not good enough. The complete and consistent treatment requires the introduction of a set of ratios of decay amplitudes between the supressed and the favored processes (with magnitude and phases), for the reconstructed (flavor eigenstate sample) and tagging sides, and for B^0 and $\bar{B}^0$ flavors. Many studies studies, discussed in section 2.10 and appendix B, suggested that the most convenient approach to deal with this competing effect is:

- consider one "effective" channel for the tagging and reconstructed sides. Effects due to more than one channel were proven to be always smaller than or equal to the single channel case;
- fix the magnitude of the ratio of decay amplitudes to 0.02 (neglecting corrections from decay constants), assuming a 100% uncertainty on this number, as discussed in section 9.12;
- fix the real parts of the phases to zero. A systematics is evaluated from the scan to all possible values (see section 9.12);
- fit for the imaginary parts of the phases, separately for flavor and tagging sides, and for B^0 and $\bar{B}^0$.

The Doubly-CKM-Suppressed decays effects are finally dominated by the tagging B, and are the main source of systematic uncertainty for $\mathrm{Re}z\frac{\mathrm{Re}\lambda_{CP}}{|\lambda_{CP}|}$, while for the other parameters the effect is small.

A long list of systematic uncertainties was considered (section 9), as well as cross-checks to verify the robustness and stability of the whole analysis chain, using data and full and toy Monte Carlo samples (section 8). The final results are:

- Analysis 2 results (unblind):

$$\Delta\Gamma/\Gamma = 0.008 \pm 0.037(\mathrm{stat}) \pm 0.018(\mathrm{syst})$$
$$|\,q/p\,| = 1.029 \pm 0.013(\mathrm{stat}) \pm 0.011(\mathrm{syst})$$

$$\frac{\mathrm{Re}\lambda_{CP}}{|\,\lambda_{CP}\,|}\mathrm{Re}z = 0.014 \pm 0.035(\mathrm{stat}) \pm 0.034(\mathrm{syst})$$
$$\mathrm{Im}z = 0.038 \pm 0.029(\mathrm{stat}) \pm 0.025(\mathrm{syst})$$

- Analysis 1 results (unblind):

$$\Delta\Gamma/\Gamma = 0.009^{+0.036}_{-0.037}(\mathrm{stat}) \pm 0.019(\mathrm{syst})$$
$$|\,q/p\,| = 1.029 \pm 0.013(\mathrm{stat}) \pm 0.011(\mathrm{syst})$$

where the first error is statistical and the second systematics. Tables 125 and 126 show the break-down of the systematic error. The parameters Δm, $\frac{\mathrm{Im}\lambda_{CP}}{|\lambda_{CP}|}$ and τ_B are reported as well, and are used as cross-check with other analyses. With the GG nominal resolution model the results are:

- Analysis 2 checks (unblind):

$$\Delta m = 0.5254 \pm 0.0076(\mathrm{stat})$$
$$\frac{\mathrm{Im}\lambda_{CP}}{|\,\lambda_{CP}\,|} = 0.762^{+0.065}_{-0.067}(\mathrm{stat})$$
$$\tau_B = 1.518 \pm 0.016(\mathrm{stat})$$

- Analysis 1 checks (unblind):

$$\Delta m = 0.5253 \pm 0.0076(\mathrm{stat})$$
$$\frac{\mathrm{Im}\lambda_{CP}}{|\,\lambda_{CP}\,|} = 0.750^{+0.066}_{-0.067}(\mathrm{stat})$$
$$\tau_B = 1.518 \pm 0.016(\mathrm{stat})$$

while with the alternative GExp parameterization we obtain:

- Analysis 2 checks (unblind):

$$\Delta m = 0.5201 \pm 0.0076(\mathrm{stat})$$
$$\frac{\mathrm{Im}\lambda_{CP}}{|\,\lambda_{CP}\,|} = 0.763 \pm 0.065(\mathrm{stat})$$
$$\tau_B = 1.531 \pm 0.015(\mathrm{stat})$$

- Analysis 1 checks (unblind):

$$\Delta m = 0.5198 \pm 0.0076(\mathrm{stat})$$
$$\frac{\mathrm{Im}\lambda_{CP}}{|\,\lambda_{CP}\,|} = 0.750 \pm 0.065(\mathrm{stat})$$
$$\tau_B = 1.531 \pm 0.014(\mathrm{stat})\ .$$

The cross-check results above deserve several remarks. The value obtained for Δm is consistent with the *BABAR* hadronic mixing measurement [23] and the 2003 world average [24]. The MC bias correction, -0.0095 ± 0.0038 for the *GG* model (table 40) and -0.0046 ± 0.0038 for the *GExp* model (table 41), has not been yet applied to the above Δm results. The difference between the *GG* and *GExp* resolution models for Δm (0.7σ statistical) and τ_B (0.8σ statistical) is due to the correlation of Δm with τ_B (-30%) and the slightly biased estimation of τ_B (towards low values) with the *GG* model, as discussed in section 8.1. Note the negligible change of Δm and τ_B between Analysis 2 and Analysis 1. The value of $\frac{\mathrm{Im}\lambda_{CP}}{|\lambda_{CP}|}$ above is consistent(inconsistent) with the value obtained from mixing/sin2β only fits (section 8.3), which agree perfectly with the standard sin2β analysis results [9].

To first order in the CPT parameter δ and the T violation in mixing parameter $\mathrm{Re}\epsilon$, we can alternatively provide the above results in the $\{\varepsilon, \delta\}$ formalism, using the relations shown in section 2.4:

- Analysis 1 results (blind):

$$\frac{\mathrm{Re}\varepsilon}{1+|\,\varepsilon\,|^2} = -0.014 \pm 0.007(\mathrm{stat}) \pm 0.006(\mathrm{syst})$$

- Analysis 1 checks (blind):

$$\frac{\mathrm{Im}\varepsilon}{1+|\,\varepsilon\,|^2} = -0.375 \pm 0.034(\mathrm{stat})$$

- Analysis 2 results (blind):

$$\frac{\mathrm{Re}\varepsilon}{1+|\,\varepsilon\,|^2} = -0.014 \pm 0.007(\mathrm{stat}) \pm 0.006(\mathrm{syst})$$

$$\frac{1-|\,\varepsilon\,|^2}{1+|\,\varepsilon\,|^2}\frac{\mathrm{Re}\delta}{1+|\,\varepsilon\,|^2} = 0.014 \pm 0.035(\mathrm{stat}) \pm 0.034(\mathrm{syst})$$

$$\frac{\mathrm{Im}\delta}{1+|\,\varepsilon\,|^2} = 0.038 \pm 0.029(\mathrm{stat}) \pm 0.025(\mathrm{syst})$$

- Analysis 2 checks (blind):

$$\frac{\mathrm{Im}\varepsilon}{1+|\,\varepsilon\,|^2} = -0.381 \pm 0.033(\mathrm{stat})$$

The 90% confidence intervals are:

$$\begin{aligned} sign(\mathrm{Re}\lambda_{CP})\Delta\Gamma/\Gamma &: [-0.068, 0.084] \\ |\,q/p\,| &: [1.001, 1.057] \\ \frac{\mathrm{Re}\lambda_{CP}}{|\,\lambda_{CP}\,|}\mathrm{Re}z &: [-0.072, 0.101] \\ \mathrm{Im}z &: [-0.028, 0.104] \end{aligned}$$

for Analysis 2, and

$$\begin{aligned} sign(\mathrm{Re}\lambda_{CP})\Delta\Gamma/\Gamma &: [-0.069, 0.087] \\ |\,q/p\,| &: [1.001, 1.057] \end{aligned}$$

for Analysis 1.

Acknowledgments

We want to thank David Kirkby and Bob Cahn for their unvaluable help to make this analysis possible, and Pat Burchat and Gerhard Raven for their advice in many issues. We are indeed grateful to the $\sin 2\beta$ AWG for providing the data sample. Special thanks to Bryam Dahmes for his help with the $J/\psi K_L^0$ systematics.

A Do UnTagged events matter?

The use of untagged events in the definition of the log-likelihood function, equations (113) and (114), provides fundamental advantages which are discussed in the following:

- allows the extraction of the detector charge asymmetries simultaneously with the physics asymmetries;
- provides additional sensitivity to the determination of $\Delta\Gamma/\Gamma$;
- improves the resolution function determination.

A.1 Detector charge asymmetries

Following the discussion in sections 2.5, 2.7 and 2.8 it becomes apparent that due to the normalization (108) and (109) and the definitions (91), T^{α} for tagged events ($\alpha = \alpha_{Tagged}$) is an overall normalization factor, irrelevant for any time-dependent analysis. However, if untagged events are also considered in the definition of the global log-likelihood function, the closure relations (96) and (97) provide additional information (the sum of the tagging efficiencies for all tagging categories determines the untagging efficiency). Any time-dependent analysis neglecting untagged events will therefore lose this information. The question may be how to incorporate the information borrowed by the untagged events, provided that the likelihood function is correctly defined (i.e. if it leads asymptotically to the correct result). Clearly, the most suitable definition is the one providing the smaller variance. It is expected that the smaller variance will be provided by a fully time-dependent analysis. This is the approach discussed in the above sections, implicit in equations (113) and (114) with $\alpha = \alpha_{Tagged}, \alpha_{UnTagged}$, and is the one used in this analysis (will be referred thereafter as **All Events method**).

Toy Monte Carlo studies were performed to check the ability of this method to extract simultaneously physics and detector charge asymmetries. The samples consisted of about 250 experiments with an statistics equivalent to about 80 fb^{-1} each, with perfect Δt resolution but mistags similar as those observed in the data. The relative populations of flavor and CP events was kept the same as observed in the data. Tagging-vertexing correlations and $B^0\bar{B}^0$ differences in reconstruction and tagging efficiencies were neglected here (not needed given we are assuming perfect resolution). We assumed no direct CP violation effects, $r_{CP,CP} = r_{CP,flav} = r_{CP,tag} = 1$. The CP phase θ_{CP} was generated to be 0.85 rad (which corresponds to $\frac{\mathrm{Im}\lambda_{CP}}{|\lambda_{CP}|}$=0.75). z and $|\,q/p\,|$ were assumed to be 0 and 1, respectively. DCKM effects were also included in the generation: the DCKM phases taken for this particular exercise were $3\pi/2$ for B^0 and $\pi/2$ for $\bar{B}^0$(for both reconstructed and tagging sides), and r_{flav}, r_{tag} were assumed to be 0.02. The samples were generated with large detector charge asymmetries: $\nu = 4\%$, $\mu^{\alpha} = 2\%, 3\%, 4\%, 4\%$ ($\alpha = \alpha_{Tagged}$). The samples were then fitted using the All Events method, fixing the tagging efficiencies $T^{\alpha_{Tagged}}$ to the values estimated from simple counting. CP untagged events were not used here (see section A.2 for a discussion about the advantages of using these events). The DCKM fitting configuration was the reference fit configuration described in appendix B. The mean residuals and Gaussian errors returned by the fits for the CPT/CPT/T/oscillation parameters are shown in figure 59. Note the slightly larger RMS values compared to the mean errors for $\Delta\Gamma/\Gamma$ and Rez (discrepancy at 15% level), as already reported in earlier studies [12], reflecting the presence of small non-Gaussian effects. The same distributions for the ν, μ^{α} parameters are shown in figure 60. We observe that we have unbiased estimates for all the parameters, and all them behave well. As an additional check, the fits were repeated using a largely different starting point (especially for $|\,q/p\,|$ and ν, μ^{α}), obtaining the same solution in all cases, up to numerical precision. Figure 61 shows the scatter and correlation coefficient distributions among $|\,q/p\,|$ and ν and μ^{Cat1}: the average correlation of $|\,q/p\,|$ with ν is about 53%, while it is about 12% with μ^{Cat1}.

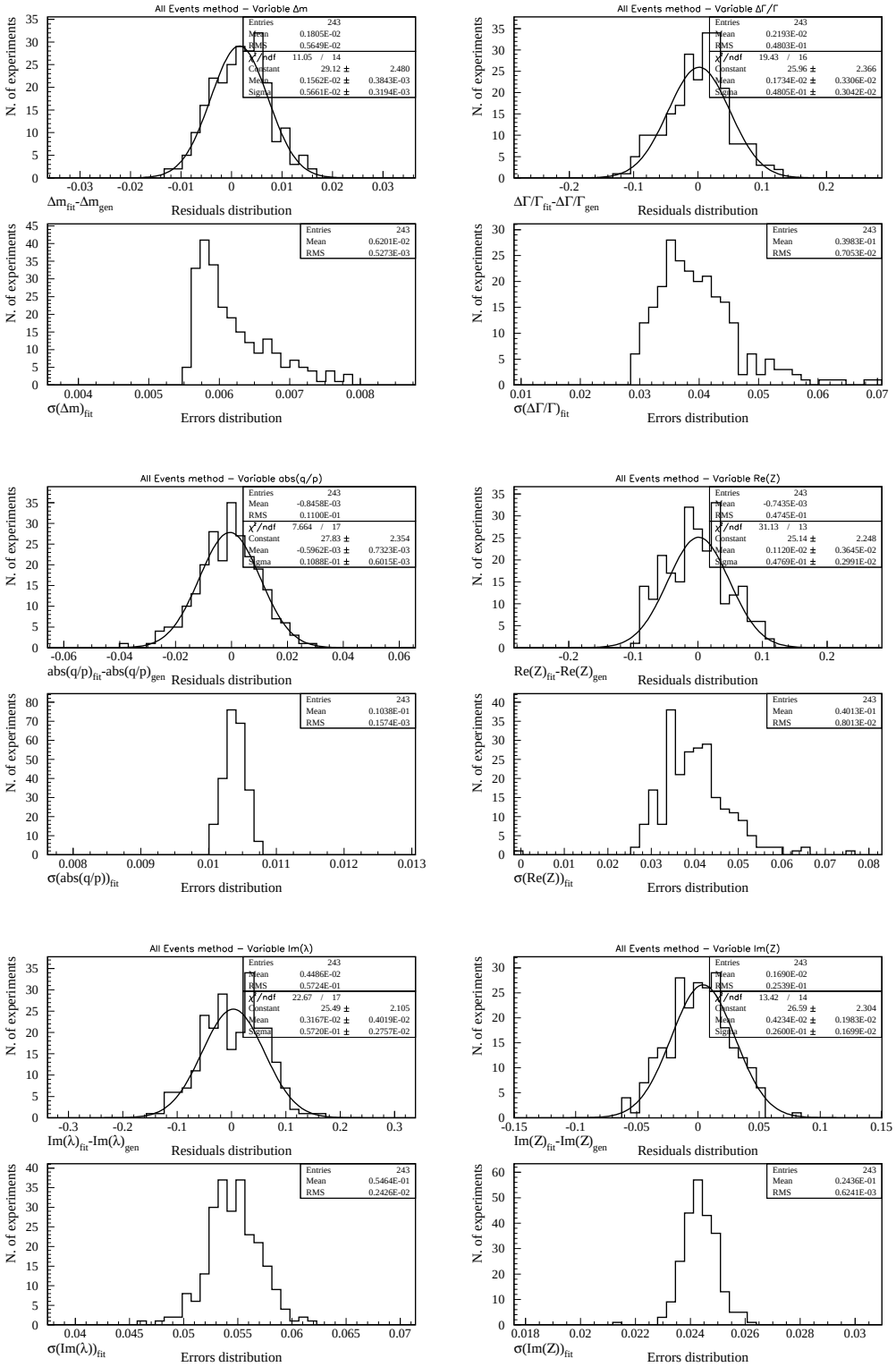

Figure 59: The residual and error (Gaussian) distributions for the CPT/CPT/T/oscillation parameters from the All Events method. The generated detector asymmetries were $\nu = 4\%$, $\mu^{\alpha} = 2\%, 3\%, 4\%, 4\%$.

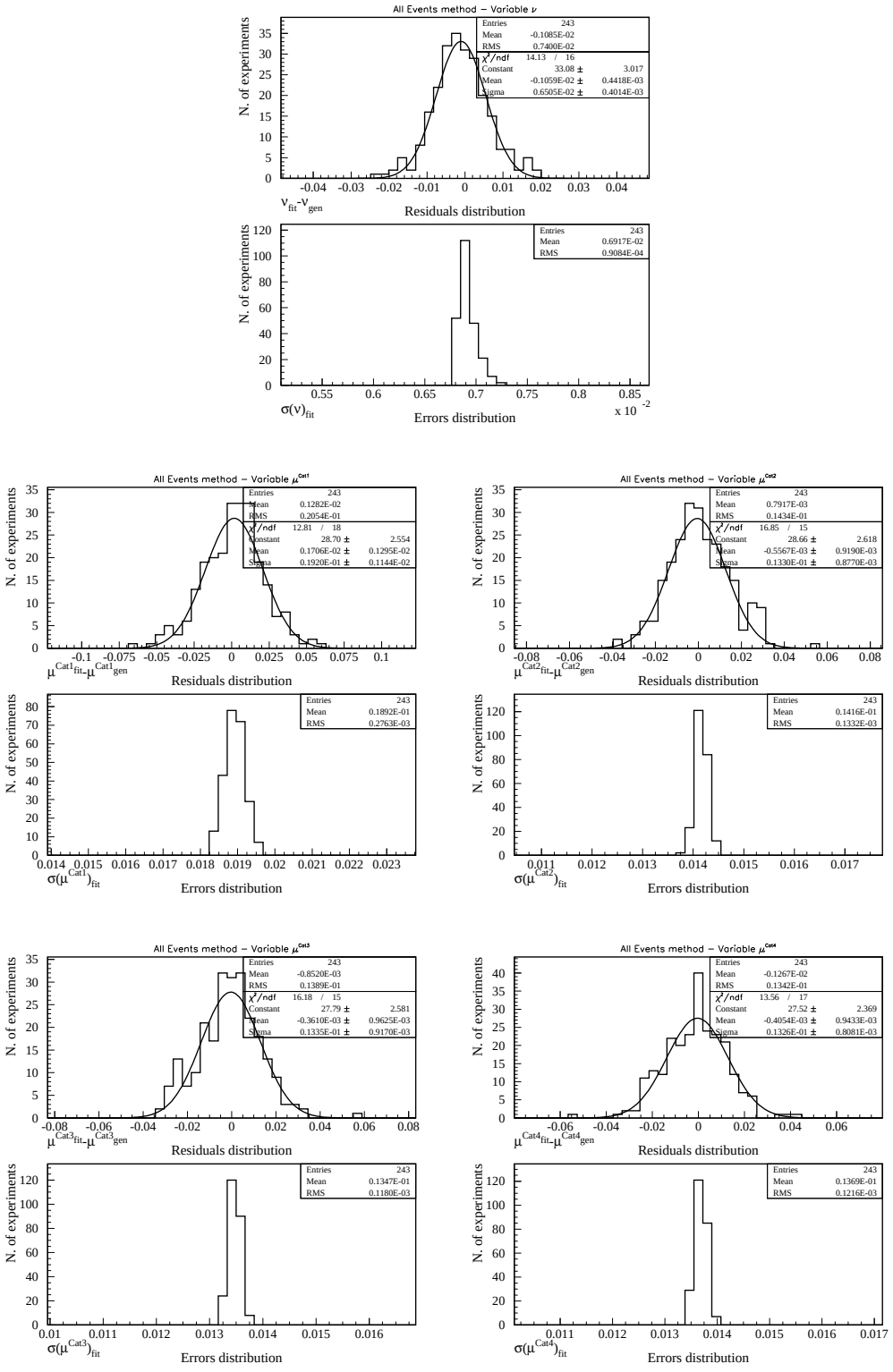

Figure 60: The residual and error (Gaussian) distributions for $B^0\bar{B}^0$ differences in reconstruction and tagging efficiencies (ν, μ^α parameters) from the All Events method. The generated values were $\nu = 4\%$, $\mu^\alpha = 2\%, 3\%, 4\%, 4\%$.

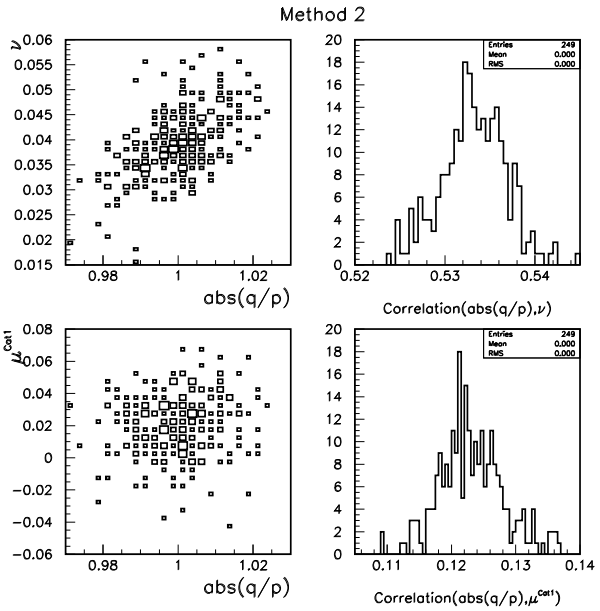

Figure 61: Scatter (left) and correlation coefficient (right) distributions among $\mid q/p \mid$ and ν (top) and μ^{Cat1} (bottom) from the All Events method. The generated detector asymmetries were $\nu = 4\%$, $\mu^{\alpha} = 2\%, 3\%, 4\%, 4\%$.

Excluding untagged events in the log-likehood function ($\alpha = \alpha_{Tagged}$ only) implies that the time-dependent analysis is insensitive to the absolute tagging and untagged rates, i.e. we are using only the shape (there is still sensitivity to the relative $B^0\bar{B}^0$and mixed/unmixed time-integrated rates within each tagging category). Intuitively, the information lost from the number of events in each category may be critical to the extraction of the $B^0\bar{B}^0$ asymmetries due to a different answer of the detector to positive and negative particles (μ^{α} and ν parameters) and any physics asymmetry parameter which sensitivity comes exclusively or mainly from $B^0\bar{B}^0$ time-integrated differences (i.e. the information is not in the time-distribution itself), like $\mid q/p \mid$. The impossibility to perform a combined determination of μ^{α}, ν and $\mid q/p \mid$ in absence of untagged events has been proven analytically in [37] (with some simplifications). The same toy Monte Carlo samples described above were used to evaluate numerically the impact of neglecting untagged events (**Tagged only method**). The mean residuals and Gaussian errors returned by the fits for the CPT/CPT/T/oscillation parameters are shown in figure 62. The same distribution for the ν, μ^{α} parameters are shown in figure 63. We observe again that we have unbiased estimates for all the parameters, and all them behave well. However, the errors on $\mid q/p \mid$ and the detector charge asymmetries parameters (ν, μ^{α}) are much larger than with the All Events method, $\sim 5\%$ compared to $\sim 1\%$, and the correlation between $\mid q/p \mid$ and ν, μ^{α} is very large, as seen in figure 64: the mean correlation of $\mid q/p \mid$ with ν is about 97%, and about 90% with μ^{Cat1}. The obvious question arising from these numerical results is why the correlation is very large but not 100%, as shown analytically in [37]. The reason of this small uncoupling is due to the fact that CP events are used together with the flavor eigenstates, and in spite of its small relative statistics, the relative amount of B^0 and $\bar{B}^0$ CP tagged events is sensitivite to $\mid q/p \mid$. In other words, the precision with which $\mid q/p \mid$ is measured in absence of untagged events comes exclusively from the CP sample. Having measured $\mid q/p \mid$ from the CP events (although with a large error) then an estimate of ν, μ^{α} can be extracted from the flavor eigenstates, although their precision is dominated by the large $\mid q/p \mid$ error. This feature was verified numerically by fitting the same toy Monte Carlo samples but now using only flavor eigenstates and fixing the parameters dominated by CP events to the generated values: $\Delta\Gamma/\Gamma$, $\frac{\mathrm{Im}\lambda_{CP}}{|\lambda_{CP}|}$ and Rez. Most of the fits failed and when they returned a converged fit with a positive-definite error matrix, the error on $\mid q/p \mid$ and ν, μ^{α} was huge, larger than two units, demostrating the non-regularity of the Hessian matrix, as

discussed in [37].

An alternative approach to extract the differences in tagging and reconstruction efficiencies together with $\mid q/p \mid$ is to use explicitely B_{flav} time-integrated rates (**Alternative method**). Historically this was the first approach used in this analysis [12], which was a generalization, to account for non-zero values of $\Delta\Gamma$, CP and CPT violation, of the former work originally proposed in [16]. We describe in the following the method.

Integrating over $-\infty < \Delta t < +\infty$ equation (93) for the most general case, we obtain ($\alpha = \alpha_{Tagged}$):

$$
\begin{aligned}
H^{\alpha}_{B^0_{tag}B^0_{flav}} &= (1+\nu)\Big\{(1+\mu^{\alpha})T^{\alpha}(1-w^{\alpha}-\Delta w^{\alpha}/2)H_{B^0_{tag}B^0_{flav}} + \\
&\quad (1-\mu^{\alpha})T^{\alpha}(w^{\alpha}-\Delta w^{\alpha}/2)H_{\overline{B}^0_{tag}B^0_{flav}}\Big\} \\
H^{\alpha}_{B^0_{tag}\overline{B}^0_{flav}} &= (1-\nu)\Big\{(1+\mu^{\alpha})T^{\alpha}(1-w^{\alpha}-\Delta w^{\alpha}/2)H_{B^0_{tag}\overline{B}^0_{flav}} + \\
&\quad (1-\mu^{\alpha})T^{\alpha}(w^{\alpha}-\Delta w^{\alpha}/2)H_{\overline{B}^0_{tag}\overline{B}^0_{flav}}\Big\} \\
H^{\alpha}_{\overline{B}^0_{tag}B^0_{flav}} &= (1+\nu)\Big\{(1-\mu^{\alpha})T^{\alpha}(1-w^{\alpha}+\Delta w^{\alpha}/2)H_{\overline{B}^0_{tag}B^0_{flav}} + \\
&\quad (1+\mu^{\alpha})T^{\alpha}(w^{\alpha}+\Delta w^{\alpha}/2)H_{B^0_{tag}B^0_{flav}}\Big\} \\
H^{\alpha}_{\overline{B}^0_{tag}\overline{B}^0_{flav}} &= (1-\nu)\Big\{(1-\mu^{\alpha})T^{\alpha}(1-w^{\alpha}+\Delta w^{\alpha}/2)H_{\overline{B}^0_{tag}\overline{B}^0_{flav}} + \\
&\quad (1+\mu^{\alpha})T^{\alpha}(w^{\alpha}+\Delta w^{\alpha}/2)H_{B^0_{tag}\overline{B}^0_{flav}}\Big\} \\
H^{\alpha}_{no\ tag B^0_{flav}} &= (1+\nu)\Big\{[1-T^{\alpha}(1+\mu^{\alpha})]H_{B^0_{tag}B^0_{flav}} + \\
&\quad [1-T^{\alpha}(1-\mu^{\alpha})]H_{\overline{B}^0_{tag}B^0_{flav}}\Big\} \\
H^{\alpha}_{no\ tag \overline{B}^0_{flav}} &= (1-\nu)\Big\{[1-T^{\alpha}(1+\mu^{\alpha})]H_{B^0_{tag}\overline{B}^0_{flav}} + \\
&\quad [1-T^{\alpha}(1-\mu^{\alpha})]H_{\overline{B}^0_{tag}\overline{B}^0_{flav}}\Big\}
\end{aligned}
\tag{136}
$$

where ν, μ^{α} and T^{α} where defined in equations (89), (90), (91) and (92); and $H_{k_1k_2} = \int_{-\infty}^{+\infty} h_{k_1k_2}(\Delta t)d\Delta t$, where $h_{k_1k_2}(\Delta t)$ was given in equation (53). Only Δt odd terms of (53) are relevant (the even terms cancel out). The above expressions have been normalized for a reconstruction efficiency $R = 1$.

We form now combinations of the above quantities:

$$
\begin{aligned}
H^{\alpha}_{any\ tag B^0_{flav}} &= H^{\alpha}_{B^0_{tag}B^0_{flav}} + H^{\alpha}_{\overline{B}^0_{tag}B^0_{flav}} = \\
&\quad (1+\nu)T^{\alpha}\left[(1+\mu^{\alpha})H_{B^0_{tag}B^0_{flav}} + (1-\mu^{\alpha})H_{\overline{B}^0_{tag}B^0_{flav}}\right]
\end{aligned}
\tag{137}
$$

$$
\begin{aligned}
H^{\alpha}_{any\ tag \overline{B}^0_{flav}} &= H^{\alpha}_{B^0_{tag}\overline{B}^0_{flav}} + H^{\alpha}_{\overline{B}^0_{tag}\overline{B}^0_{flav}} = \\
&\quad (1-\nu)T^{\alpha}\left[(1+\mu^{\alpha})H_{B^0_{tag}\overline{B}^0_{flav}} + (1-\mu^{\alpha})H_{\overline{B}^0_{tag}\overline{B}^0_{flav}}\right]
\end{aligned}
\tag{138}
$$

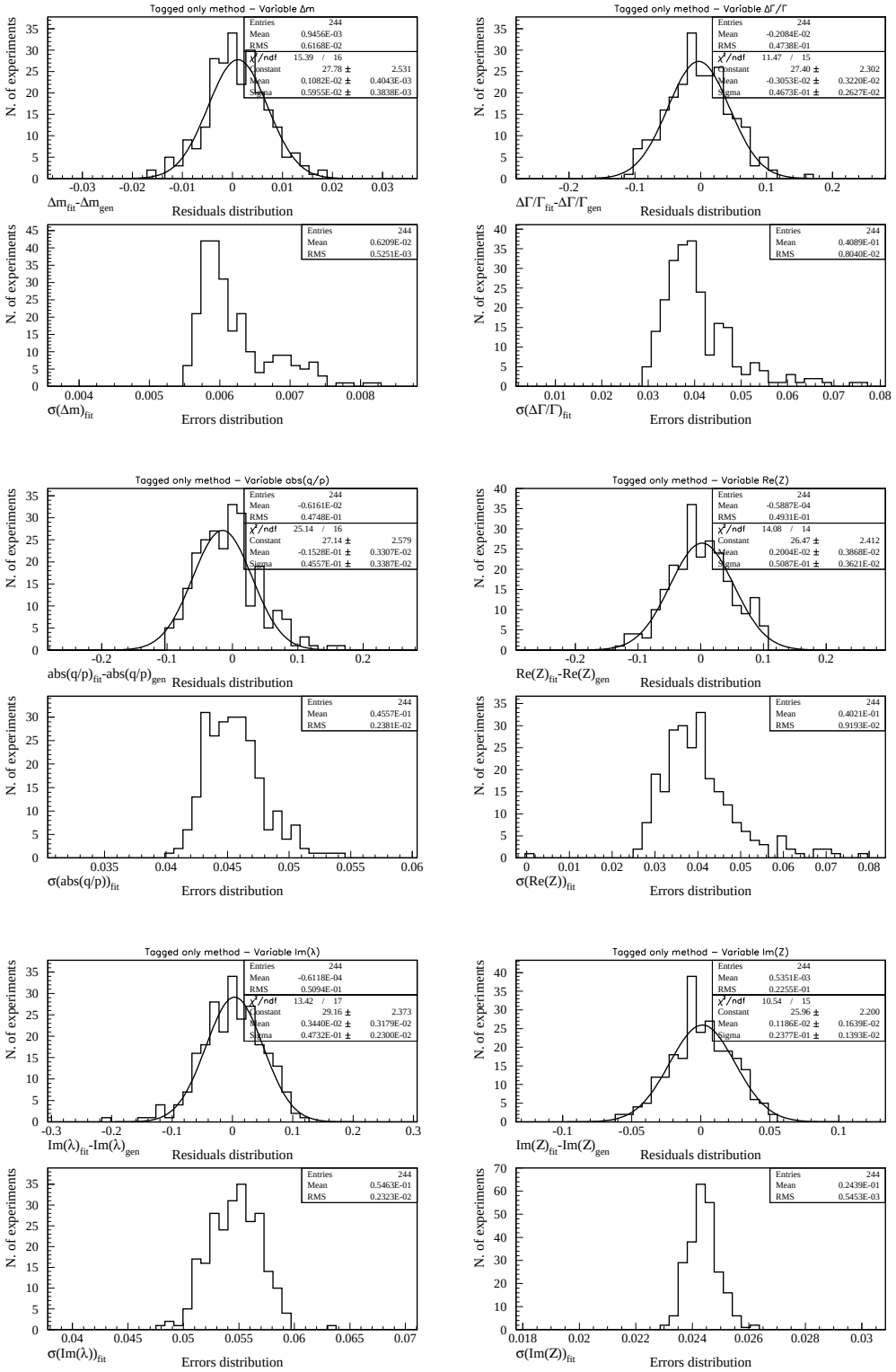

Figure 62: The residual and error (Gaussian) distributions for the CPT/CPT/T/oscillation parameters from the Tagged only method. The generated detector asymmetries were $\nu = 4\%$, $\mu^{\alpha} = 2\%, 3\%, 4\%, 4\%$.

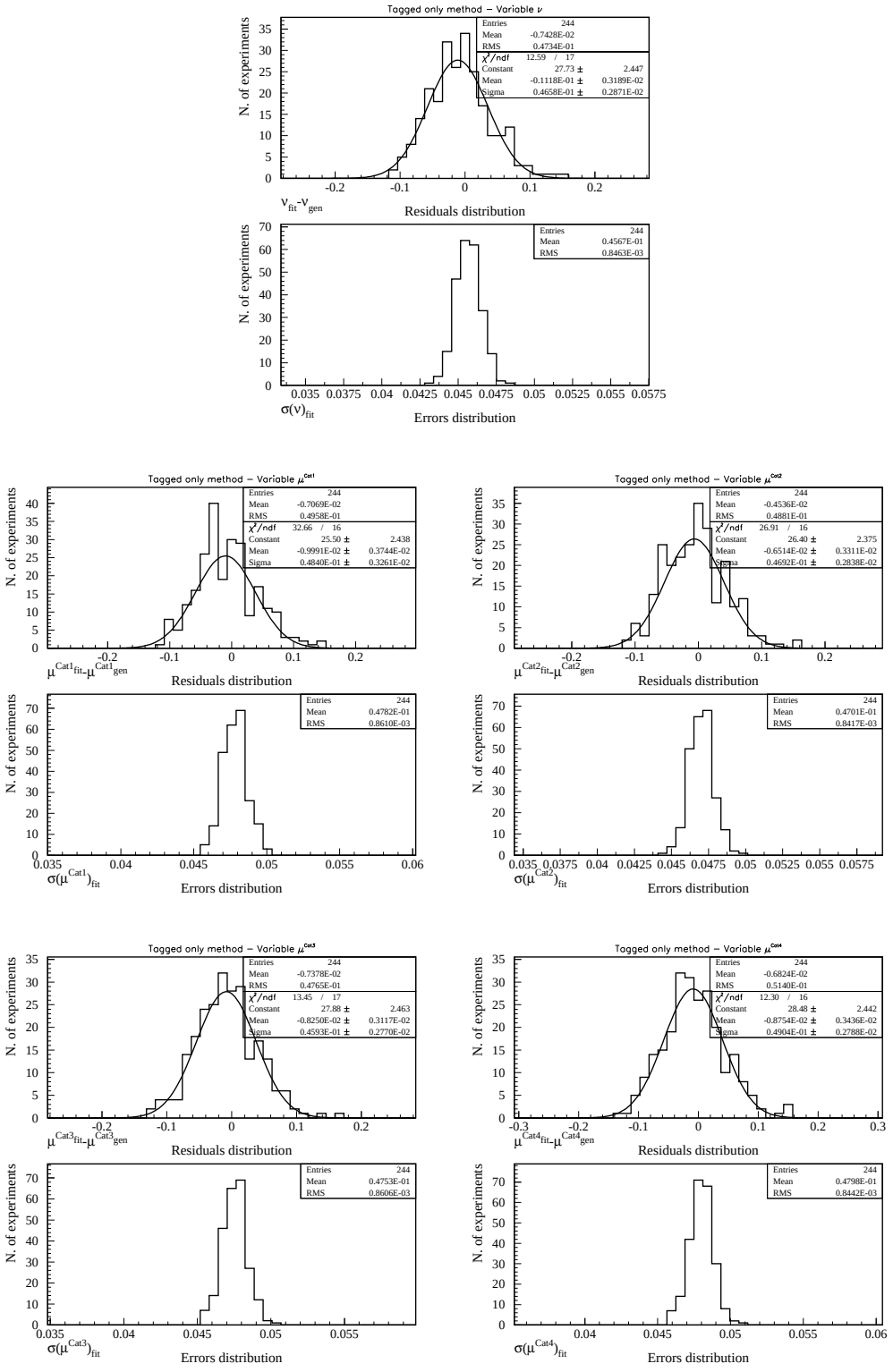

Figure 63: The residual and error (Gaussian) distributions for $B^0\bar{B}^0$ differences in reconstruction and tagging efficiencies (ν, μ^α parameters) from the Tagged only method. The generated values were $\nu = 4\%$, $\mu^\alpha = 2\%, 3\%, 4\%, 4\%$.

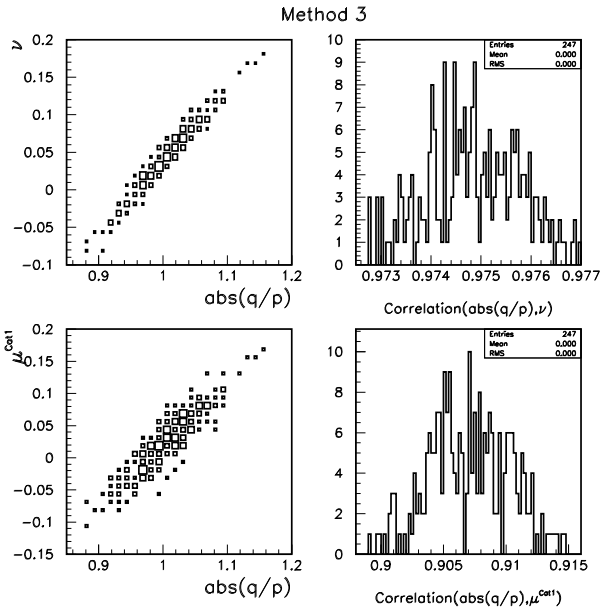

Figure 64: Scatter (left) and correlation coefficient (right) distributions among $\mid q/p \mid$ and ν (top) and μ^{Cat1} (bottom) from the Tagged only method. The generated detector asymmetries were $\nu = 4\%$, $\mu^{\alpha} = 2\%, 3\%, 4\%, 4\%$.

$$H^{\alpha}_{B^0_{flav}} = H^{\alpha}_{no\ tag B^0_{flav}} + H^{\alpha}_{any\ tag B^0_{flav}} = (1+\nu)\left[H_{B^0_{tag}B^0_{flav}} + H_{\overline{B}^0_{tag}B^0_{flav}}\right] \quad (139)$$

$$H^{\alpha}_{\overline{B}^0_{flav}} = H^{\alpha}_{no\ tag \overline{B}^0_{flav}} + H^{\alpha}_{any\ tag \overline{B}^0_{flav}} = (1-\nu)\left[H_{B^0_{tag}\overline{B}^0_{flav}} + H_{\overline{B}^0_{tag}\overline{B}^0_{flav}}\right] \quad (140)$$

or equivalently,

$$x = (1+\nu)T^{\alpha}\left[(1+\mu^{\alpha})a + (1-\mu^{\alpha})b\right] \quad (141)$$

$$y = (1-\nu)T^{\alpha}\left[(1+\mu^{\alpha})c + (1-\mu^{\alpha})d\right] \quad (142)$$

$$z + x = (1+\nu)(a+b) \quad (143)$$

$$w + y = (1-\nu)(c+d) \quad (144)$$

where

$$a = H_{B^0_{tag}B^0_{flav}}\ ,\ \ b = H_{\overline{B}^0_{tag}B^0_{flav}}\ ,\ \ c = H_{B^0_{tag}\overline{B}^0_{flav}}\ ,\ \ d = H_{\overline{B}^0_{tag}\overline{B}^0_{flav}}$$

are the time integrated theoretical rates (with $r_{CP,1} = r_{CP,2} = 1$) and

$$x = H^{\alpha}_{any\ tag B^0_{flav}}\ ,\ \ y = H^{\alpha}_{any\ tag \overline{B}^0_{flav}}\ ,\ \ z = H^{\alpha}_{no\ tag B^0_{flav}}\ ,\ \ w = H^{\alpha}_{no\ tag \overline{B}^0_{flav}}\ .$$

are the measured rates of tagged events in category α for B^0_{flav} (x) and $\overline{B}^0_{flav}$ (y) processes, and the total measured rates of B^0_{flav} and $\overline{B}^0_{flav}$ except those tagged in category α (z, w). Let us note that following the discussion at the end of section 2.5, possible direct CP violation effects (together with the detector charge asymmetries) are already included in the B counting, so that the PDF for the final fit should have $r_{CP,1} = r_{CP,2} = 1$.

Equations (141), (142), (143) and (144) can be worked out to obtain ν, μ^{α} and T^{α}:

$$\nu = \frac{1}{2}\frac{(z+x)(c+d)-(w+y)(a+b)}{(a+b)(c+d)} \tag{145}$$

$$\mu^{\alpha} = \frac{x(1-\nu)(c+d)-y(1+\nu)(a+b)}{y(1+\nu)(a-b)-x(1-\nu)(c-d)} \tag{146}$$

$$T^{\alpha} = \frac{1}{1-(\nu)^2}\frac{x(c-d)(1-\nu)-y(a-b)(1+\nu)}{2(bc-da)} \tag{147}$$

These expressions are also valid when the Δt resolution is considered. Let us note the reuse of events in the evaluation of ν, μ^{α} and T^{α}: for each tagging category $\alpha = \alpha_{Tagged}$ it is required the number of tagged events in that category together with the excluded events (events tagged by other categories plus the untagged events).

Let us stress the fact that in addition to the dependence with the number of $B^0/\bar{B}^0$/mixed/unmixed events, the extraction of ν, μ^{α} and T^{α} relies on estimates of the parameters which are going to be extracted from the time dependent analysis), independently of mistags and Δt resolution [16]. The terms with odd Δt dependence do not contribute.This is particularly critical for $\mid q/p \mid$. In order to introduce the time integrated constraint given by equations (145) and (146), an Extended Maximum Likelihood can be constructed to incorporate the Poisson uncertainties from the B counting. The modified likelihood function reads

$$\ln \mathcal{L}_{Extended} = \ln \mathcal{L} + \Delta \ln \mathcal{L} \tag{148}$$

where $\ln \mathcal{L}$ was defined in equation (114) and

$$\Delta \ln \mathcal{L} = \sum_{\alpha} \Delta \ln \mathcal{L}_{\alpha} \tag{149}$$

$$\begin{aligned} &- \ln N_{B^0_{flav},notag}! + N_{B^0_{flav},notag} \ln \eta_{B^0_{flav},notag} - \eta_{B^0_{flav},notag} \\ &- \ln N_{\overline{B}^0_{flav},notag}! + N_{\overline{B}^0_{flav},notag} \ln \eta_{\overline{B}^0_{flav},notag} - \eta_{\overline{B}^0_{flav},notag} \end{aligned} \tag{150}$$

and

$$\begin{aligned} \Delta \ln \mathcal{L}_{\alpha} = &- \ln N^{\alpha}_{B^0_{flav},tag}! + N^{\alpha}_{B^0_{flav},tag} \ln \eta^{\alpha}_{B^0_{flav},tag} - \eta^{\alpha}_{B^0_{flav},tag} \\ &- \ln N^{\alpha}_{\overline{B}^0_{flav},tag}! + N^{\alpha}_{\overline{B}^0_{flav},tag} \ln \eta^{\alpha}_{\overline{B}^0_{flav},tag} - \eta^{\alpha}_{\overline{B}^0_{flav},tag} \end{aligned} \tag{151}$$

$N^{\alpha}_{B^0_{flav}(\overline{B}^0_{flav}),tag}$ is the number of B_{flav} events reconstructed as $B^0(\overline{B}^0)$ and tagged in category α, and $N_{B^0_{flav}(\overline{B}^0_{flav}),notag}$ is the total number of untagged B_{flav} events and reconstructed as $B^0(\overline{B}^0)$. $\eta^{\alpha}_{B^0_{flav}(\overline{B}^0_{flav}),tag}$ and $\eta_{B^0_{flav}(\overline{B}^0_{flav}),notag}$ denote the corresponding expected numbers of events. This method can be applied by counting the number of signal events (estimated from m_{ES} fits). For combinatorial background components, where typically we assume Δm=0, $\Delta\Gamma/\Gamma$=0, $\mid q/p \mid$=1 and $z = 0$, there is no need to apply this method, and the parameters ν and μ^{α} can be fixed to the estimates obtained previously to the fit using events from the sideband region.

To check the feasibility of the Alternative method, the same toy Monte Carlo samples used before were fitted using this method. The mean residuals and Gaussian errors returned by the fits for the CPT/CPT/T/oscillation parameters are shown in figure 65. We observe again that we have unbiased estimates for all the parameters, with basically the same precision as with the All Events method. The scatter distributions among $\mid q/p \mid$ and ν and μ^{α} reveal that the correlation pattern between physics and detector asymmetries are similar to those of the All Events method. The values of ν and μ^{α} at the final solution were consistent with those generated. As an additional check, the fits were repeated using a largely different starting point (especially for $\mid q/p \mid$ and ν, μ^{α}), obtaining the same solution in all cases, up to numerical precision, as shown in figure 66.

A.2 Sensitivity to $\Delta\Gamma/\Gamma$

The discussion in section A.1 considers only the additional time-integrated information contained in the untagged events. There is, however, additional information in the time-dependence. Taking first order in the CPT parameter z and assuming perfect tagging states, direct CP conservation (in reconstructed CP and flavor states as well as tagging states) and $\mid q/p \mid$=1, the coefficients of the time dependence are those given in tables 129 and 130 (obtained summing the $\mid 1\rangle$ and $\mid \bar{1}\rangle$ contributions of tables 3 and 4). From an inspection of these coefficients we conclude that only the $\Delta\Gamma/\Gamma$ dependence remains (first order for CP and second order for flavor eigenstates), while the dependence on CPT/CP violation basically disappears, due either to the cancellation of coefficients or mixing. The $\Delta\Gamma/\Gamma$ sensitivity contained in untagged CP events was already suggested in [38].

Coefficient	$\mid f_{no\ tag} f_2\rangle$	$\mid f_{no\ tag}\rangle \mid f_{\bar{2}}\rangle$
c_+	2	2
c_-	0	0
Re(s)	Rez	$-$Rez
Im(s)	Imz	$-$Imz

Table 129: Coefficients of the time-dependent decay rate for flavor eigenstates (perfect tagging states), to first order in the CPT parameter z and assuming direct CP conservation and $\mid q/p \mid$=1, for untagged events.

Coefficient	$\mid f_{no\ tag} f_{CP}\rangle$
c_+	$4(1+\mathrm{Imz}\mathrm{Im}\lambda'_{CP})$
c_-	$4\mathrm{Imz}\mathrm{Im}\lambda'_{CP}$
Re(s)	$2\mathrm{Re}\lambda'^{*}_{CP}$
Im(s)	0

Table 130: Coefficients of the time-dependent decay rate for CP eigenstates (perfect tagging states), to first order in the CPT parameter z and assuming direct CP conservation and $\mid q/p \mid$=1, for untagged events.

A toy Monte Carlo study was performed to verify the gain in sensitivity to $\Delta\Gamma/\Gamma$ coming from untagged CP events. The toy Monte Carlo samples are similar to those generated previously, but now with $\nu = \mu^{\alpha} = 0$. The

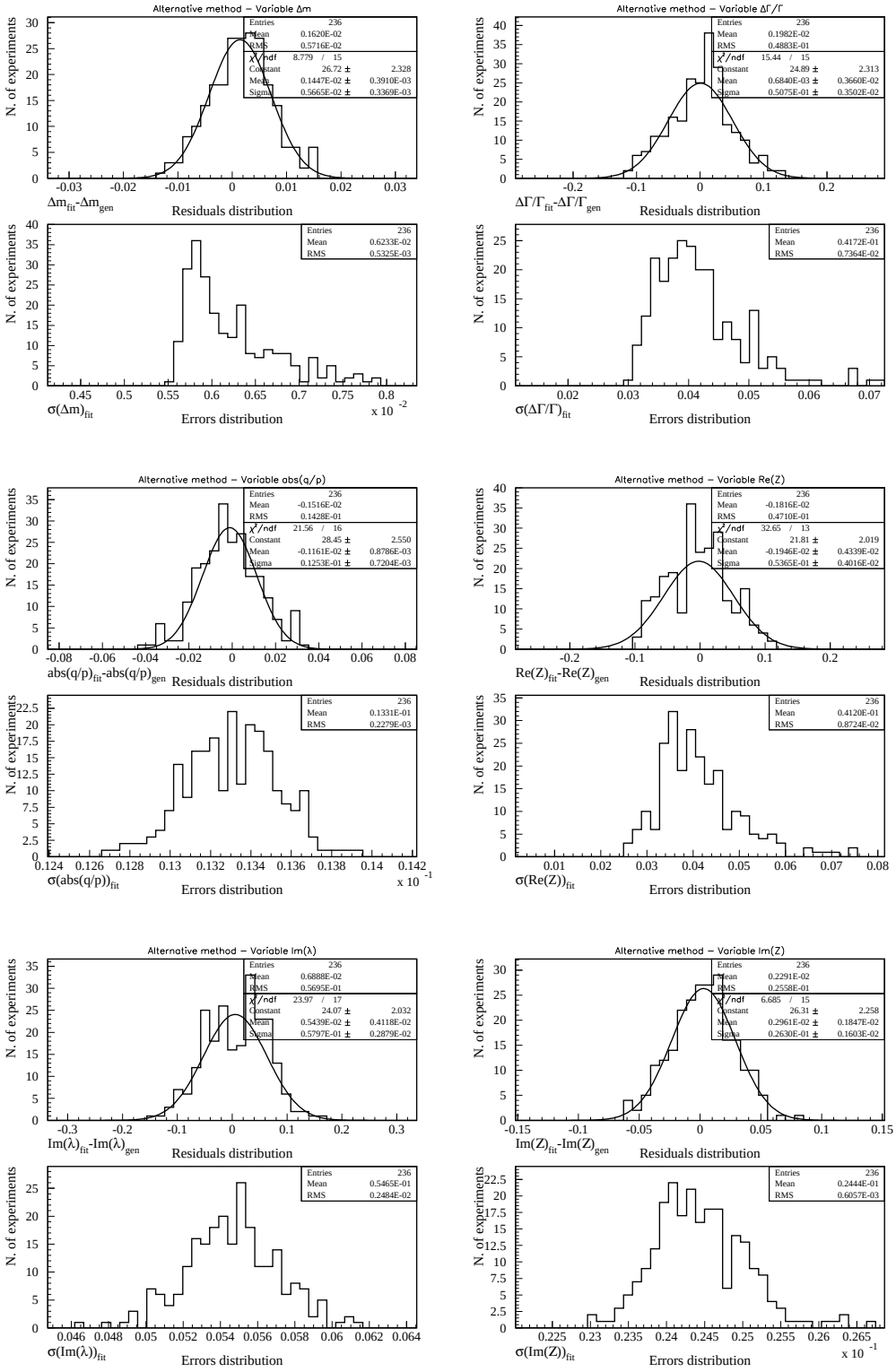

Figure 65: The residual and error (quadratic) distributions for the CPT/CPT/T/oscillation parameters from the Alternative method. The generated detector asymmetries were $\nu = 4\%$, $\mu^{\alpha} = 2\%, 3\%, 4\%, 4\%$.

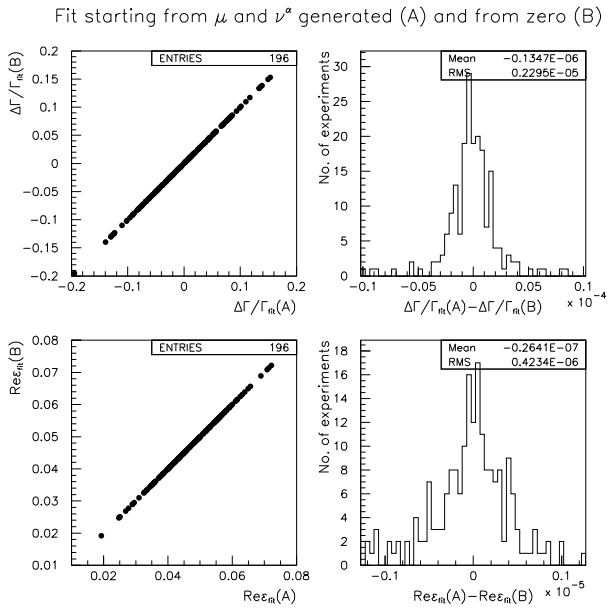

Figure 66: Comparison between the results obtained fitting the same samples generated with large $B^0\bar{B}^0$ differences in reconstruction and tagging efficiencies, using different starting points. The upper left plot shows the correlation among the fitted values of $\Delta\Gamma/\Gamma$ from the two sets of starting points, while the upper right shows the distribution of the differnce between the two fitted parameters. The lower plots show the analogous for the $\frac{\mathrm{Re}\epsilon}{1+|\epsilon|^2}$ ($\approx|\ q/p\ |$) parameter.

samples were then fitted with the All Events method, with and without untagged CP events. Table 131, which compares the RMS of the residual distributions and the average Gaussian errors for all the parameters, reveals the gain in sensitivity to $\Delta\Gamma/\Gamma$.

	Δm	$\Delta\Gamma/\Gamma$	$\lvert\ q/p\ \rvert$	$\frac{\mathrm{Re}\lambda_{CP}}{\lvert\lambda_{CP}\rvert}$Rez	$\frac{\mathrm{Im}\lambda_{CP}}{\lvert\lambda_{CP}\rvert}$	Imz
	Do not use untagged CP events					
RMS	0.0062	0.046	0.0113	0.049	0.049	0.022
Average quadratic error	0.0062	0.041	0.0104	0.041	0.054	0.024
	Do use untagged CP events					
RMS	0.0062	0.041	0.0113	0.047	0.052	0.023
Average quadratic error	0.0062	0.037	0.0104	0.043	0.055	0.024

Table 131: RMS and average Gaussian error from the All Events method configuration with and without untagged CP events.

A.3 Resolution function

Finally, it is obvious that the untagged events (which represent about the 30% of the total statistics) will contribute to the extraction of the resolution function. Nevertheless, the gain is expected to be much smaller than the above improvements since the resolution function is already very well determined from the tagged events of the high statistics B_{flav} sample.

B Doubly-CKM-Suppressed Decays Toy Monte Carlo studies

B.1 Sensitivity studies

We investigated the numerical sensitivity of the CPT/T/CPT/Mixing parameters to DCKM effects using toy Monte Carlo. For these studies, the samples were generated with the values of the phases that maximize and minimize the PDF (this occurrs at the physical region boundaries of the sines and cosines of the phases). In the most general case without model asumptions we have a total of 16 possible combinations for each B meson, reconstructed and tagging (4 possible angles for each B^0 and $\bar{B}^0$: 0, $\pi/2$, π, $3\pi/2$). In practice, the matrix of combinations is "antisymmetric" under B^0 and $\bar{B}^0$ interchange, which gives a total of 10 different combinations. In order to reduce futher the number of combinations and simplify as much as possible this study, we assumed $\theta = \phi_{strong} + \phi_{weak}$, $\bar{\theta} = \phi_{strong} - \phi_{weak}$, with $\phi_{weak} = 2\beta + \gamma = 1.85$, which reduces to 4 combinations. This assumption will be released for the systematic error evaluation in the final analysis. The rates r_{flav}, $\bar{r}_{flav}$, r_{tag} and $\bar{r}_{tag}$ were generated to be 0.05. One single effective channel contributing to the reconstructed (flavor sample) and tagging (common for the flavor and CP samples) sides was assumed here. The samples consisted of about 100 experiments with an statistics equivalent to about 60 fb^{-1} each, with perfect Δt resolution but mistags as those observed in the data. The relative populations of flavor and CP events was kept the same as observed in the data. Tagging-vertexing correlations and $B^0\bar{B}^0$ differences in reconstruction and tagging efficiencies were neglected here. We assumed no direct CP violation effects, $r_{CP,CP} = r_{CP,flav} = r_{CP,tag} = 1$. The CP phase θ_{CP} was generated to be 0.86 rad (which corresponds to $\frac{\mathrm{Im}\lambda_{CP}}{|\lambda_{CP}|}$=0.75). z and $|\,q/p\,|$ were assumed to be 0 and 1, respectively[7].

We first analyzed the effects in the tagging side. The mean residuals obtained when fitting the samples neglecting the DCKM effects in both, tagging and reconstructed sides (**fit configuration 1**), but generating DCKM effects in the tagging side only, are summarized in table 132. To evaluate the significance of the offsets, these values should be compared to the RMS reported in the same table. The statistical error on the offsets are about 10 times smaller than the reported RMS. We observe a large impact on Imz, a non-negligible effect on $\frac{\mathrm{Re}\lambda_{CP}}{|\lambda_{CP}|}Rez$ and to a less extend on $\frac{\mathrm{Im}\lambda_{CP}}{|\lambda_{CP}|}$. The effects for all the other parameters are negligible[8].

θ_{tag}	Δm	$\Delta\Gamma/\Gamma$	$\lvert q/p\rvert$	$\frac{\mathrm{Re}\lambda_{CP}}{\lvert\lambda_{CP}\rvert}Rez$	$\frac{\mathrm{Im}\lambda_{CP}}{\lvert\lambda_{CP}\rvert}$	Imz
0	0.0020	-0.0032	0.0011	-0.0263	-0.0032	0.0175
$\pi/2$	0.0016	0.0019	-0.0001	-0.0098	0.0033	-0.0615
π	0.0014	0.0066	0.0005	0.0253	-0.0050	-0.0186
$3\pi/2$	0.0020	-0.0025	0.0005	0.0008	0.0185	0.0614
RMS	0.0078	0.052	0.013	0.056	0.068	0.013

Table 132: Mean residuals and RMS for fit configuration 1, tagging side phase scan.

When the same samples are fitted letting free $\frac{\mathrm{Im}\lambda_{tag}}{|\lambda_{tag}|}$ and $\frac{\mathrm{Im}\bar{\lambda}_{tag}}{|\bar{\lambda}_{tag}|}$, with $r_{tag} = \bar{r}_{tag}$ fixed to 0.05 and $\frac{\mathrm{Re}\lambda_{tag}}{|\lambda_{tag}|} = \frac{\mathrm{Re}\bar{\lambda}_{tag}}{|\bar{\lambda}_{tag}|} = 0$[9] (**fit configuration 2**), we obtain the mean residuals and RMS listed in table 133. The large effect

[7] Although irrelevant here, the different DCKM fitting configurations investigated in this appendix were all based in the Alternative method described in appendix A, since these studies were performed before the implementation and adoption of the All Events methods as the nominal approach to deal with untagged events.

[8] The Δm mean residual should be compared to the mean residual when no DCKM effects are generated, about 0.0022. This small bias is known to be due to the simultaneous extraction of Δm with the CPT parameters. When CPT is assumed to be a good symmetry this small effect goes away.

[9] r_{flav}, $\bar{r}_{flav}$, $\frac{\mathrm{Re}\lambda_{flav}}{|\lambda_{flav}|}$, $\frac{\mathrm{Re}\bar{\lambda}_{flav}}{|\lambda_{flav}|}$, $\frac{\mathrm{Im}\lambda_{flav}}{|\lambda_{flav}|}$ and $\frac{\mathrm{Im}\bar{\lambda}_{flav}}{|\lambda_{flav}|}$ are all fixed to zero.

on Imz has disappeared here, at the price of an increase in its statistical error (from 0.013 to 0.019). The effect on $\frac{\mathrm{Im}\lambda_{CP}}{|\lambda_{CP}|}$ seems to be also reduced. The mean biases and statistical reach of all the other parameters remain basically unchanged. The RMS for $\frac{\mathrm{Im}\lambda_{tag}}{|\lambda_{tag}|}$ and $\frac{\mathrm{Im}\bar{\lambda}_{tag}}{|\lambda_{tag}|}$ is 0.32.

θ_{tag}	Δm	$\Delta\Gamma/\Gamma$	$\mid q/p \mid$	$\frac{\mathrm{Re}\lambda_{CP}}{\lvert\lambda_{CP}\rvert}$Rez	$\frac{\mathrm{Im}\lambda_{CP}}{\lvert\lambda_{CP}\rvert}$	Imz
0	0.0018	0.0014	0.0013	-0.0253	-0.0074	-0.0009
$\pi/2$	0.0021	0.0025	-0.0003	-0.0080	0.0079	-0.0017
π	0.0017	0.0068	-0.0002	0.0252	0.0022	0.0020
$3\pi/2$	0.0019	-0.0076	0.0007	-0.0002	0.0092	0.0032
RMS	0.0078	0.054	0.013	0.056	0.069	0.019

Table 133: Mean residuals and RMS for fit configuration 2, tagging side phase scan.

The same samples were also fitted with $\frac{\mathrm{Im}\lambda_{tag}}{|\lambda_{tag}|}$, $\frac{\mathrm{Im}\bar{\lambda}_{tag}}{|\lambda_{tag}|}$, $\frac{\mathrm{Re}\lambda_{tag}}{|\lambda_{tag}|}$ and $\frac{\mathrm{Re}\bar{\lambda}_{tag}}{|\lambda_{tag}|}$ free and $r_{tag} = \bar{r}_{tag}$ fixed to 0.05 (**fit configuration 3**). The mean residuals and RMS obtained are those summarized in table 134. The situation for $\frac{\mathrm{Re}\lambda_{CP}}{|\lambda_{CP}|}$Rez is now slightly better, at the price of an increase of its statistical precision. The $\mid q/p \mid$ and $\frac{\mathrm{Im}\lambda_{CP}}{|\lambda_{CP}|}$ RMS' are also slightly poorer. The RMS for $\frac{\mathrm{Im}\lambda_{tag}}{|\lambda_{tag}|}$ and $\frac{\mathrm{Im}\bar{\lambda}_{tag}}{|\lambda_{tag}|}$ is 0.32 as before, while it is 2.1 for $\frac{\mathrm{Re}\lambda_{tag}}{|\lambda_{tag}|}$ and $\frac{\mathrm{Re}\bar{\lambda}_{tag}}{|\lambda_{tag}|}$. We observe that the sensitivity to the real parts in the tagging side is poor.

θ_{tag}	Δm	$\Delta\Gamma/\Gamma$	$\mid q/p \mid$	$\frac{\mathrm{Re}\lambda_{CP}}{\lvert\lambda_{CP}\rvert}$Rez	$\frac{\mathrm{Im}\lambda_{CP}}{\lvert\lambda_{CP}\rvert}$	Imz
0	0.0010	0.0013	0.0025	0.0093	-0.0121	-0.0005
$\pi/2$	0.0017	0.0055	-0.0003	0.0031	0.0005	-0.0016
π	0.0004	0.0089	-0.0003	0.0016	0.0058	-0.0034
$3\pi/2$	0.0019	-0.0051	-0.0014	-0.0098	0.0090	0.0030
RMS	0.0077	0.054	0.017	0.065	0.070	0.019

Table 134: Mean residuals and RMS for fit configuration 3, tagging side phase scan.

Results from tables 132, 133 and 134 confirm some of the expectations discussed in the previous section: i) Rez(Imz) is mainly correlated with the DCKM real(imaginary) parts, ii) the effects on Δm and $\Delta\Gamma$ are small, iii) the effect on $\frac{\mathrm{Im}\lambda_{CP}}{|\lambda_{CP}|}$ is rather small, and seems to have contributiones from both real and imaginary DCKM parts.

The above studies have been repeated but now generating the DCKM effects in the reconstructed side only (flavor sample). The mean residuals and RMS obtained when fitting with **configuration 1** are summarized in table 135. We observe again a large offset on Imz but significantly smaller than in the previous case where the DCKM effects were generated in the tagging side. No significant effects are observed in all the other parameters. Comparing these results with those equivalent in the tagging side (table 132) we conclude that the tagging side gives the largest systematic effect to the determination of the CPT/CP/T/oscillation parameters. The effect on Imz goes away if $\frac{\mathrm{Im}\lambda_{flav}}{|\lambda_{flav}|}$, $\frac{\mathrm{Im}\bar{\lambda}_{flav}}{|\lambda_{flav}|}$ are also fitted, with $r_{flav} = \bar{r}_{flav}$ fixed to 0.05 (**fit configuration 4**) (and all the other DCKM related parameters fixed to zero), as reported in table 136. The RMS for $\frac{\mathrm{Im}\lambda_{flav}}{|\lambda_{flav}|}$ and $\frac{\mathrm{Im}\bar{\lambda}_{flav}}{|\lambda_{flav}|}$ is 0.32, as in the case of the tagging side. When $\frac{\mathrm{Re}\lambda_{flav}}{|\lambda_{flav}|}$ and $\frac{\mathrm{Re}\bar{\lambda}_{flav}}{|\lambda_{flav}|}$ were considered as additional free parameters in the fit most of them failed, due to the extremelly poor sensitivity to these parameters (RMS ~ 10).

θ_{flav}	Δm	$\Delta\Gamma/\Gamma$	$\mid q/p \mid$	$\frac{\mathrm{Re}\lambda_{CP}}{\mid\lambda_{CP}\mid}$Rez	$\frac{\mathrm{Im}\lambda_{CP}}{\mid\lambda_{CP}\mid}$	Imz
0	0.0021	0.0052	0.0001	0.0027	0.0050	0.0051
$\pi/2$	0.0040	0.0006	0.0001	-0.0094	-0.0145	-0.0178
π	0.0031	-0.0056	-0.0011	0.0031	-0.0019	-0.0049
$3\pi/2$	0.0012	-0.0032	0.0014	-0.0001	0.0153	0.0202
RMS	0.0078	0.054	0.013	0.056	0.069	0.013

Table 135: Mean residuals and RMS for fit configuration 1, reconstructed (flavor sample) side phase scan.

θ_{flav}	Δm	$\Delta\Gamma/\Gamma$	$\mid q/p \mid$	$\frac{\mathrm{Re}\lambda_{CP}}{\mid\lambda_{CP}\mid}$Rez	$\frac{\mathrm{Im}\lambda_{CP}}{\mid\lambda_{CP}\mid}$	Imz
0	0.0024	0.0046	-0.0003	0.0007	-0.0059	-0.0008
$\pi/2$	0.0037	-0.0028	0.0008	-0.0056	-0.0100	0.0003
π	0.0029	-0.0060	-0.0011	0.0030	-0.0027	0.0005
$3\pi/2$	0.0012	0.0015	0.0008	-0.0016	0.0118	-0.0009
RMS	0.0080	0.053	0.013	0.056	0.069	0.014

Table 136: Mean residuals and RMS for fit configuration 4, reconstructed (flavor sample) side phase scan.

From these sensitivity studies we verified numerically the features anticipated from the analytical study described in section 2.2.5 concluding that the optimal trade-off between statistical precision and systematic uncertainties due to Doubly-CKM-Suppressed decays requires the introduction of 4 additional fit parameters (in addition to the 6 CPT/T/CP and oscillation parameters), the sines of the DCKM phases, 2 for the tagging side and 2 for the reconstructed (flavor sample) B (**reference fit configuration**). It was verified for different DCKM phase configurations that this fitting configuration provides unbiassed estimates for all the parameters, and the quadratic errors reported by the fit give a good estimation of the statistical reach, within 10%. Table 137 summarizes the results obtained for a particular DCKM configuration where all phases were generated to be $\pi/2$, with $r_{tag} = \bar{r}_{tag} = r_{flav} = \bar{r}_{flav} = 0.05$. The residual and quadratic error distributions are shown in figure 67. Table 138 summarizes the largest average correlation coefficients among the physics parameters and any DCKM parameter.

	Δm	$\Delta\Gamma/\Gamma$	$\mid q/p \mid$	$\frac{\mathrm{Re}\lambda_{CP}}{\mid\lambda_{CP}\mid}$Rez	$\frac{\mathrm{Im}\lambda_{CP}}{\mid\lambda_{CP}\mid}$	Imz
Mean residual	0.0025	0.0039	-0.0015	-0.0052	0.0101	0.0002
Error mean residual	0.0005	0.0031	0.0010	0.0031	0.0045	0.0017
RMS	0.008	0.052	0.016	0.052	0.071	0.028
Average quadratic error	0.008	0.049	0.017	0.050	0.068	0.029

Table 137: Mean residuals, RMS and average quadratic error from the reference fit configuration. The DCKM phases were taken for this particular exercise to be $\pi/2$, with $r_{tag} = \bar{r}_{tag} = r_{flav} = \bar{r}_{flav} = 0.05$.

B.2 Effects from mistags

The feature described in the second paragraph of section 2.10 was verified fitting a common set of toy Monte Carlo experiments fixing $r_{tag} = \bar{r}_{tag}$ to 0.05 and 0.10 (the samples were generated with 0.05). Figure 68 shows the perfect one-to-one correlation (up to numerical differences) among the fitted results for all the CPT/T/CP/oscillation parameters. In this exercise the real and imaginary parts in the tagging side were left free,

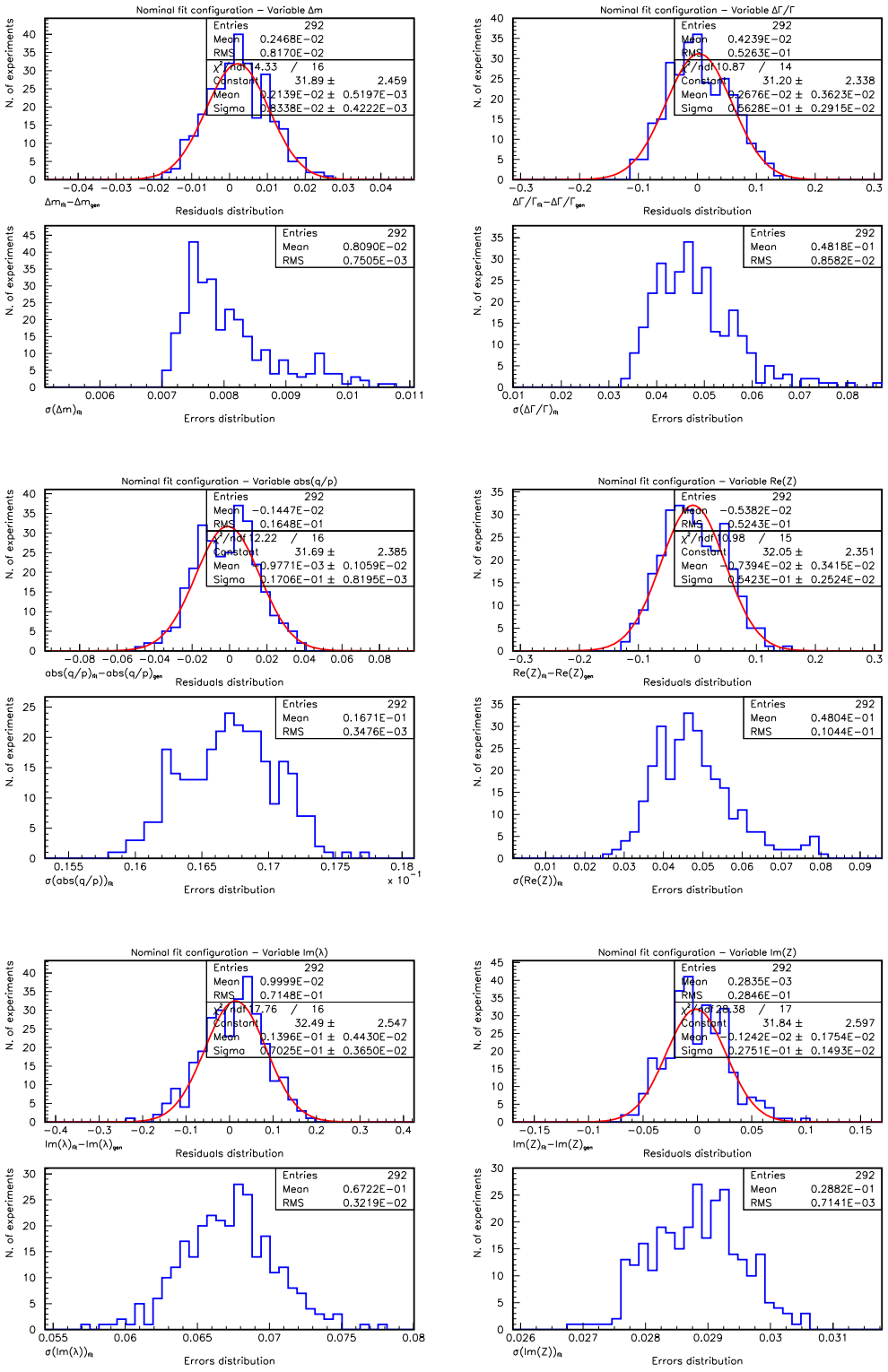

Figure 67: The residual and error (quadratic) distributions for the CPT/CPT/T/oscillation parameters from the reference fit configuration. The DCKM phases were taken for this particular exercise to be $\pi/2$, with $r_{tag} = \overline{r}_{tag} = r_{flav} = \overline{r}_{flav} = 0.05$.

Parameter	Parameter	Average correlation coefficient
Imz	$\frac{\mathrm{Im}\lambda_{flav}}{\lvert\lambda_{flav}\rvert}$	50
	$\frac{\mathrm{Im}\lambda_{flav}}{\lvert\lambda_{flav}\rvert}$	-55
	$\frac{\mathrm{Im}\lambda_{tag}}{\lvert\lambda_{tag}\rvert}$	53
	$\frac{\mathrm{Im}\lambda_{tag}}{\lvert\lambda_{tag}\rvert}$	-58
$\frac{\mathrm{Im}\lambda_{flav}}{\lvert\lambda_{flav}\rvert}$	$\frac{\mathrm{Im}\lambda_{tag}}{\lvert\lambda_{tag}\rvert}$	72
	$\frac{\mathrm{Im}\lambda_{tag}}{\lvert\lambda_{tag}\rvert}$	10
$\frac{\mathrm{Im}\bar{\lambda}_{flav}}{\lvert\lambda_{flav}\rvert}$	$\frac{\mathrm{Im}\lambda_{tag}}{\lvert\bar{\lambda}_{tag}\rvert}$	10
	$\frac{\mathrm{Im}\bar{\lambda}_{tag}}{\lvert\lambda_{tag}\rvert}$	76
$\frac{\mathrm{Im}\lambda_{tag}}{\lvert\lambda_{tag}\rvert}$	$\frac{\mathrm{Im}\lambda_{tag}}{\lvert\bar{\lambda}_{tag}\rvert}$	19

Table 138: Largest (>= 10%) correlations between the CPT/T/CP/oscillation parameters and the DCKM parameters, for the reference fit configuration. The DCKM phases were taken for this particular exercise to be $\pi/2$, with $r_{tag} = \bar{r}_{tag} = r_{flav} = \bar{r}_{flav} = 0.05$.

while only the imaginary parts in the reconstructed (flavor sample) side were considered as free parameters (real parts were fixed to zero). For the same experiments/fits, figure 69 shows the rescaling of the mistag fractions and the DCKM parameters in the tagging side.

B.3 Multiple final states

In order to check that DCKM effects from semi-inclusive channels are always smaller than those from a single channel (third paragraph of section 2.10), we generated two different sets of toy Monte Carlo samples (about 200 experiments each), similarly as described in section B.1. In the first set each sample was split into two same-sized sub-samples with phases $\theta^a_{tag}/\theta^b_{tag} = 0, \pi/2, \pi, 3\pi/2$, with $\theta_{weak} = 1.85$ fixed. In the second set only one single channel was considered. To enhance the effect we want to investigate, r was generated to be 0.1 in the tagging side. No DCKM effects in the reconstructed side (flavor sample) were generated for this study. Each sample was then fitted with the standard, single channel approach, and then we compared the results for the two-channel and single-channel samples. The mean residuals of the fit results are shown in table 139, for the two and single channel case. From the comparison of the results we conclude that the biases in the two-channel case are about the average of the biases from the samples generated with a single channel. The worse case (largest bias) in the case of a single channel is always larger than any of the two-channels configurations.

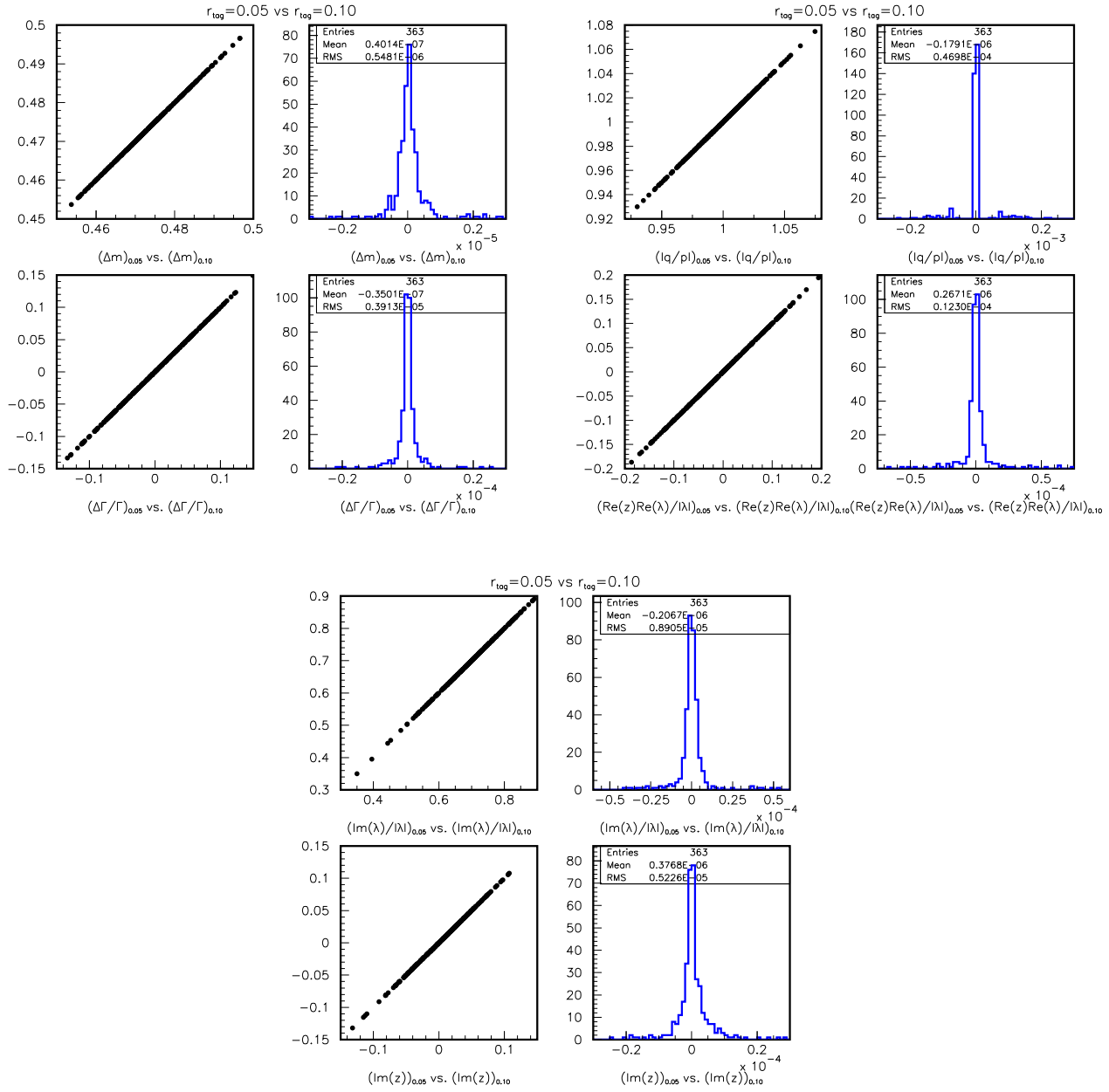

Figure 68: Experiment-by-experiment comparison (scatter and difference) of the fitted results for all the CPT/T/CP/oscillation parameters when the same toy Monte Carlo samples are fitted with different values of $r_{tag} = \bar{r}_{tag}$ (0.05 and 0.10).

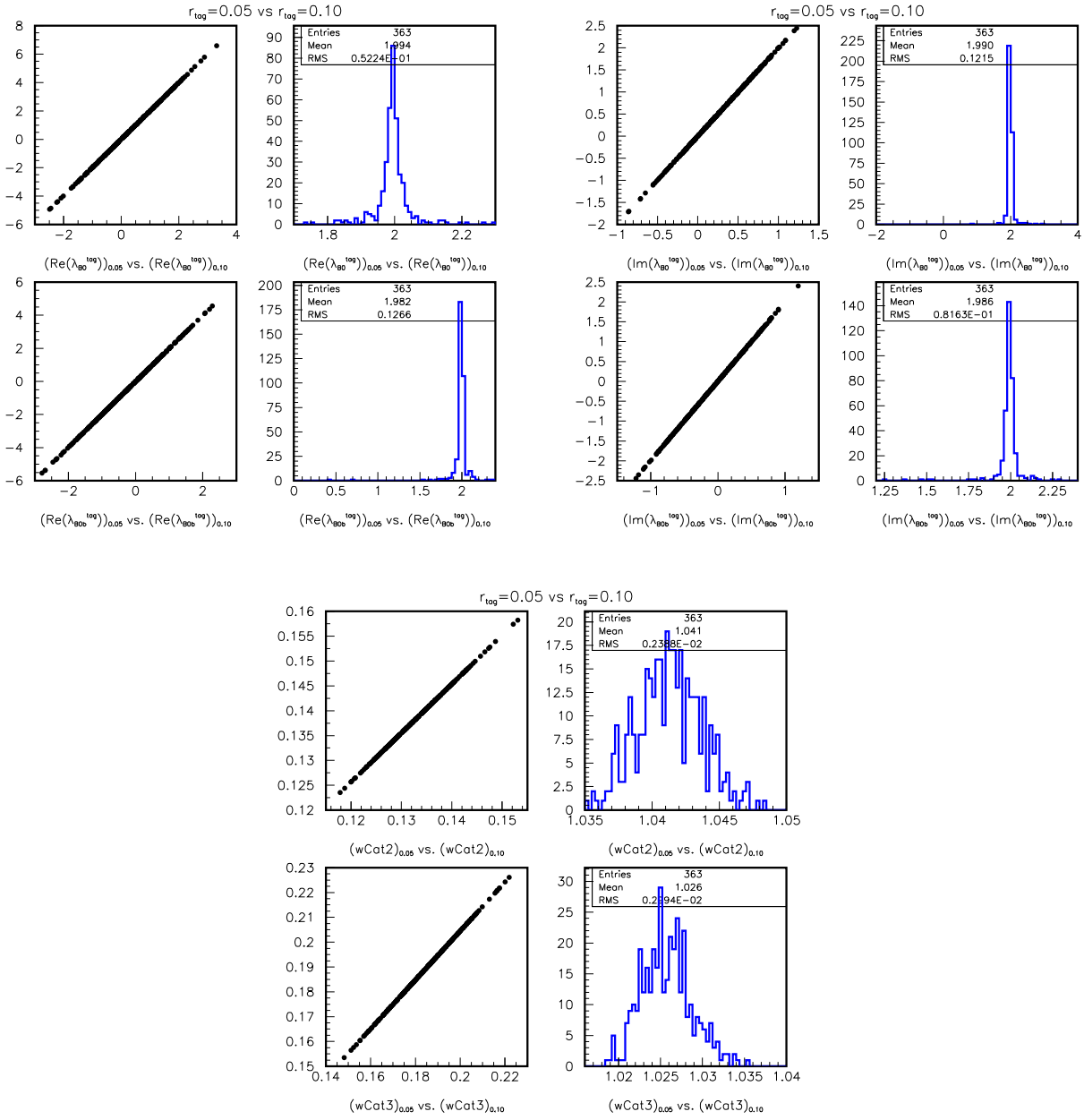

Figure 69: Experiment-by-experiment comparison (scatter and ratio) of the fitted results for the mistag fractions (`Kaon` and `NT1` tagging categories) and the DCKM parameters when the same toy Monte Carlo samples are fitted with different values of $r_{tag} = \overline{r}_{tag}$ (0.05 and 0.10).

Two channels						
θ^a_{tag} / θ^b_{tag}	Δm	$\Delta\Gamma/\Gamma$	$\mid q/p \mid$	$\frac{\mathrm{Re}\lambda_{CP}}{\mid\lambda_{CP}\mid}$Rez	$\frac{\mathrm{Im}\lambda_{CP}}{\mid\lambda_{CP}\mid}$	Imz
0 / $\frac{\pi}{2}$	$(2.67\pm0.55)\cdot10^{-3}$	$(-4.8\pm3.7)\cdot10^{-3}$	$(-1.4\pm1.3)\cdot10^{-3}$	$(-4.27\pm0.37)\cdot10^{-2}$	$(3.7\pm4.9)\cdot10^{-3}$	$(0.9\pm1.4)\cdot10^{-3}$
0 / π	$(2.94\pm0.59)\cdot10^{-3}$	$(2.7\pm3.6)\cdot10^{-3}$	$(-1.3\pm1.3)\cdot10^{-3}$	$(-5.6\pm4.5)\cdot10^{-3}$	$(5.7\pm4.8)\cdot10^{-3}$	$(0.8\pm1.5)\cdot10^{-3}$
0 / $\frac{3}{2}\pi$	$(1.86\pm0.56)\cdot10^{-3}$	$(2.7\pm3.8)\cdot10^{-3}$	$(-1.2\pm1.3)\cdot10^{-3}$	$(-1.87\pm0.40)\cdot10^{-2}$	$(-5.0\pm4.7)\cdot10^{-3}$	$(-0.2\pm1.5)\cdot10^{-3}$
$\frac{\pi}{2}$ / π	$(1.53\pm0.53)\cdot10^{-3}$	$(4.2\pm4.2)\cdot10^{-3}$	$(-2.8\pm1.3)\cdot10^{-3}$	$(1.34\pm0.40)\cdot10^{-2}$	$(0.9\pm4.1)\cdot10^{-3}$	$(1.4\pm1.2)\cdot10^{-3}$
$\frac{\pi}{2}$ / $\frac{3}{2}\pi$	$(2.49\pm0.57)\cdot10^{-3}$	$(0.4\pm4.2)\cdot10^{-3}$	$(-2.3\pm1.3)\cdot10^{-3}$	$(0.8\pm4.1)\cdot10^{-3}$	$(8.7\pm5.3)\cdot10^{-3}$	$(-0.6\pm1.3)\cdot10^{-3}$
π / $\frac{3}{2}\pi$	$(2.62\pm0.55)\cdot10^{-3}$	$(4.4\pm4.0)\cdot10^{-3}$	$(-0.9\pm1.3)\cdot10^{-3}$	$(3.03\pm0.38)\cdot10^{-2}$	$(3.8\pm5.3)\cdot10^{-3}$	$(-1.8\pm1.3)\cdot10^{-3}$
Single channel						
θ_{tag}	Δm	$\Delta\Gamma/\Gamma$	$\mid q/p \mid$	$\frac{\mathrm{Re}\lambda_{CP}}{\mid\lambda_{CP}\mid}$Rez	$\frac{\mathrm{Im}\lambda_{CP}}{\mid\lambda_{CP}\mid}$	Imz
0	$(3.62\pm0.60)\cdot10^{-3}$	$(-5.7\pm4.0)\cdot10^{-3}$	$(-0.7\pm1.3)\cdot10^{-3}$	$(-4.87\pm0.35)\cdot10^{-2}$	$(2.3\pm5.3)\cdot10^{-3}$	$(-1.0\pm1.4)\cdot10^{-3}$
$\frac{\pi}{2}$	$(1.66\pm0.61)\cdot10^{-3}$	$(1.4\pm3.9)\cdot10^{-3}$	$(-1.9\pm1.2)\cdot10^{-3}$	$(-1.98\pm0.38)\cdot10^{-2}$	$(6.5\pm4.6)\cdot10^{-3}$	$(0.0\pm1.4)\cdot10^{-3}$
π	$(2.83\pm0.59)\cdot10^{-3}$	$(-2.8\pm3.7)\cdot10^{-3}$	$(-4.5\pm1.3)\cdot10^{-3}$	$(5.27\pm0.34)\cdot10^{-2}$	$(3.2\pm4.7)\cdot10^{-3}$	$(1.1\pm1.4)\cdot10^{-3}$
$\frac{3}{2}\pi$	$(2.03\pm0.57)\cdot10^{-3}$	$(-2.5\pm3.7)\cdot10^{-3}$	$(-2.5\pm1.2)\cdot10^{-3}$	$(1.32\pm0.41)\cdot10^{-2}$	$(-1.2\pm4.8)\cdot10^{-3}$	$(-0.3\pm1.4)\cdot10^{-3}$

Table 139: Mean residuals with error from about 200 toy Monte Carlo experiments generated with two channels and one single channel in the tagging side (r_{tag} was generated to be 0.1).

C Evaluating $\delta m_d/m_d$ and $\delta\Gamma_d/\Gamma_d$ from $\Delta\Gamma_d/\Gamma_d$, Δm_d and z

The CPT parameter, z, is defined as

$$z = \frac{\Delta m - i\Delta\Gamma/2}{\Delta m_d - i\Delta\Gamma_d/2} \tag{152}$$

The quantities $\delta m_d/m_d$ and $\delta\Gamma_d/\Gamma_d$ can then be written as

$$\begin{aligned} \delta m_d/m_d &= \mathrm{Re}z\Delta m_d/m_d + \frac{1}{2}\mathrm{Im}z\Delta\Gamma_d/m_d \\ \delta\Gamma_d/\Gamma_d &= \mathrm{Re}z\Delta\Gamma_d/\Gamma_d - 2\mathrm{Im}z\Delta m_d/\Gamma_d \end{aligned} \tag{153}$$

Let us define now the following variables (related to the actual measured parameters):

$$\begin{aligned} p_1 &= \frac{\mathrm{Re}\lambda}{|\lambda|}\mathrm{Re}z \\ p_2 &= \mathrm{Im}z \\ p_3 &= \frac{\mathrm{Im}\lambda}{|\lambda|} \\ p_4 &= \Delta m_d/m_d \\ p_5 &= sign\left(\frac{\mathrm{Re}\lambda}{|\lambda|}\right)\Delta\Gamma_d/m_d \\ p'_4 &= \Delta m_d/\Gamma_d \\ p'_5 &= sign\left(\frac{\mathrm{Re}\lambda}{|\lambda|}\right)\Delta\Gamma_d/\Gamma_d \end{aligned} \tag{154}$$

In terms of these variables, $\delta m_d/m_d$ and $\delta\Gamma_d/\Gamma_d$ can be written as

$$\begin{aligned} q_1 \equiv \delta m_d/m_d &= s\left[\frac{p_1}{\sqrt{1-p_3^2}}p_4 + \frac{1}{2}p_2 p_5\right] \\ q_2 \equiv \delta\Gamma_d/\Gamma_d &= \frac{p_1}{\sqrt{1-p_3^2}}p'_5 - 2p_2 p'_4 \end{aligned} \tag{155}$$

where s is the sign choice for $\mathrm{Re}\lambda/|\lambda|$. Note the overall sign ambiguity in q_1, while q_2 is insensitive to it.

Similarly as we did to produce Fig.1 of the PRL, we can estimate the total error σ_{tot} on each p_k by combining its statistical error (σ_{stat}) with its additive (σ_{syst}) and multiplicative (f_{syst}) systematic error according to

$$\sigma_{tot} = \sqrt{(1+f_{syst})^2\sigma_{stat}^2 + \sigma_{syst}^2}$$

Parameters p_1, p_2 and p_3 are just measured parameters of the CPT analysis:

$$p_1 = 0.014 \pm 0.053 \quad , \quad p_2 = 0.038 \pm 0.040 \quad , \quad p_3 = 0.762 \pm 0.074$$

For p_3 we take the value and error from the standard $\sin 2\beta$ analysis, assuming $f_{syst} = 0$.

To evaluate p_4, we take the Δm_d PDG2002 average assuming as well $f_{syst} = 0$: $\Delta m_d = 0.489 \pm 0.005 \pm 0.007$ $\hbar\text{ps}^{-1} = (0.322 \pm 0.006) \times 10^{-9}$ MeV. For m_d we use the PDG2002 average, $m_d = 5279.4 \pm 0.5$ MeV. When evaluating the error on p_4, the contribution from m_d is completely negligible (by several orders of magnitude). Finally we obtain:

$$p_4 = (6.10 \pm 0.11) \times 10^{-14}$$

The parameter p_5 can be evaluated similarly, using the PDG2002 central value of the B^0 lifetime, 1.542 ± 0.016 ps: $\Delta\Gamma_d = -0.005 \pm 0.030$ $\hbar\text{ps}^{-1} = (-0.003 \pm 0.020) \times 10^{-9}$ MeV. Note that the error on the average B^0 lifetime is already part of the systematic error on $\Delta\Gamma_d/\Gamma_d$, so we do not need to propagate it here. Finally we get:

$$p_5 = (-0.006 \pm 0.37) \times 10^{-14}$$

The variables p'_4 and p'_5 can be evaluated in the same way (here, again, we do not need to propagate the uncertainty on the average B^0 lifetime since it is already part of the systematic error on the measured parameters):

$$p'_4 = 0.754 \pm 0.013 \quad , \quad p'_5 = -0.008 \pm 0.047$$

We estimate the overall correlations (i.e. statistical+systematic) using the statistical correlations reported by the CPT fit (note that the correlations involving p_4, p_5, p'_4, p'_5 are the same as with the corresponding measured parameters, Δm_d and $\Delta\Gamma_d/\Gamma_d$ since the relative factors can be considered as constants, as discussed above):

$$\rho(p_1,p_2) = -3.4\% \quad , \quad \rho(p_1,p_3) = -10.9\% \quad , \quad \rho(p_1,p_4) = \rho(p_1,p'_4) = +7.0\%$$
$$\rho(p_1,p_5) = \rho(p_1,p'_5) = -7.9\%$$
$$\rho(p_2,p_3) = +17.4\% \quad , \quad \rho(p_2,p_4) = \rho(p_2,p'_4) = -0.2\% \quad , \quad \rho(p_2,p_5) = \rho(p_2,p'_5) = -1.8\%$$
$$\rho(p_3,p_4) = \rho(p_3,p'_4) = -5.6\% \quad , \quad \rho(p_3,p_5) = \rho(p_3,p'_5) = +0.4\%$$
$$\rho(p_4,p_5) = \rho(p'_4,p'_5) = -1.3\%$$

We now evaluate the error on q_1 and q_2 using the usual error propagation prescription,

$$(dq_k)^2 = \sum_{ij} \frac{\partial q_k}{\partial p_i} \frac{\partial q_k}{\partial p_j} V_{ij}$$

where V_{ij} is the covariance matrix of p_i estimated above. The partial derivatives are:

$$\frac{\partial q_1}{\partial \vec{p}} = s \left(\frac{p_4}{\sqrt{1-p_3^2}}, \frac{1}{2}p_5, 4p_1p_4p_3(1-p_3^2)^{-3}, \frac{p_1}{\sqrt{1-p_3^2}}, \frac{1}{2}p_2 \right)$$

$$\frac{\partial q_2}{\partial \vec{p}} = \left(\frac{p_5'}{\sqrt{1-p_3^2}}, -2p_4', 4p_1 p_5' p_3 (1-p_3^2)^{-3}, -2p_2, \frac{p_1}{\sqrt{1-p_3^2}} \right)$$

The $\delta\Gamma_d/\Gamma_d$ interval is then:

$$\delta\Gamma_d/\Gamma_d : [-15.6, 4.2]\% \ @90\%CL$$

Similarly, the $\delta m_d/m_d$ interval is (assuming $s = +1$, same convention as used in the CPT fit):

$$\delta m_d/m_d : [-0.75, 1.01] \times 10^{-14} \ @90\%CL$$

If we assume instead $s = +1$, the corresponding interval is

$$\delta m_d/m_d : [-1.01, 0.75] \times 10^{-14} \ @90\%CL$$

D $\Delta\Gamma_d/\Delta m_d$ from $\Delta\Gamma_d/\Gamma_d$ and Δm_d

To evaluate $\Delta\Gamma_d/\Delta m_d$ using the measured values of $\Delta\Gamma_d/\Gamma_d$ and Δm_d, we can apply the usual error propagation. If we call $x = \Delta\Gamma_d$, $y = \Delta m_d$ and $z = \Delta\Gamma_d/\Delta m_d$, we have

$$dzdz = \frac{1}{y^2}\left(dxdx + z^2 dydy - 2zdxdy\rho(x,y)\right)$$

As before, let us take for Δm_d the PDG2002 average, assuming $f_{syst} = 0$: $\Delta m_d = 0.489 \pm 0.005 \pm 0.007$ ps^{-1}. From the measured value of $\Delta\Gamma_d/\Gamma_d = -0.008 \pm 0.037 \pm 0.018$ ps^{-1}, and using the PDG2002 average B^0 lifetime central value, 1.542 ps, we estimate $\Delta\Gamma_d = -0.005 \pm 0.024 \pm 0.012$ ps^{-1}. Note, again, that the error on the average B^0 lifetime is already part of the systematic error on $\Delta\Gamma_d/\Gamma_d$, so we do not need to propagate it here.

The evaluation of the central value and statistical and systematic errors of $\Delta\Gamma_d/\Delta m_d$ are now straightforward. We first evaluate the statistical error using the -1.3% correlation extracted from the fit. We get 0.049. This error is unchanged if we assume no error on Δm_d (i.e. the error on $\Delta\Gamma_d/\Delta m_d$ is completely dominated by the error on $\Delta\Gamma_d$). The systematic error depends on the assumed systematic correlation: changing it from -100% to $+100\%$ changes the systematic error from 0.0237 to 0.0240; assuming no systematic error on Δm_d the error is 0.0239. Therefore, we have

$$\Delta\Gamma_d/\Delta m_d = -0.011 \pm 0.049 \pm 0.024$$

independently of the assumed correlations between $\Delta\Gamma_d$ and Δm_d.

To evaluate the 90%CL interval we proceed exactly in the same way but now multiplying the statistical error on $\Delta\Gamma_d$ by the multiplicative factor f_{syst}, and rescaling all errors by 1.64. The resulting interval is

$$\Delta\Gamma_d/\Delta m_d : [-0.112, 0.091] \ @90\%CL$$

Using alternative values of Δm_d (BaBar average, BaBar hadronic mixing, etc) makes very small changes on $\Delta\Gamma_d/\Delta m_d$.

Similarly, with CPT is assumed to be a good symmetry,

$$\Delta\Gamma_d/\Delta m_d = -0.012 \pm 0.049 \pm 0.024 \quad [-0.113, 0.090] \ @90\%CL$$

References

[1] A.S. Dighe et al., Measurement of the Lifetime Difference of B_d^0 Mesons: possible and Worthwhile?, *Nucl. Phys.* **B624** (2002) 377-404.

[2] R.F. Streater and A.S. Wightman, *PCT, Spin and Statistics, and All That*, Benjamin, New York, 1964.

[3] M.B. Gavela et al., *Mod. Phys. Lett.* **A9** (1994) 795.

[4] I.I. Bigi, A.I. Sanda, *CP Violation*, Cambridge University Press, 2000.

[5] M. Kobayashi and A. I. Sanda, *Phys. Rev. Lett.* **69** (1992) 3139; Z. Xing, *Phys. Rev.* **D50** (1994) 2957; D. Colladay and V. A. Kostelecký, *Phys. Lett.* **B344** (1995) 259; V. A. Kostelecký and R. Van Kooten, *Phys. Rev.* **D54** (1996) 5585; P. Colangello and G. Corcella, *Eur. Phys. J.* **C1** (1998) 515.

[6] S.W. Hawking, *Phys. Rev.* **D14** (1975) 2460; *Commun. Math. Phys.* **87** 395 (1982); V.V. Barmin et al., *Nucl. Phys.* **B247** (1985) 293.

[7] B. Aubert et al., The BaBar Collaboration, Observation of CP Violation in the B^0 meson system, *Phys. Rev. Lett.* **87** 091801 (2001).

[8] Ed. V. A. Kostelecký, *CPT and Lorentz Symmetry*, World Scientific, Singapore, 1999.

[9] *BABAR* Analysis Document # 442, Supporting document for the summer 2002 $\sin 2\beta$ analysis.

[10] *BABAR* Analysis Document # 188, A general model for Neutral B decay time distributions.

[11] The *BABAR* Physics Book, Ed. P.F. Harrison and H.R. Quinn, SLAC-R-504 (1998).

[12] *BABAR* Analysis Document # 385, A study of indirect violation of CPT/CP and CP/T using fully reconstructed CP and flavor eigenstates.

[13] *BABAR* Analysis Document # 436 (v6.0) Measurement of $\Delta\Gamma/\Gamma$ and study of CPT and T violation using fully reconstructed CP and flavor eigenstates.

[14] For a comparison of different formalisms, see for instance V. A. Kostelecký, *Phys. Rev.* **D64** 076001 (2001).

[15] M. C. Bañuls, J. Bernabéu, *Phys. Lett.* **B423** (1998) 151; *Phys. Lett.* **B464** (1999) 117; *JHEP* **9906:032** (1999); *Nucl. Phys.* **B590** (2000) 19.

[16] R. Cahn, Determining efficiency differences from time-integrated data, $\sin 2\beta$ HNs #183, or `http://www.slac.stanford.edu/~cahn/internal/differing_efficiencies.ps`

[17] R. Cahn, Some Things about $\Delta\Gamma$, `http://www.slac.stanford.edu/~cahn/internal/delta_Gamma.ps`

[18] *BABAR* Analysis Document # 18, A User's Guide to the RootFitTools Package for Unbinned Maximum Likelihood Fitting.

[19] *BABAR* Analysis Document # 56, Analysis of $B^0 \to J/\psi K_L^0$ decays.

[20] *BABAR* Analysis Document # 452, Aspects of the summer 2002 $\sin 2\beta$ measurement specific to the decay mode $B^0 \to J/\psi K_L^0$.

[21] *BABAR* Analysis Document # 119, B Tagging in BaBar: Status for the 2001 $\sin 2\beta$ Publications.

[22] *BABAR* Analysis Document # 317, BTagger-A Multivariate Tagging Algorithm with Categories Based on the Physics of the Btag Decay.

[23] *BABAR* Analysis Document # 125, Measurement of $B^0\overline{B}^0$ mixing with fully reconstructed hadronic B decays.

[24] Give here the new world average for Δm.

[25] *BABAR* Analysis Document # 91, Draft Guidelines for Blind Analyses in *BABAR*, V2.0, section 3.2.

[26] Particle Data Group, K. Hagiwara *et al.*, *Phys. Rev.* **D66** 010001 (2002).

[27] *BABAR* Analysis Document # 102, The BaBar Vertexing.

[28] *BABAR* Analysis Document # 106, Study of Material Interactions with Gamma Conversions and Protons.

[29] *BABAR* Analysis Document # 144, Measurements of the charged and neutral B meson lifetimes using fully reconstructed B decays.

[30] *BABAR* Analysis Document # 14, Measuring the PEP-II Boost.

[31] NAG software, `http://wwwinfo.cern.ch/asd/nag/`

[32] F. James, MINUIT reference manual, CERN program library.
`http://wwwinfo.cern.ch/asdoc/Welcome.html`

[33] *BABAR* Analysis Document # 349, Correlation between mistag of kaon tag and calculated error on Δt.

[34] *BABAR* Analysis Document # 254, Vertexing supporting document for Summer 2001 Conferences.

[35] R. Cahn, Dealing with lambda for Doubly Cabibbo-Suppressed Decays,
`http://babar-hn.slac.stanford.edu:5090/HyperNews/get/pubboard08/83/1/4.html`

[36] Pat Burchat, Can we bound r from doubly-CKM-suppressed B decays?,
`http://www.slac.stanford.edu/BFROOT/www/Physics/Analysis/AWG/BBMixingHadr/Meetings/21Nov2002/`

[37] R. Cahn, Double-Cabbibo Suppressed Decays, μ, ν, $|\,q/p\,|$, CPT, and All That,
Mixing HNs #385, `http://babar-hn.slac.stanford.edu:5090/HyperNews/get/Bmixing/385.html`

[38] Sibylle Petrak, Impact of a Lifetime Difference $\Delta\Gamma$ of B^0 mesons on *BABAR* measurements, *BABAR* Note 472, November 1998.

E Document history

Changes between version 5.0 and 4.0

- Abstract: add unblind results and 90% confidence limits.
- Add unblind results and Δt distributions (section 7.6) and asymmetries on data (section 7.7, as an additional check of goodness-of-fit).
- Remove section with asymmtries from Monte Carlo.
- Add setting limits section 9.23.
- Update section 10 with unblind results and limits.

Changes between version 4.0 and 3.0

- Sections 7.2 and 7.3: compare unblind Δm results with *BABAR* hadronic mixing result and 2003 world average. Explain the origin of the difference in the Δm result between the *GG* and *GExp* resolution models.
- Remove cross-check results from the abstract and add discussion about the cross-check measurements in the summary (section 10).
- Clarify that the *GG* resolution model is used as nominal parameterization while the *GExp* is used to assign systematics (sections 6 and 10).
- Fix binomial errors in plots of asymmetries.
- Add a section (7.7) for asymmetries in data, and modify section on asymmetries on Monte Carlo (**??**). Add a discussion about about the questions of points consistently below the curve in the mixing asymmetry in the Monte Carlo (as requested by David Williams).
- Run period check (section 8.14), merge run2c and run2d (run2d luminosity too small).
- Final results of goodness-of-fit and expected errors (section 7.5) for Analysis 1 and Analysis 2. Likelihood fit systematics updated accordingly (section 9.14).
- Sections 7.2 and 7.3: clarify the origin of the change in the values of $\frac{\mathrm{Im}\lambda_{flav}}{|\lambda_{flav}|}$, $\frac{\mathrm{Im}\bar{\lambda}_{flav}}{|\lambda_{flav}|}$, $\frac{\mathrm{Im}\lambda_{tag}}{|\lambda_{tag}|}$, $\frac{\mathrm{Im}\bar{\lambda}_{tag}}{|\lambda_{tag}|}$ among the `GG` and `GExp` resolution models and between Analysis 1 and Analysis 2.
- Section 8.12: update results after bug fix in the script used to select the common events. This bug was introducing additional fluctuations due to the use of uncommon events. The results are now more consistent and some of the large 3-5 sigma discrepancies observed before went away. Add some remarks about the interpretation and significance of the checks.
- Beam spot systematics (9.3) slightly changed (fixed a small bug in the selection of common events, before some events were not common).

Changes between version 3.0 and 2.0

- Section 2: change to BaBar Physics Book sign conventions for q/p and $\Delta\Gamma$.
- Add a new short section (2.3) clarifying which are the sign conventions adopted in the text and in the results presented in the document.
- Added results of goodness-of-fit and expected errors, section 7.5. Likelihood fit systematics updated accordingly (section 9.14). Processing for Analysis 1 still not finished and the final statistics will be ready for version 4.0. Assign for now as likelihood systematics for Analysis 1 the same as Analysis 2.
- Blinding strategy description, section 5, clarified and completed (thanks to Pat's questions).
- Section 4: add checks of $\sigma_{\Delta t}$ and Δt dependence of μ^{α} and ν. For completeness, add also Δt dependence of w^{α} and Δw^{α}.

Changes between version 2.0 and 1.0

- Abstract: has been improved including final results and giving some additional information.
- Introduction (section 1): modified according to Bob requests (relative weight of $\Delta\Gamma$ measurement vs CPT/T test was opposite to the title and abstract). A more clear road-map to related documentation is also included.
- Parameter counting, section 2.9. Moved ahead and completed with missing parameters. Added reference to other closely related sections.
- Added table 6 (section 3) detailing the signal event yields per sample and tagging category after vertexing cuts.
- Summary, section 10. Expanded with more wording in an attempt to give a quick overview of the analysis.
- Section 9.2 updated including a check for the flat outlier component with finite normalization (Pat's request).
- Sections 8.1 and 9.6 updated clarifying the relationship between the fixed lifetime to the world average and its dependence with the $\Delta\Gamma$=0 assumption. Take as systematics twice the error from the world average to account for the effect. Justifies the prescription. No change on overall systematics, however.
- K_L^0 systematics due to ΔE shape and MC reweighting have been updated/added in section 9.21.
- Section 7.1.1: clarify the origin of the apparent bias in the fitted B^+ lifetime, remarking that is has no effect on the relevant parameters (mistag fractions and detector charge asymmetries for B^+).
- Likelihood fit systematics (section 9.14) clarified.
- Blinding strategy description, section 5, clarified.
- Figure **??**: added curves with $\Delta\Gamma/\Gamma$=0, $|\,q/p\,|$=1, $z=0$.
- Section 9.20, clarify why we do not evaluate/assign an explicit systematics from charm content.
- Final tables 123– 126 updated consistently to systematics changes/additions.